UNIVERSITA' DEGLI STUDI DI PARMA

Dottorato di ricerca in "Progettazione e sintesi di composti biologicamente attivi"

Ciclo XXIV

Application of comparative modelling to the design and discovery of novel GPCR ligands

Coordinatore:
Chiar.mo Prof. Marco Mor

Tutor:
Chiar.ma Prof.ssa Silvia Rivara

Dottorando: Daniele Pala

A Claudia, il mio rifugio

Summary

CHAPTER 1

Introduction

G protein-coupled receptors

G protein-coupled receptors (GPCRs) constitute the largest superfamily of transmembrane receptors whose primary function is to convert extracellular stimuli to an intracellular response through the action of G proteins. The overall architecture of GPCRs is characterized by seven membrane-spanning helices connected by three intracellular (ICL) and three extracellular (ECL) loops. It was estimated that up to 800 GPCRs are encoded by the human genome,[1] of which ~400 are expected to bind endogenous ligands.[2,3] Such a diversity is deeply related to two fundamental aspects of the GPCR machinery: the necessity to respond to a broad spectrum of chemically diverse extracellular signals (including light, neurotransmitters, hormones, peptides, lipids, amino acids and many others) and to activate different intracellular signalling pathways.
Nowadays, more than 30% of currently marketed drugs target GPCRs,[4] underlining the physiological importance of this receptor family and their therapeutical relevance. Due to these reasons, in the last decades a growing interest has been shown for the study of GPCRs functions, mechanisms and modulation: the intimate understating of the receptor structural features and of the signalling mechanism could lead to the development of new drugs useful in the treatment of a variety of diseases.

Classification

The first attempt to classify GPCRs was made in 1993,[5] when sequence-based fingerprints were developed for the seven hydrophobic domains of GPCRs: this study was subsequently extended[6] to incorporate a higher number of sequences taken from different species and the term “clan” was then created to designate different GPCR families. This classification system was updated in 1994, with the introduction of the “A-F” notation to describe GPCR classes:[7] nowadays this classification is widely used and accepted as standard from the International Union of Pharmacology, Committee on Receptor Nomenclature and Classification (NC-IUPHAR)[8]. A different method of classification was proposed in 1999, in which GPCRs were divided in different families (from 1 to 5) on the basis of their common structural motifs and of the nature of their endogenous ligands.[9] The sequencing of the human genome in 2001 re-opened the issue of GPCR classification, since a plenty of new sequences belonging to the human GPCR repertoire were mapped and characterized.

The last GPCRs classification method relied on a phylogenetic approach and divided GPCRs in five different families, named Glutamate, Rhodopsin, Adhesion, Frizzled/taste2 and Secretin (GRAFS).[10] Two of the main advantages of this method are the inclusion of a wider number of classified proteins and the presence of the bitter taste 2 receptor subtype, not covered in the previous classifications.

A brief description of GPCR families is reported below: each family is indicated using both the GRAFS and the NC-IUPHAR nomenclature systems.

Class A (Rhodopsin)

The rhodopsin family is the most populated one and contains more than 600 human proteins. The GRAFS classification further divided this family into four groups, named α, β, γ and δ. While group α includes some of the most interesting targets currently under investigations in the majority of drug discovery campaigns, such as histamine, dopamine, adrenergic and serotoninergic receptors, group β contains mostly peptide-binding receptors, like oxytocin, gonadotropin-releasing hormone and neuropeptide Y receptors. Few examples of proteins included in group γ are somatostatin, opioid and angiotensin receptors, whereas group δ comprises the glycoprotein-binding receptors, the olfactory receptors and others.

Class A of GPCRs is characterized by some peculiar characteristics, like a considerably short N-terminus portion and the presence of common structural motifs. However, despite their similarities, proteins belonging to class A show a high heterogeneity in terms of primary sequence and ligand preference. Indeed, an extremely wide spectrum of extracellular substances, such as amines, photons, purines, hormones and peptides are able to bind members of class A GPCRs. It was estimated that about 27% of currently marketed drugs target class A GPCRs, which highlights the therapeutic potential and the importance of this class of membrane receptors.[11,12]

Due to the presence of common structural domains among class A members, some attempts were made to found a common numbering scheme to label corresponding pairs of amino acids. Schwartz[13] and Ballesteros[14] proposed two different nomenclatures to assign numbers to conserved residues in the transmembrane (TM) domains: while in the former approach the most conserved residue in a helix receives a generic number according to its position in the helix, in the latter method the most conserved residue is indicated as X.50, where X is the number of the TM helix. Nowadays, the Ballesteros-

Weinstein numbering scheme is commonly used and widely accepted in the GPCRs community and will be used thorough the text to indicate amino acid positions.

Class B (Secretin)

In contrast to the highly-populated rhodopsin family, the secretin family includes only a small number of members characterized by a high sequence identity, such as the calcitonin-like receptors, the corticotrophin-releasing hormone receptors and the glucagon-like peptide receptors. The direct consequence of such a high degree of sequence similarity is a reduced ability of these targets to respond to a wide spectrum of exogenous ligands: indeed, the receptors comprised in this family preferably bind peptide hormones. While in the rhodopsin family the ligand binding site is located approximately into a cavity delimited by the TM portions, in the secretin family the hormone-binding domain is located mainly in the extracellular milieu.[15,16,17] The binding region of the secretin-like receptors is constituted by three distinct domains, that span from the N-terminus through the extracellular loops (ECLs):[18,19,20,21] an extended network of cysteine bridges located at the hormone-binding pocket brings to an overall stabilization of the binding site structure.

Class B (Adhesion)

The members of the adhesion family differ from secretin-like receptors for at least three main characteristics: i) the architecture of the N-termini,[22] ii) the nature of ligands able to bind them and iii) the presence of functional domains,[23] like the GPCR proteolytic domain, absents in the secretin family. Adhesion-like receptors preferably bind extracellular matrix molecules and the architecture of their N-termini is peculiar among other GPCRs families, since it contains several domains that have been shown to play a key role in determining the specificity of ligand-receptor interactions.[24]

Class C (Glutamate)

Cass C contains about 20 GPCRs,[10] including the metabotropic glutamate receptors and the calcium-sensing receptor. Similarly to what observed for class B GPCRs, the binding site region of the glutamate-like receptor family is located at the N-terminus region. Crystallization studies have been used to clarify the architecture of the extracellular portion of these receptors:[25] it was seen that the binding site structure is organized into two domains whose tertiary structures are fixed through several disulphide bridges. From these observations, it was hypothesized that the ligand binding mechanism resembled that

of a Venus flytrap, in which the two extracellular domains could accommodate the endogenous ligand and trigger the subsequent receptor activation.

Frizzled/taste2

The frizzled group of receptors comprises ten frizzled receptors and the smoothened receptor:[10] while the formers preferably bind a specific family of glycoproteins, the latter seems to be able to trigger the activation cascade in a ligand-indipendent manner. Similarly to class B and C, also the frizzled receptors are characterized by a long N-terminus domain which is formed by 200-300 amino acids and acts like a binding site region that could accommodate the glycoprotein.[26] On the other hand, the taste2 group of receptors shows slightly different characteristics compared to the frizzled cluster. As seen for class A GPCRs, also the members of the taste2 group are characterized by a heterogeneous amino acid composition and low sequence similarities.[27] This could explain the ability of these receptors to detect a variety of bitter compounds present in nature.[28] In contrast to what observed for frizzled receptors, the taste2 ligand binding site is not enclosed in the long N-terminus domain: indeed, recent studies identified some residues located on extracellular loop portions as crucial for ligand binding.[29]

Signalling pathways and second messengers

As described before, GPCRs convey an extracellular stimulus to the intracellular environment. However, this response is not driven by GPCRs themselves, but requires the activation of other proteins and second messengers that could trasmit the signal from the extracellular milieu into the cell. The cascade of events that follows GPCRs activation starts with the involvement of heterotrimeric guanine-nucleotide-binding regulatory proteins, called G proteins. G proteins bind to the cytoplasmic portion of GPCRs and are constituted by three different subunits: α (36-52 kDa), β (35-36 kDa) and γ (8-10 kDa).[30] The last two subunits (β and γ) are strongly connected to form functional units. G proteins transmit the signal from GPCRs to second messengers and to other proteins. However, to avoid altered signal transmissions, G proteins follow an activation-deactivation cycle that is triggered by GPCR activation. When a GPCR activates a G protein, it leads the replacement of guanosine diphosphate (GDP, that preferentially binds the inactive state of G protein) with guanosine triphosphate (GTP) at the α subunit. This nucleotide exchange drives the release of the G protein from its cognate GPCR and allows the dissociation of

the G protein into two different subunits, α and βγ. These two functional units activate other downstream effectors (such as adenylyl cyclase, phospholipases and lipid kinases) to transmit and amplify the initial signal. The effector targets usually regulate the intracellular concentrations of second messengers, such as inositole-triphosphate, diacylglycerol, cyclic AMP and calcium cations which finally exert a physiological response, typically through the regulation of gene transcription. The cycle is then terminated with the cleavage of GTP in GDP by the α subunit: the increased affinity of the α subunit towards the βγ unit leads to their re-association and the re-coupling of the G-protein with the cognate GPCR.

So far, 20, 6 and 12 isoforms have been identified for α, β and γ subunits, respectively: different combinations of isoforms lead to different G proteins with different characteristics and functions. G proteins are currently classified in four distinct classes based on their sequence homology: G_s, G_i, G_q and G_{12}.[31] Different G protein subtypes exert different functions and mediate different intracellular responses.[32,33,34,35] Indeed, while G_s activates adenylyl cyclase and regulates calcium channels, the G_i subtype inhibits adenylyl cyclase, activates cyclic GMP phosphodiesterase and regulates potassium and calcium channels. Similarly to G_s, also the G_q subtype leads to the activation of an effector target, namely the phospholipase Cβ. The functional mechanism of the G_{12} subtype has been recently characterized:[34] it was shown that this G protein not only regulates sodium and potassium channels but also binds and stimulates the Bruton's tyrosine kinase.

As stated previously, the downstream signal produced by GPCR activation is transmitted to effectors through the action of G proteins. After the discovery of the GPCR-G protein signalling mechanism, it was hypothesized that only the α subunits could activate downstream effectors, while the βγ complex could only inhibit or negatively tune the α subunit-induced effects. Recent experimental evidences brought to a reassessment of the GPCR-G protein transduction mechanism. Indeed, it was shown that also the βγ subunit could activate effector targets, like potassium channels,[36] adenylyl cyclase, phospolipase Cβ, phospholipase A_2 and other kinases.[37] While the β subunits seem to share a common amino acid composition, the γ subunits are characterized by a lower sequence similarity: thus, it could be hypothesized that the different characteristics and functions seen among different βγ complexes are mainly due to the γ subunit.

Although some effector proteins have been shown to be regulated by both α and βγ subunits, it must be noted that the ability of a specific subunit to activate a particular

effector strongly depends on the effector subtype.[38] For example, different subtypes of adenylyl cyclase show different responses to α and βγ subunits: while one subtype is activated by α and unaffected by βγ, a second subtype can be only activated by α and is inhibited by βγ.

The mechanism and functions of G proteins are regulated by some covalent modifications, acted by three main types of lipids: these covalent adducts occur mostly at the α and γ subunits.[39,40] The α subunit can undergo both myristoylation and palmitoylation: while the former is an irreversible reaction crucial for anchoring the unit to the membrane, the latter is a reversible modification that was thought to regulate and tune the downstream response. On the contrary, the γ subunit is usually prenylated: this modification is thought to facilitate the anchoring of the βγ complex to the membrane and to promote the association between α and βγ subunits. Although several studies have been already performed, the functions of these G protein-lipids adducts are matter of evaluation. However, it seems reasonable that the covalent bond with these hydrophobic substituents could facilitate the seizure of G protein towards specific lipid-enriched membrane domains, like calveole.[40]

It must be noted that G protein transduction mechanism does not usually follow a “one protein-one effector-one signal” relationship and that the activation of a specific receptor does not imply the involvement of a predetermined pattern of downstream effectors. On the contrary, the starting signal coming from a single GPCR could diverge or converge depending on some specific conditions, such as the cell type or the tissue: thus, i) a single GPCR could activate different G proteins and effector targets, leading to the activation of different signaling routes[41,42,43,44,45,46,47,48] or ii) different GPCRs could activate the same G protein, in order to tune and integrate the activation signals coming from different extracellular stimuli.[49,50,51,52,53] A third case, called “cross-talk”, is characterized by the integration and the cross-regulation of two or more different signal routes coming from different GPCRs.[54,55,56]

Available GPCR crystal structures: similarities and differences

GPCR crystallization is extremely challenging due to different factors: i) the instability of these proteins in detergents, ii) the presence of highly-flexible regions (e.g. loops) and iii)

their low expression levels. Recently, the field of GPCR structural biology has achieved new remarkable results due to the development of improved crystallization techniques.

The first crystal structure of a GPCR was that of bovine rhodopsin, released in 2000.[57] For the subsequent 7 years rhodopsin has been the sole GPCR crystal structure available. Although this crystal structure represented an impressive breakthrough in the field of structural biology, it belongs to a very specific branch of GPCRs and could not completely clarify the mechanism and function of GPCRs machinery, especially for diffusible ligands. In 2007, the structure of the β_2 adrenergic receptor in complex with an inverse agonists was solved.[58,59,60] The release of the crystal structure of a "druggable" GPCR threw light for the first time on the interactions between a drug-like compound and its receptor and on the differences occurring between GPCR subfamilies. The β_2 adrenergic receptor was followed by other class A GPCRs: the β_1 adrenergic receptor,[61] the A_{2A} adenosine receptor,[62] the CXCR4 chemokine receptor,[63] the D_3 dopamine receptor[64] and the H_1 histamine receptor.[65]

Although the crystal structures of the ligand-free form of rhodopsin (opsin) were released in 2008,[66,67] year 2011 saw the dawn of a new era for GPCR structural biology: indeed, the crystal structures of the active states of β_2, β_1 and A_{2A} adenosine receptors were released.[68,69,70,71,72,73] The availability of the active form of "druggable" GPCRs helps to clarify at a molecular level the major structural modifications occurring upon agonist binding.

Nowadays, 55 GPCR crystal structures are available in the Protein Data Bank,[74] divided as follows: 16 of bovine rhodopsin,[57,75,76,77,78,79,80,81,82,83,84,85,86] 2 of squid rhodopsin,[87,88] 2 of opsin,[66,67] 11 of the β_2 adrenergic receptor,[58,59,60,68,69,70,89,90,91] 10 of the β_1 adrenergic receptor,[61,71,92] 7 of the A_{2A} adenosine receptor,[62,72,73,93] 5 of the CXCR4 chemokine receptor,[63] 1 of the D_3 dopamine receptor[64] and 1 of the H_1 histamine receptor.[65]

A detailed comparison between available crystal structures is presented below.

Extracellular region

Class A GPCRs can respond to a variety of chemically diverse compounds. To favor the entrance and the accommodation of such a diverse set of chemical entities into the ligand binding pocket, class A GPCRs developed highly-flexible extracellular domains, that can differ even between members of the same subfamily. The release of the new GPCR crystal structures threw light on the architecture of the extracellular regions belonging to

different GPCR subfamilies, highlighting their striking differences as well as specific structural motifs.

ECL1 is usually small and it is constituted by few amino acids. Although its residue composition can vary remarkably between different receptors, its length remains conserved since more than 70% of class A GPCRs are characterized by 52 amino acids between residues 2.50 and 3.50[94] (according to the Ballesteros numbering scheme[14]). A sequence-based analysis revealed the presence of two conserved motifs into the ECL1 sequence: the WXFG[95] and the DXXCR.[96] The WXFG seems to be the most conserved one, as it is present in 80% of class A GPCRs: since site-directed mutagenesis targeting this sequence altered receptor activation but not ligand binding,[95,97,98] it has been hypothesized that this specific motif could be involved in the transmission of the ligand binding signal to the TM portions,[95] triggering the conformational changes associated with receptor activation. On the contrary, the DXXCR motifs was found at the C-terminus of ECL1 in the vasopressin and oxytocin receptors: due to its proximity to the extracellular portion of TM3, this motif is probably involved in the formation and stabilization of the conserved disulfide bridge between TM3 and ECL2. Moreover, additional studies provided some clues for a role of this specific domain in the receptor activation mechanism.[96,99] The inspection of available GPCR crystal structures revealed that ECL1 can form an extended network of interactions with neighboring domains. With the only exception of the A_{2A} adenosine receptor, the ECL1 is characterized by an unfolded structure. Its C-terminus sequence points towards the conserved disulfide bridge between TM3 and ECL2 (Figure 1): in particular, for aminergic GPCRs (β_1, β_2, H_1 and D_3), the tryptophan residue belonging to the WXFG domain can form favorable hydrophobic interactions with the cysteine residues of the disulphide bridge. In the rhodopsin sequence, this tryptophan is substituted by a phenylalanine. However, also in this case, a hydrophobic interaction occurring between the conserved cysteines and the FXFG motif could be identified. ECL1 domains of the A_{2A} and the CXCR4 receptors represent two extreme cases, in which the overall structural arrangement is remarkably influenced by additional molecular interactions. ECL1 segment of the CXCR4 receptor is shifted outwards compared to other GPCR structures, due to the peculiar architecture of ECL2, that leans on ECL1 to retain the binding pocket accessible from the extracellular side. In this case, beside the hydrophobic interaction between the tryptophan of the WXFG motif and the disulphide bridge, an additional polar interaction could be detected between Asn101 (ECL1) and the backbone NH group of

Tyr184 (ECL2). ECL1 of the A_{2A} adenosine receptor is characterized by the presence of an unique β-strand at the interaction interface with ECL2: this secondary structure arrangement and the presence of a disulphide bridge linking ECL1 with ECL2 (between Cys71 and Cys159) bring to an overall stabilization of ECL1 and to an inward shift of this domain compared to other GPCR crystal structures.

Although several evidences exclude an involvement of the ECL1 portion in ligand binding, the interactions occurring between this short segment and the highly conserved cysteine bridge between TM3 and ECL2 could impact the binding site shape.[95,97,98,100,101]

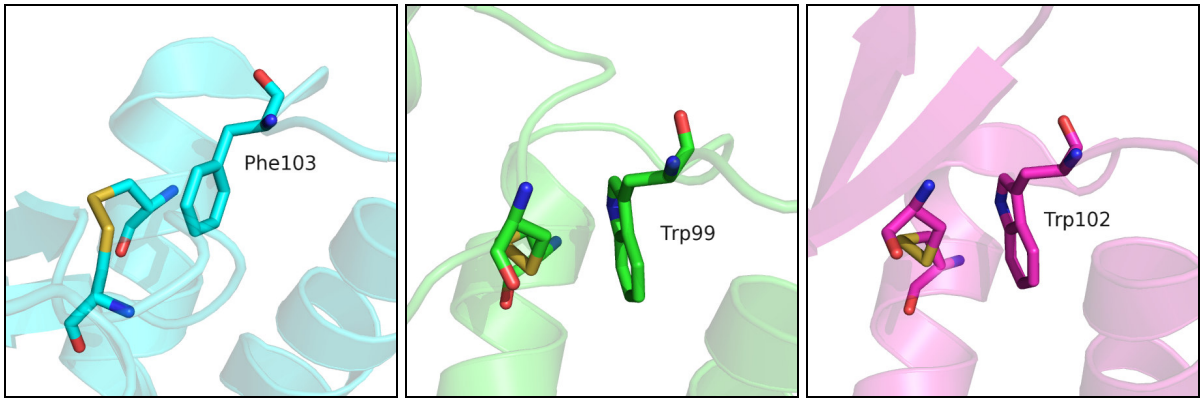

Figure 1: representation of the interaction between ECL1 and the conserved disulfide bridge connecting ECL2 to TM3. Phe or Trp residues belonging to the W(F)XFG domain are represented in sticks as well as the cysteines forming the disulphide bond. Rhodopsin (PDB: 1GZM), β_2 adrenergic receptor (PDB: 2RH1) and CXCR4 chemokine receptor (PDB: 3ODU) are depicted with cyan, green and magenta cartoons, respectively.

ECL2 is the extracellular domain with the highest heterogeneity in terms of structural arrangement and primary sequence among different GPCRs (Figure 2). Due to its peculiar position at the top of the helix bundle and, consequently, at the entrance of the binding pocket, this loop has been extensively studied as a key structural feature of GPCRs, that could directly influence both ligand stabilization and receptor activation.

The role of ECL2 in the regulation of ligand trafficking from the extracellular milieu to the receptor binding crevice was highlighted by several experimental evidences. Although the overall ECL2 structure is stabilized by a conserved disulphide bridge connecting ECL2 with the extracellular end of TM3, the flexibility of this domain has to be maintained to some extent to preserve receptor functionality.[102,103,104] Indeed, attempts to constrain ECL2 structure using additional cysteine bridges has been shown to inhibit signal transduction for some GPCRs.[102] The enhanced flexibility of this extracellular domain led to hypothesize additional mechanisms that can regulate its conformational equilibrium and, consequently, the trafficking of ligand molecules. The presence of such “molecular

triggers" at the extracellular surface of GPCRs was then confirmed by recent studies, that correlated the structural rearrangement observed at the ECL2 domain with ligand stabilization and receptor activation. [91,105,106,107]

The overall architecture of this extracellular portion greatly vary between different GPCR crystal structures. Rhodopsin represents a peculiar case, in which ECL2 forms a four-stranded β sheet in conjuction with the N-terminus: this particular arrangement of ECL2 seals the binding site crevice, avoiding solvent penetration into the ligand binding pocket. Conversely, ECL2 domains of aminergic GPCRs as well as those of CXCR4 and A_{2A} receptors, assume a more open conformation, that allows the accommodation of diffusible ligands. While β_1 and β_2 receptors are characterized by a short α helix segment from the tip of TM4 to the conserved cysteine on ECL2, in H_1 and D_3 receptors ECL2 segments show an unfolded structure. CXCR4 and A_{2A} receptors are characterized by a more complex architecture of ECL2 domains.

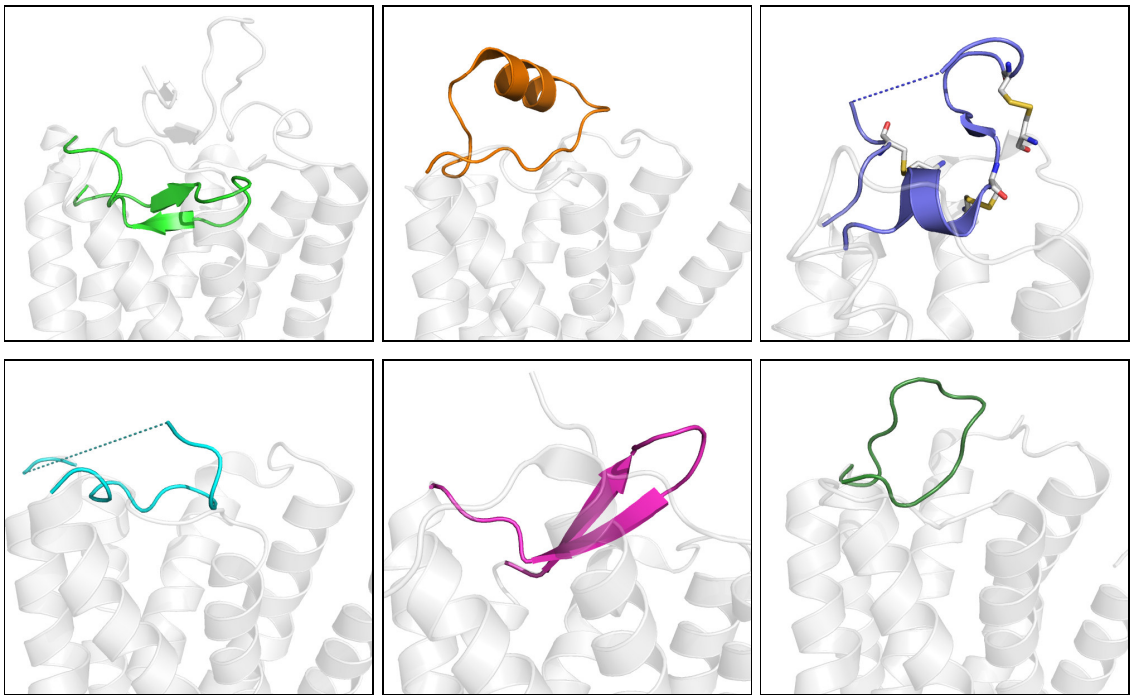

Figure 2: cartoon representations of the ECL portions for available GPCRs: rhodopsin (PDB: 1GZM, green), β_2 adrenergic receptor (PDB: 2RH1, orange), A_{2A} adenosine receptor (PDB: 3EML, blue), H_1 histamine receptor (PDB: 3RZE, cyan), CXCR4 chemokine receptor (PDB: 3ODU, magenta) and D_3 dopamine receptor (PDB: 3PBL, dark green). The three disulphide bridges present in the ECL2 segment of the A_{2A} receptor are depicted in sticks.

In the A_{2A} adenosine receptor, ECL2 tertiary structure is highly constrained by 3 disulphide bonds (Figure 2): these covalent interactions are aimed to fix the position of ECL2 with respect to ECL1 and TM3 and to stabilize a short α helix segment shown to be crucial for

ligand binding, located between the conserved cysteine and the tip of TM5. The CXCR4 receptor has another, different, arrangement of the extracellular domains, where ECL2 leans on ECL1, leaving the ligand binding pocket completely exposed to the solvent.
These different conformations seen for ECL2 mirror the differences of GPCRs endogenous ligands. Indeed, while ECL2 of rhodopsin tends to enclose the hydrophobic molecule of retinal in a solvent-inaccesible pocket, aminergic GPCRs bind to diffusible ligands, withdrawn from the extracellular milieu: in this case a more open conformation of the ECL2 domain is required to facilitate ligand penetration.
With the availability of new GPCR crystal structures, it is becoming clear that ECL2 domain is strongly involved in shaping the binding site crevice, since an extended network of interactions could be identified between ligands and the amino acids belonging to ECL2. For example, a phenylalanine residue belonging to ECL2 of the β_1 and β_2 adrenergic receptors (Phe201 and Phe193 in the β_1 and β_2 receptors, respectively) inserts deeply into the binding site crevice, forming hydrophobic interactions with the aromatic cores of both agonist and antagonist molecules. A similar interaction was seen in the A_{2A} adenosine receptor, in which two different residues located on ECL2 (Phe168 and Glu169) stabilize the binding of agonists and antagonists through an extended network of hydrophobic and polar interactions.

Similarly to ECL1, also ECL3 domain is characterized by a small number of amino acids, from 6 to 8.[94,108] A possible role of this extracellular domain in signal transduction and G protein activation has been recently proposed.[95,109] A variety of contacts have been observed either between ECL3 and other extracellular domains or within the amino acids included in the ECL3 segment (Figure 3). In CXCR4 receptor Cys274, located on ECL3, forms a disulphide bridge with Cys28 belonging to the N-terminus: this interaction further stabilizes the open conformation of the CXCR4 extracellular domain, allowing the accommodation of bulky ligands into the binding site crevice. The presence of additional disulfide bridges within ECL3 has been identified in H_1 histamine receptor, as well as in A_{2A} adenosine receptor. It could be hypothesized that these additional restraints help ECL3 to make favorable contacts with other receptor counterparts. For example, in the A_{2A} adenosine receptor, hydrogen bond interactions were identified between a histidine residue on ECL3 (His264) and Glu169 on ECL2: since the latter was found to form crucial interactions for ligand stabilization, it could be hypothesized that His264 acts like an anchor, that forces Glu169 to assume a conformation favorable for ligand binding.

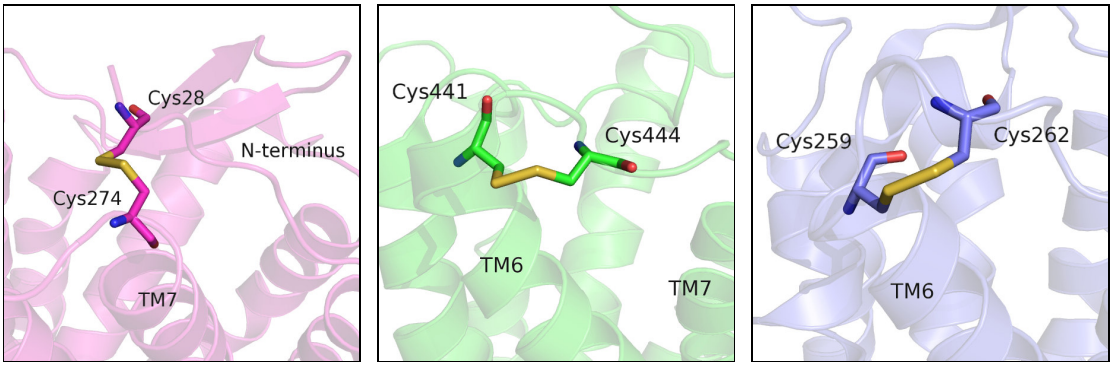

Figure 3: disulphide bridges located on the ECL3 for CXCR4 chemokine receptor (PDB: 3ODU, magenta), H_1 histamine receptor (PDB: 3RZE, green) and A_{2A} adenosine receptor (PDB: 3EML, blue).

Transmembrane portions and ligand binding sites

Available X-ray crystal structures of GPCRs share a common tertiary structure, formed by 7 TM helices that span through the lipid bilayer. The overall organization of these domains is conserved among different GPCRs and only small deviations have been observed. To highlight the structural similarity shared by these structures it could be noted that, taking into account only GPCRs crystallized in an inactive state, the root mean square deviation (RMSD) calculated on the Cα carbons of TM segments do not exceed 3 Å between any pair of structures.[108] Thus, besides some minor differences, like deviations from the ideal α helix conformation and shifts occurring at the tips of TM domains, the overall architecture of the transmembrane portion seems to be conserved among different members of class A GPCRs.

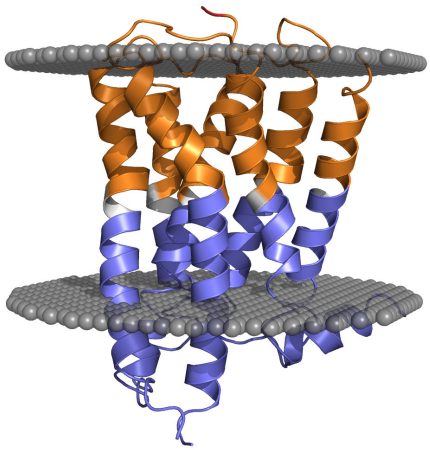

Figure 4: schematic representation of a GPCR embedded in a lipid bilayer. The hypothetic location of phospholipids polar heads are represented with gray spheres. Extracellular and intracellular portions of the TM bundle are depicted with orange and blue cartoon, respectively.

Ideally, the transmembrane domains of a prototypic GPCR could be divided into two different portions: an extracellular part, mainly involved in ligand binding and an

intracellular part, whose primary function is to couple with G protein. Not surprisingly, these two portions of the transmembrane domain are characterized by a different degree of sequence similarity that mirrors their functional role. For example, the higher diversity in terms of amino acid composition of the extracellular portions of the TM domains is explicable by the wide range of ligands and endogenous molecules acting on GPCRs: the sequence heterogeneity of the extracellular domains allows the recognition and the accommodation of a variety of chemically diverse compounds. On the contrary, the intracellular portion of the TM bundle interacts and binds to a finite number of G proteins: thus, a common recognition pattern of amino acids is required for an optimal protein-protein interaction and, therefore, the sequence conservation is more pronounced. To stress the differences in sequence similarity between these two portions of the transmembrane domain, it was calculated that, among available GPCR crystal structures, only 6% of residues are highly conserved in the extracellular part, compared to 26% of residues in the intracellular branch.[108]

All available GPCR crystal structures show a common location of the ligand binding site, placed towards the extracellular side of the receptor. Although all the ligands tend to occupy this shared crevice, the nature and the location of the ligand binding pockets strongly differ between different GPCR structures.

As described previously, rhodopsin is characterized by a deeply buried binding pocket, sealed by a complex tertiary structure formed by the N-terminus along with ECL2: this complex extracellular architecture allows retinal to be deeply inserted into the binding site, reaching almost the middle of the TM domain (Figure 5, left).[101] The retinal binding site is mostly constituted by hydrophobic amino acids and the overall structure of ECL2 is aimed at preventing solvent penetration: the retinal-bound conformation is therefore stabilized by an extended network of hydrophobic interactions, occurring with residues located on TM3, TM5 and TM6. Interestingly, no residues belonging to ECL2 directly interact with retinal. The binding site of aminergic GPCRs has a completely different organization compared to rhodopsin.

As described before, ECL2 structure of β_1, β_2, H_1 and D_3 receptors tends to be more open compared to rhodopsin: thus, ligands do not penetrate deeply into the helix bundle and occupy a pocket in the proximity of ECL2. A structural comparison showed that the main core of β_1 and β_2 antagonists is shifted almost 5 Å towards the extracellular side compared to the β–ionone ring of retinal (Figure 5, center).[101] Moreover, the binding site of aminergic GPCRs is shifted toward the extracellular portion of the receptor to allow the interaction of

the ligand protonated nitrogen with an aspartic residue located on TM3 (Asp3.32): this residue is highly conserved among aminergic GPRCs and several studies already identified this amino acid as crucial for the binding of endogenous amines.[110,111,112,113]

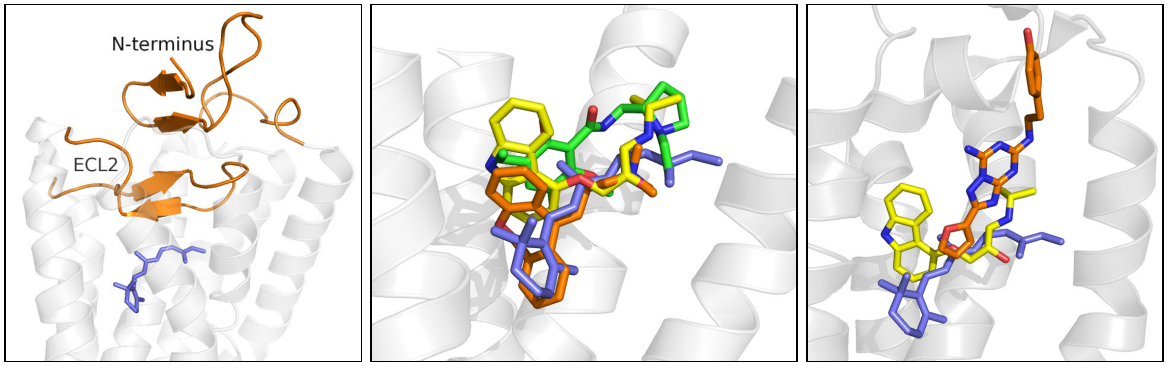

Figure 5: Left: accommodation of retinal (blue sticks) into the rhodopsin binding site (PDB: 1GZM). N-terminus and ECL2 portions are depicted in orange. Center: superposition of retinal (blue), carazolol (yellow), doxepin (orange) and eticlopride (green) within the binding site of rhodopsin (PDB: 1GZM), β_2 adrenergic receptor (PDB: 2RH1), H_1 histamine receptor (PDB: 3RZE) and D_3 dopamine receptor (PDB: 3PBL), respectively. Right: comparison between binding modes of retinal (blue), carazolol (yellow) and ZM241385 (orange) into the binding site region of rhodopsin (PDB: 1GZM), β_2 adrenergic receptor (PDB: 2RH1) and A_{2A} adenosine receptor (PDB: 3EML), respectively.

Besides the interaction with $Asp^{3.32}$, all co-crystallized ligands of β_1, β_2, H_1 and D_3 receptors form an extended network of both hydrophobic and polar interaction with the residues delimiting the binding site region. In particular, a broad spectrum of contacts could be identified with residues located on TM3, TM5, TM6 and TM7, including positions 3.34, 3.37, 5.42, 5.43, 6.48, 6.51, 6.52, 6.55 and 7.39. Interestingly, doxepin, the co-crystallized ligand of the H_1 histamine receptor, adopts a slightly different binding mode compared to that observed for β_1, β_2 and D_3 ligands. Indeed, the bulky tricyclic structure of doxepin is deeply inserted into the binding site region to preserve the key interaction with Asp3.32; thus, in the co-crystallized conformation, the aromatic moiety of doxepin lays in the proximity of $Trp^{6.48}$, similarly to what observed for the β-ionone ring of retinal (Figure 5, center).

The A_{2A} receptor shows a different architecture of the ligand binding site. The A_{2A} binding pocket extends vertically into the helix bundle and protrudes out of the receptor extracellular surface (Figure 5, right). The co-crystallized ligands are stabilized into the binding site by several hydrophobic and polar interactions with residues located on TM5, TM6 and TM7. However, due to the peculiar ligand conformation that spans vertically towards the extracellular domain, a number of different residues located on both ECL2 and ECL3 are involved in ligand stabilization (e.g., Phe168 and Glu169 on ECL2 and His264 on ECL3). It was shown that A_{2A} binding pocket is shifted outward of about 5-6 Å

compared to the β_1 and β_2 binding sites and of about 10-11 Å compared to that of rhodopsin.[101]

The location of the binding site in the CXCR4 receptor is more challenging, due to the different nature of its endogenous ligands. As described previously, the extracellular portion is shifted outward from the center of the helix bundle, favoring the accommodation of bulky peptides. However, the CXCR4 structure co-crystallized with a small antagonist molecule gave more precise clues to the location of the ligand binding site. The small antagonist occupies a cavity different from that observed in rhodopsin and in the aminergic GPCRs: this cleft is delimited by TM2, TM3, ECL2 and the N-terminus and is located at the extracellular surface of the receptor (Figure 6). Once again, the location of this unusual binding cavity is explicable by the nature of the endogenous ligands acting on the CXCR4 receptor. The binding process of peptide molecules (the typical CXCR4 ligands) requires the presence of an extended recognition interface, that usually comprises specific extracellular domains: therefore, it is likely that small molecules could be easily accommodated in this wide binding cleft, located towards the extracellular side of the receptor.

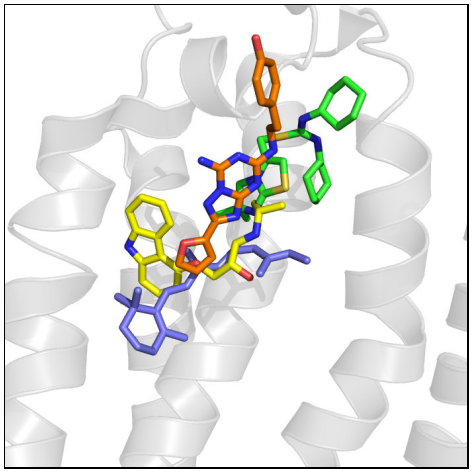

Figure 6: comparison between binding modes of retinal (blue), carazolol (yellow), ZM241385 (orange) and IT1t (green) into the binding site region of rhodopsin (PDB: 1GZM), β_2 adrenergic receptor (PDB: 2RH1), A_{2A} adenosine receptor (PDB: 3EML) and CXCR4 chemokine receptor (PDB: 3ODU), respectively.

Intracellular domain

The main role of the intracellular domains of GPCRs is to interact with the cognate G protein, as well as with a number of different downstream effectors to activate the signal transduction cascade. The newly released GPCR crystal structures revealed a certain degree of similarity between different intracellular structural elements, letting to

hypothesize a common coupling mechanism with effector targets among GPCRs of class A.

Similarly to what observed for ECL1 and ECL2 portions, also ICL1 segment is formed by a small number of residues. Although available GPCR structures reveal that this segment preferably assume an unfolded secondary arrangement, a highly conserved architecture of ICL1 backbone was observed among different crystal structures. Interestingly, a highly conserved isoleucine residue, located on ICL1, inserts into the TM bundle, forming a network of hydrophobic interactions with residues located at the extracellular ends of TM1 and TM2, as well as with residues belonging to helix 8.[108,114] Interestingly, this specific interaction was not observed in the CXCR4 receptor: this could be due to the presence of a disordered helix 8, that prevents the contacts with the isoleucine of ICL1. The A_{2A} adenosine receptor differs from all the other structures solved so far since an α helix turn could be observed in the ICL1 segment: however, despite the presence of such a structurally diverse motif, the helix turn seems to preserve the isoleucine-mediated contacts with helix 8. Recent experimental evidences highlighted the fundamental role played by ICL1 in the signal transduction mechanism,[115] as well as in the regulation of receptor translocation from the endoplasmatic reticulum.[114] Moreover, increasing experimental data support the role of ICL1 residues in the stabilization of the cognate G protein.[116,117]

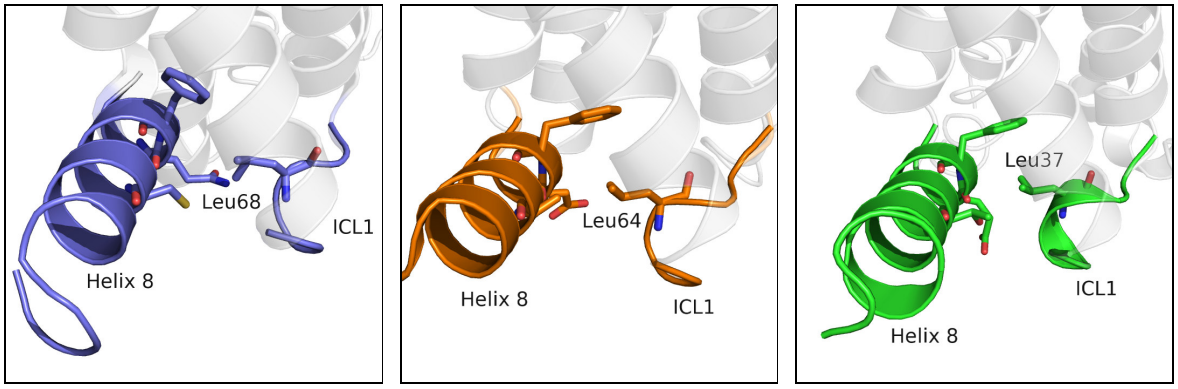

Figure 7: representation of the interaction occurring between the conserved Leu residue on ICL1 and the amino acids located on helix 8 for rhodopsin (PDB: 1GZM, blue), β_2 adrenergic receptor (PDB: 2RH1, orange) and A_{2A} adenosine receptor (PDB: 3EML, green).

Compared to ICL1, ICL2 domain is few amino acids longer and is characterized by an enhanced flexibility: indeed, a conserved architecture of this domain among available GPCRs is not observed (Figure 8). A broad spectrum of spatial arrangements has been observed among ICL2 domains of available GPCR structures, even within a single crystal

form. While in rhodopsin and in the H_1 histamine receptor ICL2 assumes an unfolded structure, in the A_{2A} adenosine receptor a two-turn α helix segment is observed. Also the CXCR4 receptor is characterized by a lack of secondary structural elements in the ICL2 portion: it is interesting to note that, in this case, the extracellular end of TM5 is two-turns longer compared to other TM5 domains of other GPCR structures and it is tilted towards TM3, shortening ICL2 segment. β_1 and the β_2 adrenergic receptors show both unfolded and α-helix arrangements of ICL2 portion among different crystal structures, highlighting the great flexibility of this intracellular domain. The D_3 dopamine receptor represents a peculiar case in this scenario, since two different arrangements of its ICL2 portion could be observed in two receptor structures solved into the same asymmetric unit: while one ICL2 shows a well-resolved α-helix structure, no electron density is available for the other unfolded ICL2. These structural evidences along with additional experimental data[107] clearly indicated a complex conformational equilibrium acting at the ICL2 level, that could be involved in the selective coupling with cognate G proteins and, therefore, in the determination of the receptor functional state.[118,119]

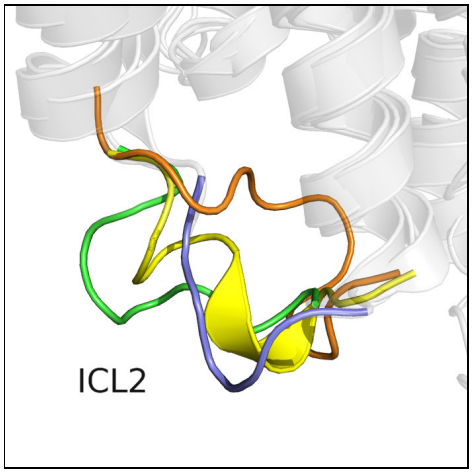

Figure 8: superposition of ICL2 segments for rhodopsin (PDB: 1GZM, blue), β_2 adrenergic receptor (PDB: 2RH1, orange), A_{2A} adenosine receptor (PDB: 3EML, yellow) and H_1 histamine receptor (PDB: 3RZE, green).

ICL3 is the most peculiar portion among the three intracellular loops. Its length strongly vary between different GPCRs, ranging from few to hundreds of amino acids. Several experimental evidences showed that ICL3 is mainly involved in G protein recognition and, consequently, in the regulation of the receptor functional state.[120,121,122,123] Due to its crucial role in the recognition of the G protein partner, ICL3 is characterized by a remarkable intrinsic flexibility, that allows to provide an optimal protein-protein recognition interface. In contrast to what has been observed in the rhodopsin structure, in which a

well-defined geometry of the ICL3 could be observed, in all the other class A GPCRs crystallized so far ICL3 domain is not present. Indeed, it seems that the plasticity of ICL3 tended to destabilize the receptor structure during the crystallization procedure:[59] therefore, a T4-lysozyme molecule has been used in a number of different GPCRs crystal structures to replace the ICL3 segment, improving the overall stabilization of the receptor. Due to this reason, all the structural information regarding ICL3 were lost during the crystallization phase. Only recently, the thermostabilized structures of the A_{2A} adenosine receptor and the β_1 adrenergic receptor were solved:[71,93] the thermostabilization obtained by site-directed mutagenesis brought to an overall stabilization of the GPCR structure and allowed to avoid the T4-lysozime insertion technique previously adopted. In these structures, ICL3 segments are well-resolved and they are characterized by an unfolded arrangement. Interestingly while in the A_{2A} crystal structures the ICL3 segments show a conserved architecture (Figure 9, left), in the structures of the β_1 adrenergic receptor ICL3 could assume two different conformations, depending on the orientation of the extracellular tip of TM6 (Figure 9, right). These recent structures highlight and confirm the high degree of flexibility exhibited by this portion, as well as its importance in shaping the intracellular domain to favor the accommodation of the G protein.

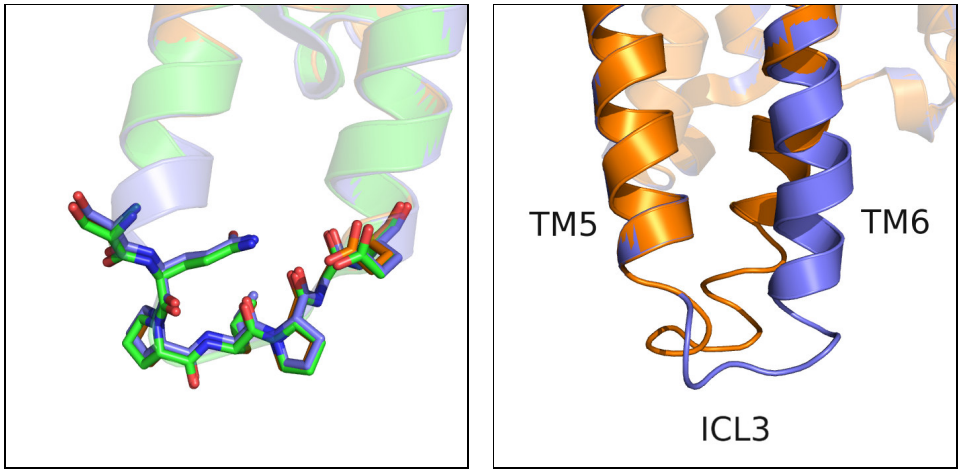

Figure 9: Left: superposition of the ICL3 segments of the thermostabilized A_{2A} receptor crystal structures: 3REY (orange), 3PWH (green) and 3RFM (blue). Right: superposition of chain A (orange) and B (blue) for the thermostabilized β_1 receptor crystal structure in complex with carazolol (PDB: 2YCW).

Similarly to what observed for the extracellular domain, the presence of “molecular locks” regulating GPCRs activation and functions has been detected at the intracellular interface. Particularly, a specific ionic interaction, called the “ionic lock”, has been identified between a highly conserved arginine at the C-terminus of TM3 (Arg3.50), a glutamic or aspartic acid at position 3.49 and a glutamic residue located at the intracellular end of TM6.[124] This

complex interaction pattern has been proposed to play a crucial role in the activation mechanism of GPCRs and several experimental evidences support the role of this motif in stabilizing the receptor inactive state. For example, a number of studies showed that the neutralization of the aspartic/glutamic acid residue at position 3.49 through site-directed mutagenesis brought to an increase in basal activity in different GPCRs:[125,126,127] this increased receptor activity confirmed that the polar interaction between the extracellular ends of TM3 and TM6 stabilize the GPCRs inactive state. Surprisingly, among available GPCR inactive conformations, only rhodopsin, the D_3 dopamine receptor and the recently released crystal structures of the thermostabilized A_{2A} and β_1 receptors show the presence of the "ionic lock" interaction (Figure 10, left and center). More interestingly, this pattern of polar interactions could be either present or not among crystal structures of the same GPCR: this is the case, for example, of the A_{2A} and the β_1 adrenergic receptors, in which the "ionic lock" could be either disrupted or formed (Figure 10, right).

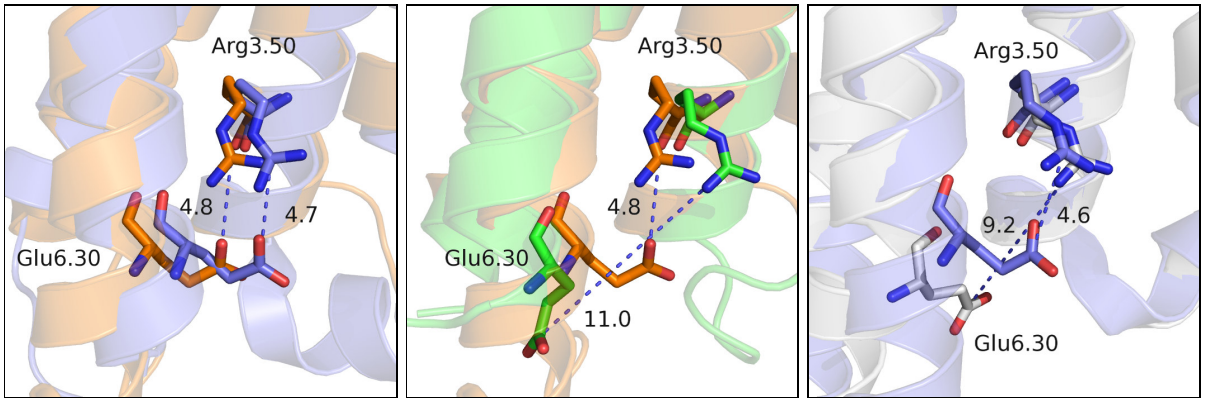

Figure 10: representation of molecular interactions occurring between the conserved $Arg^{3.50}$ and the acid residue located at the N-terminus of TM6 ($Glu^{6.30}$). Left: superposition of the crystal structures of rhodopsin (PDB: 1GZM, orange) and of the D_3 dopamine receptor (PDB: 3PBL, blue) Center: superposition of the crystal structures of rhodopsin (PDB: 1GZM, orange) and of the β_2 adrenergic receptor (PDB: 2RH1, green). Right: superposition of the ZM241385-A_{2A} (PDB: 3EML, white) and of the caffeine-A_{2A} (PDB: 3RFM) crystal complexes. The "ionic lock" distance was measured between the guanidine carbon of $Arg^{3.50}$ and the carboxyl carbon of $Glu^{6.30}$.

A possible explanation for this striking discrepancy between crystal structures and other experimental evidences relies on the different basal activities shown by these receptors. It was postulated that, while rhodopsin shows a degree of basal activity that is virtually zero, β_1 and A_{2A} receptors show a higher level of basal activity, that is reflected in an enhanced flexibility and instability of the ionic lock interaction. It must be noted that the peculiar architecture of the ICL2 of both β_1 and A_{2A} receptors helped to destabilize the ionic lock interaction. Indeed, a tyrosine residue in the ICL2 domain (Tyr112 in the A_{2A} receptor and Tyr149 in the β_1 receptor located at position 3.60) protrudes into the TM bundle and forms

a hydrogen bond interaction with the aspartic residue at position 3.49, weakening the 3.49-3.50 salt bridge (Figure 11). Consistently with the hypothesis that the strength of the ionic lock interaction mirrors the basal activity level, the β_2 adrenergic receptor architecture reveals a even more disrupted structure of polar interactions between charged residues at the end of TM3 and TM6 compared to rhodopsin, β_1 and A_{2A} receptors (Figure 11, center): this disordered structure of the intracellular domain could be due to the high basal activity showed by this GPCR. Moreover, also the unfolded structure of the ICL2 segment of the inactive β_2 crystal structure seems to reveal an improved level of basal activity.

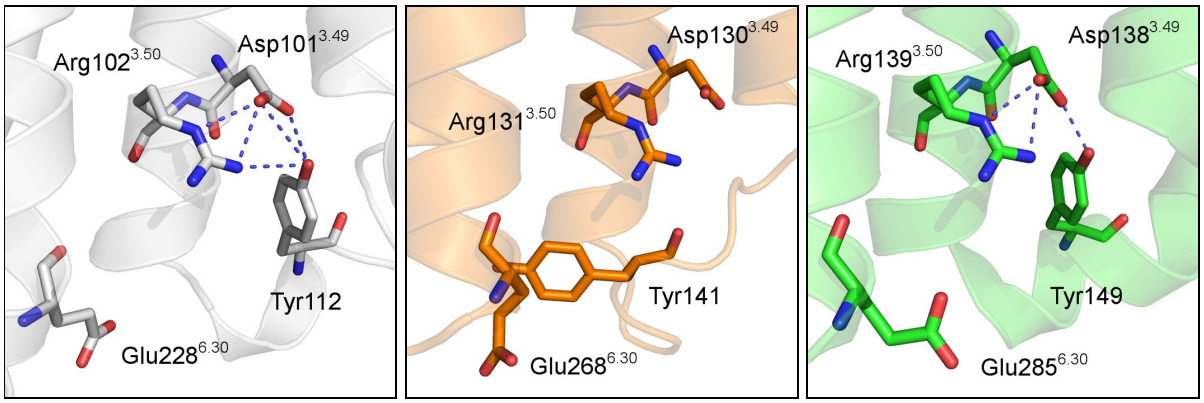

Figure 11: representation of molecular interactions occurring at the conserved Arg$^{3.50}$ for A_{2A} adenosine receptor (PDB: 3EML, white), β_2 adrenergic receptor (PDB: 2RH1, orange) and β_1 adrenergic receptor (PDB: 2VT4, green). Residues located at positions 3.49, 3.50, 3.60 (on the ECL2) and 6.30 are depicted in sticks.

In this perspective, the lack of the ionic lock interaction in some GPCR crystal structures could be seen as an effect of the high degree of flexibility shown by the GPCR intracellular domain, allowing the formation of a complex conformational equilibrium between different receptor states, characterized by a either broken or formed ionic lock. Although this explanation seems the most biologically-consistent one, it could be speculated that the crystallization procedures can strongly impact the overall architecture of the GPCR, leading to biased protein structural arrangement. The available crystal structures of the β_2 adrenergic receptor seem to discard this hypothesis, since a common disrupted geometry of the ionic lock was observed among all the structures, crystallized with different techniques and with different covalent adducts (T4-lysozyme and antibodies). Conversely, the A_{2A} adenosine receptor shows a preserved ionic lock interaction only in the thermostabilized receptor crystal structure, that does not contain the T4-lysozyme fragment. All these observations could lead to speculate on the potential structural modifications induced during the crystallization phase.

The activation mechanism

The molecular basis of GPCR activation have been extensively investigated in earlier studies. It was proposed that GPCR activation mechanism follow precise stages at different levels of the GPCR structure.

For a long time rhodopsin was used as a prototypical receptor to elucidate the activation mechanism of class A GPCRs. Site-directed mutagenesis studies were initially performed on a cluster of highly conserved residues located on TM6. Results suggested that an overall rotamer change (called rotamer "toggle switch") occurring at that level of the binding site is needed to trigger the subsequent structural rearrangements that finally lead to receptor activation.[128] In particular, several experimental evidences highlighted a remarkable conformational change of $Trp^{6.48}$ during rhodopsin activation, suggesting a key role of this residue in the overall activation mechanism.[129,130,131] These experimental evidences were confirmed by the observation, through different experimental techniques, that GPCR activation implies large movements of TM6 with respect to TM3 and the subsequent disruption of the "ionic lock" interaction.[125,124,132,133,134,135,136,137] These observations brought to an unambiguous definition of GPCR activation mechanism, that seemed to be triggered in the ligand binding site region and then to proceed downwards through TM6, causing an outward movement of its intracellular end with respect to TM3.

The first structural evidences of the receptor active state came from the rhodopsin framework. In contrast to other class A GPCRs, rhodopsin binds its endogenous ligand (retinal) through a covalent interaction: thus, it was shown that the light-induced receptor activation requires a complex rearrangement of the retinal molecule into the binding site, leading to the breaking of the covalent bond and the subsequent dissociation between the ligand (all-*trans*-retinal) and the ligand-free form of rhodopsin (opsin). This complex mechanism of activation implies the presence of different conformational states corresponding to different steps of the covalent reaction: five different stages have been detected from the inactive form to opsin, comprising photo, batho, lumi, meta I and meta II, with the meta II stage being predicted as the active form of rhodopsin. The batho and lumi crystal structures containing the all-*trans*-retinal were recently released[83,84] along with a meta I and an unprotonated intermediate.[78,138] Although all these structures bind the agonist form of retinal (namely, the all-*trans*-retinal), the outward tilt previously predicted for the TM6 N-terminus was not observed,[132,137] indicating that these structures retain an inactive conformation. The first crystal structures of opsin were finally released in 2008,[66,67]

giving the first clues for the structural rearrangement occurring upon receptor activation (Figure 12).

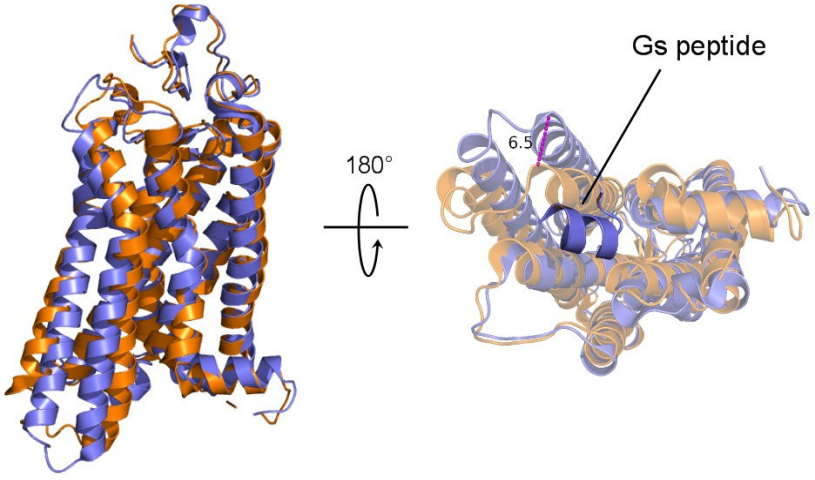

Figure 12: superposition between rhodopsin (PDB: 1GZM, orange) and opsine (PDB: 3DQB, blue) crystal structures.

These structures showed the predicted outward movement of the intracellular end of TM6 and the subsequent breaking of the "ionic lock" interaction between TM6 and TM3, harmonizing for the first time experimental data and structural observations. Moreover, one of these opsin structure was solved with a short peptide molecule belonging to the C-terminal domain of G protein, known to bind preferentially the active state of GPCRs: this element not only confirmed the active nature of the opsin structure but threw light, for the first time, on the pattern of interaction governing GPCR-G protein recognition mechanism (Figure 12).

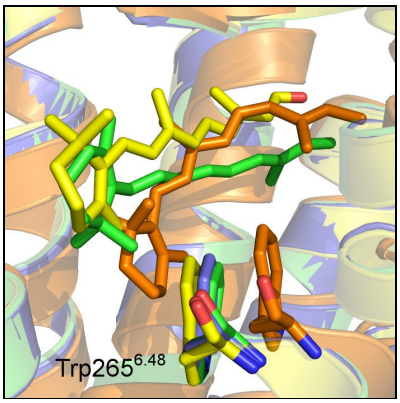

Figure 13: superposition of rhodopsin (PDB: 1GZM, orange), opsine (PDB: 3DQB, blue), metarhodopsin II (PDB: 3PQR, green) and constitutively active rhodopsin (PDB: 2X72, yellow) crystal structures. The conserved tryptophan residue located on the CWXP domain (Trp265$^{6.48}$) is represented in sticks.

The recent development of newer crystallization techniques brought to the release of the first crystal structure of the meta II state[86] as well as of a constitutively active form of rhodopsin.[85] These new X-ray crystal structures contain the all-*trans*-retinal inside the binding site, providing new evidences for the structural rearrangements occurring at the ligand binding site upon the conversion of retinal from its antagonist (*cis*) to agonist (*all*-trans) forms.

Interestingly, the rotamer change of $Trp^{6.48}$ shown to be associated with receptor activation was observed neither in opsin nor in the meta II state (Figure 13). Several justifications were proposed to explain this striking discrepancy between experimental and structural data, and it is likely that the predicted conformational change occurring at the $Trp^{6.48}$ side chain is a temporary event rather than a stable rearrangement: thus, it is probable that such a fast conformational transition may not be captured by the crystallization process.

Year 2011 saw the dawn of a new era for GPCRs structural biology, with the release of the crystal structures of the agonist-bound forms of the A_{2A} adenosine receptor as well as the β_1 and β_1 adrenergic receptors. These structures represented a real breakthrough in the field of GPCRs structural biology, since they clarified for the first time the molecular basis of agonist recognition occurring at “druggable” GPCRs. Intriguingly, some unexpected behaviors were observed among crystal structures of different receptors.

None of the agonist-bound forms of the β_1 adrenergic receptor and the A_{2A} adenosine receptor showed the outward movement of TM6 observed in both opsin and meta II state, indicating that these structures represent an initial state of receptor activation in which the agonist molecule did not trigger yet the TM6 rearrangement. A comparison between these structures and the opsin-Gs peptide complex revealed that the slight movement of TM6 observed in both the agonist-bound structures of A_{2A} and β_1 receptors is not sufficient to accommodate the G protein partner at the intracellular side. Although initially it was hypothesized that the lack of TM6 movement was related to the presence of the T4-lysozyme molecule that could impede a correct TM6 relocation, the newest crystal structures of the A_{2A} adenosine receptor were obtained through thermostabilization, without the T4-lysozyme adduct. Thus, it is likely that the absence of the predicted shift of TM6 is related not to the crystallization procedure but to the lack of a G protein counterpart that could stabilize the outward movement of the TM6 end.

Although these crystallographic structures did not provide additional information on the involvement of intracellular domains in receptor activation, they gave important hints on the ligand binding site modifications occurring upon agonist binding. Indeed, in both β_1 and

A_{2A} receptors, an inward shift of the extracellular end of TM5 was observed, contracting the binding site region and favoring the formation of an extended network of ligand-receptor interactions. For example, in the β_1-isoprenaline complex, a contraction of the ligand binding pocket of about 1 Å was observed, bringing known key residues of TM5 (namely Ser211$^{5.42}$ and Ser215$^{5.46}$) to interact with the agonist molecule.[71] Also in the A_{2A}-NECA complex, a bulge on TM5 was detected. This inward movement of the helix and the resulting insertion of Cys185$^{5.46}$ and Val186$^{5.47}$ into the binding site crevice cause a conformational rearrangement of His250$^{6.52}$, that shifts about 2 Å towards the TM bundle and forms a hydrogen bond interaction with NECA. Similarly to what observed for β_1 and A_{2A} receptors, also the β_2 crystal structure covalently bound to an agonist molecule[69] does not show the predicted outward tilt of TM6 helix but it displays an inward movement of the extracellular side of TM5.

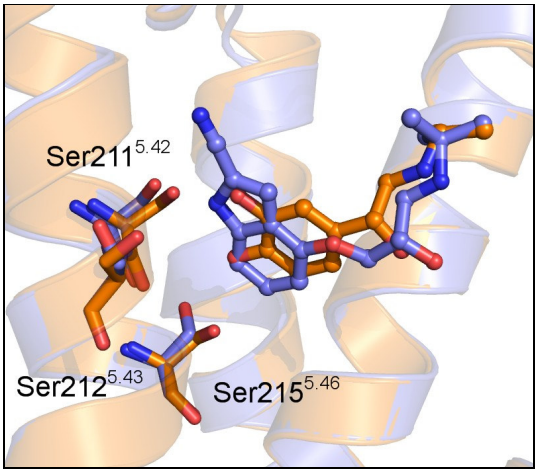

Figure 14: Left: superposition of the antagonist- (PDB: 3EML, white) and agonist-bound forms (PDB: 2YDV, blue) of the A_{2A} adenosine receptor. NECA is depicted with yellow carbons. Right: superposition of the cyanopindolol-β_1 (PDB: 2VT4, blue) and isoprenaline-β_1 (PDB: 2Y03, orange) crystal complexes. Cyanopindolol and isoprenaline are represented with ball and sticks.

The first β_2 receptor-agonist complexes that showed the predicted TM6 displacement were recently released.[68,70] In these structures the outward movement of TM6 was allowed by the presence of either a camelid antibody or a G protein at the cytoplasmic surface, that are known to stabilize the receptor active state. Taken together, these observation suggest that agonist binding is required to trigger the activation signal but is not sufficient to produce the conformational rearrangements needed to efficiently couple with the cognate G protein.

Very interestingly, also in the agonist-bound crystal structures of “druggable” GPCRs the rotamer “toggle switch” was not observed: once again, the lack of conformational changes

occurring at the $Trp^{6.48}$ could be explained by the transient nature of the switching event, that could not be captured during the crystallization process. Another possible explanation is the complete lack of such a "toggle switch" in the β_2 adrenergic receptor: indeed, mutagenesis studies performed on other class A GPCRs showed that the mutation $Trp^{6.48}$Ala did not abolish receptor activation,[139] highlighting that $Trp^{6.48}$-mediated activation could be shared only among a specific subset of GPCRs.

Although $Trp^{6.48}$ conformation does not change remarkably in available agonist-bound structures of GPCRs, different rigid shifts of TM6 could be observed among different crystal structures. Indeed, while in A_{2A} and β_2 receptors $Trp^{6.48}$ shifts leftward towards TM5 of about 1 Å (measured on Cα) upon agonist binding (Figure 15, left), in the structures of opsin, metha II state and of the constitutively active rhodopsin, the $Trp^{6.48}$ is shifted of about 2 Å away from TM7 compared to rhodopsin and moves in a cleft previously occupied by the β-ionone ring of retinal (Figure 15, right).

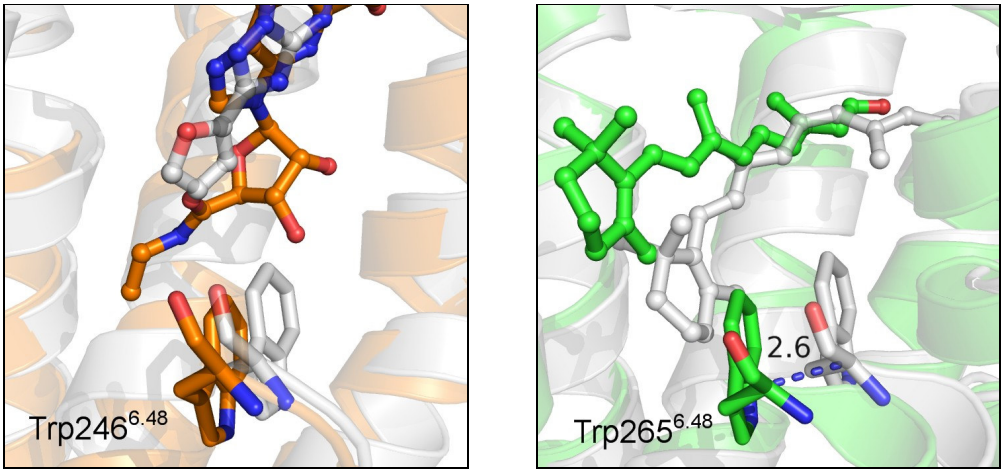

Figure 15: Left: superposition of the antagonist- (PDB: 3EML, white) and agonist-bound (PDB: 3QAK, orange) crystal structures of the A_{2A} adenosine receptor. Right: superposition of rhodopsin (PDB: 1GZM, white) and the constitutively active form of rhodopsin (PDB: 2X72, green).

Several rearrangements around the conserved $Trp^{6.48}$ have been observed in the available GPCR active conformations. The crystal structures of opsin, meta II state and of the β_2 receptor in complex with either the camelid nanobody or G protein show a particular structural rearrangement one turn below the conserved tryptophan residue ($Trp^{6.48}$). A highly conserved phenylalanine located at position 6.44 seems to undertake an outward rotation towards TM5, triggering the outward tilting of TM6. Simultaneously, the residue 3.40 located at the same level of $Phe^{6.44}$ (Leu125 in opsin and Ile121 in the β_2 receptor) shifts away from the highly conserved proline residue 5.50 (Figure 16). This complex rearrangement is likely to be responsible of the outward movement of the cytoplasmic end

of TM6, being Phe$^{6.44}$ the pivot point that triggers TM6 relocation. Conversely, the β_2 receptor crystal structure covalently bound to an agonist and the β_1 receptor structures in complex with both agonists and partial agonists do not show the same conformational changes at the Phe$^{6.44}$, confirming that they are representative of a receptor inactive state. More interestingly, in the agonist-bound structures of the A_{2A} adenosine receptor, the concerted translocation of residues Ile92$^{3.40}$ and Phe242$^{6.44}$ is observed, but without the expected TM6 outward movement. Thus, it could be hypothesized that the agonist-bound forms of the A_{2A} receptor represent an intermediate state of the signal transduction pathway, in which the conformational rearrangements have been already transmitted from the ligand binding site to Trp$^{6.48}$ but without affecting TM6 orientation. Once again, increasing structural evidences highlight that the agonist binding alone is needed to trigger the conformational rearrangements but is not able to stabilize the fully activated receptor state.

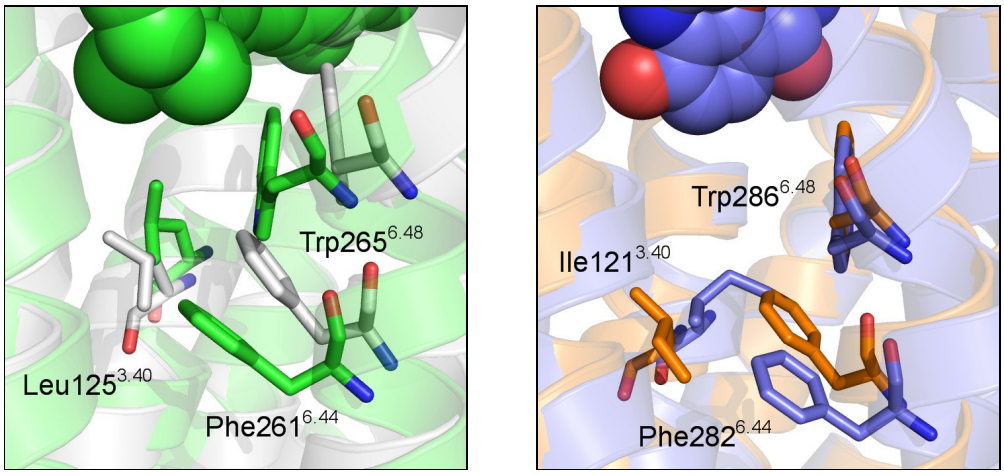

Figure 16: Left: superposition of rhodopsin (PDB: 1GZM, white) and meta II state (PDB: 3PQR, green) crystal structures. Right: superposition of the inverse agonist- (PDB: 2RH1, orange) and agonist-bound (PDB: 3P0G, blue) structures of the β_2 adrenergic receptor. The all-*trans* retinal and the β_2 agonist are represented with spheres.

Comparative modeling

Despite the great interest in the field of GPCRs, few crystal structures have been solved so far, belonging to 4 different subfamilies: rhodopsin (rhodopsin and opsin), aminergic (β_1, β_2, D_3 and H_1) peptide (CXCR4) and nucleotide-like (A_{2A}). The achievement of new GPCR crystal structures is still limited by the intrinsic instability shown by these proteins during expression and crystallization procedures, hampering the assessment of the molecular

basis of ligand recognition as well as the characterization of the receptor functions at a molecular level.

Since the optimization of expression and crystallization procedures could be achieved in years, an alternative approach to overcome the lack of GPCR crystal structures is needed. A common strategy adopted nowadays is the comparative modeling, that allows to build a molecular model of the target under study and to investigate its mechanism, functions and behavior applying a variety of *in silico* techniques.

Workflow overview

This study was focused on different GPCRs, for which structural information was either available or not: in the latter case, a comparative modeling procedure was applied to obtain a 3D model of the receptor.

The first phase of the comparative modeling procedure is the template selection. With the recent availability of new GPCR crystal structures belonging to different class A subfamilies, a finer selection of the starting structure could be made. In this scenario, the model building could follow three different approaches: i) the use of one template, ii) the use of multiple templates and iii) the so-called “fragment-based” modeling. The selection of a single template structure for homology modeling of a target receptor could be based on the similarity/identity shared among their sequences,[140] on the similarity of the regions defining their binding pockets,[141] or on the similarity occurring at some common structural motifs.[142] Although the single template methodology seems to be the most straightforward one since it usually follows the “higher homology-better template” criterion, a growing body of literature has been trying to investigate the role of the newly released GPCR crystal structures in the context of a multi-template modeling approach. Although some cases showed that the use of multiple templates could remarkably improve the enrichment during virtual screenings,[143] the application of this approach should be carefully evaluated: indeed the quality of receptor models is often not growing with the number of templates.[144] The application of a multi-template approach should be assessed also considering the quality of available templates: a recent study performed on the β_2 adrenergic receptor clearly showed that docking simulations performed on a multi-template model provided worse results compared to models built using a single template.[140] This finding was probably due to the poor sequence homology shared between templates and the target receptor: in this case, the enhanced sequence diversity could not be compensated by the inclusion of

different template structures. The principle guiding the "fragment-based" modeling approach is to use portions belonging to different templates and to reassemble them in a new receptor structure using a threading alignment. One of these methods, called I-TASSER, provided good results in the prediction of the A_{2A} adenosine receptor structure.[145]

The main pitfall of the comparative modeling procedure lays in the fact that the receptor model remarkably relies on the template structure, biasing the final secondary and tertiary structure rearrangements. An alternative approach is represented by *ab initio* techniques (like MembStruk[146,147] and Predict[148]), that generate a receptor model without relying on a template structure. Membrane helices are firstly identified and built based on the hydrophobic character of the amino acid sequence and then assembled together using either geometrical criteria (derived from diffraction data or available helix rearrangements of GPCR crystal structures) or contacts with the membrane environment. This method showed reliable results for different GPCRs, including rhodopsin,[147,148] the S25 odorant receptor,[149] the 5-HT_{2C} receptor,[150] the histamine receptors[151] , the D_2 and the neurokinin 1 receptors.[152]

The modeling of loop sequences is widely recognized as a challenging task, due to the low sequence identity and the different length between template and target receptors. The building of these receptor portions is of particular interest since available GPCR crystal structures clearly reveal a role of loop domains (especially ECL2) in ligand stabilization: thus, the correct prediction of the architecture of these segments is crucial to understand the molecular basis of ligand recognition and, consequently, to obtain reliable receptor models. So far, GPCR crystal structures showed that loop architecture was conserved between different receptor subtypes: for example, the β_1 and the β_2 adrenergic receptors share a similar arrangement of loop sequences and, more importantly, of the ECL2 segment. This means that, if the query sequence is very close to one of the crystallized structures, the 3D coordinates of the template could represent a good starting point for loop building. On the contrary, loop architecture is very receptor-specific and could strongly vary even within the same group of receptors: for example, although H_1, D_3 and β_2 receptors belong to group α of class A GPCRs, they show a completely different rearrangement of the loop portions, especially of the ECL2. As stated before, due to the fact that ECL2 has one of the longest loop sequences and is directly involved in ligand binding, many efforts have been made to model this portion along with all the other loop segments. A widely-used strategy relies on the *de novo* building of these regions, without

using any 3D coordinates taken from the template structure. So far, a huge body of literature on loop building is available but all cases showed that the prediction of loop sequences longer than 10-12 residues is still a difficult task,[153,154,155,156,157,158] especially for membrane proteins. Only recently, accurate predictions of long loop structures were made:[159,160] it is likely that, with the constant improvement of computational techniques, the prediction of loop structures will become more reliable and affordable. Some studies also suggested a different strategy: indeed, it was seen that a remarkable improvement of docking results could be simply obtained by the deletion of loop sequences, that hindered the binding site cavity impeding the correct ligand accommodation:[140,161,162] this approach is computationally cheaper compared to the de novo modeling but, at the same time, completely avoid the determination of the ligand-receptor interactions occurring at the ECL2, hampering a complete understanding of the molecular basis of ligand recognition.

Once the template is selected, the template(s) and the target sequences have to be aligned. Usually, the alignment of class A GPCR sequences relies on conserved structural motifs, identified within TM helices.[14,163,164] They comprise an asparagine on TM1 (Asn1.50), an aspartate on TM2 (Asp2.50), the DRY or ERY motif at the extracellular end of TM3, a tryptophan on TM4 (Trp4.50), a proline on TM5 (Pro5.50), the CWXP domain on TM6 and the NPXXY motif on TM7. Recently, more accurate comparisons of TM helices that include a vast number of GPCR sequences, showed the presence of additional conserved residues and motifs.[164,165] For example, besides the conserved Asn1.50, Gly, Leu and Val residues were found at positions 1.49, 1.52 and 1.53 within more than 50% class A GPCRs.[164] At the same time, six conserved aromatic/hydrophobic residues were identified at the cystoplasmic end of TM2, including Phe2.42, Leu2.46, Ala2.47, Ala2.49, Leu2.51 and Leu2.52.[164] In addition to the DRY (or ERY) motif, TM3 has other three conserved amino acids, located at positions 3.39 (Ser), 3.43 (Leu) and 3.46 (Ile). Moreover, while TM4 is characterized by the occurrence of a highly-conserved proline residue at position 5.59, TM5 shows a FXXP motif between Phe5.47 and Pro5.50. An additional conserved Phe residue at position 6.44 was also detected among more than 80% of class A GPCRs and conserved leucine, asparagine and serine residues were found at positions 7.41, 7.45 and 7.46 in more than 60% of class A GPCRs.[164] Also the short helix 8, that runs parallel to the lipid bilayer, shows some conserved positions, like a small FR domain that occurs in more than 50% of GPCRs of class A.[164]

Due to the broad occurrence of these structural motifs among class A GPCRs, the alignment should be built taking into account these conserved sequences to fix key amino acids positions within the TM domains.

The subsequent phase of the comparative modeling procedure includes the identification of the binding site region. Although usually the location of the binding site could be hypothesized on the basis of mutagenesis data, useful information could be also retrieved from available GPCR crystal structures. Indeed, although different ligand spatial orientations have been recognized among different GPCR subfamilies, a similar location of the ligand binding site could be identified. As already described, the binding pocket is located at the extracellular side of the transmembrane domains, in the proximity of ECL2. In most of the cases, the ligand binding pocket is formed by residues located on TM3, TM5, TM6 and TM7. Moreover, some interactions are found to be highly conserved within GPCR subfamilies: for example, a hydrogen bond interaction between the ligand protonated nitrogen and the aspartic residue at position 3.32 could be detected among available crystal structures of aminergic GPCRs (β_1, β_2, D_3 and H_1). Thus, although the location of the binding site could differ between GPCRs, indications from both literature and crystallized homologues could guide the identification of residues important for ligand binding.

Once the 3D coordinates of the receptor model are obtained and refined, several techniques could be applied to validate the homology model: this validation phase is a crucial point, since it influences the reliability of the receptor in the drug design process. Docking studies and MD simulations are currently two of the most widely used techniques to assess the receptor model quality.

The docking approach tries to build energetically favored conformations of the ligand into the receptor binding pocket: in brief, the algorithm tries to find the best match between detected ligand features and receptor functional groups within the binding site region. Alternative binding poses obtained by docking studies are ranked according to their ability to occupy the binding site cleft as well as to form favorable interactions with receptor functional groups. During this phase, the consistency between energetically favored ligand poses and both experimental and ligand-based information should be carefully considered. The importance of including additional information during model building and docking studies was clearly highlighted by a recent study, aimed at evaluating the state-of-art of the modeling techniques by the prediction of the A_{2A} adenosine receptor structure before its release.[145] Interestingly, the receptor models characterized by the smallest RMSD

compared to the crystal structure were those that integrated available mutagenesis and ligand-based information during model building.[166] Several examples of this knowledge-supported homology modeling procedure have been described in literature,[185,167,168,169,170,171] highlighting the importance to harmonize structural information derived from X-ray crystal structures with both ligand-based and mutagenesis data.

To reduce the computational demand and to allow the evaluation of hundreds to million compounds in an affordable time, docking studies represent a good compromise between accuracy and speed. One of the main limitations of docking studies is the lack of a flexible treatment of the protein structure: although this allows to remarkably reduce the computation time, it prevents protein structural rearrangements that occur upon ligand binding. To obtain a "flexible" description of the target structure and to carefully evaluate the receptor structural relocations, another computational technique is required. Molecular dynamics (MD) represents a widely used methodology that allows to describe the dynamic evolution of the system under investigation following the Newtonian equation of motion. This approach is useful to evaluate the stability of the ligand-receptor interactions found, for example, during docking studies and to assess the occurrence of receptor structural rearrangements that can take place after ligand binding: basing on observations provided by the MD simulations, new ligand modifications, aimed at increasing the overall binding affinity, could be suggested. With the recent advances in computer speed and performances, timescales grown exponentially, bringing to a new era of MD in which simulations of up to μs or ms became finally feasible.[172] MD simulations have been extensively applied to GPCRs, to assess the presence of different conformational states,[69,173,174,175] to investigate their interactions with the membrane components[176] or to evaluate the preferred ligand pose into the binding site.[169,177]

Nowadays, virtual screening (VS) represents one of the most powerful techniques that could be used in the validation phase of the homology modeling as well as in early stages of the drug design process. In both cases, VS is mainly employed to identify a small subset of candidates among a larger set of compounds according to both chemical-physical criteria and predicted ligand-receptor interactions. In this scenario, VS could be used either to assess the ability of a receptor model to retrieve known compounds in a larger set of decoys or to evaluate its capacity to recognize new small molecules candidates endowed with acceptable affinities. Beside the remarkable performances obtained using GPCR X-ray crystal structures,[178,179,180,181,182,183] a growing body of literature reports several examples of virtual screening campaigns applied on GPCR

homology models to identify known compounds[184,185,186,187,188,189] or new chemical entities.[167,183,190,191,192,193,194,195]

Conclusions

Since the release of the first crystal structure of a "druggable" GPCR in 2007, a growing interest has been shown for GPCRs, also confirmed by the increase of GPCR-related publications available in the literature.[196] The availability of a number of different GPCR crystal structures provides a valuable amount of structural information; on the other hand they show subtle but critical differences, that could be hardly predicted by state-of-art modeling techniques (e.g. ECL2). In addition, the analysis of the agonist-bound structures revealed that the binding sites for agonists, inverse agonists and antagonists overlap considerably and share a common arrangement of residues delimiting the binding site region: due to these subtle differences observed among different receptor functional states, it will be even more difficult to predict the efficacy of newly designed compounds targeting GPCRs. In this picture, homology-model-based drug design has to deal with i) the prediction of a reliable receptor 3D structure and ii) the identification of new chemical entities. Although a general skepticism around the application of structure-based drug design on GPCRs has recently influenced the field of medicinal chemistry,[197,198] the advances in modeling techniques as well as the availability of a huge amount of high quality information retrieved from experimental and ligand-based data definitely re-opened that issue, bringing to the dawn of a new era for the GPCR homology modeling.

CHAPTER 2

Aim of the work

This Ph.D. project was mainly focused on the building and validation of the three-dimensional structures of G protein-coupled receptors and on the assessment of their reliability and usefulness in the drug design process.

Different GPCRs have been extensively investigated, for which X-ray crystal structures were either available or not: the MT_1 and MT_2 melatonin receptors, the 5-HT_{2C} serotonin receptor, the H_3 histamine receptor, the β_2 adrenergic receptor and the A_{2A} adenosine receptor.

A number of different computational techniques were applied to build and refine the receptor 3D coordinates, to characterize the ligand recognition process at a molecular level and to evaluate the main receptor rearrangements occurring upon ligand binding. This allowed in some cases to propose a binding mode for new series of ligands and/or to suggest an explanation for the agonist or antagonist behavior of known ligands or for receptor subtype selectivity. The results provided by these *in silico* investigations were compared with available experimental data and ligand-based information, such as mutagenesis data, pharmacophore models and structure-activity relationships, to assess the consistency of 3D models with available experimental information. After this validation procedure, structural information provided by 3D models of ligand-receptor complexes were used to suggest possible ligand modulations aimed at improving binding affinity, selectivity or at attaining dual-acting activity.

This study threw light on the role of GPCR crystal structures and homology models in the current medicinal chemistry landscape, highlighting their usefulness for the characterization of the ligand recognition mechanism at a molecular level.

CHAPTER 3

MT_1 and MT_2 melatonin receptors

Therapeutic relevance

Melatonin (N-acetyl-5-methoxytryptamine) is a tryptophan-derived hormone secreted by the pineal gland with peak concentrations occurring during the night. The release and production of this hormone follow a circadian rhythm and are regulated by the suprachiasmatic nucleus, a brain area widely recognized as the main circadian clock in mammals.[199] Although the release of melatonin mainly occurs at the pineal gland, other tissues were shown to be involved in the secretion of this hormone.[200,201,202] Since its discovery, a variety of studies highlighted the involvement of melatonin in a plethora of physiological functions, such as the regulation of circadian rhythms, sleep[203] and immune system,[204] blood pressure control,[205] pain perception[206] and bone formation.[207] An antioxidant activity has also been ascribed to melatonin,[208] suggesting an additional role of this substance as a "radical scavenger". Due to its involvement in a variety of different physiological processes, melatonin has been proposed as a therapeutic agent in a number of diseases, including sleep disturbances,[209] mood disorders,[210] depression,[211] neurodegenerative syndromes,[212] cancer,[213] epilepsy[214] and stroke.[215] The last two decades showed a remarkable advancement in the design and discovery of novel MT_1 and MT_2 receptor ligands.[216,217] While a prolonged-release formulation of melatonin[218] and ramelteon[219] (a non-selective agonist) have been marketed for the treatment of insomnia, agomelatine,[220,221] an MT_1/MT_2 agonist and $5HT_{2C}$ antagonist, has been approved for the treatment of major depressive disorders. Moreover, tasimelteon[222] and PD-6795[223] are currently being evaluated in clinical trials for their sleep promoting properties and for the treatment of insomnia.

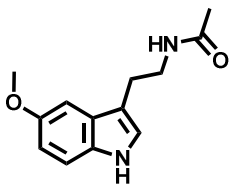

melatonin

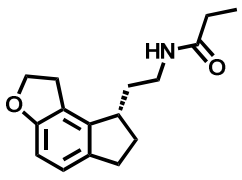

ramelteon

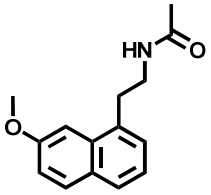

agomelatine

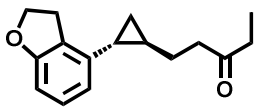

tasimelteon

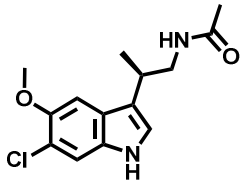

PD-6795

The availability of novel chemical entities, especially selective agents, is fundamental to investigate and clarify the physiological roles of melatonin and its receptors, as well as to identify new potential therapeutic applications.

Receptors signalling pathways

Melatonin binds to and activates two G protein-coupled receptors, named MT_1 and MT_2.[224,225] An additional melatonin binding site, named *MT_3*, has been recently reported as the hamster homologue of the human enzyme quinone reductase 2;[226,227] due to its catalytic action, this third site has been proposed to be involved in the melatonin-mediated antioxidant activity.[228,229] These binding sites show different affinities for melatonin. Indeed, while MT_1 and MT_2 receptors are characterized by high affinity towards their endogenous ligand (in the nM scale), the *MT_3* binding site shows a low affinity profile for this hormone. Both MT_1 and MT_2 receptors couple with the inhibitory G_i protein, leading to deactivation of the adenylyl cyclase and a consequent decrease of intracellular cAMP concentrations.[230] In addition to their cognate G proteins, melatonin receptor have also been shown to interact with other intracellular second messengers.[231,232] In humans, melatonin receptors are expressed in different areas of the central nervous system[233,234,235] as well as in many peripheral tissues.[236,237,238] The different roles of the two melatonin receptor subtypes have been clarified only partially. While MT_1 activation inhibits neuronal firing in the suprachiasmatic nucleus[239] and reduces hormones release,[240] the activation of MT_2 receptors promotes splenocyte proliferation, inhibition of dopamine release in the eye and vasodilatation of coronary arteries.[236,241,242] Experiments conducted on the rat caudal artery showed a vasoconstrictive effect of MT_1 receptor in contrast to a MT_2-mediated vasodilation.[243,244]

Modeling melatonin receptors: state of the art

During the last two decades, both ligand-based and structure-based approaches have been extensively applied to clarify the molecular basis of ligand recognition and to understand the main requirements for ligand potency and selectivity.

Due to the paucity of available GPCR crystal structures, all the melatonin receptor models published so far[245,246,247,248,249,250,251,252,253,254,255,256,257,258] have been built starting from the

crystal structure of bovine rhodopsin. Different binding modes have been proposed for melatonin and other ligands. This is in part a consequence of the available mutagenesis data: indeed, while site-directed mutagenesis recognized a number of residues that could potentially influence ligand binding, it was not able to unambiguously identify key residues involved in direct ligand-receptor interactions. For example, while the amide group was proposed to interact with either $Ser^{3.35}$ and $Ser^{3.39}$ or with $Tyr^{7.43}$ or with some ECL2 residues, suggested counterparts for the methoxy group were $His^{5.46}$ and $Tyr^{7.43}$. Thus, binding hypothesis retrieved from previous models reflect the uncertainty of the structural information available for melatonin receptors.

Moreover, the proposed receptor models were not able to fully explain structure-activity relationships (SARs) of melatoninergic ligands.

Given the intrinsic limits of these models, several research groups tried to investigate melatoninergic ligands applying ligand-based strategies. Several publications described the application of CoMFA analysis,[259] pharmacophore models[260,261] and scaffold hopping[262,263,264] to discover and characterize new melatoninergic compounds without the use of receptor 3D coordinates. These investigations provided an impressive amount of high-quality information about SARs, that should be harmonized with structure-based models.

Template selection

At the time of this study, only the crystal structures of rhodopsin, opsin, β_1, β_2 and A_{2A} receptors were available.

A sequence-based comparison made between MT_1 and MT_2 receptors and available GPCR crystal structures showed identity percentages lower than 30% within TM domains: considering that the accuracy of homology models of membrane proteins was predicted to strongly decrease below 30% of shared identity,[265] melatonin receptors represent a challenging task from a modeling point of view. Calculated identity percentages between both melatonin receptors and all available crystallized GPCRs are in the range of 20%-29% within TM domains.[266] Since all available template structures shared low identity percentages with target sequences, an increase in model quality was not expected using a multiple template approach. In this scenario, the template selection was made taking into account not only the sequence identity percentage but also the structural features of each template structure. Rhodopsin was rejected due to i) its poor sequence identity shared with

melatonin receptors (22% and 20% with MT_1 and MT_2 receptors, respectively) and ii) for the peculiar arrangement of ECL2 segment: as described previously, its N-terminus and ECL2 portions "seal" the retinal binding site and could impede a correct accommodation of diffusible ligands. The A_{2A} adenosine receptor shares sequence identities of 29% and 24% with MT_1 and MT_2 receptors, respectively. Although these percentages are higher than those observed for rhodopsin, the ligand binding site architecture and the ECL2 secondary structure arrangement brought to discard this template: indeed, the A_{2A} binding cleft is completely exposed to the solvent and could prevent a correct accommodation of a molecule with a strong hydrophobic character like melatonin. Moreover, the overall structure of the A_{2A} adenosine receptor is strongly optimized to accommodate bulky nucleotide-like ligands: thus, it is likely that this specific architecture could not be suitable to accommodate a less polar and bulky molecule like melatonin. β_1 and β_2 adrenergic receptors share the same location of the binding site and the same architecture of the ECL2 portion. Although the β_1 receptor shares higher sequence identities with both melatonin receptors (~28% between β_1 and both MT_1 and MT_2) compared to the β_2 (~25% between β_2 and both MT_1 and MT_2), these percentages are too low to provide an unambiguous identification of the best template: due to the fact that the crystallized β_1 receptor derives from turkey, the human β_2 receptor was chosen as the reference structure.

Sequence alignment and model building

The X-ray crystal structure of the human β_2 receptor in complex with the inverse agonist timolol (PDB ID: 3D4S)[89] was selected as the template structure. The amino acid sequences of the β_2, MT_1 and MT_2 receptors (UniProt IDs P07550, P48039 and P49286, respectively) were retrieved from the Universal Protein Resource.[267,268] Initial alignment was carried out with ClustalW,[269] using default parameters and subsequently optimized considering conserved sequence motifs among class A GPCRs (Figure 17).[14,164] Highly conserved residues within TM domains, as well as the conserved disulfide bridge connecting ECL2 and TM3 have been taken into account during alignment refinement.

```
b2      WVVGMGIVMSLIVLAIVFGNVLVITAIAKFERLQTVTNYFITSLACADLVMGLAVVPFGAAHILMK-MWTFGNFWCE
hMT1    LASALACVLIFTIVVDILGNLLVILSVYRNKKLRNAGNIFVVSLAVADLVVAIYPYPLVLMSIFNN-GWNLGYLHCQ
hMT2    VAPALSAVLIVTTAVDVVGNLLVILSVLRNRKLRNAGNLFLVSLALADLVVAFYPYPLILVAIFYD-GWALGEEHCK

b2      FWTSIDVLCVTASIWTLCVIAVDRYFAITSPFKYQSLLTKNKARVIILMVWIVSGLTSFLPIQMHWYRATHQEAINC
hMT1    VSGFLMGLSVIGSIFNITGIAINRYCYICHSLKYDKLYSSKNSLCYVLLIWLLTLAAVLPNLRAG-T-LQ-YDP-R-
hMT2    ASAFVMGLSVIGSVFNITAIAINRYCYICHSMAYHRIYRRWHTPLHICLIWLLTVVALLPNFFVG-S-LE-YDP-R-

b2      YAEETCCDFF--TNQAYAIASSIVSFYVPLVIMVFVYSRVFQEAKRQL-----------KFCLKEHKALKTLGIIMG
hMT1    -I--YSCTFAQSVSSAYTIAVVVFHFLVPMIIVIFCYLRIWILVLQVRQRVKPDRKPKLK--PQDFRNFVTMFVVFV
hMT2    -I--YSCTFIQTASTQYTAAVVVIHFLLPIAVVSFCYLRIWVLVLQARRKAKPESRLCLK--PSDLRSFLTMFVVFV

b2      TFTLCWLPFFIVNIVHVIQDN----LIRKEVYILLNWIGYVNSGFNPLIYCRSPD-FRIAFQELLCL
hMT1    LFAICWAPLNFIGLAVASDPASMVPRIPEWLFVASYYMAYFNSCLNAIIYGLLNQNFRKEYRRIIV-
hMT2    IFAICWAPLNCIGLAVAINPQEMAPQIPEGLFVTSYLLAYFNSCLNAIVYGLLNQNFRREYKRILL-
```

Figure 17: alignment of β_2, MT_1 and MT_2 sequences. Conserved residues within TM domains (X.50 positions) are in bold while TM domains of β_2 receptor crystal structure are underlined in grey.

As previously described, in the β_2 crystal structure the ICL3 portion was substituted with the T4-lysozyme to enhance receptor stabilization during the crystallization process: for this reason, residues 223 to 263 belonging to the β_2 adrenergic receptor are missing in the crystal structure and therefore were not considered during alignment building. The N- and C- termini of the β_2 adrenergic receptor were not solved due to their low resolution: these portions were not modeled and they were excluded from the alignment.

The MT_1 receptor was modeled in an advanced stage of the workflow, starting from the optimized structure of the MT_2 receptor: thus, in the initial phase of the comparative modeling, only the MT_2 receptor model was taken into account. The MT_2 homology model was built using Modeller software[270,271] applying standard parameters. 5 receptor models were initially built and the model characterized by the best value of the objective function implemented in the Modeller package was chosen. Hydrogens were added to the model structure and the protonation state of polar residues was calculated at a neutral pH; the hydrogen bond network was optimized by modifying polar hydrogens orientation. An initial minimization was applied to relax the major steric clashes, using a RMSD of 0.3 Å as convergence criterion.

The Ramachandran plot of the final MT_2 melatonin receptor is shown in Figure 18.

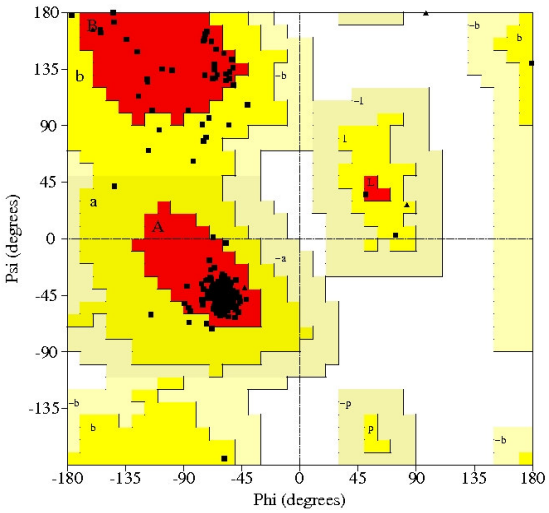

Figure 18: Ramachandran plot of the MT$_2$ melatonin receptor model.

Identification of binding sites

Mutagenesis studies were used to identify the binding site location. For MT$_1$ and MT$_2$ receptors, residues located on TM3, TM4, TM5, TM6 and TM7 were found to be involved in ligand stabilization, including positions 3.32, 4.60, 5.42, 5.46, 6.52 and 7.43 (Figure 19, left).[250,252,258,272]

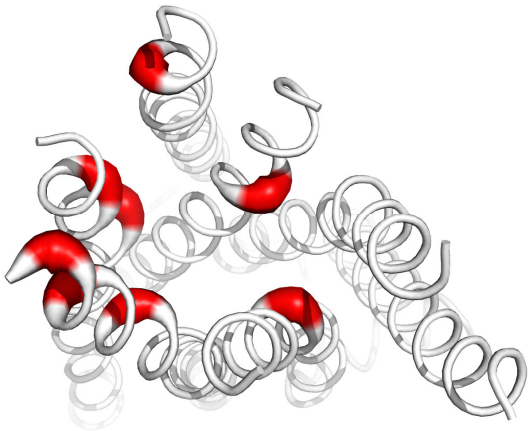

Figure 19: location of key residues (thick red cartoons) within the MT$_2$ receptor.

Mutagenesis studies on MT$_1$ and MT$_2$ receptors outlined a peculiar binding site location, that seems to be shifted towards TM4 and TM5 compared to aminergic GPCRs. One clue that could confirm this hypothesis is the involvement of position 4.60 in ligand binding. This position is occupied by an asparagine residue in less than 5% of class A GPCRs;[164] about 30% of GPCRs belonging to class A has proline or valine residues at position 4.60.[164] Thus the presence of an asparagine residue, able to form extensive H-bond interactions

compared to non-polar proline or valine residues, could indicate a direct interaction of the melatonin molecule with this specific position of TM4. Another hint suggesting a binding site shift towards TM4/5 is the peculiar amino acid composition of TM3 and TM5. For example, position 3.33 in melatonin receptors is occupied by a glycine: this residue occurs only in about 5% of class A GPCRs, whereas bulkier residues such as tyrosine, phenylalanine or valine are located at the same position in more than 40% of receptors.[164] The presence of such a small residue at position 3.33 could lead to a simultaneous rotation and shift of the ligand core towards TM4, being TM3 the pivot point for ligand relocation. Interestingly, two tyrosine residues occupy positions 7.40 and 7.39 in both melatonin receptors. While position 7.40 is occupied by an even bulkier tryptophan residue in more than 20% of class A GPCRs,[164] position 7.39 is commonly characterized by smaller amino acids, such as valine, threonine and leucine.[164] All these observations outline a peculiar binding site architecture for melatonin receptors, comprising: i) a hindered room at the interface between TM3 and TM7, delimited by three tyrosines at positions 7.39, 7.40 and 7.43; ii) a more open cavity delimited by TM3, TM4 and TM5, characterized by a pattern of smaller amino acids compared to other class A GPCRs.

Binding mode hypothesis

Position 5.46 of β_2 and β_1 adrenergic receptors is known to be crucial for ligand binding: indeed, mutagenesis studies performed on the β_2 receptor revealed a key role of $Ser207^{5.46}$ in the binding of catecholamines.[273] The importance of this residue is also confirmed by available β_2 and β_1 receptor crystal structures in which serine residues at position 5.46 form favorable interactions with co-crystallized ligands. Position 5.46 in melatonin receptors is occupied by a histidine residue (His195 and His208 in MT_1 and MT_2 receptors, respectively). Mutagenesis studies showed a role of this amino acid in ligand binding, since the point mutation $His208^{5.46}Ala$ brings to a 4-fold decrease in melatonin binding at the MT_2 melatonin receptor.[272] Although mutagenesis studies evidenced the importance of this residue for ligand stabilization, its interaction with melatoninergic compounds is still unclear at an atomistic level. $His^{5.46}$ is unlikely to bind the methoxy oxygen of melatonin since the mutation $His208^{5.46}Ala$ brings to a 4-fold decrease in binding affinity also for N-acetyltryptamine, that lacks the methoxy group on position 5 of the indole ring.[272] On the other hand, it is unlikely to be a counterpart for the indole NH group, since

agomelatine (a naphthalene derivative of melatonin lacking the indole NH functionality) shows Ki values in the nanomolar range for both melatonin receptors.[274] Thus, it could be speculated that His$^{5.46}$ may form a π-π or even a NH-aromatic interaction with the indole ring of melatonin.

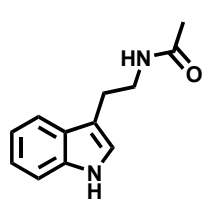

N-acetyltryptamine

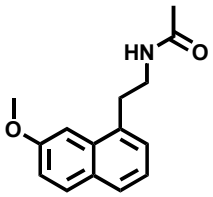

agomelatine

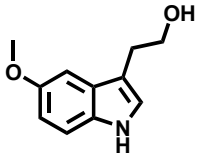

5-methoxytryptophol

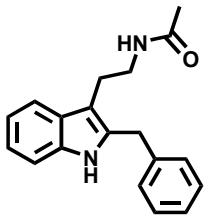

luzindole

Val$^{5.42}$ is located one turn above His$^{5.46}$. This amino acid plays a crucial role in ligand recognition, since the point mutation Val204$^{5.42}$Ala nullifies melatonin binding at the MT$_2$ melatonin receptor. In addition, while mutagenesis studies have been also performed on other GPCRs to clarify the key role of this amino acid in ligand stabilization and receptor activation,[275] the newly released crystal structures of aminergic GPCRs helped to elucidate the involvement of this residue in ligand recognition at a molecular level. In β_1 and β_2 receptors, position 5.42 is occupied by a serine, that was thought to bind the *meta*-hydroxyl group of catecholamines.[275] In contrast to endogenous amines, melatonin is a highly hydrophobic molecule, in which the *meta*-hydroxyl group of catecholamines is methylated to form a methoxy group. In this scenario, one could speculate that the Ser$^{5.42}$ → Val$^{5.42}$ substitution observed among β adrenergic and melatonin receptor sequences could be seen as a consequence of the different chemical structures of their endogenous ligands. Indeed, while the hydroxyl group of catecholamines tends to form favorable interactions with a polar residue (e.g. serine or threonine) at position 5.42,[275] the methoxy group of melatonin is likely to be stabilized by a more hydrophobic residue: in this perspective, it could be hypothesized that the valine residue at position 5.42 of melatonin receptors might be the counterpart for the methoxy group of melatonin.

Another residue shown to be crucial for melatonin binding is Asn$^{6.52}$. Interestingly, this residue is a phenylalanine in β_1, β_2, D_3 and H_1 receptors and it forms edge-to-face interactions with the aromatic core of co-crystallized ligands. While point mutations Asn268$^{6.52}$Ala, Asn268$^{6.52}$Asp and Asn268$^{6.52}$Leu completely abolish melatonin binding at the MT$_2$ melatonin receptor, the mutation Asn268$^{6.52}$Gln does not affect melatonin affinity.[258] Thus, it can be hypothesized that the required H-bond donor (glutamine or

asparagine) at position 6.52 may interact with the neighboring $His^{5.46}$ through a H-bond interaction. In this scenario, $Asn^{6.52}$ may re-orient the imidazole ring of $His^{5.46}$ in a conformation capable of favorable interactions with the ligand indole ring.

$Asn^{4.60}$ was proven to be involved in melatonin binding or stabilization. The point mutation $Asn175^{4.60}Ala$ on the MT_2 receptor brings to a 4-fold decrease in melatonin binding and a 13-fold decrease in 5-methoxytryptophol binding. Conversely, binding affinities of compounds lacking the 5-methoxy group, namely luzindole and N-acetyltryptamine, were unaffected. These evidences suggest that $Asn^{4.60}$ could be a counterpart for the methoxy group of melatonin.

A tyrosine residue at position 7.43 is highly conserved among aminergic GPCRs and more than 30% of class A receptors carry a tyrosine at this position.[164] Looking at available X-ray crystal structures of β_1, β_2, D_3 and H_1 receptors, it is clear that this residue plays a key role in ligand binding, since it promotes a suitable orientation of $Asp^{3.32}$ into the ligand binding site. The point mutation $Tyr298^{7.43}Ala$ completely abolishes melatonin binding at the MT_2 receptor.[250] Due to the lack of $Asp^{3.32}$ in MT_1 and MT_2 receptors, $Tyr^{7.43}$ may directly interact with the side chain of melatonin and, particularly, with the terminal amide group. A recent study investigated the role of melatonin amide functionality using a novel class of melatoninergic ligands in which the amide side chain was partially constrained within a ring.[276] The absence of the amide hydrogen did not produce a remarkable effect on ligand binding. Thus, it could be hypothesized that the hydroxyl group of $Tyr^{7.43}$ may interact with the carbonyl oxygen of melatonin amide chain through a H-bond interaction. Taken together, the evidences described above suggest a specific orientation of melatonin into the binding site, with the 5-methoxy group facing $Asn^{4.60}$ on TM4, the indole ring accommodated in proximity of $Val^{5.42}$ and $His^{5.46}$ on TM5 and the amide group bound to $Tyr^{7.43}$ on TM7.

A key aspect in the identification of the binding mode for MT_2-selective antagonists came from the 3D-QSAR models previously proposed by our group.[259] One of the main outcomes of this study was that MT_2-selective antagonists require a bulky lipophilic group bound to positions 1 or 2 of the indole ring of melatonin arranged in an “out-of-plane” conformation. A sequence inspection of melatonin receptors revealed that positions 3.40 and 5.51 of the MT_2 receptor are occupied by smaller residues compared to the MT_1 subtype (Figure 20), leading to the presence of a lipophilic pocket between TM5 and TM3, which is wider in the MT_2 receptor compared to the MT_1 subtype. Thus, this additional cleft could accommodate the prototypical “out-of-plane” lipophilic substituent carried by MT_2-

selective antagonists. Interestingly, crystal structures of GPCRs active state showed a crucial role of position 3.40 in receptor activation: as previously described, the receptor activation mechanism implies the simultaneous rotation of residues 3.40 and 6.44, triggering the outward movement of the intracellular end of TM6. In this scenario, it could be hypothesized that the "out-of-plane" substituent conferring the MT_2 selectivity could sterically interfere with position 3.40, impeding the outward tilt of TM6 and the subsequent receptor activation.

On the contrary, positions 4.57, 4.61 and 3.29 are occupied by bulkier amino acids in the MT_2 receptor compared to the MT_1 (Figure 20). SAR studies clearly indicated that the presence of a bulky lipophilic substituent in a position corresponding to that of the methoxy group of melatonin could improve MT_1 selectivity. Thus, it could be hypothesized that the bulky substituent conferring MT_1 selectivity could be accommodated in this additional cleft between TM3 and TM4, present in the MT_1 but not in the MT_2 receptor.

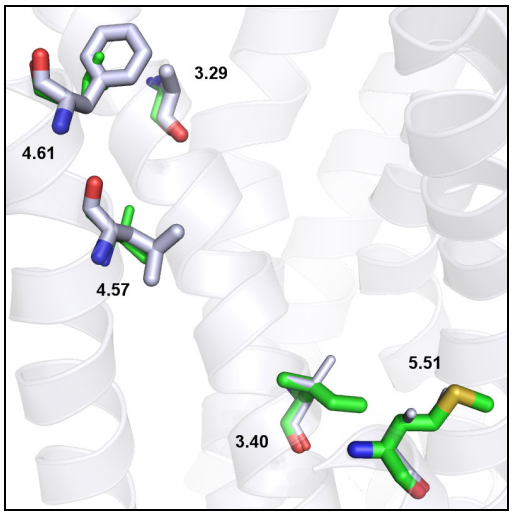

Position	MT_1	MT_2
3.29	Gly104	Ala117
3.40	Ile115	Val128
4.57	Val159	Leu172
4.61	Leu163	Phe176
5.51	Met200	Ile213

Figure 20: comparison between MT_1 (green carbons) and MT_2 (grey carbons) receptor models. Residues delimiting the additional pockets are depicted with sticks. For the same position, the bulkiest residue is represented by thick sticks.

Additional ligand-based information could be used to define the binding mode of melatoninergic ligands. A chiral pharmacophore model, recently described for non-selective melatoninergic agonists, was built starting from conformationally-constrained, chiral and stereoselective ligands.[260] The main common pharmacophore features found among selected compounds were: i) an aromatic nucleus, ii) an amide fragment and iii) a methoxy, or other equivalent groups, placed on the aromatic nucleus. The melatonin conformation with the best fit to this model has the ethylamidoethyl side chain below the plane of the indole ring (in the orientation depicted in Figure 21), oriented perpendicularly

to the aromatic plane: in this peculiar conformation the Cα-Cβ-N-C-CH_3 chain adapts an all-*anti* configuration.[260]

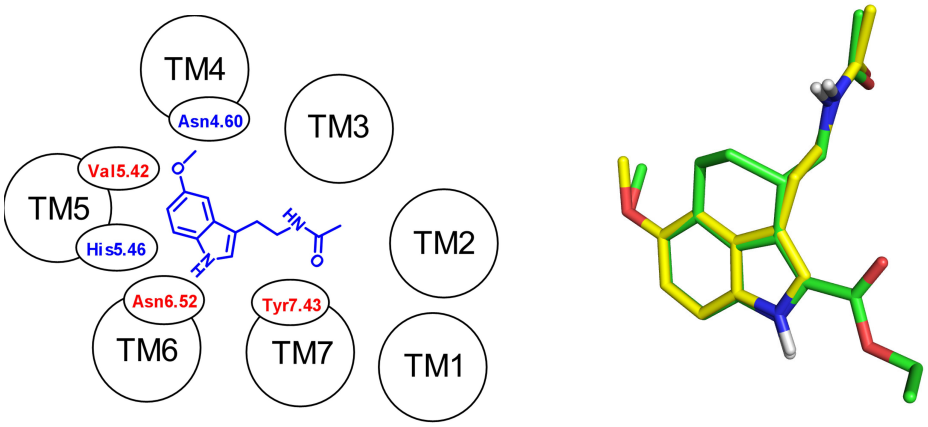

Figure 21: Left: hypothesized binding mode of melatonin into the melatonin receptors. Amino acids important for melatonin binding are depicted in the figure. Residues whose mutation abolish or decrease melatonin binding are depicted in red and blue, respectively. Right: superposition of the constrained analogue synthesized to assess the putative active conformation of the melatonin amide side chain (green carbons, ref. 260) and melatonin (yellow carbons).

Refinement of the MT_2 receptor model

To adapt the binding site shape around the bulky melatonin receptor antagonists, UCM454[277] was manually docked into the putative binding site in a conformation consistent with pharmacophore model, mutagenesis studies and SARs. The resulting UCM454-MT_2 complex was energy minimized using MMFFs force field to a convergence gradient of 0.001 kJ/(molÅ): during this phase, to allow a better ligand accommodation without affecting the geometry of the TM portion, UCM454 and TM helices backbone atoms were maintained frozen.

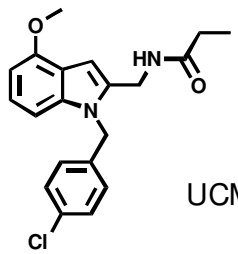

UCM454

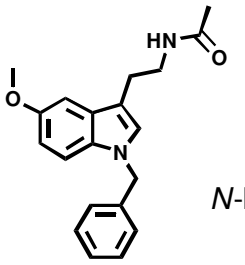

N-benzyl-melatonin

The resulting complex was then submitted to a simulated annealing (SA) process. 10 cycles in which the system was heated and cooled gradually from 1000 K to 298 K were performed, collecting the complex coordinates at the end of each cycle. To avoid α-helix disruptions and to enhance mutual adaptation between the ligand and receptor side

chains, some constrains were applied on receptor structure. While distance constraints were applied between the backbone N and O atoms of TM regions involved in hydrogen bonds, with a force constant of 500 kJ/(molÅ^2) and a tolerance of 0.3 Å to keep the α-helical secondary structure, positional constraints were introduced for all the TM backbone atoms, with a force constant of 50 kJ/(molÅ^2) and a tolerance of 2.0 Å, to allow slight adjustments in the relative position of the helices. To facilitate the adaptation of the binding site cavity, UCM454 was retained frozen during each SA cycle.

The ten resulting structures were minimized with TM backbone atoms frozen, using MMFFs and applying a convergence criterion of 0.05 kJ/(molÅ); the structure with the best arrangement of the amino acids involved in ligand binding was chosen for further optimizations. A MD simulation was performed to relax the MT_2 receptor-UCM454 complex derived from the SA procedure. The same set of constrains used for SA were applied in MD simulation and a gradual increase in temperature was applied, to prevent structure disruption. After 100 ps at 50 K, 100 ps at 100 K and 100 ps at 200 K, 600 ps of simulation at 310 K were performed. The final structure obtained was energy minimized with the same set of constrains used in MD simulation.

Another bulky antagonist was then docked into the MT_2 binding site: *N*-benzyl-melatonin (a MT_2-selective antagonist).[259] A docking grid was built using Glide[278] software, centered on UCM454 in the complex obtained from MD simulation. Enclosing box and bounding box were set to 25 and 10 Å, respectively and a scaling factor of 0.8 was applied on Van der Waals radii of protein heavy atoms. Coulomb-Van der Waals energy cutoff was set to 100 kcal/mol, to avoid the deletion of poses with proper geometry, but with a high energy contribution due to steric hindrance. The best pose according to the GScore was retained and the resulting complex was further minimized with frozen backbone, applying the MMFFs force field to a convergence gradient of 0.05 kJ/(molÅ). The modified complex was then minimized with frozen backbone and the resulting structure was submitted to MD simulation. During MD simulation, all constrains used for SA were applied, and same temperature steps described above were used: 100 ps at 50 K, 100 ps at 100 K, 100 ps at 200 K and a production phase of 600 ps at 310 K. The final structure obtained from this simulation was energy minimized using the protocol previously described (Figure 22).

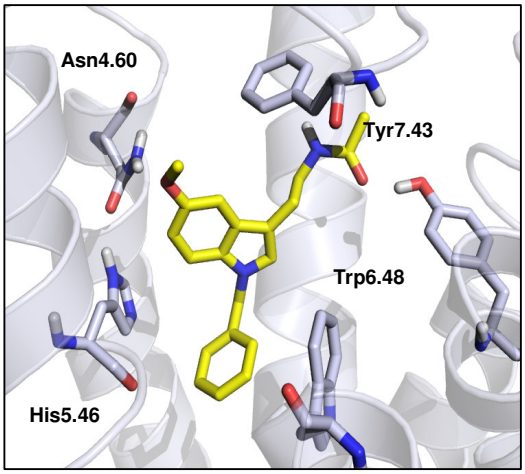

Figure 22: *N*-benzyl-melatonin within the MT_2 receptor binding site. The methoxy group is H-bonded to Asn175$^{4.60}$ and the amidic oxygen interacts with Tyr298$^{7.43}$. The benzyl substituent is located near Trp264$^{6.48}$. Amidic chain orientation is consistent with the pharmacophore hypothesis.

The 3D structure of the MT_2 receptor receptor after the SA and MD simulations previously described was used as the template to build the MT_1 receptor model. Based on the alignment reported in Figure 1, amino acids belonging to MT_2 were substituted with the corresponding residues of the MT_1 receptor using Maestro[279] software. Finally, side chains of MT_1 receptor model were minimized with MMFFs, to a convergence gradient of 0.05 kJ/(molÅ) (Figure 23).

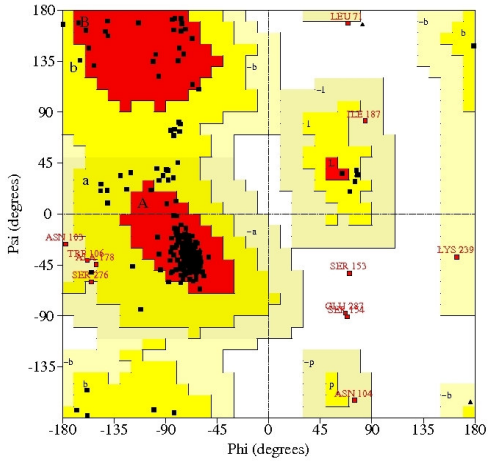

Figure 23: Ramachandran plot of the MT_1 receptor model. Only 4 residues, belonging to loop segments, are located in disallowed regions.

To evaluate if receptor models were consistent with available SARs and mutagenesis data, docking studies and MD simulations were performed on these structures using known active compounds.

Receptor models validation

Docking studies within the MT$_2$ receptor model

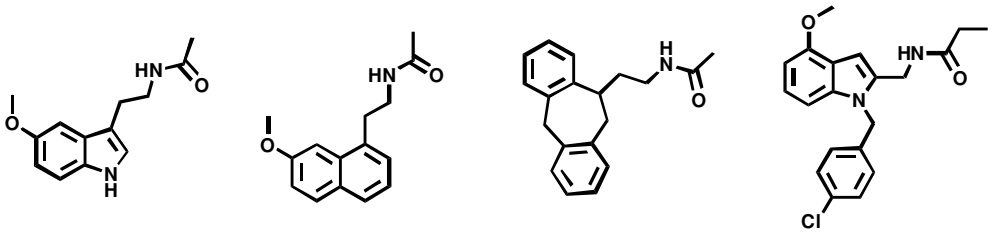

melatonin agomelatine UCM545 UCM454

A ligand subset comprising UCM454, (*S*)-UCM545,[280] agomelatine[281] and melatonin was selected for docking studies. Automatic docking was performed using Glide software.[278] Docking grids were centered on *N*-benzyl-melatonin in the complex with the MT$_2$ receptor (previously described) and enclosing and bounding boxes were set to 22 and 10 Å, respectively. Van der Waals radii of protein heavy atoms were scaled to 0.8 and 20 poses were retained for each docking run. Coulomb-van der Waals energy cutoff was set to 100 kcal/mol to avoid discarding of poses with proper geometry, but with a high energy contribution due to steric hindrance.

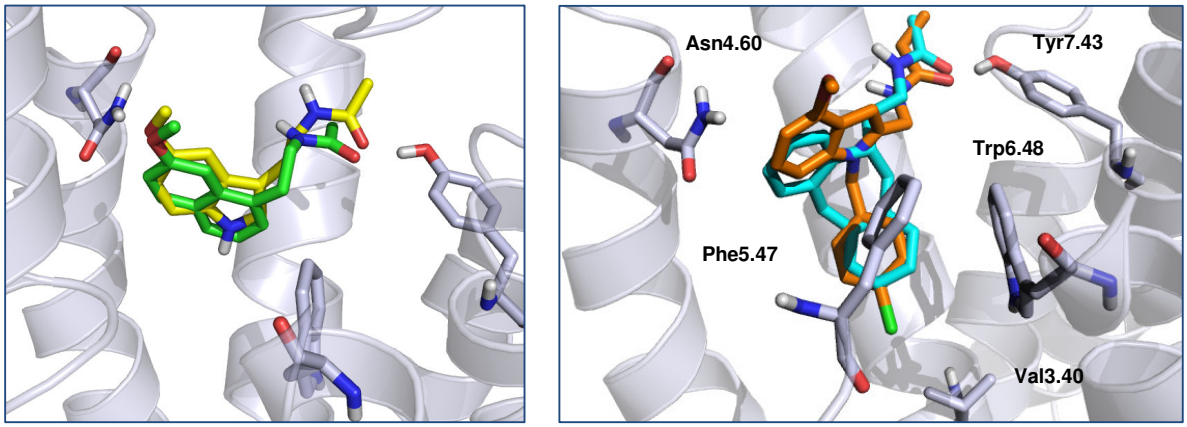

Figure 24: melatonin (yellow), agomelatine (green), UCM454 (orange) and UCM545 (cyan) docked into MT$_2$ binding site.

The automatic docking procedure could not find a correct accommodation of melatonin within the MT$_2$ binding cavity: in particular, none of the docking poses could form favorable interactions with Tyr298$^{7.43}$ and Asn175$^{4.60}$. This was probably due to the increased volume of the MT$_2$ binding site, adapted around two bulky MT$_2$-selective antagonists. thus, the endogenous ligand tended to occupy additional regions and cavities different from the

putative binding site. For this reason, melatonin was manually docked into MT_2 binding site. All resulting complexes were minimized applying MMFFs force field, with frozen backbone atoms, to a convergence gradient of 0.05 kJ/(molÅ). Minimized complexes are depicted in Figure 24. All ligands interacted with Tyr298$^{7.43}$ with their amidic oxygen, retaining an amide chain conformation consistent with the pharmacophore model. Moreover, UCM454 and UCM545 accommodated their "out-of-plane" substituent in a pocket formed by TM5 and TM6, in the proximity of Val128$^{3.40}$. The methoxy group of melatonin, agomelatine and UCM454 interacted with Asn175$^{4.60}$, whose mutation leads to a 4-fold decrease in melatonin binding.[272] His208$^{5.46}$ did not directly interact with the ligand but it was H-bonded to Asn175$^{4.60}$, favoring the interaction between Asn175$^{4.60}$ and the ligand methoxy group.

To evaluate the stability of ligand-receptor interactions found with docking studies, the resulting complexes were submitted to MD simulations. After 60 ps of equilibration, 600 ps of production phase were run at 310 K, applying MMFF force field and with all backbone atoms frozen. Minimized complexes after MD simulations are depicted in Figure 25: all the four complexes were stable during MD simulations as well as H-bond interactions with key residues within the binding site region.

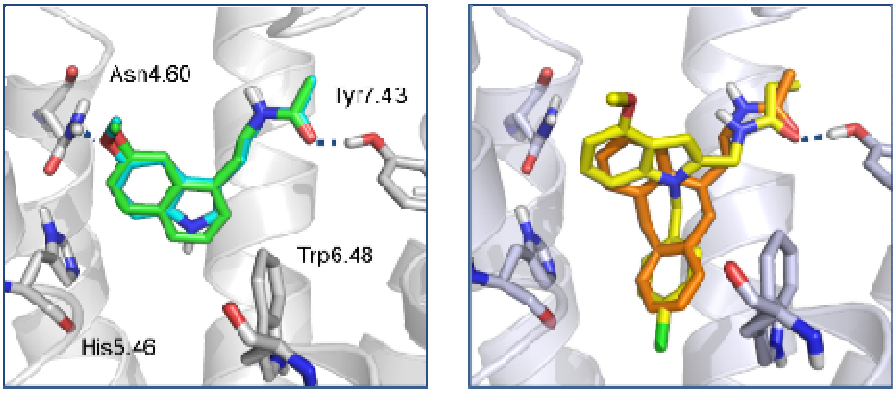

Figure 25: minimized complexes of melatonin (cyan), agomelatine (green), UCM545 (orange) and UCM454 (yellow) into MT_2 receptor model after MD simulations.

Docking study within the MT_1 receptor model

Docking studies were performed to evaluate the consistency of the MT_1 receptor model with the available experimental data. Melatonin and UCM871 (MT_1-selective partial agonist) were chosen as reference compounds.

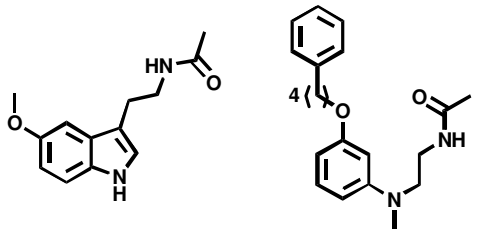

Melatonin UCM871

To model the binding site shape, ligands were manually docked into the active site of the MT$_1$ receptor in a conformation consistent with the pharmacophore model. Resulting complexes were energy minimized with frozen backbone to a convergence gradient of 0.05 kJ/(molÅ), applying MMFFs force field. Melatonin and UCM871 interacted with Tyr285$^{7.43}$ (Tyr298$^{7.43}$ in the MT$_2$ receptor) with their amidic oxygen and with His195$^{5.46}$ (His208$^{5.46}$ in the MT$_2$ receptor) with their oxygen atoms connected to the aromatic nucleus. In addition, the phenylbutyloxy substituent of UCM871 was accommodated into a region located at the top of TM3 and TM4, where it formed extensive hydrophobic interactions with Phe105$^{3.30}$, Val159$^{4.57}$ and Leu163$^{4.61}$ (Figure 26).

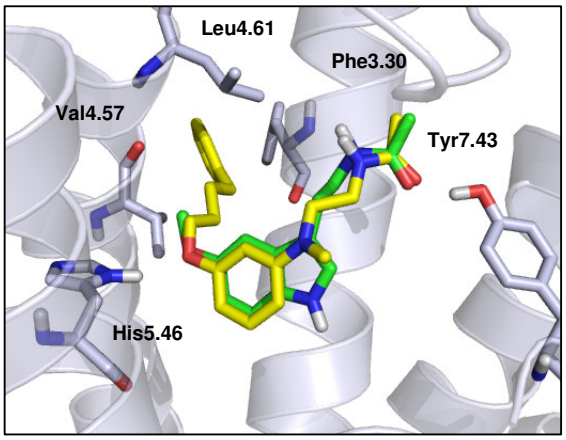

Figure 26: UCM871 (yellow) and melatonin (green) within the MT$_1$ receptor model; both ligands interacted with Tyr285$^{7.43}$.

Comparison between MT$_1$ and MT$_2$ receptor models

Docking studies within the two melatonin receptor models allowed to evidence some differences between MT$_1$ and MT$_2$: in particular, some regions of the binding site that could allow a better ligand accommodation in MT$_1$ compared to MT$_2$ (and vice versa) for selective ligands were identified.

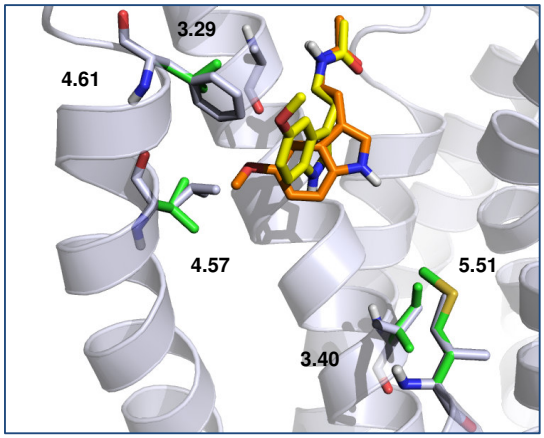

Position	MT_1	MT_2
3.29	Gly104	Ala117
3.40	Ile115	Val128
4.57	Val159	Leu172
4.61	Leu163	Phe176
5.51	Met200	Ile213

Figure 27: MT1 (green carbons) and MT2 (gray carbons) complexes with melatonin (orange for MT1 and yellow for MT2).

As described previously, while the MT_1 receptor has bulkier residues in the region surrounding position 1 and 2 of the indole ring (3.40 and 5.51), the MT_2 receptor model has smaller residues in this zone. In fact, Ile115$^{3.40}$ and Met200$^{5.51}$ in MT_1 receptor correspond to Val128$^{3.40}$ and Ile213$^{5.51}$ in the MT_2 receptor. Moreover, the MT_1 receptor binding site is characterized by the presence of a region, surrounded by residues belonging to TM3 and TM4, where a portion of the MT_1-selective ligands can be accommodated. The corresponding area in the MT_2 model is not or less available for the ligand, due to the presence of amino acids with bulkier side chains, hampering a correct ligand accommodation. Ala$^{3.29}$, Leu$^{4.57}$ and Phe$^{4.61}$ in the MT_2 receptor correspond to Gly, Val and Leu in MT_1 receptor, respectively. These differences could account for the slightly different orientation of melatonin into the two binding sites (Figure 27): indeed, while in MT_1 receptor melatonin found an accessible volume near TM4 and TM3, in the MT_2 this region is occupied by amino acid side chains, and melatonin is therefore located near TM3 and TM5, closer to Trp$^{6.48}$, Val$^{3.40}$ and Ile$^{5.51}$.

Figure 28 shows UCM871 (MT_1-selective partial agonist) and UCM454 (MT_2-selective antagonist) docked within the MT_1 and MT_2 binding sites, respectively. Solvent accessible surfaces surrounding the five residues cited above (3.29, 3.40, 4.57, 4.61 and 5.51) are represented. While the MT_1 receptor is characterized by an accessible pocket near TM3-TM4 interface (upper left of the picture, orange surface), it has no or very limited space available in the region surrounded by TM3 and TM5 (lower right of the picture). On the contrary, the MT_2 receptor surface (blue) evidences a hindered region near TM3-TM4 and an accessible volume between TM3 and TM5.

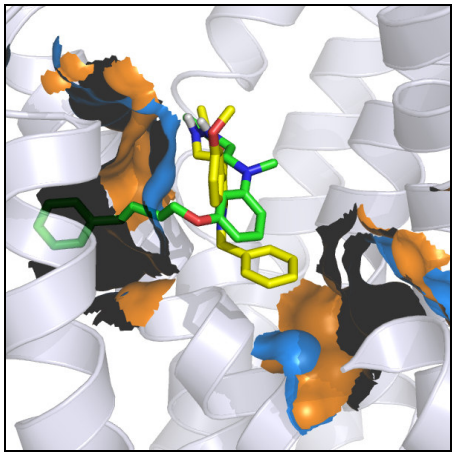

Figure 28: UCM871 (green) and UCM454 (yellow) into the MT_1 (orange surface) and MT_2 (blue surface) binding site; only a cartoon representation of the MT_1 receptor is reported for clarity.

MD simulations in a solvated lipid bilayer: the MT_1 melatonin receptor

Model building and refinement

The newly released crystal structures of GPCR active state gave the chance to investigate the agonist recognition process at a molecular level. Thus, to investigate the agonist binding at melatonin receptors, a new homology model of the MT_1 subtype was built starting from a template structure crystallized in an active state.

As described previously, only certain β_2 receptor crystal structures (PDB ID: 3P0G and 3SN6) and opsin structures show the complete pattern of conformational transitions predicted for the GPCR activation mechanism. Among these two potential templates, opsin shows the lowest homology and identity percentages with the MT_1 melatonin receptor; consequently, the β_2 receptor was chosen as template structure. Since the complex β_2 receptor-Gs protein (PDB ID: 3SN6) was not available when this study started, the β_2 receptor structure co-crystallized with a camelid nanobody (PDB ID: 3P0G) was selected as template for the MT_1 receptor modeling.

The alignment between the β_2 and MT_1 sequences used for model building is reported below.

```
b2      DVTQQRDEVWVVGMGIVMSLIVLAIVFGNVLVITAIAKFERLQTVTNYFITSLACADLVMGLAVVPFGAAHILMKMWTFGNFWCE
hMT1    RGDGARPSWLASALACVLIFTIVVDILGNLLVILSVYRNKKLRNAGNIFVVSLAVADLVVAIYPYPLVLMSIFNNGWNLGYLHCQ

b2       FWTSIDVLCVTASIWTLCVIAVDRYFAITSPFKYQSLLTKNKARVIILMVWIVSGLTSFLPIQMHWYRATHQEAINCYAEETCC
hMT1     VSGFLMGLSVIGSIFNITGIAINRYCYICHSLKYDKLYSSKNSLCYVLLIWLLTLAAVLPNLRAGTLQ--Y-DPRI-Y----SC

b2       DFF--T-NQAYAIASSIVSFYVPLVIMVFVYSRVFQEAK----------------LKEHKALKTLGIIMGTFTLCWLPFFIVNIV
hMT1     T-FAQSVSSAYTIAVVVFHFLVPMIIVIFCYLRIWILVLQVRQRVKPDRKPKLKPQDFRNFVTMFVVFVLFAICWAPLNFIGLA

b2       HVIQD-N-L--IRKEVYILLNWIGYVNSGFNPLIYCRSP-DFRIAFQELLCLRR
hMT1     VASDPASMVPRIPEWLFVASYYMAYFNSCLNAIIYGLLNQNFRKEYRRIIVSLC
```

A different alignment was used for the ECL2 portion compared to that used for the previous MT_1 receptor model. Indeed, in the melatonin receptor models previously described and built on the inactive form of the β_2 receptor, the unique phenylalanine belonging to the ECL2 of melatonin receptors was aligned to Phe193 of the β_2 sequence. A visual inspection of crystal structures revealed that Phe193 protrudes into the β_2 binding site, forming favorable hydrophobic interactions with co-crystallized ligands. Retaining the previous alignment, this phenylalanine belonging to the ECL2 lays in the middle of the binding cleft, impeding a correct ligand accommodation in melatonin receptors (Figure 29).

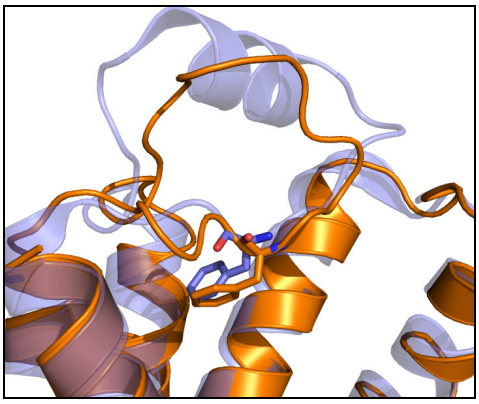

Figure 29: superposition of the β_2 receptor crystal structure (PDB: 3D4S, blue) and the MT_2 receptor model built on the inactive state of the β_2 receptor (orange). Phe193 of the β_2 receptor and Phe192 of the MT_2 melatonin receptor are represented in sticks.

Since the β_2 receptor is characterized by the presence of two phenylalanines in its ECL2 sequence, it could be hypothesized that Phe179 in the MT_1 receptor (or Phe192 in the MT_2 receptor) corresponds to Phe194 instead of Phe193 of the β_2 sequence. In contrast to Phe193, Phe194 points towards the extracellular milieu, far from the binding site. Thus, a new alignment, in which MT_1 Phe179 is aligned on Phe194 of the β_2 receptor sequence, could provide a wider binding site cavity, facilitating the agonist accommodation.

Comparative modeling was carried out with Modeller 9.7[270,271] and thirty MT_1 receptor models were initially generated. The structural quality of the models was evaluated using Procheck[282], as well as the Protein Report tool implemented in Maestro 9.0.[283] The best model was selected on the basis of geometrical parameters quality and on Modeller objective function. The initial ECL3 conformation of the chosen model had to be optimized prior to further studies, since it protruded into the membrane bilayer and was not suitable for MD simulations. This peculiar ECL3 geometry was probably due to the implicit solvation treatment implemented in the Modeller package for loop optimization, which has shown not to be suitable for the prediction of loop geometries in membrane proteins.[159] Therefore, an extensive loop optimization procedure was conducted for ECL3, resulting in an energetically-favored conformation consistent with the presence of the membrane bilayer. The resulting receptor model was then refined with the Protein Preparation Wizard workflow of Maestro 9.0.[283] Hydrogen atoms were added and the protonation state of polar residues was consistent with physiological pH.

Preliminary MD simulations performed in a solvated lipid bilayer for both MT_1 and MT_2 receptors showed some disruptions of the helix secondary structure. In particular, a disordered α-helix structure was found near the conserved $Asn^{1.50}$. A visual inspection of trajectories revealed that an aspartic acid located at position 1.46 undertook a downward rotation, forming a stable H-bond interactions with both the backbone NH group and the NH_2 group of the side chain of $Asn^{1.50}$: this double polar interaction caused the disruption of the TM1 α-helix structure in both melatonin receptors (Figure 30).

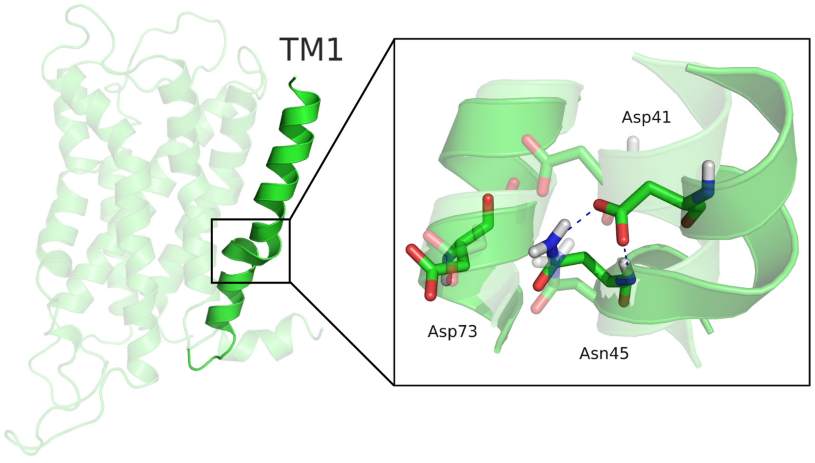

Figure 30: superposition of the initial (trasparent) and final snapshots retrieved from the MD simulation of the MT_1 receptor.

Interestingly, while in the majority of class A GPCRs, small and/or polar amino acids like glycine, alanine, valine and serine are located at position 1.46,[164,284] in melatonin receptors this position is occupied by an aspartic acid. The presence of an acid residue at this position is not common among class A GPCRs since only 1% of them carry an aspartic residue at position 1.46.[164] Looking at available GPCR crystal structures it could be observed that position 1.46 is deeply buried into the TM bundle and points towards TM7 and TM2 (Figure 31, left).

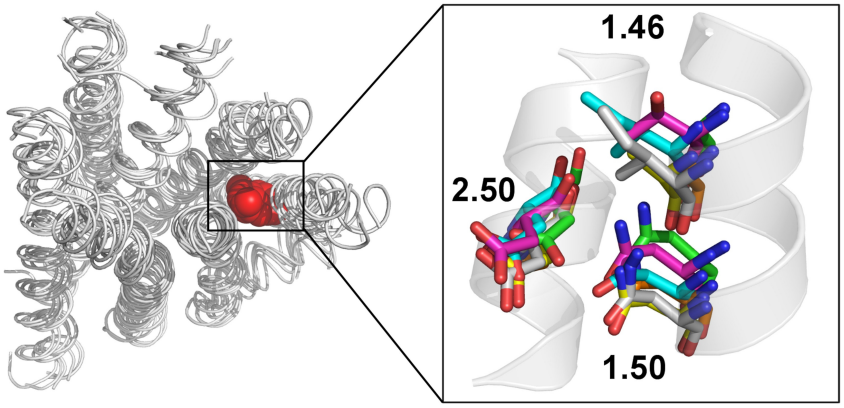

Figure 31: Left: superposition of crystal structures of inactive GPCRs: residues located at position 1.46 are depicted with red spheres. Right: relative orientations of positions 1.50, 2.50 and 1.46 in available GPCRs crystal structures: rhodopsin (green), β_2 and β_1 receptors (grey), A_{2A} (yellow), D_3 (blue), H_1 (magenta) and CXCR4 (orange).

A visual inspection revealed that neighboring residues in the proximity of position 1.46 form a hydrophobic environment, suitable to accommodate small and hydrophobic amino acids rather than charged acidic residues. The peculiar orientation of position 1.46 and the hydrophobic character of its environment led to hypothesize a different protonation state for this particular acidic residue in the MT_1 receptor. PROPKA [285,286,287] and MCCE [288,289] were therefore used to estimate the pKa for this aspartate using the 3D structure of the MT_1 melatonin receptor model. Both approaches returned extremely high pKa values (~9 and ~13 for PROPKA and MCCE, respectively), suggesting the neutral form of this aspartic acid as the most favored one. According to these results, the uncharged Asp41$^{1.46}$ could form an extensive H-bond network with neighboring residues, leading to an overall stabilization of the receptor structure (Figure 32).

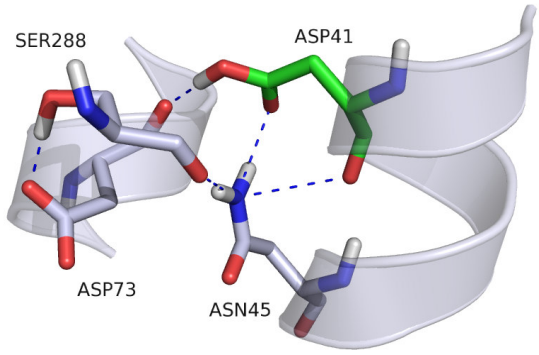

Figure 32: H-bond network stabilized by the protonation of Asp41$^{1.46}$. The carboxylic group of Asp41$^{1.46}$ could interact with the side chain of Asn45$^{1.50}$ on TM1 and Asp73$^{2.50}$ on TM2. Also Ser288$^{7.46}$ concurs to the overall stabilization of the TM1-TM2-TM7 interface.

C- and N- termini were capped with acetyl and methylamino groups, respectively. The resulting receptor model was then subjected to a restrained minimization to an RMSD of 0.5 Å. The Ramachandran plot for the final refined structure is reported below.

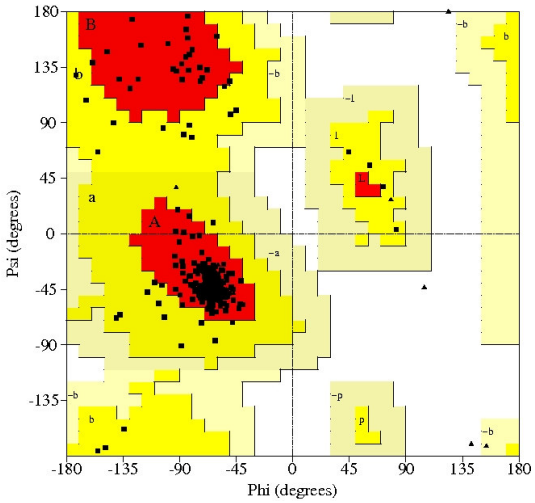

Figure 33: Ramachandran plot of the final MT$_1$ receptor model. No residues are in disallowed regions.

To adapt the binding site region, a potent MT$_1$/MT$_2$ non-selective melatoninergic ligand, 2-phenylmelatonin (2PhMLT), was docked into the ligand binding site. To overcome the difficulties experienced with initial docking studies on melatonin receptors, a “tailored” induced fit docking procedure was applied, in which experimental and ligand-based information has been used during pose selection.

The initial geometry of 2PhMLT was optimized through a minimization procedure, applying the OPLS2005 force field[290] in implicit water. The amide side chain conformation was consistent with the chiral pharmacophore model for melatoninergic agonists (Figure 34).

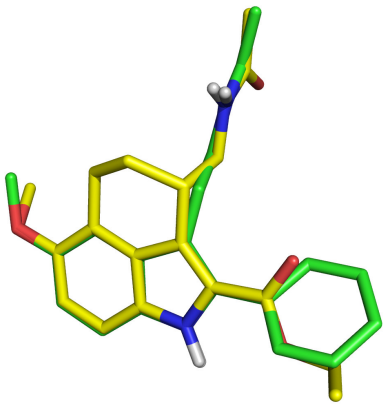

Figure 34: superposition of 2PhMLT (green carbons) with the chiral constrained analogue reported in ref. 276.

To create a suitable space for 2PhMLT accommodation, side chains of Val111$^{3.36}$, Trp251$^{6.48}$ and Tyr281$^{7.39}$ were deleted prior to docking studies. Enclosing and bounding boxes were centered on Met107$^{3.32}$ and His195$^{5.46}$, retaining default sizes of 20 Å and 10 Å, respectively. To soften the potential for nonpolar portions of the receptor, van der Waals (vdW) radii of receptor atoms with partial atomic charges lower than 0.25 (absolute value) were scaled to 0.7. 2PhMLT was docked rigidly into the MT_1 receptor model and 50 poses were collected. vdW radii of ligand atoms with partial atomic charges lower than 0.15 (absolute value) were scaled to 0.5 and the Coulomb-vdW energy potential was increased to 100 kcal/mol to avoid discarding of poses with proper geometry, but with a high energy contribution due to steric hindrance.

Only the poses with the methoxy group pointing towards the cluster of smaller residues found at the interface of TM3 and TM4 (3.29, 4.57, 4.61) in the MT_1 receptor and with the amide side chain facing Tyr285$^{7.43}$ were selected for further refinement: as stated previously, the residues on TM3 and TM4 are thought to allow accommodation of the bulky substituent conferring MT_1-selectivity.

For each protein-ligand complex, a Prime side-chain prediction was run on residues within 6 Å from the ligand molecule: after side-chain optimization, a Prime minimization of the same set of residues and the ligand was performed to relax the structure.

Among selected poses, only one retained both the amide side chain conformation consistent with the pharmacophore model and the main H-bond interaction with Tyr$^{7.43}$: thus, this pose was selected for further refinement. Since the ECL2 segment spanning from the conserved cysteine to the tip of TM5 formed sub-optimal interactions with 2PhMLT, a Prime loop searching procedure was conducted on this specific protein

segment: the loop conformation showing the best Prime Energy value was selected for further studies.

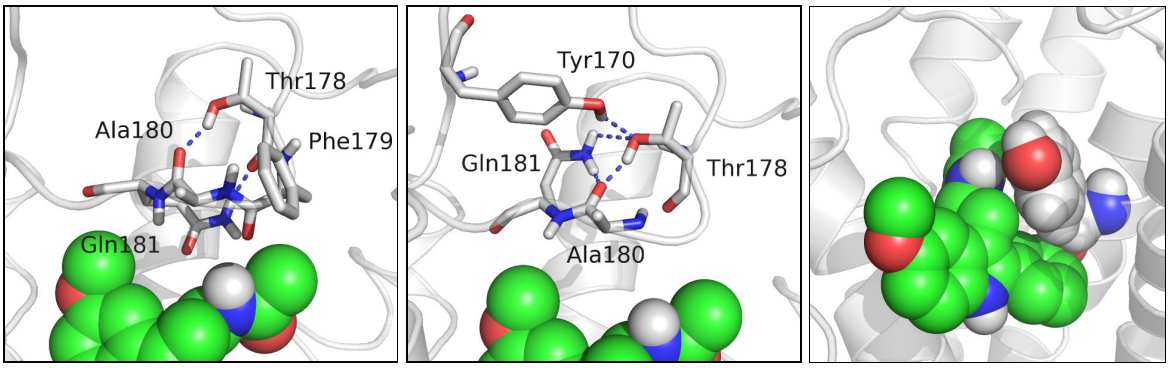

Figure 35: pattern of H-bond interactions occurring at the ECL2 before (left) and after (center) the loop optimization procedure. Only residues in the proximity of 2-phenylmelatonin (green spheres) are depicted in sticks. Right: sphere representation of 2PhMLT (green) and Tyr281$^{7.39}$ (white) into the MT$_1$ binding site.

In the final ECL2 conformation, an upward rotation of the Glu181 side chain could be observed: this movement facilitated the formation of an extended network of H-bond interactions that stabilized the overall geometry of the ECL2 portion. Interestingly, none of the residues located between the conserved cysteine on ECL2 and the extracellular end of TM5 interacted with the ligand molecule. This was probably due to the close proximity of the bulky Tyr281$^{7.39}$ side chain to the ligand amide functionality: indeed, the Tyr281$^{7.39}$ side chain sterically impeded the formation of favorable contacts between 2PhMLT and residues located on the ECL2 portion (Figure 35, right).

The final complex was minimized using AMBER* force field[291,292,293] applying a convergence gradient of 0.05 kJ/(molÅ): atoms comprised in a shell of 8 Å center on ligand molecule were free to move while all the other residues were retained fixed. The resulting complex is depicted below.

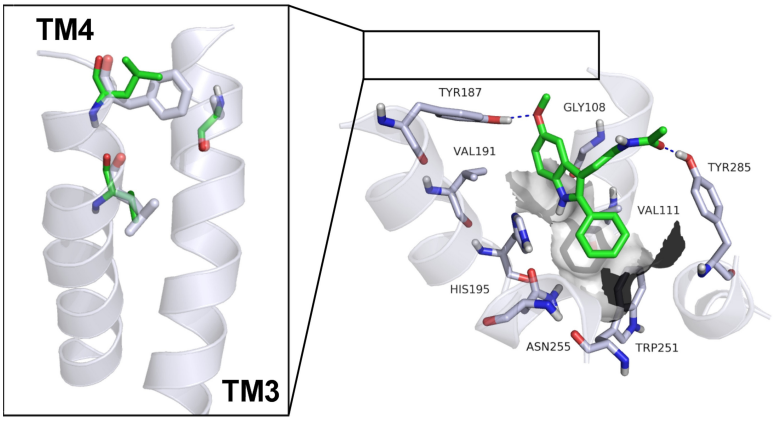

Figure 36: Left: superposition of TM3 and TM4 of MT$_1$ (green residues) and MT$_2$ (grey residues) receptor models. Positions 3.29, 4.57 and 4.61 are highlighted. Right: 2PhMLT (green carbons) into the MT$_1$ receptor model (gray carbons).

As can be seen in Figure 36, the amide side chain orientation of 2PhMLT is consistent with the pharmacophore model for melatonin receptor agonists. Two main H-bond interactions could be detected between the methoxy oxygen of 2PhMLT and Tyr187$^{5.38}$ and between the carbonyl oxygen of 2PhMLT and Tyr285$^{7.43}$. While mutagenesis studies highlighted the importance of Tyr$^{7.43}$ for melatonin binding in the MT_2 melatonin receptor,[250] no site-directed mutagenesis studies have been performed for Tyr$^{5.38}$ on TM5. However, Tyr$^{5.38}$ is highly conserved among class A GPCRs (~30%)[164] and data retrieved from other receptors showed a crucial role of residue 5.38 in both agonist and antagonist binding[170,294] as well in receptor activation.[295] The indole core of 2PhMLT interacted with residues known to play a crucial role in melatonin binding such as Val191$^{5.42}$, His195$^{5.46}$ and Asn255$^{6.52}$. In addition, the 2-phenyl substituent of 2PhMLT formed a edge-to-face interaction with Trp251$^{6.48}$, known to be fundamental for the receptor activation mechanism.[128]

As expected, the MT_1 binding site is shifted towards TM3 and TM4 compared to those observed in available GPCRs: this shift also causes a different orientation of the 2PhMLT core compared to that of the β_2 agonist co-crystallized into the template structure (Figure 37).

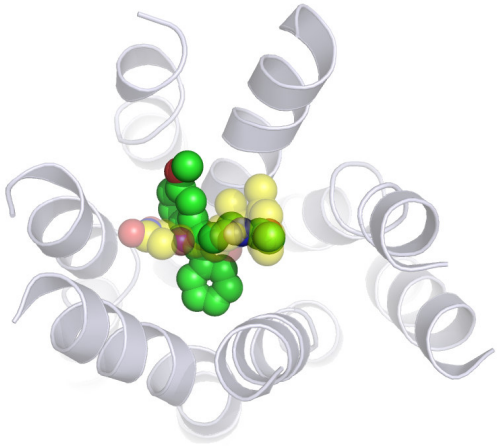

Figure 37: comparison between the binding pose of 2PhMLT (opaque green spheres) and the co-crystallized β_2 agonist (PDB ID: 3P0G, transparent yellow spheres).

Protocol

Desmond v2.2[296] was used to built the system and to perform the dynamics simulations. Protein-ligand complex was aligned to the 3P0G crystal structure deposited into the

Orientations of Protein in Membranes database (OPM)[297] to find the best protein orientation with respect to the membrane bilayer. The MT_1-2PhMLT complex was then embedded in a POPC lipid bilayer with at least 12 Å between the protein and its closest periodic image. The system was solvated by approximately 10800 TIP3P water, resulting in a simulation box of approximately 80 Å x 70 Å x 100 Å. The Amber99SB force field[298] was used to model the protein, while ligands and lipids were parameterized using the GAFF.[299] Partial charges of 2PhMLT were calculated at the AM1-BCC level. The GAFF/TIP3P combination was applied on this system since it proved to give reliable results in MD simulations of membrane systems.[300] Preliminary MD simulations performed on GPCR crystal structures and melatonin receptor models clearly showed that the latter structures could not be simulated in the same conditions as those used for crystallized complexes. Indeed, they needed a longer and "tailored" equilibration procedure to avoid structure disruptions.

The steps applied during the equilibration phase of the system are listed below:

1. System was energy-minimized with 2000 steps of steepest-descent with a convergence gradient of 50 kcal/(molÅ). All protein and ligand heavy atoms were constrained with a force constant of 50 kcal/(molÅ^2).
2. System was energy-minimized with 2000 steps of steepest-descent with a convergence gradient of 5 kcal/(molÅ). All atoms were free to move.
3. 1 ns-long NVT simulation was performed using the Langevin barostat and thermostat.[301] Temperature was linearly increased from 10 to 310 K and heavy atoms of both protein and ligand were constrained with a force constant of 50 kcal/(molÅ^2), that linearly decreased to 10 kcal/(molÅ^2). To avoid the penetration of water molecules into the membrane bilayer, a gaussian potential was applied during the NVT simulation to water molecules.
4. 1 ns-long NPT simulation was performed using the Langevin barostat and thermostat. Temperature was set to 310 K and the Gaussian potential inserted in the previous step was retained. Constraints on protein and ligand heavy atoms were retained, applying a force constant of 10 kcal/(molÅ^2).
5. 1 ns-long NPT simulation was run applying the same settings of the previous step, without the inclusion of the Gaussian potential.
6. 2 ns-long NPT simulation was performed using the Langevin barostat and thermostat. Temperature was set to 310 K and positional constraints were applied

on both protein and ligand heavy atoms. The constraint force was linearly decreased from 10 kcal/(molÅ^2) to 2 kcal/(molÅ^2).

7. 5 ns-long NPT simulation was run using the Langevin barostat and thermostat, at a temperature of 310 K. Positional constraints were applied on protein alpha carbons as well as on heavy atoms of 2PhMLT, Tyr187$^{5.38}$ and Tyr285$^{7.43}$ with a force constant of 2 kcal/(molÅ^2). This phase was mainly used to facilitate the ligand adaptation into the binding site preserving the main H-bond interactions.
8. A final equilibration step of 500 ps was performed using the NPT ensemble, applying no constraints.

The production phase was performed in NPT conditions under constant pressure of 1 atm and a temperature of 310 K, applying Langevin thermostat and barostat. M-SHAKE[302] algorithm was employed to constrain all bond lengths to hydrogen atoms. Short-range electrostatic interactions were cut off at 9 Å, whereas long-range electrostatic interactions were computed using the Particle Mesh Ewald method.[303] A RESPA integrator[304] was used with a timestep of 2 fs, and long-range electrostatics were computed every 6 fs. The production phase of the MD simulations was 50 ns-long.

Results

The receptor structure proved to be stable during the MD simulation, as well as the main ligand receptor interactions. Moreover, the time evolution of the dihedral angle τ_1 indicated a stable conformation of the amide side chain (Figure 38, right).

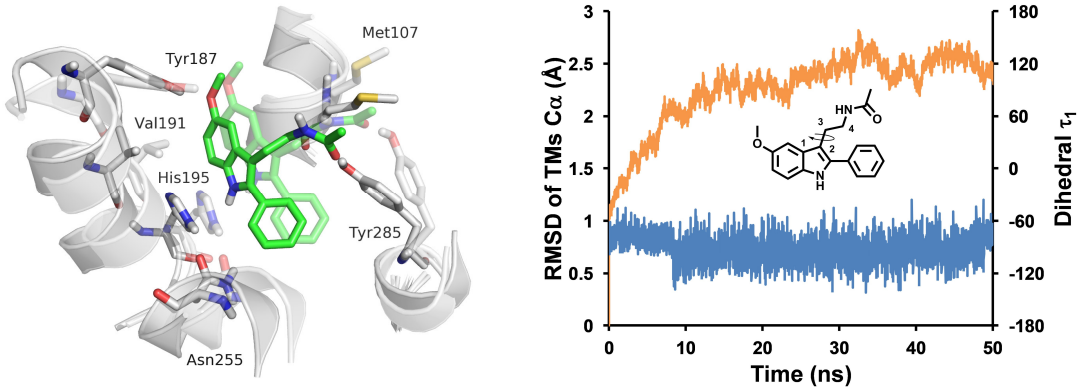

Figure 38: Left: starting (transparent) and final (opaque) conformations retrieved from MD simulation of the 2PhMLT-MT_1 complex. Right: time evolution of the RMSD value (orange) and the τ_1 dihedral angle value (blue).

The last frame of the MD simulation containing the entire system was submitted to a minimization procedure applying a convergence gradient of 0.5 kcal/(molÅ). The protein structure was then extracted from the system and was used to perform docking studies with the MT_1-selective partial agonist, UCM871. To adapt the binding site shape to this anilinoethylamide derivative, an induced fit docking run was applied using a slightly different protocol compared to that employed for 2PhMLT. In this case, docking grids were centered on 2PhMLT and, before docking studies, the side chain of Asn181 belonging to ECL2 was trimmed to create a room for the accommodation of the phenylbutyloxy chain. Since H-bond interactions with Tyr187$^{5.38}$ and Tyr285$^{7.43}$ were maintained by 2PhMLT during MD simulation, 2 distance constraints were applied between the two oxygen atoms belonging to UCM871 and the hydroxyl hydrogens of both Tyr187$^{5.38}$ and Tyr285$^{7.43}$.

The pose showing the best fitting with the pharmacophore features of melatoninergic agonists was selected for MD simulations in a solvated lipid bilayer. The UCM871-MT_1 complex was minimized using the AMBER* force field[291,292,293] applying a convergence gradient of 0.05 kJ/(molÅ): during the minimization phase, only atoms comprised in a shell of 8 Å centered on UCM871 were free to move. The receptor structure was re-inserted into the lipid bilayer obtained at the end of the previous simulation with 2PhMLT and water molecules within 1 Å of receptor structure were deleted. The MD simulation of the UCM871-MT_1 complex was performed applying the same protocol used for 2PhMLT.

The 30 ns simulation showed a stable receptor structure, as well as a stable H-bond interaction between UCM871 amide group and Tyr285$^{7.43}$, that concurred to the stabilization of the amide side chain conformation. In contrast, the interaction with Tyr187$^{5.38}$ was lost during the first stages of the MD simulation and the hydroxyl group of Tyr187$^{5.38}$ formed a OH-π interaction with the benzene ring of UCM871. The terminal phenyl ring of the MT_1-selective ligand formed extensive hydrophobic interactions with Leu163$^{4.61}$ and Gly104$^{3.29}$ at the top of TM3 and TM4, belonging to the cluster of residues thought to accommodate the bulky lipophilic substituents of MT_1-selective compounds.

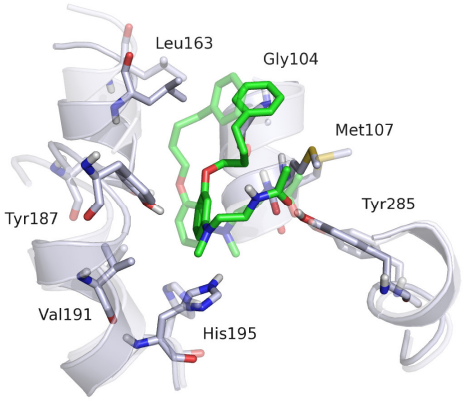

Figure 39: starting (transparent) and final (opaque) conformations retrieved from MD simulation of the UCM871-MT_1 complex.

These studies provided a new binding mode hypothesis for melatoninergic agonists into the MT_1 receptor model. This binding mode showed high stability during MD simulations in a solvated lipid bilayer and was consistent with available data, such as pharmacophore models, mutagenesis data and SARs. A similar binding mode has been recently proposed for melatoninergic antagonists into a rhodopsin-based receptor model[256] but, in this case, $Tyr^{7.43}$ was not involved in ligand binding and the binding site cavity was shifted towards TM6 and TM7 compared to that found in this study.

Moreover, a structure-based explanation for the MT_1 selectivity was proposed, for which the bulky substituents typical of MT_1-selective compounds could be accommodated into an additional pocket present in the MT_1 melatonin receptor, but not in the MT_2 subtype, located at the extracellular ends of TM3 and TM4.

Conformational analysis of melatoninergic ligands

4-phenyl-2-propionamidotetralin derivatives

As described previously, the investigation on the physiological roles of melatonin receptors strongly depends on the availability of potent and selective ligands. So far, two selective melatoninergic compounds have been extensively used as pharmacological tools to discriminate the role of MT_1 and MT_2 receptors in melatonin-mediated effects: luzindole, an antagonist with modest binding affinity and limited selectivity for the MT_2 receptor,[305] and 4-phenyl-2-propionamidotetralin[305] (4-P-PDOT). 4-P-PDOT shows nM binding affinity for the MT_2 receptor, with about one hundred times selectivity over the MT_1 receptor and a partial agonist behavior.

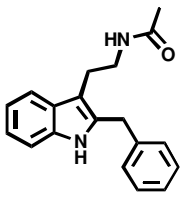

Luzindole

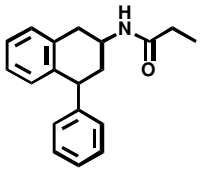

4-P-PDOT

Despite the importance of 4-P-PDOT in the pharmacological characterization of melatonin receptors, structure-activity relationships (SARs) within the 4-phenyl-2-acylaminotetralin series are still fairly unexplored. So far, only two analogs of 4-P-PDOT were characterized (i.e. the *N*-acetyl and *N*-chloroacetyl derivatives), showing binding affinities comparable to that of 4-P-PDOT.[305] In addition, the role of two crucial elements for the pharmacophore of melatonin receptor ligands, i.e. the 5-methoxy group of melatonin and the amidic group orientation, still have to be assessed in the 4-P-PDOT series. Although the 4-phenyl-2-alkylamidotetralin structure can be easily superposed to other chemically diverse MT_2-selective antagonists[306] and the issue of *cis*/*trans* isomers had been already investigated,[307] the relationship between conformational equilibria, pharmacophoric-based superpositions and ligand binding affinities has not been assessed yet.

The aim of this work was to investigate the active conformation of 4-P-PDOT derivatives, combining structural information derived from two different pharmacophore models, one for melatonin receptor agonists[260] and one for MT_2-selective antagonists.[306,308] The crucial pharmacophore points found for MT_2-selective antagonists and partial agonists are the following: i) an aromatic nucleus, ii) an amide fragment and iii) a bulky lipophilic group characterized by an “out-of plane” arrangement with respect to the aromatic nucleus. Moreover, 3D-QSAR analysis had shown that a methoxy substituent occupying a position corresponding to that of the methoxy group of melatonin, is positively correlated with binding affinity.[259] Although pharmacophore models provided an impressive amount of information that has been extensively exploited to design novel MT_2-selective ligands,[261,280] further investigations are needed to clarify some unsolved issues. For example, due to the lack of available data regarding the stereoselectivity of MT_2-selective antagonists, specular pharmacophore models could be fitted by known compounds: in addition, the amide side chain fragment and the “out-of-plane” bulky substituent could assume different relative spatial arrangements, resulting in different pharmacophore models.[277]

A chiral pharmacophore model has been recently described for nonselective melatoninergic agonists, in which conformationally-constrained, chiral and stereoselective

ligands have been superposed to identify a similar arrangement of common ligand elements.[260] The main pharmacophore points were: i) an aromatic nucleus, ii) an amide fragment and iii) a methoxy, or other equivalent groups, bound to the aromatic nucleus. In the melatonin conformation that shows the best fit with this model the acetylaminoethyl side chain points below the plane of the indole ring (in the orientation depicted in Figure 21), assuming a perpendicular orientation: in this putative active conformation the Cα-Cβ-N-C-CH_3 chain adapts an all-*anti* arrangement.[260]

Although the two pharmacophores previously described share common elements (i.e., the aromatic nucleus and the amide fragment), so far no experimental evidences clearly showed that these elements have the same mutual arrangement in the "agonists" and "MT_2-selective antagonists" active conformations.

To test the hypothesis that, in its active configuration and conformation, the aromatic portion and the amide fragment of 4-P-PDOT are arranged similarly to those of melatonin, a conformational analysis has been carried out for *cis*- and *trans*-8-methoxy derivatives of 4-P-PDOT (Table 1), applying a combined study of molecular dynamics simulations and NMR experiments.[309]

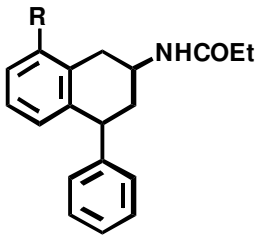

R	Stereochemistry	pK_i MT_1	pK_i MT_2
melatonin		9.58	9.47
OCH_3	(±)-*cis*	7.83	10.22
OCH_3	(±)-*trans*	7.04	9.71
H[a]	(±)-*cis*	7.12	9.16
H[a]	(±)-*trans*	6.65	8.06
H[b]	(+)-*cis*-(*2S,4S*)	7.02	9.26
H[b]	(-)-*cis*-(*2R,4R*)	6.59	7.01
H[b]	(+)-*trans*-(*2R,4S*)	6.89	8.02
H[b]	(-)-*trans*-(*2S,4R*)	5.67	6.10

Table 1: pKi values measured for 4-P-PDOT derivatives of ref. 309. a: see ref. 307. b: see ref. 310.

Protocol

Molecular modeling studies were performed with Macromodel 9.7.[311] Starting geometries of *cis* and *trans* isomers of 8-methoxy-4-P-PDOT were optimized using the MM2 force field,[312] applying a convergence criterion of 0.2 kJ/(molÅ) with implicit $CHCl_3$. Stochastic

dynamics (SD) simulations were performed with the MM2 force field, applying the GB/SA $CHCl_3$ solvation treatment. A time step of 1 fs was applied during SD simulations and temperature was set to 298 K. A 1 μs-long SD simulation was run after 1 ns of equilibration. 50000 frames were collected for analysis. SD was chosen among other computational techniques since it proved to be able to reproduce the conformational equilibrium of small molecules in implicit $CHCl_3$.[313,314,315,316,317,318,319] Preliminary SD simulations were performed on both enantiomers of *cis* and *trans* isomers: since a similar behavior was observed for each couple of enantiomers, SD simulations are described for Compound 1 and 2 in the picture below. For the *trans* derivative, different starting conformations were used for SD simulations, with axial amide substituent and pseudo-equatorial phenyl ring or with equatorial amide group and pseudo-axial phenyl substituent: data showed that the starting point did not significantly affect the results. Coupling constants were calculated with Maestro 9.0,[283] employing an implemented version of the Karplus equation.[320]

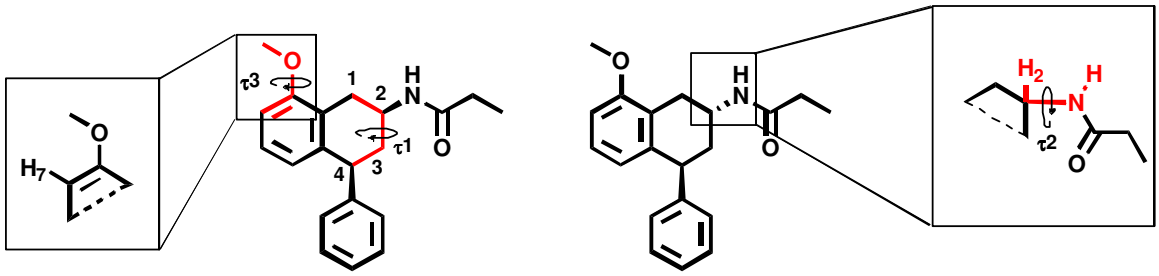

(2*S*,4*S*)-enantiomer
Compound 1

(2*R*,4*S*)-enantiomer
Compound 2

Results

The time evolution of dihedral angle τ_1 (C1-C2-C3-C4) showed that the half-chair conformation of the *cis* derivative characterized by both substituents in equatorial arrangement (τ_1=60°) was conserved throughout the simulation, with only a small number of snapshots (1.4%) showing a di-axial arrangement (τ_1=300). On the contrary, τ_1 values for the *trans* derivative revealed multiple interconversions between two cyclohexene conformations, I and II. While in conformation I (τ_1=60°) the 2-propionamido and the 4-phenyl ring substituents are in axial and pseudo-equatorial arrangement, respectively, in conformation II (τ_1=300°) these two substituents assume opposite arrangements, with the amide group in axial conformation and the phenyl ring in the pseudo-equatorial one.

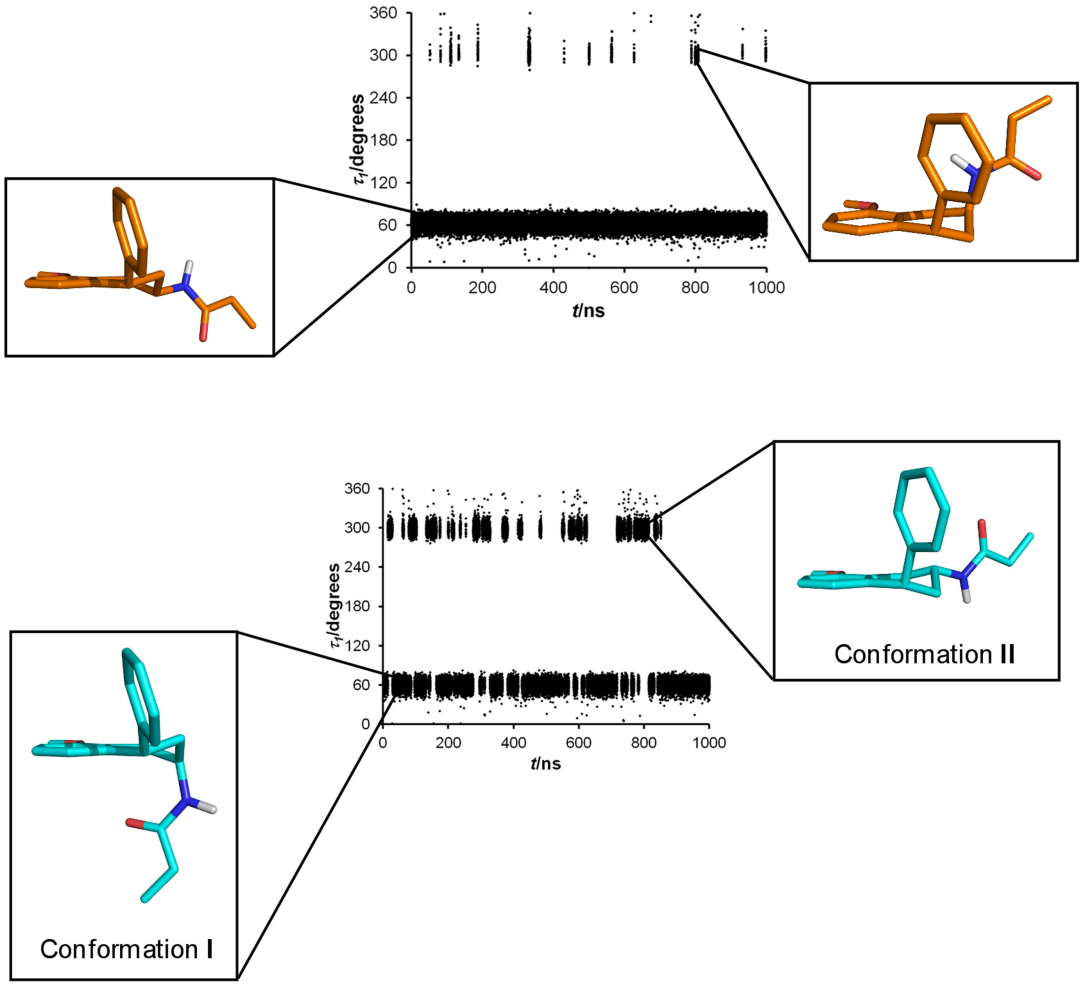

Figure 40: Graphical representation of τ_1 (C1-C2-C3-C4) dihedral angle values for compound 1 (up) and 2 (down). Representative structures collected during SD simulations for compound 1(orange) and 2 (cyan) are depicted in black squares.

A ratio of 28/72 was observed for these two conformations, being I the more abundant. Calculated coupling constants (*J*) for vicinal protons were obtained from 50000 conformations collected during SD simulations (see table below).

Protons[a]	type of coupling	*Cis*		*Trans*			
					calc.		
		obs.	calc.[b]	obs.	I[c]	II[d]	Aver.[b]
H1a-H1b	geminal (^2J)	16.8	-	17.4	-	-	-
H3a-H3b	geminal (^2J)	12.0	-	12.6	-	-	-
H1b-H2	vicinal (^3J)	10.8	10.7	5.4	5.3	3.8	4.2
H1a-H2	vicinal (^3J)	5.4	4.5	6.0	10.3	2.9	5.0
H3b-H2	vicinal (^3J)	12.0	11.0	3.0	3.2	2.9	3.0
H3a-H2	vicinal (^3J)	2.4	3.1	7.8	11.2	3.8	5.8
H3b-H4	vicinal (^3J)	12.0	11.1	7.2	2.0	11.0	8.4
H3a-H4	vicinal (^3J)	4.8	4.8	6.0	5.2	5.2	5.2
NH-H2	vicinal (^3J)	7.2	-	7.2	-	-	-

Table 2: [a] Protons are marked “a” or “b” according to their relative position with respect to the tetraline plane: while protons “a” lay below the ring plane, protons “b” are placed above the plane. [b] Average values obtained from SD simulations. [c] Calculated from conformations of the *trans* derivative having the amide side chain in axial arrangement. [d] Calculated from conformations of the *trans* derivative having the amide side chain in equatiorial arrangement.

While for the *cis* analogue a substantial agreement between experimental and theoretical values could be observed, for the *trans* derivative some slight deviations were detected between observed and calculated *J* values, in particular $J_{H3a\text{-}H2}$ (experimental = 7.8; calculated = 5.8) and $J_{H3b\text{-}H4}$ (experimental = 7.2; calculated = 8.4). Although SD simulations showed I as the preferred conformation for the *trans* isomer, observed *J* values suggest a more uniform distribution between conformations I and II: indeed, the theoretical ratio showing the best agreement between experimental and calculated *J* values is 45/55 (with $J_{calc,H3a\text{-}H2}$ = 7.1 and $J_{calc,H3b\text{-}H4a}$ = 6.9). During SD simulations the 8-methoxy group assumed one preferred orientation in which the methyl group points toward H7: this observation is consistent with the presence of strong NOE signals between protons belonging to the methoxy group and H7 (Figure 41).

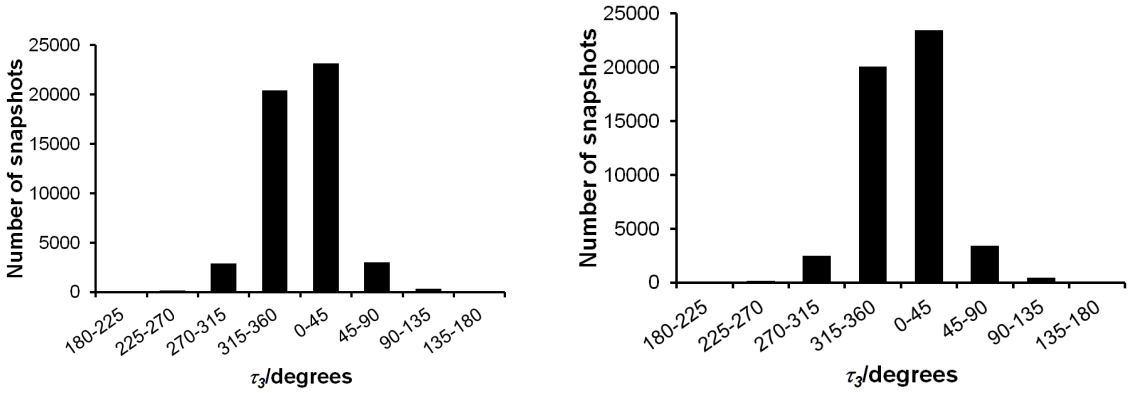

Figure 41: Distribution of τ_3 values for compound 1 (left) and 2 (right) during stochastic dynamics simulation.

SD simulations of both *cis* and *trans* isomers showed a preferred orientation also for the amide NH group, that was oriented *anti* to H2 during most of the simulation time (>99%): only in a small number of snapshots with an opposite orientation of the amide NH (i.e. with τ_2 ~0°) was observed (Figure 42). Although SD simulations showed a favored conformation for the amide NH group, both the coupling constant between H2 and NH protons (7.2 Hz) and the lack of strong NOE signals between NH and protons belonging to the tetralin ring suggest a free rotaion around the C2-N bond.

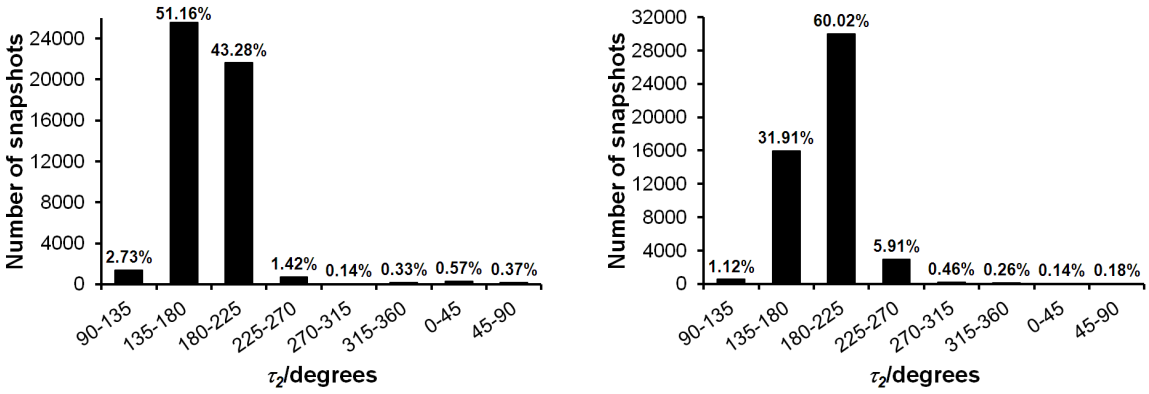

Figure 42: Distribution of τ_2 values for compound 1 (left) and 2 (right) during stochastic dynamics simulation.

Combined information derived from both NMR data and SD simulations indicated: i) a preferred di-equatorial arrangement of amide and phenyl substituents for the *cis* isomer; ii) an equilibrium, with an approximate ratio of 50:50, between conformations I and II of the *trans* isomer; iii) a preferred *anti* orientation of H2 and NH protons, with a possible free rotation around the C2-N bond.

The most abundant conformer of compound 1 obtained from SD simulation could be easily superposed on the active conformation of melatonin, inferred from the pharmacophore model recently proposed by our group (Figure 43, left).[260] Moreover, consistent with the high stereoselectivity observed for the agonist (*S*)-8-M-PDOT,[321] the *cis*-(2*S*,4*S*) enantiomer of 8-methoxy-4-P-PDOT (compound 1) was the one with the best fitting to the agonists pharmacophore. The "out-of-plane" phenyl ring of compound 1 represents an additional pharmacophore element, which had been shown to improve MT_2-selectivity and reduce intrinsic activity.[259] Accordingly, the same conformer of compound 1 fits the common pharmacophore elements of the MT_2-selective antagonist UCM454 (Figure 43, center). These two superpositions suggest that the pharmacophore models for melatoninergic agonists and for MT_2-selective antagonists share the same relative arrangement of the common features.

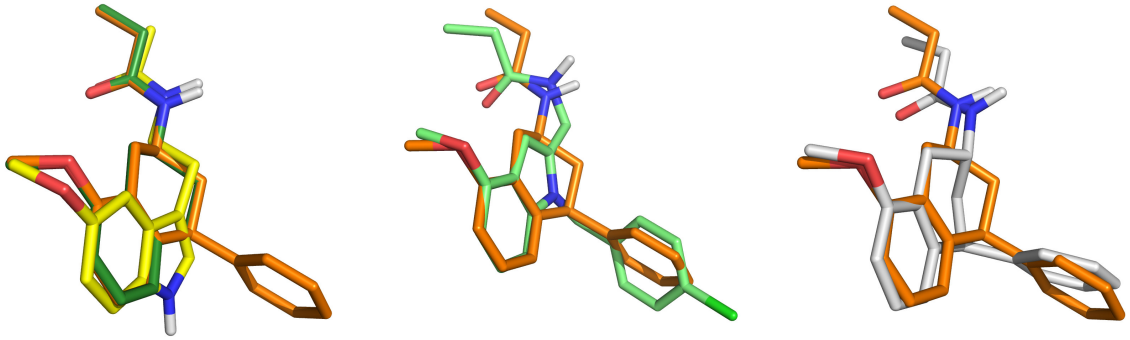

Figure 43: Left: superposition of melatonin (yellow carbons), (*S*)-8-MPDOT (dark green carbons), and compound 1 (orange carbons). Center: superposition of compound 1 (orange carbons) and UCM454 (light green carbons). Right: superposition of compound 1 (orange carbons) and compound 2 (white carbons).

As for the *trans* stereoisomers, only the *trans*-(2*R*,4*S*) enantiomer (compound 2) could give a strict superposition of its phenyl substituent to the 4-phenyl group of the *cis*-(2*S*,4*S*) derivative. On the other hand, the same orientation of the amide fragments of these two stereoisomers could only be achieved selecting for compound 2 a τ_2 dihedral angle of ~0°: this angle is consistent with NMR data, but is strongly disfavored in SD simulations. In particular, the conformation of compound 2 reported in Figure 43 has an equatorial arrangement of the amide chain, with the NH bond pointing toward H2: this represented a minimum-energy conformation, belonging to a subset of snapshots accounting for about 0.5% of the total simulation ensemble (see Figure 42). The presence of a limited number of snapshots that could fit the common pharmacophore features could explain, to some extent, the lower potency observed for the *trans* isomer compared to the *cis* one (Table 1).[309]

Thus, while for melatoninergic agonists the "active" conformation of the amide side chain had been previously identified on the basis of chiral and constrained analogues,[260] the present results suggest that, also for MT_2-selective antagonists or partial agonists, the NH bond of the amide functionality should assume a perpendicular orientation respect to the aromatic nucleus of the tetralin ring (Figure 43, center). To further test this hypothesis, two derivatives carrying a double bond between positions 1 and 2 of the tetralin nucleus were tested (compounds A and B): the insertion of the double bond could impede the NH group to assume a perpendicular orientation, hampering a correct ligand binding.

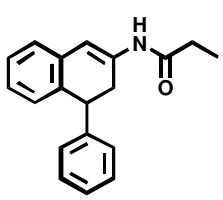

(±)-Compound **A**

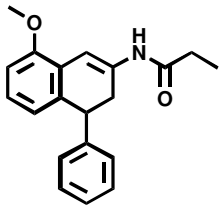

(±)-Compound **B**

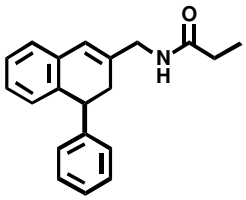

(±)-Compound **C**

As expected, compounds A and B showed a remarkable decrease in binding affinity for melatonin receptors,[309] suggesting that these compounds could not interact within the binding site with a pharmacophore-consistent pose. To further validate the hypothesis that the decreased binding affinity is mainly due to the non-perpendicular orientation of the NH group, a new compound was synthesized, in which an additional flexible methylene spacer was inserted between the dihydronaphthalene ring and the amide side chain (compound C). The inclusion of a flexible linker on the amide functionality allowed a better superposition of the pharmacophore features on those of compound 1 (Figure 44), bringing to a partial recovery of MT_2 binding affinity.[309]

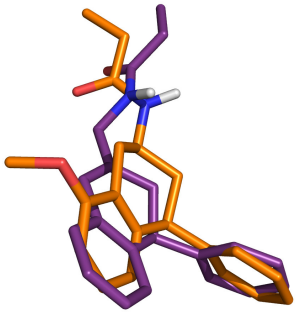

Figure 44: superposition of compound 1 (orange carbons) and compound C (violet carbons).

Phenlyalkylamides

Recently, a new series of melatoninergic ligands, characterized by a phenyl ring connected to the amide group through an ethyloxy or ethylthio chain, has been described.[264] Interestingly, the insertion of a methyl group on the alkyl chain strongly affected ligand binding affinity, depending on the stereo-configuration of the carbon atom carrying the methyl group.

	R	pKi MT$_1$	pKi MT$_2$	Compound[a]
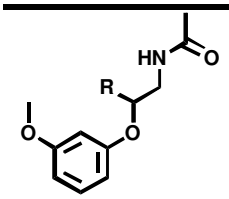	H	7.39	7.17	12d
	(*S*)-Me	8.77	8.33	(S)-7d
	(*R*)-Me	7.31	6.96	(R)-7d
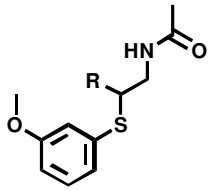	H	7.26	7.40	12e
	(*S*)-Me	8.24	8.15	(S)-7e
	(*R*)-Me	5.56	6.18	(R)-7e

[a] = compound names taken from ref. 264.

In both series, the introduction of a (*R*)-methyl group brought to a decrease in binding affinities for both melatonin receptors compared to the unsubstituted compound. On the contrary, the insertion of a (*S*)-methyl substituent brought to a slight increase in binding affinities for both MT$_1$ and MT$_2$ receptors.

These molecules retain the main pharmacophore features identified for melatoninergic agonists,[260] i.e., i) an aromatic ring, ii) an amide functionality and iii) a methoxy group bound to the aromatic nucleus (Figure 45). The higher binding affinity of the (S) enantiomer can be due favourable interactions with the receptor, or to an alteration of the conformational equilibrium of the acylaminoalkyl-oxy or –thio chain favoring a good superposition to the pharmacophore model for melatoninergic agonists.

To test the latter hypothesis, SD simulations were performed on the unsubstituted compound 12d and the (*S*)-methyl derivative (*S*)-7d to evaluate the impact of methyl insertion on the conformational equilibrium in solution.

Protocol

Starting conformations of 12d and (*S*)-7d were optimized using the OPLS2005 force field.[290] SD simulations were performed applying the OPLS2005 force field in implicit water. A time step of 1 fs was employed during equilibration (1 ns) and production (500 ns) phases of the SD simulations and temperature was set to 298 K. 10000 snapshots were collected for data analysis.

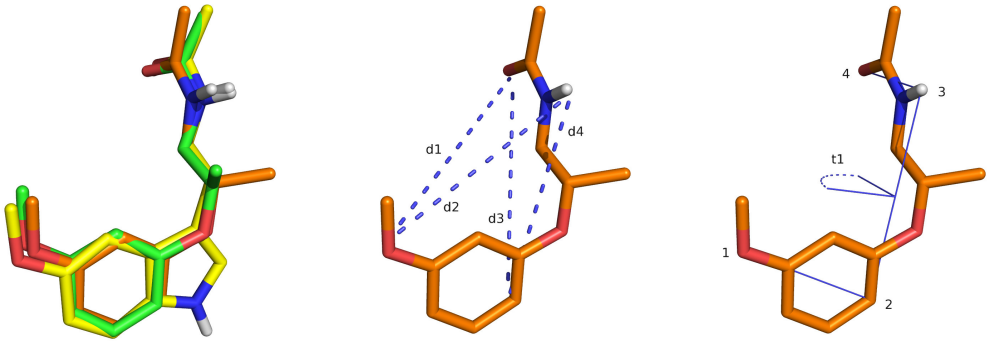

Figure 45: Left: superposition of melatonin (yellow carbons), compound (*S*)-7d of ref. 264 (orange carbons) and compound (*R*)-7d of ref. 264 (green carbons). Center and right: schematic representation of the four distances and the dihedral angle monitored for compound (*S*)-7d of ref. 264.

A set of 4 distances and 1 dihedral angle were monitored during SD simulations. Measured distances were compared to those found in the putative active conformation of melatonin, applying the following equation:

$$\text{Squared Deviation from Pharmacophore (SDP)} = \sum_{i=1}^{4} (di_{compound} - di_{melatonin})^2$$

The SDP gives a measure of the deviation from the "ideal" distances observed in the putative active conformation of melatonin. However, since SDP could not discriminate between mirror amide side chain arrangements with respect to the aromatic nucleus, the dihedral angle τ_1 (Figure 35, left) was used to assess the relative orientations of the amide functionality and the aromatic ring. The expected "ideal" value of τ_1 dihedral angle is 270°, corresponding to a sine value of -1.

Results

SD simulations revealed a different behavior of the unsubstituted compound compared to the (*S*)-methyl derivative. Indeed, an inspection of the first 100 snapshots having the lowest SDP values for compounds 12d and (*S*)-7d showed remarkable differences in the distribution of τ_1 values.

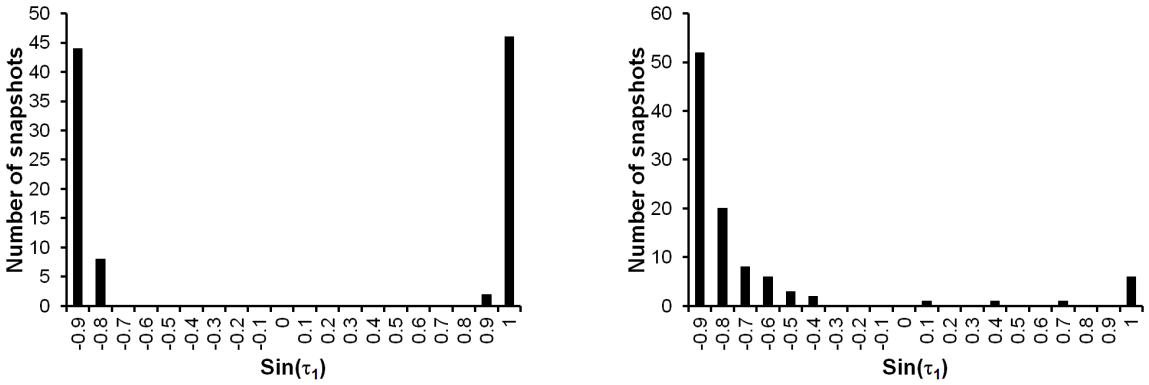

Figure 46: distribution of τ_1 values for compounds 12d (left) and (*S*)-7d (right) taken from the first 100 snapshots ranked by SDP.

As depicted in Figure 46, a roughly symmetrical distribution of τ_1 values could be observed for the unsubstituted 12d, indicating that the amide side chain could assume two specular conformations, both perperdicular to the phenyl ring: one extends below the plane of the aromatic ring (with $\sin(\tau_1)$ around -1, in the orientation depicted in Figure 45) while the other points above the aromatic nucleus (with $\sin(\tau_1)$ around 1). Conversely, for (*S*)-7d 72% of the 100 snapshots with best SDP values assume a conformation in which the amide side chain points below the plane of the phenyl ring and extend perpendicular to the aromatic plane ($-1 < \mathrm{Sin}(\tau_1) < -0.8$). Structures with this arrangement of the amide chain are superposable to the chiral pharmacophore model developed for melatoninergic agonists.[260] Only 6% of the best 100 snapshots assume an opposite orientation of the amide group, extended above the phenyl ring and not consistent with the agonists pharmacophore model.

In conclusion, these simulations suggest an atomistic explanation for the increased affinity of the (*S*)-enantiomers of the series compared to the unsubstituted derivatives. SD simulations showed that the insertion of the methyl substituent influences the conformational equilibrium of the alkyl chain, favoring an orientation similar to that observed in the putative active conformation of melatonin.

The two studies prevoiusly reported described a computational approach based on the screening of an ensamble of conformations (created through SD simulations) against a pharmacophore model, to try to rationalize the different binding affinity profiles observed among different derivatives. This procedure provided good indications regarding the ligand conformational abundances: these information were subsequently used to rationalize the differences in binding affinities for some melatoninergic compounds. Thus, although this

specific protocol requires an extensive validation process, it represents a feasible and computationally cheap approach that could be used to evaluate the ability of newly designed compounds to fulfill the structural requirements defined by the pharmacophore models.

CHAPTER 4

5-HT_{2C} serotonin receptor

Therapeutic relevance

Serotonin (5-hydroxytryptamine) is an important endogenous neuromodulator which is mainly located in the gastrointestinal tract, in platelets and in the central nervous system. More than 70% of the total amount of serotonin is synthesized in the enterchromaffin cells, whereas the remainder is synthesized in serotonergic neurons located in the central nervous system.[322] Serotonin was found to be involved in a variety of physiological and behavioral functions, including the regulation of cardiovascular system, muscle contraction, sleep, body temperature, weight, pain, mood, appetite and cognitive functions, including memory and learning.[323] For this reason, serotonin has been extensively studied as a prototypic therapeutic substance, useful in the treatment of obesity,[324] anxiety,[325,326] depression,[327] schizophrenia[328] and epilepsy.[329]

Receptor signalling pathways

The 5-HT$_{2C}$ receptor is mainly coupled to the G_q protein subtype, leading to the activation of phospholipase C and a consequent increase of intracellular calcium levels. Although G_q represents its main intracellular partner, it must be noted that the 5-HT$_{2C}$ receptor can also couple to other target effectors through the activation of other G protein subtypes.[330,331] 5-HT$_{2C}$ receptors are primarily expressed in the choroid plexus, where they decrease the secretion of the cerebrospinal fluid.[332] Beside the choroid plexus, 5-HT$_{2C}$ receptors are widely distributed among different brain regions, including the olfactory bulb, the substantia nigra, the hypothalamus, the hippocampus and the spinal cord.[333,334,335]

Modeling the 5-HT$_{2C}$ receptor: state of the art

So far, few homology models of the 5-HT$_{2C}$ receptor have been reported.

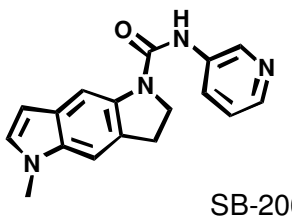

SB-206553

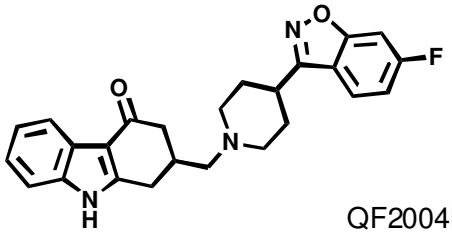

QF2004B

SmithKline research group described a 5-HT$_{2C}$ receptor model[336,337] in which only the transmembrane regions were built by the "active analogue approach"[338] and a standard cationic neurotransmitter template (a default template of GPCR_builder program) was used for model building. The antagonist SB-206553 was docked into the 5-HT$_{2C}$ receptor model: interactions were found between the carbonyl group of the ligand, Ser138$^{3.36}$ and Ser141$^{3.39}$ on TM3; moreover, the methyl substituent was accommodated in a pocket near two valines belonging to TM2 and TM6. No interactions were described with Asp134$^{3.32}$, supposed to be the receptor counterpart for serotonin amine group.

Brea *et al.* built a 5-HT$_{2C}$ receptor model[339] in which transmembrane regions were modeled and their packing was adjusted on the basis of the crystal structure of bovine rhodopsin. Ligand interactions were found with Cys127$^{3.25}$, Asp134$^{3.32}$ and Ser138$^{3.36}$.

Rashid *et al*. investigated the binding mode of sapogrelate, a serotonin antagonist, to 5-HT$_{2A}$, 5-HT$_{2B}$ and 5-HT$_{2C}$ receptors.[340] The 5-HT$_{2C}$ receptor model was built based on bovine rhodopsin as the template. Strong interactions were described between the ligand and Asp134$^{3.32}$ and an additional contact was found with Ser361$^{7.46}$.

Brea *et al*. proposed complete models of both 5HT$_{2A}$ and 5HT$_{2C}$ receptors,[341] built using bovine rhodopsin as template. The inverse agonist QF2004B docked into the 5-HT$_{2C}$ binding site interacted with Asp134$^{3.32}$ and Ser138$^{3.36}$; an additional interaction was found with a serine on TM2.

Another 5-HT$_{2C}$ receptor model was developed by Chavatte *et al.* using bovine rhodopsin as the template;[342] agomelatine was docked into the binding site, showing extensive interactions with Asp134$^{3.32}$, Ser138$^{3.36}$ and Asn204 belonging to ECL2. Docking of the bulky agonist lisuride revealed the same pattern of interactions seen for agomelatine, with key interactions involving Asp134$^{3.32}$, Asn204, Phe328$^{6.52}$ and Tyr358$^{7.43}$.

Finally, another rhodopsin-based 5-HT$_{2C}$ receptor model was published by Zuo *et al.*:[343] this receptor was investigated applying docking studies of agonist compounds, identifying Asp134$^{3.32}$, Ser138$^{3.36}$, Tyr358$^{7.43}$ as the putative binding elements.

Only recently, the first 5-HT$_{2C}$ receptor model built starting from the crystal structure of the β_2 adrenergic receptor in its inactive conformation was published.[188] The authors described the use of potent 5-HT$_{2C}$ antagonists to adapt the binding site region during MD simulations: to evaluate the ability of these 3D models to retrieve known 5-HT$_{2C}$ ligands, virtual screenings campaigns and docking studies were applied on these ligand-adapted receptors.

Template selection

At the time of this study, only the crystal structures of rhodopsin, opsin, β_1, β_2 and A_{2A} receptors were available. Calculated identity percentages between the human 5-HT$_{2C}$ sequence and available GPCR crystal structures within TM domains were 21%, 36%, 37% and 28% for rhodopsin, β_1, β_2 and A_{2A} receptor, respectively. In this case two receptors shared an identity percentage higher than 30% with the target sequence, being the human β_2 receptor the closest homologue: for this reason, it was chosen as the template structure.

Sequence alignment and model building

The X-ray crystal structure of the human β_2 receptor in complex with the inverse agonist timolol (PDB ID: 3D4S)[89] was selected as the template structure. The amino acid sequences of the β_2 and 5-HT$_{2C}$ receptors (UniProt IDs P07550 and P28335, respectively) were retrieved from the Universal Protein Resource.[267,268] Initial alignment was carried out with ClustalW2,[269] using default parameters and subsequently optimized considering conserved sequence motifs among class A GPCRs.[14,164] Highly conserved residues within TM domains, as well as the conserved disulfide bridge connecting ECL2 and TM3 have been taken into account during alignment refinement.

```
b2       WVVGMGIVMSLIVLAIVFGNVLVITAIAKFERLQTVTNYFITSLACADLVMGLAVVPFGAAHILMK-MWTFGNFWCE
5-ht2c   VQNWPALSIVIIIIMTIGGNILVIMAVSMEKKLHNATNYFLMSLAIADMLVGLLVMPLSLLAILYDYVWPLPRYLCP

b2       FWTSIDVLCVTASIWTLCVIAVDRYFAITSPFKYQSLLTKNKARVIILMVWIVSGLTSFLPIQMHWYRATHQEAINC
5-ht2c   VWISLDVLFSTASIMHLCAISLDRYVAIRNPIEHSRFNSRTKAIMKIAIVWAISIGVSVPIPVIGLRDEEKV-----

b2       YAEETCCDFF--TNQAYAIASSIVSFYVPLVIMVFVYSRVFQEAKRQL-----------KFCLKEHKALKTLGIIMG
5-ht2c   FVNNTTCVLN--D-PNFVLIGSFVAFFIPLTIMVITYCLTIYVLRRQA-----------QAINNERKASKVLGIVFF

b2       TFTLCWLPFFIVNIVHVIQDN----LIRKEVYILLNWIGYVNSGFNPLIYCRSPD-FRIAFQELLCL
5-ht2c   VFLIMWCPFFITNILSVLCEKSCNQKLMEKLLNVFVWIGYVCSGINPLVYTLFNKIYRRAFSNYLR-
```

Figure 47: alignment of β_2 and 5-HT$_{2C}$ sequences. Conserved residues within TM domains (X.50 positions) are in bold while TM domains of β_2 receptor crystal structure are underlined in grey.

As previously described, in the β_2 crystal structure the ICL3 portion was substituted with the T4-lysozyme to enhance receptor stabilization during the crystallization process: for this reason, residues 223 to 263 belonging to the β_2 adrenergic receptor are missing in the crystal structure and therefore were not considered during alignment building (Figure 47). The N- and C- termini of the β_2 adrenergic receptor were not solved due to their low

resolution: these portions were not modeled and they were excluded from the alignment. In the 5-HT$_{2C}$ receptor the ICL3 segment is formed by up to 50 amino acids. Since loop modeling algorithms proved to be feasible for sequences constituted by a maximum of 10-15 residues, the 5-HT$_{2C}$ cytoplasmic ends of TM5 and TM6 were linked by a bridge formed by 7 alanines. This connection allowed to preserve the relative distance between the tips of TM helices, favoring, at the same time, their α-helix propensity.[344,345,346,347,348]

The 5-HT$_{2C}$ homology model was built using Modeller software[270,271] applying standard parameters. 10 receptor models were initially built and the model characterized by the best value of the objective function implemented in the Modeller package was chosen. Hydrogens were added to the model structure and the protonation state of polar residues was calculated at a neutral pH; the hydrogen bond network was optimized by modifying polar hydrogens orientation. An initial minimization was applied to relax the major steric clashes, using a RMSD of 0.3 Å as convergence criterion.

The Ramachandran plot of the final 5-HT$_{2C}$ receptor is shown in Figure 48: only two residues belonging to loop segments and located far from the binding site were in disallowed regions: these geometrical deviations were fixed later.

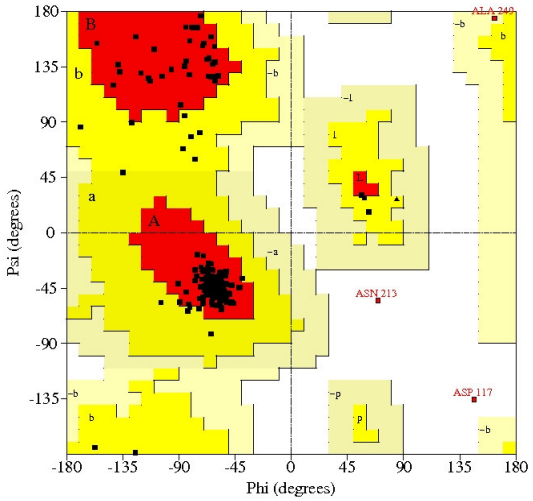

Figure 48: Ramachandran plot of the 5-HT$_{2C}$ receptor model.

Identification of binding site

Mutagenesis studies were used to identify the binding site location. Site-directed mutagenesis performed on the 5-HT$_{2C}$ receptor investigated only few residues, positioned on TM3 and TM5:[112,113,349] although they provided limited indications regarding the binding site location, these studies helped to clarify the key role of residues 3.32, 3.36 and 5.46 in

ligand binding (Figure 49). In addition, since the 5-HT_{2C} receptor binds and endogenous amine (serotonin), it is likely that the location of its binding site can be similar to that observed for other aminergic GPCRs, like β_1, β_2, D_3 and H_1 receptors.

Figure 49: location of key residues (thick red cartoons) within the 5-HT_{2C} receptor.

Binding mode hypothesis

For 5-HT_{2C} receptor mutagenesis data and information provided by ligand-based studies, such as pharmacophore models and SARs, have been used to guess an initial binding mode for potent 5-HT_{2C} ligands into the receptor model.

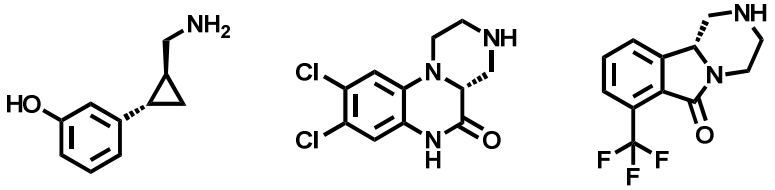

An alignment was initially performed for stereoselective agonists (see figure above) to assess the putative active conformation of the aminoethyl chain of serotonin.[350,351,352] Also in this case, a pattern of common pharmacophore features could be identified, comprising i) an aromatic core and ii) a basic amine group. The aminoethyl chain in the serotonin conformation showing the best fit has a C3-Cα-Cβ-NH_2 dihedral angle close to 180°. Similarly to what observed for melatonin, also in this case the aminoalkyl side chain of the endogenous molecule points below the plane of the indole ring (in the orientation depicted in the images below), extending perpendicularly to the indole plane (Figure 50).

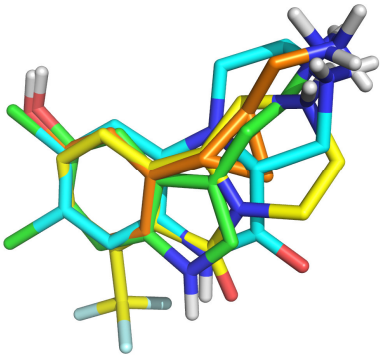

Figure 50: superposition of serotonin (green carbons), compound 40 of ref. 350 (orange carbons), compound 29 of ref. 351 (yellow carbons) and WAY161503 (cyan carbons). Compounds are depicted in their protonated state.

Receptor validation

Test set preparation

The set of 5-HT$_{2C}$ receptor antagonists used for docking studies is reported below along with the binding affinities. The set comprises both basic and non-basic antagonists, with different bulkiness.

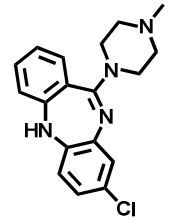

Clozapine
pKi 5-HT$_{2C}$ = 7.9

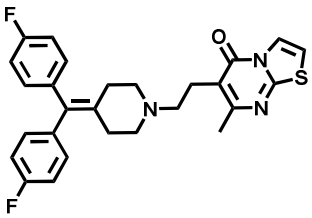

Ritanserine
pKi 5-HT$_{2C}$ = 9.7

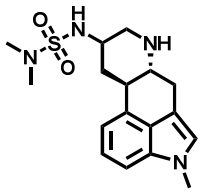

Mesulergine
pKi 5-HT$_{2C}$ = 9.0

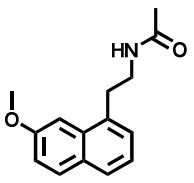

Agomelatine
pKi 5-HT$_{2C}$ = 6.2

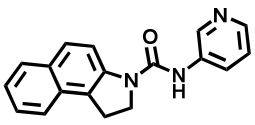

S32006
pKi 5-HT$_{2C}$ = 8.4

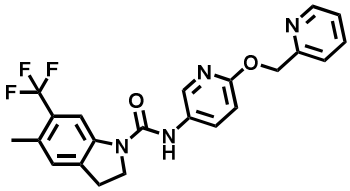

SB247853
pKi 5-HT$_{2C}$ = 9.3

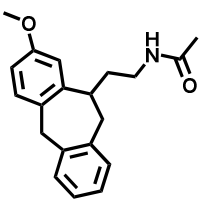

UCM546
pKi 5-HT$_{2C}$ = 6.7

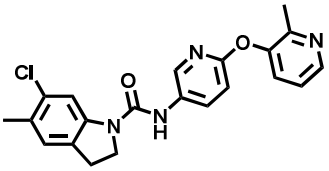

SB242084
pKi 5-HT$_{2C}$ = 9.0

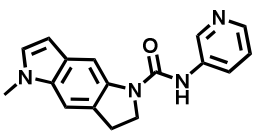

SB206553
pKi 5-HT$_{2C}$ = 7.9

Docking protocol

Glide grid was centered on Asp134$^{3.32}$ and Ser219$^{5.43}$. Enclosing and bounding boxes were retained at default dimensions and no scaling factors were applied on protein non-polar atoms. Van der Waals (vdW) radii of ligand non-polar atoms (i.e. atoms having a partial charge lower than ±0.15) were down-scaled to 0.8 during docking run to achieve a better ligand accommodation. No post-docking minimizations were performed and the Coulomb-vdW energy potential was increased to 100 kcal/mol to avoid discarding of poses with proper geometry, but with a high energy contribution due to steric hindrance. 20 poses were collected for each docking run and ranked using the Emodel score. The selection of the final pose was based on both ligand-receptor complementarity and available experimental information, such as mutagenesis studies and structure-activity relationships.

When the described protocol failed to find a suitable docking pose, the induced-fit docking protocol[353] implemented in Maestro software was applied: since it takes into account protein flexibility during docking process it could facilitate ligand accommodation into the binding site. Docking grids were centered on the same residues cited above and box dimensions were retained at default values. The induced fit workflow applied on the 5-HT$_{2C}$ receptor is summarized below:

1. Constrained minimization of the receptor with an RMSD cutoff of 0.18 Å
2. Initial Glide docking using a softened potential (scaling of van der Waals radii to 0.7 and 0.5 for receptor and ligand heavy atoms, respectively). Side chains of Phe223$^{5.47}$ and Phe328$^{6.52}$ were temporarily removed to facilitate ligand accommodation into the binding site.
3. Prime side chain prediction for each protein–ligand complex, applied on residues within 5 Å of any ligand pose. Side chains of Phe223$^{5.47}$ and Phe328$^{6.52}$ were re-introduced.
4. Prime minimization of each ligand-receptor complex.
5. Glide re-docking of each protein–ligand complex structure. The ligand is now rigorously docked, using default Glide settings (van der Waals radii scaling of 1 and 0.8 for receptor and ligand, respectively), into the induced-fit receptor structure.
6. Estimation of the binding energy for each output pose using a combination of Prime energy and GScore (IFDScore).

Results

The docking poses obtained for basic antagonists (i.e. clozapine, ritanserine and mesulergine) showed a similar accommodation, in which the aromatic core of the ligand is placed in a cavity between TM6 and TM5, forming extensive hydrophobic/π-π interactions with Phe223$^{5.47}$, Phe327$^{6.51}$ and Phe328$^{6.52}$ (Figure 51). Moreover, the ligand protonated nitrogen interacted with the conserved acid residue (Asp134$^{3.32}$) on TM3 through a salt bridge.

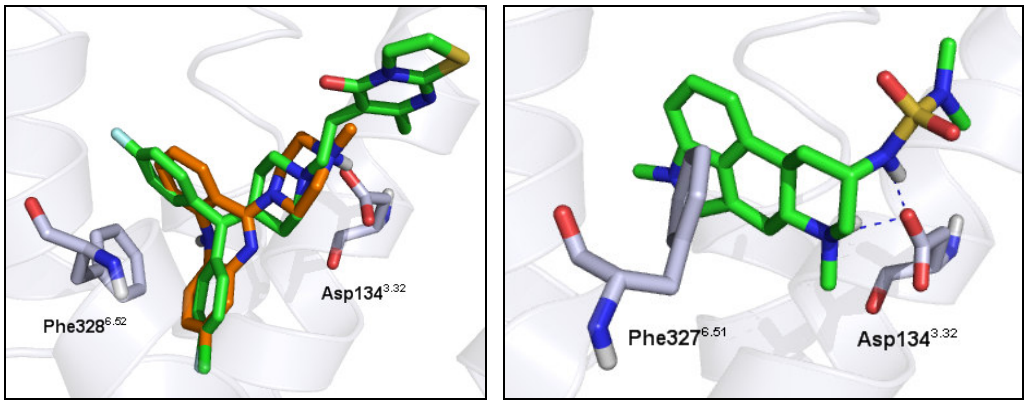

Figure 51: Left: clozapine (orange carbons) and ritanserine (green carbons) docked into the 5-HT$_{2C}$ receptor model. Right: proposed binding mode of mesulergine (green carbons) into the 5-HT$_{2C}$ receptor model.

While mutagenesis data supported the key role of Asp134$^{3.32}$ residue in ligand binding at the 5-HT$_{2C}$ receptor,[112,113] no direct data is available for Phe223$^{5.47}$, Phe327$^{6.51}$ and Phe328$^{6.52}$. However, mutagenesis data retrieved from the 5-HT$_{2A}$ receptor subtype showed that Phe$^{5.47}$ is involved in the binding of serotonin[354] and, more generally, of serotoninergic agonists. Moreover, Phe$^{6.51}$ and Phe$^{6.52}$ residues are involved in ligand binding, since their mutation to leucine brought to a decrease in serotonin affinity for 5-HT$_2$ receptor subtypes.[355]

The binding mode observed for rintanserine and mesulergine is similar to that proposed in a recent publication,[188] in which a 5-HT$_{2C}$ receptor model was optimized and refined using potent 5-HT$_{2C}$ antagonists.

Once the ability of our receptor model to accommodate potent charged antagonists was assessed, further docking studies were performed with non-charged compounds. UCM546 and agomelatine were selected as representative neutral antagonists, having binding affinities in the micromolar range for the 5-HT$_{2C}$ receptor. Docking studies showed a similar binding mode for these ligands, where the naphthalene core of agomelatine and

the tricyclic ring of UCM546 laid in the hydrophobic cavity previously described, delimited by Phe223$^{5.47}$, Phe327$^{6.51}$ and Phe328$^{6.52}$ (Figure 52, left). As depicted in Figure 52, the aromatic rings of both UCM546 and agomelatine form π-π interactions with the side chain of Phe328$^{6.52}$. Moreover, an additional H-bond interaction is observed between Asn331$^{6.55}$ side chain and the methoxy group of UCM546: mutagenesis studies made on the β_2 adrenergic receptor showed that this residue plays a crucial role in agonist recognition and in receptor activation.[356]

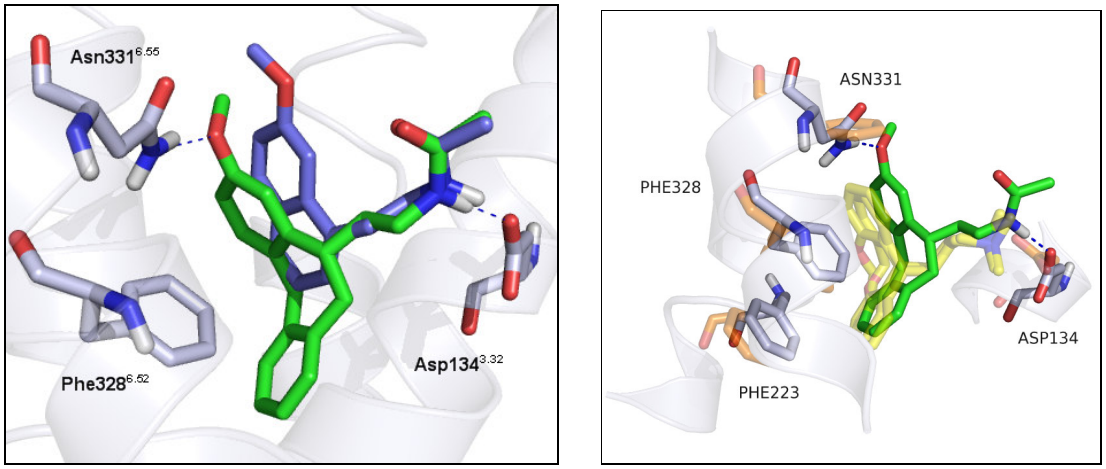

Figure 52. Left: agomelatine (purple carbons) and UCM546 (green carbons) docked into the 5-HT$_{2C}$ receptor model. Right: superposition of the 5-HT$_{2C}$ (grey carbons)-UCM546 (green carbons) complex and the H_1 histamine receptor (orange carbons) co-crystallized with doxepin (yellow carbons).

Interestingly, the conformation of UCM546 into the 5-HT$_{2C}$ binding site is similar to that observed for doxepin into the H_1 histamine receptor (Figure 52, right).[65] These compounds share a common 6-7-6 ring system and an aminoethyl chain connected to the 7-membered ring. While the amino group of both compounds interacts with the conserved acid residue Asp$^{3.32}$ on TM3, the tricyclic core is accommodated deeply into the binding site crevice, near positions 5.47 and 6.52.

The third set of 5-HT$_{2C}$ antagonists included carbomoyl-indolines derivatives: nowadays these compounds represent the most important class of neutral and selective 5-HT$_{2C}$ receptor antagonists. Docking studies showed a common binding orientation for all the ligands tested, in which the ligand molecule adopted an extended conformation that spanned from TM5 to TM2 (Figure 53).

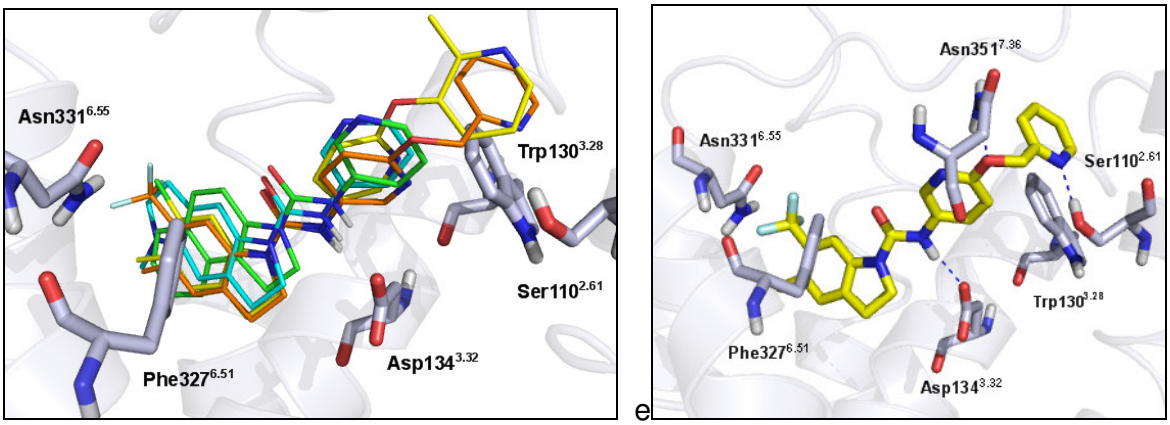

Figure 53. Left: a set of carbomoyl-indoline compounds docked into the 5-HT$_{2C}$ receptor model: S32006 (green carbons), SB242084 (yellow carbons), SB247853 (orange carbons) and SB206553 (cyan carbons). Right: best pose obtained for SB247853 into the 5-HT$_{2C}$ receptor binding site.

The indoline core is positioned near TM5 and TM6, forming extensive hydrophobic interactions with Phe327$^{6.51}$ and Phe328$^{6.52}$. The amide group of Asn331$^{6.55}$ is close to the H-bond acceptor group attached to position 6 of the indoline core, such as CF_3 of SB247853 or the chlorine atom of SB242084. The ureidic NH group interacts with the conserved aspartic acid on TM3 (Asp134$^{3.32}$) through a H-bond interaction. While the pyridine ring bound to the urea group was sandwiched between Leu209 (ECL2) and Val354$^{7.39}$, the terminal pyridine of both SB247853 and SB242084 was accommodated in a cavity between helices 2 and 3, delimited by Trp130$^{3.28}$, Ser110$^{2.61}$ and Ile114$^{2.65}$. In addition, Asn351$^{7.36}$ could form a H-bond interaction with the oxygen atom of SB247853 attached to the pyridine ring (Figure 53, right).

This accommodation of carbamoyl-indoline derivatives resemble the one observed in a recent publication, in which a wider set of compounds has been docked into an optimized 5-HT$_{2C}$ receptor model.[188] Although the overall accommodation of compounds is very similar in both receptor models, there are also some subtle but critical differences. Indeed, in the previously published 5-HT$_{2C}$ receptor model, Arg195$^{4.66}$ on TM4 forms a H-bond interaction with the ureidic oxygen, and Asn210 located on ECL2 can interact with the acceptor groups bound to position 6 of carbamoyl-indoline core. These small differences are probably due to the different approaches used for the homology modeling procedure and for the optimization phase.

Taken together, these results showed that our receptor model was able to accommodate a set of diverse 5-HT$_{2C}$ antagonists into the ligand binding site. Docking poses obtained for these compounds were consistent with available mutagenesis studies, made either on the 5-HT$_{2C}$ receptor or on other different serotoninergic receptors subtypes.

MD simulations in a solvated lipid bilayer

For the 5-HT$_{2C}$ receptor, a MD simulation was performed in a solvated lipid bilayer to evaluate i) the stability of the main ligand-receptor interactions and ii) the main protein rearrangements that occur upon ligand binding.

Protocol

S32006 (see below) was initially docked into the 5-HT$_{2C}$ receptor model using the docking procedure described above: the resulting complex was energy-minimized and used as input for the MD simulation.

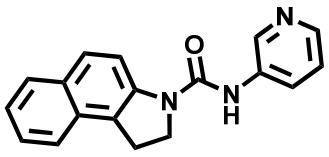

S32006
pKi 5-HT$_{2C}$ = 8.4

Desmond v2.2[296] was used to built the system and to set up the dynamics simulation. Protein-ligand complex was embedded in a POPC lipid bilayer by aligning the receptor to the 2RH1 crystal structure deposited into the Orientations of Protein in Membranes database (OPM),[297] with at least 13 Å between the protein and its closest periodic image. Protein-membrane system was solvated by approximately 9700 SPC water molecules in a simulation box of approximately 80 Å x 70 Å x 100 Å. The Amber99SB force field[298] was used to model the protein, while ligand and lipids were parameterized using the GAFF.[299] The system was relaxed using a modified version of a membrane relaxation protocol implemented in the Schrodinger 2009 Suite, summarized below:

1. System was energy-minimized with 2000 steps of steepest-descent with a convergence gradient of 50 kcal/(molÅ). All protein heavy atoms were constrained with a force constant of 50 kcal/(molÅ^2).
2. System was energy-minimized with 2000 steps of steepest-descent with a convergence gradient of 5 kcal/(molÅ). All atoms were free to move.
3. 60 ps-long MD simulation in the NVT ensemble was run using the Langevin barostat and thermostat.[301] Temperature was linearly increased from 10 to 310 K and protein heavy atoms were constrained with a force constant of 50 kcal/(molÅ^2), that linearly decreased to 10 kcal/(molÅ^2). In the initial system, the protein was inserted into a pre-equilibrated lipid bilayer through a “replacement” methodology, in

which the lipid molecules whose center of mass overlap that of the protein residues were deleted from the membrane: this procedure built a “hole” into the membrane bilayer to accommodate the protein. Although the membrane tried to adapt itself around the protein structure, empty spaces are always present between the protein and the lipid molecules. To avoid the penetration of water molecules into the membrane bilayer, a gaussian potential was applied during the NVT simulation.

4. 200 ps-long MD simulation in the NPT ensemble was run using the Langevin barostat and thermostat. Temperature was set to 310 K and the Gaussian potential inserted in the previous step was retained. Protein heavy atoms were constrained with a force constant of 10 kcal/(molÅ^2).
5. 100 ps-long MD simulation on the NPT ensemble was run using the Langevin barostat and thermostat. Temperature was set to 310 K but the Gaussian potential was removed. Constraints were the same used in the previous step.
6. 600 ps-long MD simulation on the NPT ensemble was run using the Langevin barostat and thermostat. Temperature was set to 310 K and positional constraints were applied on both ligand and protein heavy atoms. The constraint force was linearly decreased from 10 kcal/(molÅ^2) to 2 kcal/(molÅ^2) during the simulation.
7. 100 ps-long MD simulation on the NPT ensemble was run using the Langevin barostat and thermostat, with a temperature of 310 K. Positional constraints were applied only on protein alpha carbons with a force constant of 2 kcal/(molÅ^2).
8. A final equilibration step of 100 ps was performed using the NPT ensemble, applying no constraints.

The production phase of the simulations was performed in the NPT ensemble under constant pressure of 1 atm and a temperature of 310 K, thermostated and barostated using the Langevin method. All bond lengths to hydrogen atoms were constrained using M-SHAKE.[302] Short-range electrostatic interactions were cut off at 9 Å whereas long-range electrostatic interactions were computed using the Particle Mesh Ewald method.[303] A RESPA integrator[304] was used with a timestep of 2 fs, and long-range electrostatics were computed every 6 fs. The production phase of the MD simulations was 10 ns-long.

Results

The root mean squared deviation (RMSD) calculated on TM alpha carbons showed a plateau at 1.8-2 Å, confirming the stability of the receptor secondary and tertiary structures (Figure 54, left).

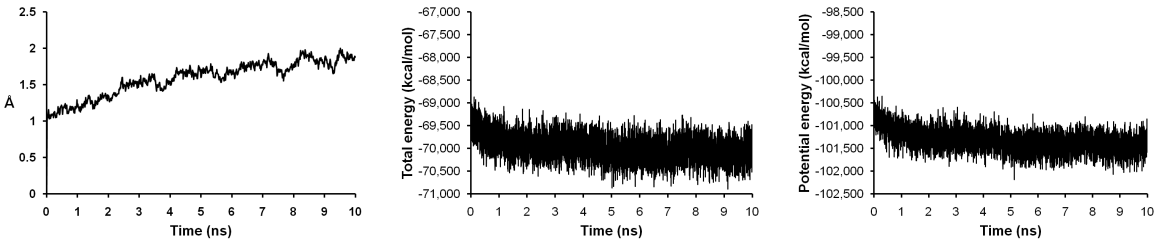

Figure 54: Left: RMSD graph calculated on transmembrane alpha carbons. Center: time evolution of the total energy during the MD simulation. Right: time evolution of the potential energy during the MD simulation.

The time evolution of the total energy of the system and of the potential energy (Figure 54, right and center) confirmed the stability of the complex during MD simulation: indeed, both energies reached a plateau at 2-3 ns that was retained till the end of the simulation. As depicted in Figure 55, the temperature oscillated around the equilibrium value of 310 K, confirming the energetic stability of our MD simulation.

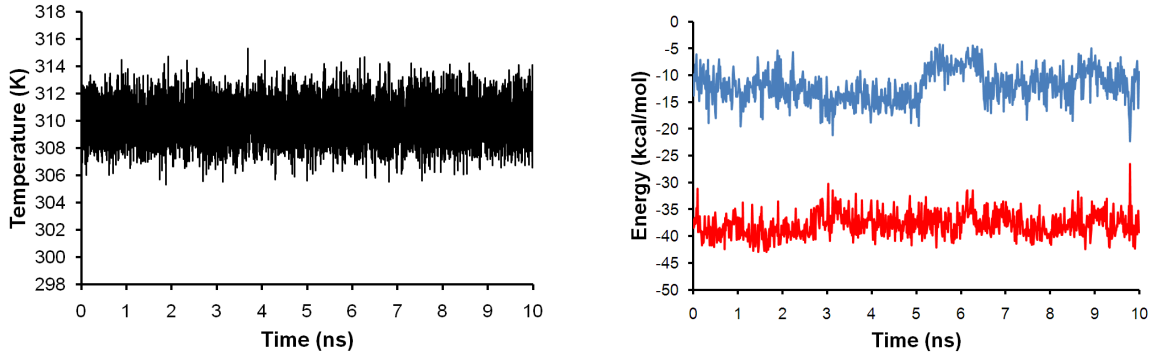

Figure 55: Left: time evolution of the temperature along the MD trajectory. Right: time evolution of Coulombic (blue) and van der Waals (red) energies.

The time evolution of long-range electrostatic interactions (Coulombic) and van der Waals energies could be used as additional criteria to evaluate the degree of convergence of a MD simulation: in this case, both van der Waals and Coulombic energies stabilized to equilibrium values around 3-4 ns (Figure 55, right). Once the energetic profile of MD simulation was inspected, we evaluated the behavior of the main ligand-receptor interactions through the whole trajectory.

As described previously for the carbomoyl-indoline 5HT$_{2c}$ antagonists, S32006 was accommodated in a pocket delimited by TM3, TM5, TM6 and TM7. It formed extensive hydrophobic interactions with a subset of aromatic residues located on TM6 and TM5 (e.g., Phe327$^{6.51}$ and Phe328$^{6.52}$) and undertook a hydrogen bond with Asp134$^{3.32}$. Moreover, the pyridine nitrogen could form an additional H-bond with the side chain of Asn351$^{7.36}$. During the MD simulation S32006 retained its starting accommodation, as well as the main interactions with residues located on TM5 and TM6 and with the conserved Asp134$^{3.32}$ (Figure 56, left). A transient H-bond interaction was observed between the pyridine nitrogen and Asn351$^{7.36}$ side chain. This might be due to the shift of the naphthalene portion of S32006 towards Phe327$^{6.51}$ and Phe328$^{6.52}$: this movement brought the pyridine nitrogen far from TM7 and, consequently, from the Asn351$^{7.36}$ side chain (Figure 56, right).

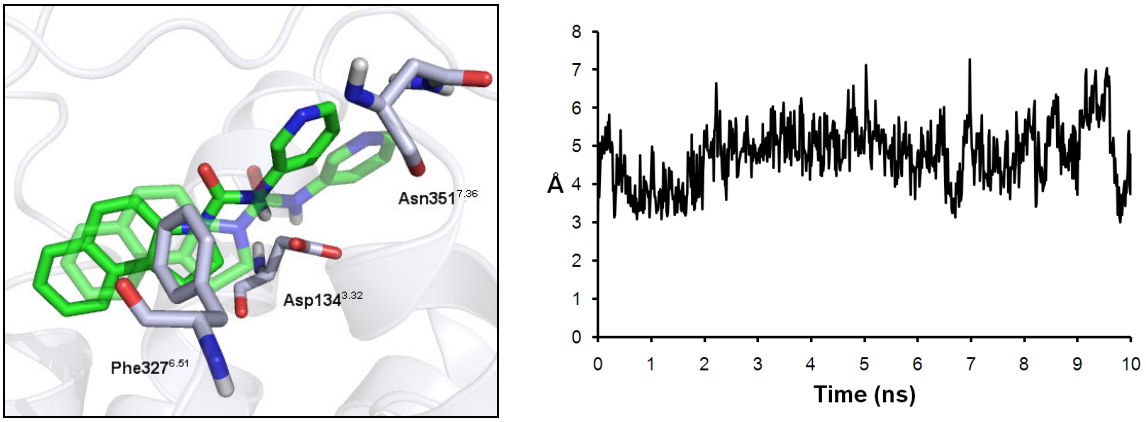

Figure 56: Left: starting (transparent) and final (opaque) conformation of S32006 (green carbons) retrieved from MD simulation. Right: time evolution of the N-N distance between Asn351$^{7.36}$ side chain and the pyridine nitrogen of S32006.

In contrast with what has been observed in a previously published 5-HT$_{2C}$ receptor model,[188] the carbonyl group did not interact with residues located near the binding site region. Indeed, the carbonyl group of S32006 laid near ECL2 and was directly exposed to solvent molecules. During the equilibration phase of the MD simulation, water molecules moved into the receptor binding cavity and solvated the carbonyl group of S32006, preventing its interactions with neighboring residues (Figure 57, left). Consequently, many water-mediated interactions were formed between the carbonyl oxygen and the residues of ECL2 segment (Figure 57, right). Particularly, a water-mediated H-bond interaction was formed between the carbonyl oxygen of S32006 and the backbone NH group of Asp211 residue. This H-bond network was also stabilized by a salt bridge between the side chains of Arg195 and Asp211 belonging to ECL2: this ionic interaction forced the positively

charged chain of Arg195 to form a favorable cation-π interaction with the naphthalene ring of S32006.

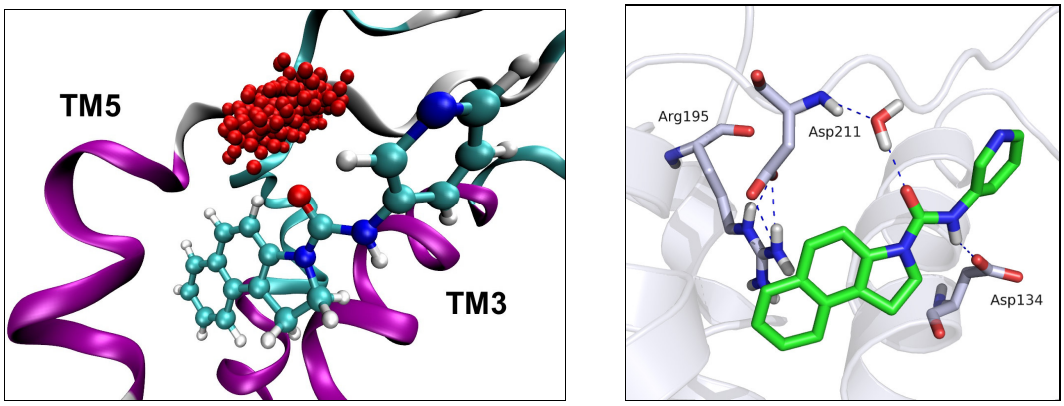

Figure 57: Left: positions of water oxygens within 2 Å from the carboxyl oxygen of S32006 for all the frames of the trajectory. Right: frame taken from MD trajectory. S32006 is colored with green carbons and residues are depicted with gray sticks.

CHAPTER 5

A_{2A} adenosine receptor

Therapeutic relevance

Adenosine is a fundamental endogenous nucleoside, continuously released on both extracellular and intracellular sides of the cell. However, while the intracellular production involves specific enzymatic reactions,[357,358,359] the extracellular release is mediated by the action of other neurotransmitters, such as NMDA or kainate.[360,361] The primary function of adenosine is to act as a signal of metabolic distress during severe tissue injuries such as hypoxia, ischemia or inflammation.[362] In this scenario, adenosine promotes tissue protection through different mechanisms, including the increase of oxygen demand, the conditioning of cells against ischemic damages and the trigger of anti-inflammatory cascades.[363] Beside its cytoprotective functions, adenosine has also been recognized to play a key role in a variety of physiological processes, like sleep,[364] the regulation of heart rate and contractility,[365,366] vasodilation,[362] behavioral stimulation,[367,368] pain perception,[369] neuroprotection[370] and the regulation of cell growth and proliferation.[371] Due to the pleiotropic effects of this endogenous substance and the wide distribution of adenosine receptors in tissues, the use of either agonist or antagonist ligands has been proposed for the treatment of numerous diseases, including arrhythmia,[372,373] ischemia,[374] hypertension,[375] Parkinson's disease,[376,377] epilepsy,[378] chronic obstructive pulmonary disease,[379] asthma,[380] cancer,[381] and diabetes.[382]

Nowadays, four different types of adenosine receptors have been identified and characterized in humans, namely A_1, A_{2A}, A_{2B} and A_3. All four receptors belong to the superfamily of GPCRs and each of them owns its peculiar pharmacological properties, tissue distribution and transduction signalling pathways.[383]

Due to the crucial role played by adenosine in humans as well as its several therapeutic applications, an increased interest has grown for the development of selective and potent adenosine agonist and antagonist molecules. However, despite the increasing efforts in the design of novel chemical entities, only adenosine itself is currently marketed (Adenocard) for the treatment of supraventricular tachycardia. The paucity of marketed adenosine receptor ligands could be due to i) the ubiquity of adenosine receptors that facilitate the onset of side effects and ii) the species-specificity of ligand binding affinities, that complicate the readability of preclinical results.

Due to the broad spectrum of clinical applications in which adenosine compounds could be involved, nowadays the design of new chemical entities able to target and interact with

adenosine receptors represents a critical field of the current medicinal chemistry landscape.

Receptor signalling pathways

The A_{2A} adenosine receptor is mainly coupled to the G protein subtype G_s, whose activation causes an increase in intracellular cAMP concentrations mediated by adenylyl cyclase. Beside the key role of the G_s protein in the A_{2A}-mediated signal transduction mechanism, other G protein partners can couple with this receptor. For example, it has been shown that in rat striatal neurons the A_{2A} receptor subtype exerts its action through the G_{olf},[384] a G protein similar to G_s. Experimental evidences employing chimeric A_1/A_{2A} receptors indicated that the cognate G_s protein binds to specific receptor features located in the ICL3 but not in the C-terminus segment of the A_{2A} receptor.[385]

Available crystal structures

Nowadays, 7 different crystal structures of the A_{2A} adenosine receptor are available in the protein data bank: while 4 of them are co-crystallized with antagonists, 3 are co-crystallized with agonist molecules.

As described previously, although the overall arrangement of the TM bundle is similar to that observed in other X-ray crystal structures of GPCRs, the A_{2A} receptor shows some remarkable differences compared to other class A GPCRs. For example, the ECL2 portion of the A_{2A} receptor is characterized by a complex structure, constrained by a network of three cysteine bridges and several secondary structural elements. The three disulphide bridges (Cys71(ECL1)-Cys159(ECL2), Cys74$^{3.22}$(TM3)-Cys146(EC2), Cys77$^{3.25}$(TM3)-Cys166(ECL2)) strongly link ECL2 to TM3 and ECL1, defining a stable network of interactions delimiting the binding site region. In addition to these cysteine bridges, a short β-sheet formed by Val164 and Ala165 and an α-helix structure from Leu167 to Val172 further stabilize the geometry of the ECL2, as well as of the binding site crevice. Moreover, a fourth disulphide bond within ECL3 segment (Cys259-Cys262) leads to an overall stabilization of the whole extracellular portion of the A_{2A} receptor structure. This network of covalent and polar interactions within extracellular loops stabilizes a open conformation of the binding site entrance, completely exposed to the solvent, facilitating ligand

accommodation. Loop geometries strongly influence the shape of the binding cavity, that extends vertically between TM5, TM6 and TM7. Due to its position, ECL2 directly interacts with co-crystallized molecules and play a crucial role in shaping the binding site cleft. Mutagenesis studies already highlighted the importance of Phe168 and Glu169 belonging to the ECL2 for both agonist and antagonist binding:[170,386,387] according to experimental evidences, these two residues protrude into the binding crevice, forming extensive interactions with co-crystallized ligands. Another polar contact that could be found in the extracellular portion of the receptor links Glu169 on ECL2 with His264 on ECL3. Indeed, in the first crystal structure of the A_{2A} receptor co-crystallized with the adenosine-like antagonist ZM241385 (PDB: 3EML),[62] His264 belonging to the ECL3 segment forms H-bond interactions with Glu169 side chain placed on ECL2. It is likely that this additional polar interaction forces Glu169 side chain to form favorable contacts with the NH_2 functionality of the antagonist molecule. However, it is not possible to exclude that this Glu169-His264 H-bond could be an artifact due to crystallization conditions: indeed, in the recent A_{2A}-ZM241385 complex crystallized using a thermostabilized receptor, His264 points away from the binding site (Figure 58, left), without interacting with Glu169 side chain.

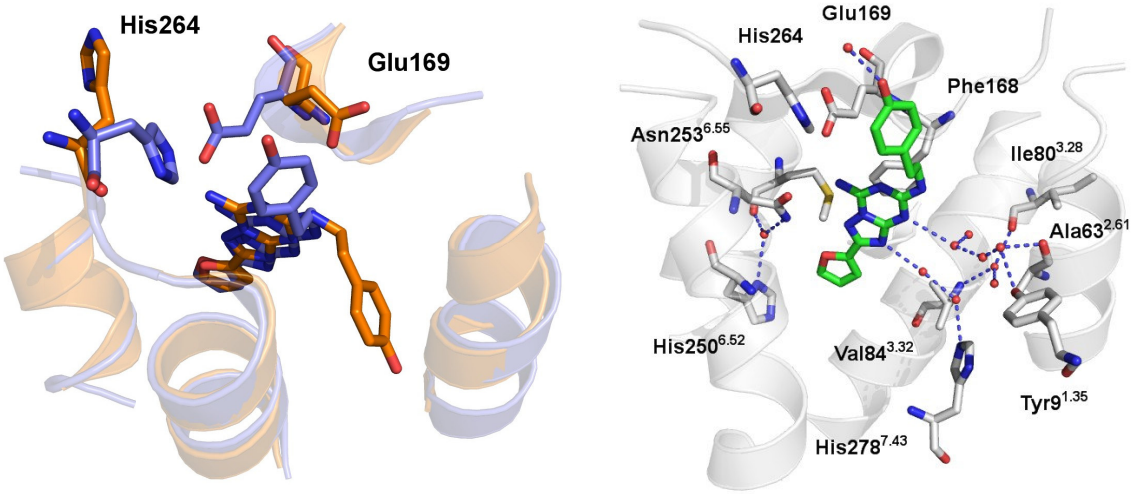

Figure 58: Left: superposition of two different crystal structures of the A_{2A} adenosine receptor in complex with the antagonist ZM241385: 3EML is depicted in blue, whereas 3PWH is depicted in orange. Right: close view of the binding site region of the A_{2A}-ZM241385 complex (PDB: 3EML, white carbons). Water molecules forming H-bonds with the ligand or neighboring residues are depicted with red spheres. ZM241385 is represented with green carbons.

Interestingly, the two crystal structures of the A_{2A}-ZM241385 complex were obtained applying different pH conditions: indeed, while 3EML was crystallized using a pH of 5.5-6, the new thermostabilized structure was solved in a more basic environment, with a pH of

about 8-8.75. This difference in crystallization procedures probably affected the protonation state of amino acids delimiting the binding site region, including His264: in this scenario, it is likely that the major differences observed for either polar or hydrophobic contacts occurring within the binding site regions of the two complexes were due to the different experimental protocols applied during the crystallization phase.

As described previously, the ligand binding site is exposed to solvent. As a consequence, several water molecules penetrate into the binding cleft, forming extensive contacts with the co-crystallized ligand (Figure 58, right). However, these water molecules could be observed only in the first crystal structure of the A_{2A} adenosine receptor in complex with ZM241385.[62] Thus, it is not possible to identify conserved water molecules among available X-ray structures of the A_{2A} receptor. 11 water molecules could be found in a shell of 6 Å centered on the co-crystallized antagonist (PDB: 3EML): these hydration sites form an extensive network of H-bond interactions with both the antagonist molecule and neighboring residues, leading to an overall stabilization of the ligand conformation into the binding site region. The ligand molecule is further stabilized by an extensive network of polar and hydrophobic interactions with amino acids delimiting the binding cavity. For example, while the furan ring of ZM241385 is sandwiched between Leu85$^{3.33}$, Met177$^{5.38}$ and Leu249$^{6.51}$, the main triazolo-triazin core is stabilized by a π-π interaction with Phe168 located on ECL2 and by additional hydrophobic contacts with Leu249$^{6.51}$ and Ile274$^{7.39}$.

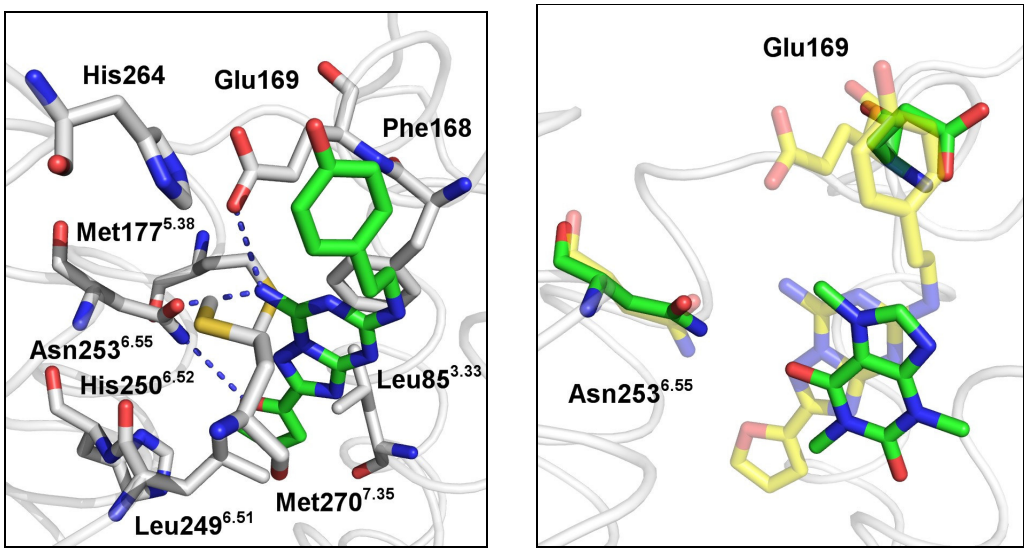

Figure 59: Left: close view of the binding site of the A_{2A}-ZM241385 complex (PDB: 3EML, white carbons). H-bond interactions between the co-crystallized antagonist and surrounding residues are depicted with dashed blue lines. ZM241385 is represented with green carbons. Right: superposition of caffeine (PDB: 3RFM, green carbons) and ZM241385 (PDB: 3EML, yellow transparent carbons) into the A_{2A} receptor binding site.

Two residues shown to be crucial for ligand binding,[170,386,387] namely Asn253$^{6.55}$ and Glu169, form a network of H-bond interactions with both the furan substituent and the triazolo-triazin ring of the co-crystallized antagonists (Figure 59).

In the xanthine-bound crystals of the A_{2A} adenosine receptor, a similar pattern of polar and hydrophobic interactions are observed. Indeed, also in the case of caffeine-A_{2A} and XAC-A_{2A} complexes, the xanthine core is located at the bottom of the binding cavity, sandwiched between Phe168, Leu249$^{6.51}$ and Ile274$^{7.39}$. Conversely, the bulky substituent bound to position 8 of the xanthine ring of XAC extends towards the extracellular part of the receptor: this terminal portion accommodates into an additional cleft between TM1, TM2 and TM7, formed by Tyr9$^{1.35}$, Leu267$^{7.32}$ and Tyr271$^{7.36}$ (Figure 60).

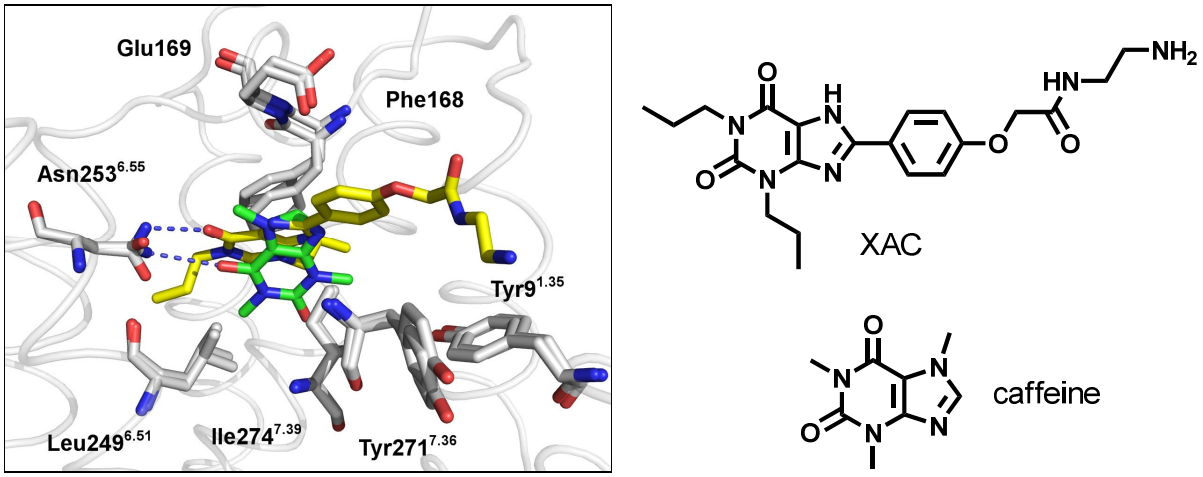

Figure 60: close view of the binding site region of the caffeine-A_{2A} (PDB: 3RFM) and the XAC-A_{2A} (PDB: 3REY) complexes. XAC and caffeine are depicted with yellow and green carbons, respectively. H-bonds between the xanthine core and Asn253$^{6.55}$ are depicted with blue dashed lines.

Interestingly, in the alternative binding mode observed for ZM241385, the terminal phenol group accommodates in an additional pocket between TM1, TM2 and TM7: however, the terminal aromatic portion of ZM241385 tends to occupy a slightly different volume, more shifted towards TM2 and less exposed to the solvent (Figure 61). Nevertheless, structural data clearly showed the presence of a peculiar cleft located in the proximity of the tips of TM1, TM2 and TM7 for both adenosine-like and xanthine A_{2A} antagonists. Since binding affinities shown by both XAC and ZM241385 (pKi ~9) [388,389,390] are higher than that of caffeine (pKi ~6),[391] it could be hypothesized that substituents able to target this additional crevice might increase the ligand binding affinity.

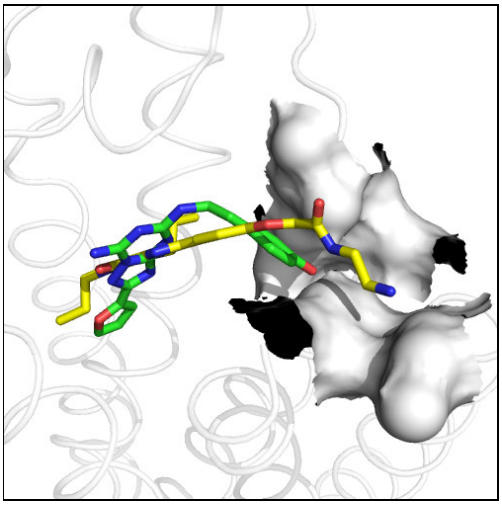

Figure 61: superposition of the binding site regions of XAC-A_{2A} (PDB: 3REY) and ZM241385-A_{2A} (PDB: 3PWH) seen from the extracellular side. XAC and ZM241385 are depicted with yellow and green carbons, respectively. The additional pocket between TM1 and TM7 is represented with white surface.

Since this study was mainly focused on the design of novel A_{2A} antagonists, only the X-ray structures crystallized in their inactive state were used to perform docking studies and MD simulations: as a consequence, agonist-bound forms of the A_{2A} adenosine receptor were not included in the current analysis.

Docking studies within the A_{2A} adenosine receptor

At the time of this work, only the A_{2A} receptor crystal structure in complex with ZM241385 was available (PDB: 3EML).[62]

A set of potent A_{2A} antagonists, belonging to different chemical classes, was used to evaluate the consistency between ligand binding poses and available information, such as SARs and mutagenesis data.

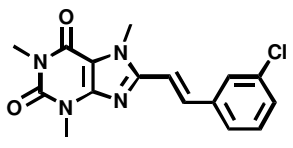

CSC (Compound 1)
Ki = 36 nM
(from J. Med. Chem. 1997,40,4396)

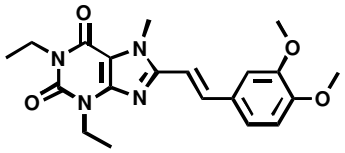

KW-6002 (compound 2)
Ki = 2.2 nM
(from Bioorg. Med. Chem. Lett. 1997,18,2349)

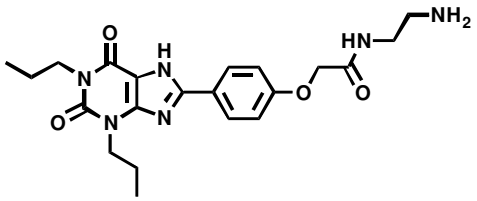

XAC (compound 3)
Ki = 3.6 nM
(from Br. J. Pharmacol. 1997, 121, 353)

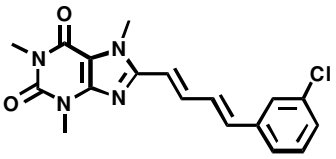

Compound 4
Ki = 104 nM
(from Bioorg. Med. Chem. 2008, 16, 8676)

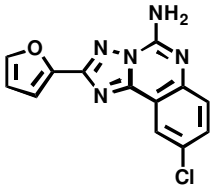

CGS15943 (Compound 5)
Ki = 0.53 nM
(from Br. J. Pharmacol. 1997, 121, 353)

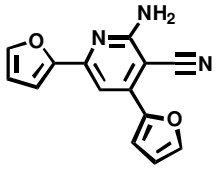

Compound 6
Ki = 1 nM
(from J. Med. Chem. 2008, 52, 4449)

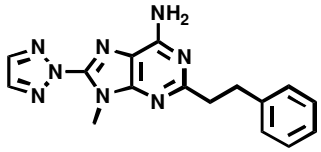

Compound 7
Ki = 4.7 nM
(from J. Med. Chem. 2005, 48, 6887)

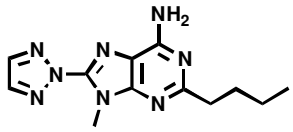

Compound 8
Ki = 6.6 nM
(from J. Med. Chem. 2005, 48, 6887)

Receptor structure refinement

The 3D structure of the A_{2A} adenosine receptor in complex with ZM241385 was retrieved from the PDB (PDB: 3EML)[62] and all the non-protein elements were deleted. As stated previously, the ICL3 segment of GPCRs is characterized by a remarkable flexibility, that could hamper the crystallization process: for this reason, in the A_{2A} crystal structure the ICL3 portion was substituted with a lysozyme molecule to decrease the overall intrinsic instability of the receptor structure. Beside the ICL3 segment, another portion showing high flexibility in the A_{2A} receptor structure is the N-terminus of the ECL2: indeed, no

diffraction data was available for residues from 149 to 155, indicating a high intrinsic instability for this small cluster of residues. Thus, to obtain a complete set of 3D coordinates for the A_{2A} adenosine receptor, Modeller 9.4[270,271] was used to re-built both the ICL3 portion and the small segment belonging to the ECL2.

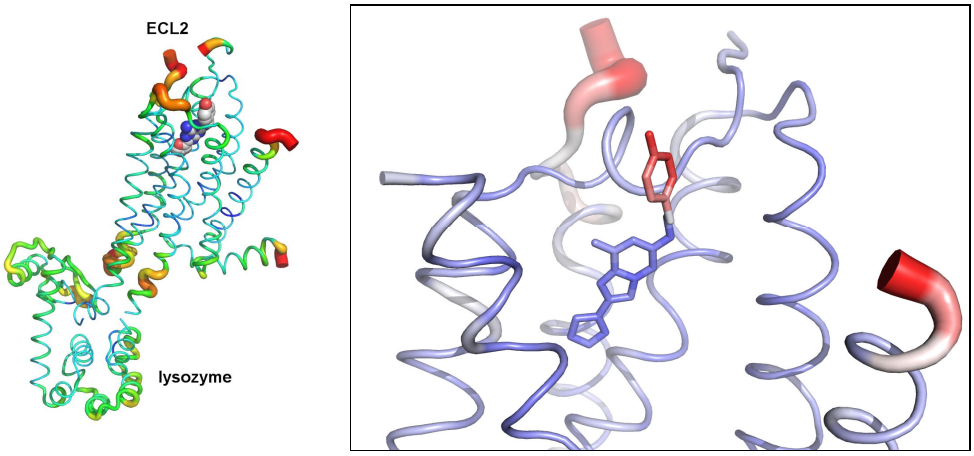

Figure 62: Left: ZM241385-A_{2A} crystal structure (PDB: 3EML). The cartoons thickness and color depend on the b-factor: thick red cartoons and thin green cartoons represents high and low b-factor values, respectively. The co-crystallized antagonist is depicted with spheres. Right: close view of the ligand binding site. Also in this case both cartoons and co-crystallized ligand are colored and modeled according to the b-factor, from red (highly flexible regions) to blue (poorly flexible segments). It could be observed a peculiar b-factor distribution in the antagonist molecule, in which the terminal phenol substituent is characterized by an enhanced flexibility compared to the rest of the molecule.

The best model was then selected on the basis of geometrical parameters quality and on Modeller objective function.

As described previously, His264 formed an extensive network of interactions with neighboring residues: in particular, while one nitrogen pointed towards the backbone carbonyl group of Ala265, the other nitrogen laid within a H-bond distance from Glu169 side chain (Figure 63, left).

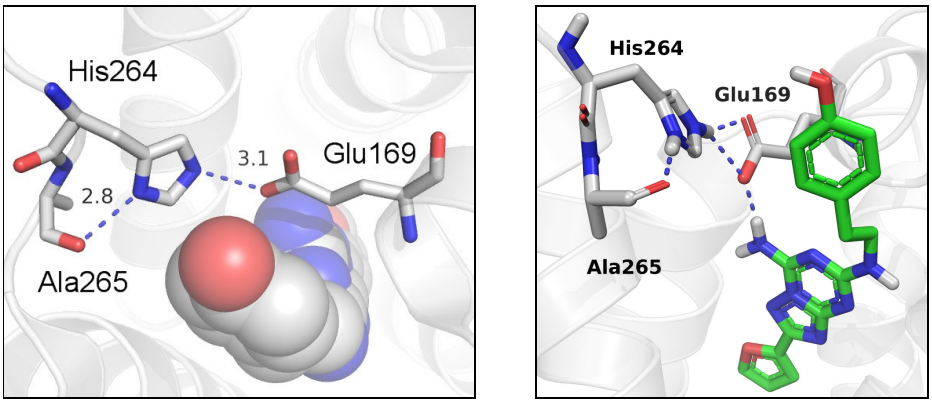

Figure 63: Left: close view of the ligand binding site of the ZM241385-A_{2A} complex (PDB: 3EML, white carbons). The co-crystallized antagonist is represented with spheres. Right: schematic view of the H-bond interactions occurring between residues of ECL2, ECL3 (white carbons) and the co-crystallized ligand (green carbons).

Since the crystallization process was conducted using acid pH (5.5-6)[62] and the calculated pKa of His264 was 7.75 (using PROPKA),[285,286,287] it could be hypothesized that His264 was protonated under crystallization conditions. This hypothesis was further supported by the fact that the protonation of His264 brought to the formation of an extended network of H-bond interactions, leading to an overall stabilization of the binding site architecture. Once protonated, His264 side chain formed not only a stable H-bond interaction with the carbonyl backbone group of neighboring Ala265, but also with Glu169 side chain: this latter contact seemed crucial for ligand stabilization, since it forced Glu169 to interact with the exocyclic NH_2 group of the antagonist molecule (Figure 63, right). On the basis of these observations, the protonation state of His264 was adjusted prior to docking studies.
To relax the crystal structure without losing the overall secondary and tertiary structure arrangements, a constrained minimization was conducted on the ZM241385-A_{2A} complex applying OPLS2005 force field:[290] a maximum RMSD of 0.3 Å was set as convergence criterion. The Ramachandran plot of the final structure is reported in Figure 64: no residues laid in disallowed regions, confirming the quality of the receptor structure from a geometrical point of view.

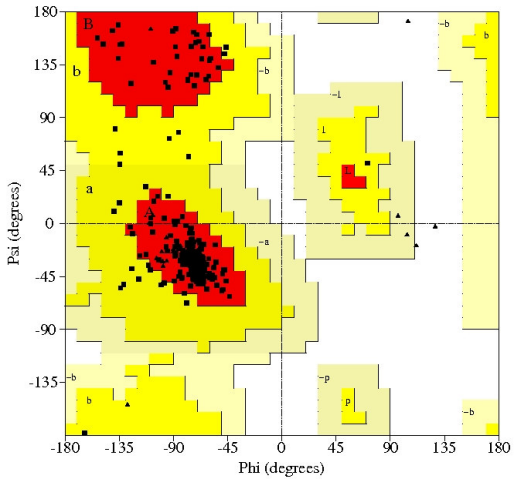

Figure 64: Ramachadran plot of the final ZM241385-A_{2A} complex obtained after the constrained minimization procedure.

Docking protocol

Docking studies were performed with Glide software.[392] Docking grids were centered on the co-crystallized antagonist and both enclosing and bounding boxes were retained at default dimensions: during grid generation, no scaling factors were applied on protein non-

polar atoms. Van der Waals (vdW) radii of ligand non-polar atoms (i.e. atoms having a partial charge lower than ±0.15) were down-scaled to 0.8 during docking run to achieve a better ligand accommodation and to allow the generation of alternative binding modes. The Coulomb-vdW energy potential threshold was increased to 100 kcal/mol and post-docking minimizations were conducted for all the generated ligand conformations. 20 poses were retained for each docking run and they were ranked according to the Emodel scoring function.

Docking results for non-xanthine antagonists

Docking results obtained for non-xanthine antagonists showed a common orientation into the binding site region.

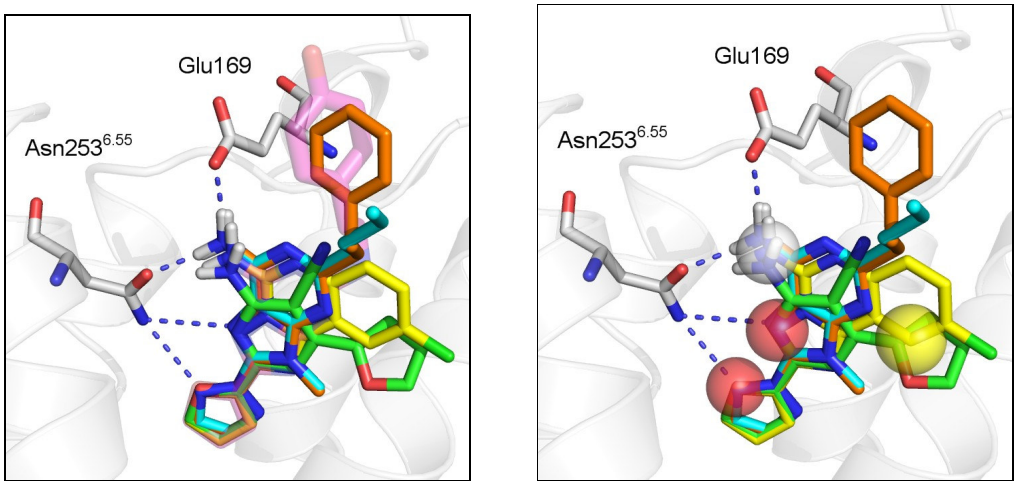

Figure 65: Left: docking poses obtained for compound 5 (yellow carbons, ref. [393], [394]), compound 6 (green carbons, ref. [395]), compound 7 (orange carbons, ref. [396]) and compound 8 (ref. 396). ZM241384 is depicted with magenta transparent sticks. Right: custom pharmacophore features identified among docked compounds: donor, acceptor and hydrophobic sites are depicted in blue, red and yellow, respectively.

Similarly to the co-crystallized antagonist, non-xanthine derivatives are characterized by a peculiar pattern of polar groups, constituted by one H-bond donor and two H-bond acceptors. In some cases, an additional lipophilic group could be present (e.g., in compounds 5 and 6). Similarly to what observed for ZM241385, while the H-bond donor group interacted with Glu169 and Asn253$^{6.55}$ side chains, the two H-bond acceptors formed extensive interactions with Asn253$^{6.55}$ side chain (Figure 65). Interestingly, the additional hydrophobic group of compounds 5 and 6 was accommodated in a volume occupied by several water molecules in the A_{2A} crystal structure. A recent study investigated the stability of these crystallized water molecules in the A_{2A} adenosine

receptor by means of MD simulations.[397] Results clearly showed that waters located in the binding site region, in the proximity of ZM241385, were characterized by unfavored energies, reflecting their remarkable instability. These observations could explain, at least in part, the high affinity conferred by substituents able to occupy this hydrated cleft.

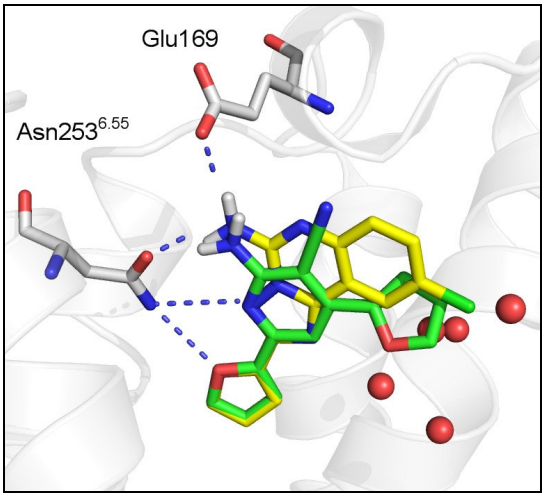

Figure 66: best docking poses obtained for compounds 5 (yellow carbons) and 6 (green carbons) into the A_{2A} receptor binding site. Water molecules found in the A_{2A} crystal structure (PDB: 3EML) are represented with red spheres.

The instability of these water molecules was also confirmed by the recent crystal structure of the A_{2A} adenosine receptor in complex with ZM241385 (PDB: 3PWH). In contrast to what observed in the previous X-ray crystal structure (PDB: 3EML), the terminal phenol group of the co-crystallized antagonist did not extend towards the extracellular side of the receptor, but was bent towards the TM bundle, interacting with residues placed at the interface between TM1, TM2 and TM7.

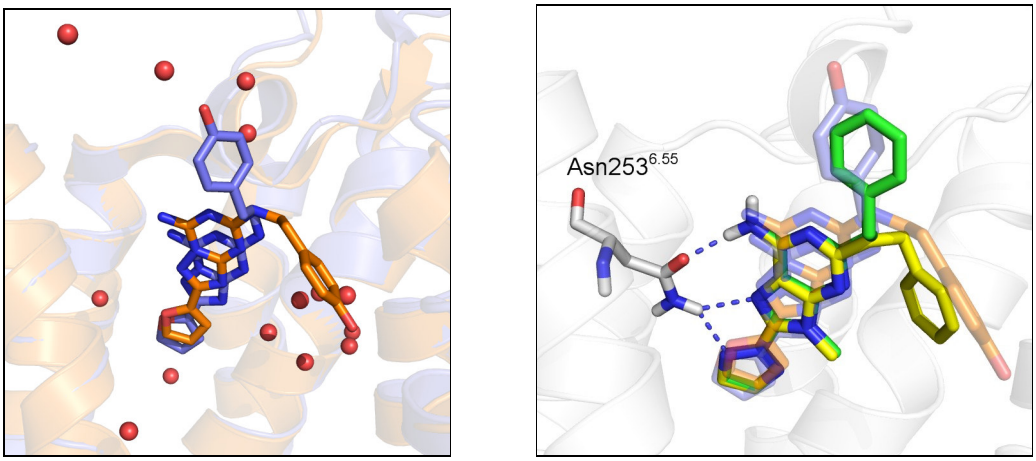

Figure 67: Left: superposition of the two A_{2A} receptor crystal structures in complex with ZM241385: 3EML (blue) and 3PWH (orange). Water molecules present in the 3EML structure are represented with red spheres. Right: first (yellow carbons) and fifth (green carbons) poses of compound 7 superposed to the co-crystallized poses of ZM241385 (blue and orange transparent carbons).

In this conformation, the phenol group laid in the proximity of the highly-hydrated site previously observed, disrupting the network of water-mediated H-bond interactions (Figure 67, left). A bent conformation of the terminal arylakyl chain could be observed also for compound 7. Indeed, in the first ranked pose of this triazolyl-purine derivative the terminal phenyethyl group did not extend vertically towards the extracellular milieu but was bent towards the binding site cleft, occupying the highly-hydrated cleft. Only in the fifth pose the terminal hydrophobic side chain pointing towards the extracellular side of the receptor (Figure 67). These two alternative binding modes observed for compound 7 resembled the two orientations observed for ZM241385 into the A_{2A} binding site (Figure 67, right).

Docking results for xanthine antagonists

Xanthine derivatives showed a common accommodation into the binding site region, in which the xanthine core was located deeply into the binding site crevice and the lipophilic substituent bound to position 8 pointed towards the extracellular side of the receptor. In particular, the carbonyl group located at position 6 of the xanthine ring formed a H-bond interaction with the Asn253$^{6.55}$ side chain.

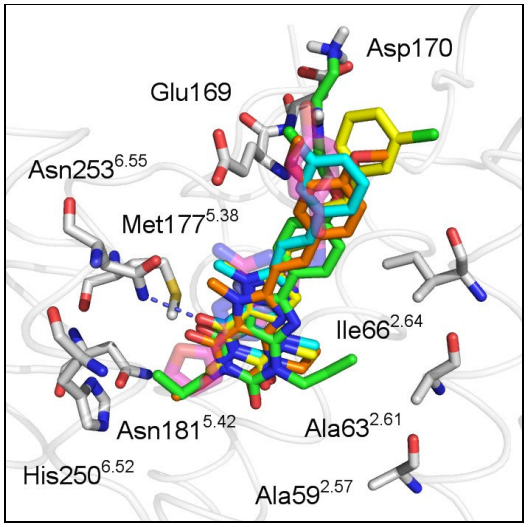

Figure 68: docking poses obtained for CSC (cyan carbons), KW-6002 (orange carbons), XAC (green carbons) and compound 4 (yellow carbons) into the A_{2A} binding site. ZM241385 is depicted with transparent magenta carbons.

The binding pose found for xanthine derivatives seemed to be consistent with available data. For example, SAR studies conducted on different xanthine analogues showed that, while the carbonyl group in position 2 of the xanthine core could be removed without affecting binding affinity, the carbonyl group bound to position 6 was crucial for ligand

binding.[398] This evidence is consistent with docking results, where the only polar interaction occurred between Asn253$^{6.55}$ side chain and the carbonyl oxygen at position 6. SAR studies[399,400,401,402] also showed that methylation of position 7 of the xanthine core often increased the ligand binding affinity for the A_{2A} receptor. Once again, the orientation of the xanthine derivatives into the A_{2A} binding site was consistent with this experimental evidence. Indeed, position 7 of the xanthine ring faced a small cavity formed by Glu169, Met174$^{5.35}$ (not shown in Figure 68), Asn253$^{6.55}$ and Met270$^{7.35}$ (not shown in Figure 68). The 7-methyl group could occupy this additional cleft, leading to an increase in ligand binding affinity. It was recently proposed that also the insertion of an ethyl group in position 7 of the xanthine core brought to a slight increase in binding affinity for the A_{2A} adenosine receptor:[403] thus, it could be hypothesized that the additional cleft cited above could probably accommodate bulkier substituents compared to the methyl group. Data taken from SAR studies also showed that positions 1 and 3 of the xanthine ring could carry methyl, ethyl and propyl substituents without affecting ligand binding affinity for the A_{2A} adenosine receptor. Accordingly, nitrogens located at positions 1 and 3 of the docked xanthine compounds pointed towards two additional clefts present in the binding site crevice, formed by Met177$^{5.38}$, Asn181$^{5.42}$, His250$^{6.52}$ and Trp246$^{6.48}$ and Ala59$^{2.57}$, Ala63$^{2.61}$ and His278$^{7.43}$, respectively: these cavities are able to accommodate a small methyl group, as in the case of CSC or compound 4, as well as a bulkier propyl substituent, as observed for XAC.

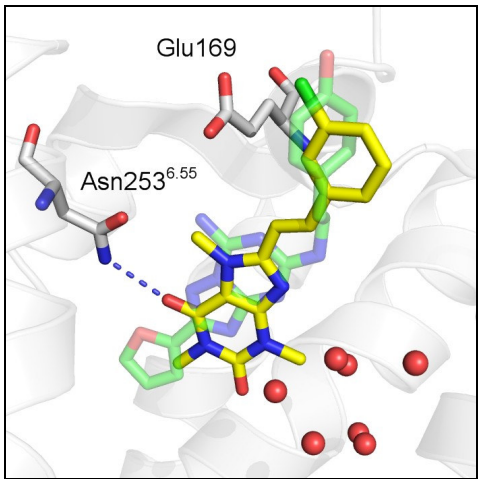

Figure 69: CSC (yellow carbons) docked into the A2A adenosine receptor. ZM241385 is depicted with transparent green carbons and water molecules present in the X-ray structure are represented with red spheres.

The effect of the atom located at position 9 of the xanthine ring has been extensively investigated.[404] Results clearly showed that substitution of the 9-nitrogen with a carbon

atom did not significantly affect binding affinity. This experimental observation was in agreement with docking results obtained for xanthine antagonists: indeed, although position 9 faced a hydrated cavity in the A_{2A} receptor binding site, it was not able to form favorable interactions with residues delimiting the binding site region or water molecules (Figure 69). Thus, docking results could explain, the similar binding affinities showed by xanthines and their 9-deaza analogues.

The favored binding mode observed for the subset of xanthine antagonists showed the bulky lipophilic group bound to position 8 extended towards the extracellular side of the receptor. This observation was consistent with available SARs, that showed that the elongation of the liphophilic substituent from a styryl to a phenylbutadienyl group brought to an increase in binding affinity for the A_{2A} adenosine receptor.[403] The bulky substituent bound to position 8 could form extensive hydrophobic interactions with residues placed at the extracellular side of the receptor, such as Leu167 and Leu267$^{7.32}$. In addition, since the elongation of the 8-substituent slightly increased the affinity for the A_{2A} receptor, this group has to point towards a cavity able to accommodate such bulky and hindered moieties: because of the vertical orientation of the binding site, it is likely that these substituents accommodate towards the extracellular side of the receptor rather than towards the intracellular portion of the cavity.

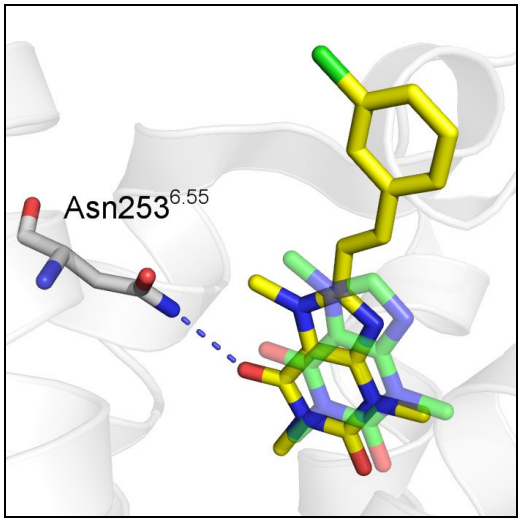

Figure 70: superposition of the co-crystallized caffeine (green transparent carbons) and the best docking pose of CSC (yellow carbons) into the A_{2A} receptor binding site.

The recent publication of two xanthine-bound structures of the A_{2A} adenosine receptor[93] gave the chance to compare the docking results with crystallized complexes. According to crystal structures, the xanthine core is placed at the bottom of the binding site, forming a

H-bond interaction with Asn253$^{6.55}$ via the carbonyl oxygen located at position 6 (Figure 70). Moreover, the xanthine core is stabilized by extensive hydrophobic interactions with Phe168, Leu249$^{6.51}$ and Ile274$^{7.39}$.

While the caffeine-A_{2A} complex helped to clarify the key interactions occurring between the xanthine core and residues delimiting the binding site region, the XAC-bound structure threw light on the ligand-receptor interactions involving the substituent bound to position 8 of the xanthine ring. Similarly to what observed in docking studies, the bulky moiety linked to the xanthine core extends vertically towards the extracellular side of the receptor. The terminal aminoethyl chain of the co-crystallized antagonist is accommodated in a cleft located between TM1, TM2 and TM7, delimited by Tyr9$^{1.35}$, Leu267$^{7.32}$ and Tyr271$^{7.36}$. In contrast to what observed in the crystal structure, the docking poses showed a different disposition of the XAC terminal chain, in which the amine group form a H-bond interaction with Asp170 located on ECL2 (Figure 71).

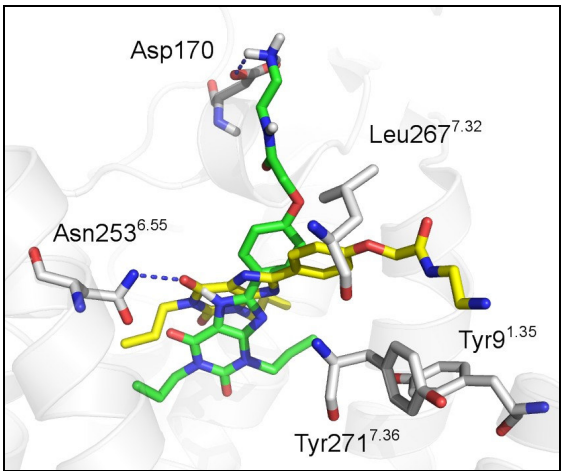

Figure 71: comparison between the crystallized (yellow carbons) and the docked (green carbons) poses of XAC into the A_{2A} receptor binding site.

This discrepancy between docking results and the co-crystallized pose of XAC was probably due to the lack of a suitable room between TM1, TM2 and TM7 in the ZM241385-bound structure of the A_{2A} adenosine receptor. On the other hand the extremely high b factor values detected in the XAC-A_{2A} complex indicated a high degree of flexibility of the co-crystallized antagonist into the binding site crevice: thus, it could be hypothesized that the ligand molecule could adopt different binding conformations into the receptor binding cleft (Figure 72).

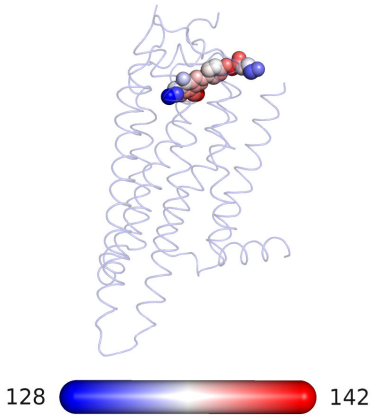

Figure 72: XAC-A_{2A} complex (PDB: 3REY). XAC is represented with spheres colored according to atomic b factor values, from 128 (blue) to 142 (red).

MD simulations in a solvated lipid bilayer

MD simulation of the ZM241385-A_{2A} complex

Computational studies described in the previous sections were primarily conducted to evaluate ligand-receptor interactions occurring between known A_{2A} antagonists and residues delimiting the binding site region. Although these studies were fundamental to search for alternative ligand conformations into the binding site cleft, they did not incorporate a flexible treatment of the target structure, that is known to be crucial for a correct ligand accommodation. MD simulations represent a feasible technique that can overcome the lack of flexibility characteristic of docking studies, leading to a better evaluation of the main protein rearrangements that occur upon ligand binding. During MD simulations, a complete and explicit description of the environment surrounding the ligand-receptor complex was preferred: the explicit description of all the elements forming the membrane environment (i.e., lipids, water and ions) could lead to a better description of the dynamic rearrangements occurring at the protein level as well as of the main structural elements involved in ligand stabilization. The analysis of the receptor relocations as well as of the dynamic behavior of the ligand-receptor interactions could provide clues to design novel chemical entities and to suggest possible chemical modifications aimed at improving ligand binding affinity.

MD protocol

The refined structure of the A_{2A} receptor employed for the generation of docking grids was used as input for MD simulation. Water molecules deleted during docking runs were reintroduced into the receptor structure: indeed, although their removal was needed to allow the accommodation of chemically different A_{2A} antagonists (e.g., compounds 5 and 6), water sites were found to be crucial for the stabilization of the triazolo-triazine core of ZM241385 as well as of the receptor binding site through a number of water-mediated contacts (Figure 73, left). Only water molecules comprised in a shell of 15 Å centered on ligand molecule were taken into account. An inspection of the B factors of these water molecules revealed a broad range of values, comprised between 39 and 101. Thus, while some of them are characterized by a limited mobility around their crystallographic position, other waters show a remarkable degree of flexibility. However, the incorporation of highly flexible water molecules into the binding site region was fundamental to maintain the network of water-mediated interactions and, consequently, to preserve the overall stabilization of the ligand-receptor complex.

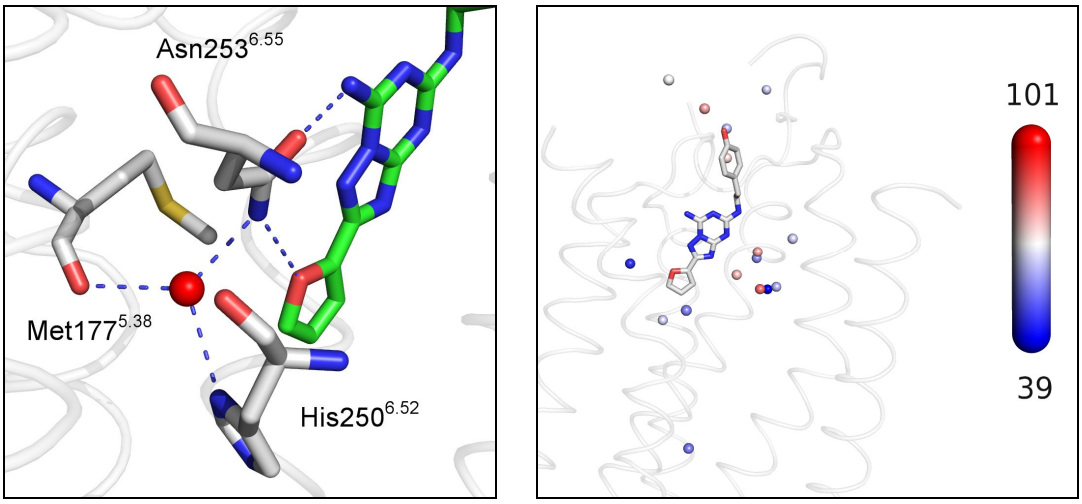

Figure 73: Left: example of the water-induced stabilization of the receptor-ligand complex. ZM241385 is represented with green carbons. Right: waters comprised in a shell of 15 Å centered on ligand molecule are depicted with spheres and colored according to their B factor, from high (red) to low (blue).

A Monte Carlo sampling was applied on water molecules to adjust their orientation and to optimize the overall H-bond network. Finally, a constrained minimization procedure was conducted on the resulting hydrated ZM241385-A_{2A} complex, applying OPLS2005 force field[290] and setting a maximum RMSD of 0.3 Å as the convergence criterion.

Desmond v2.2[296] was used to built the system and to set up the dynamics simulation. The hydrated ZM241385-A_{2A} complex was embedded in a POPC lipid bilayer by aligning the

receptor to the 3EML crystal structure deposited into the Orientations of Protein in Membranes database (OPM),[297] with at least 13 Å between the protein and its closest periodic image. Protein-membrane system was solvated by approximately 13300 SPC water molecules in a simulation box of approximately 70 Å x 70 Å x 120 Å. Amber99SB force field[298] was used to model the protein, while ligand and lipids were parameterized using the GAFF.[299] GAFF was used to parameterize lipid molecules since recent MD simulations showed that this force filed could reproduce experimental data obtained for membrane systems.[405] The final ligand-receptor complex embedded in a solvated lipid bilayer was relaxed using a modified version of a membrane relaxation protocol implemented in the Schrodinger 2009 Suite, summarized below:

1. System was energy-minimized with 2000 steps of steepest-descent with a convergence gradient of 50 kcal/(molÅ). All protein heavy atoms were constrained with a force constant of 50 kcal/(molÅ^2).
2. System was energy-minimized with 2000 steps of steepest-descent with a convergence gradient of 5 kcal/(molÅ). All atoms were free to move.
3. 60 ps-long MD simulation in the NVT ensemble was run using the Langevin barostat and thermostat. Temperature was linearly increased from 10 to 310 K and protein heavy atoms were constrained with a force constant of 50 kcal/(molÅ^2), that linearly decreased to 10 kcal/(molÅ^2). During this initial MD stage, a gaussian potential was applied on water molecules to avoid their penetration into the membrane bilayer.
4. 200 ps-long MD simulation in the NPT ensemble was run using the Langevin barostat and thermostat. Temperature was set to 310 K and the Gaussian potential inserted in the previous step was retained. Protein heavy atoms were constrained with a force constant of 10 kcal/(molÅ^2).
5. 100 ps-long MD simulation on the NPT ensemble was run using the Langevin barostat and thermostat. Temperature was set to 310 K but the Gaussian potential was removed. Constraints were the same used in the previous step.
6. 600 ps-long MD simulation on the NPT ensemble was run using the Langevin barostat and thermostat. Temperature was set to 310 K and positional constraints were applied on both protein heavy atoms and protein backbone. The constraint force was linearly decreased from 10 kcal/(molÅ^2) to 2 kcal/(molÅ^2) during the simulation.

7. 100 ps-long MD simulation on the NPT ensemble was run using the Langevin barostat and thermostat, with a temperature of 310 K. Positional constraints were applied only on protein alpha carbons with a force constant of 2 kcal/(molÅ^2).
8. A final equilibration step of 100 ps was performed using the NPT ensemble, applying no constraints.

The production phase of the simulations was performed in the NPT ensemble under constant pressure of 1 atm and a temperature of 310 K, thermostated and barostated using the Langevin method.[301] All bond lengths to hydrogen atoms were constrained using M-SHAKE.[302] Short-range electrostatic interactions were cut off at 9 Å, whereas long-range electrostatic interactions were computed using the Particle Mesh Ewald method.[303] A RESPA integrator[304] was used with a timestep of 2 fs, and long-range electrostatics were computed every 6 fs. During 30 ns of production phase, frames were extracted and subsequently used for the analysis.

Trajectory clustering

Ptraj is an application of the AMBER simulation package[406] that allows to perform statistical analyses on MD trajectories. It includes a clustering procedure that can be applied on an ensemble of snapshots extracted from a MD simulation. As stated previously, the main aim of the MD simulation study performed on the ZM241385-A_{2A} complex was to investigate the main receptor rearrangements occurring upon ligand binding. In this scenario, the clustering approach represented a useful technique to analyze the MD trajectory because it allows to examine a number of different receptor conformation and to evaluate the statistical relevance of their structural deviations, as it permits to assess if two conformations are truly different from a structural point of view. Thus, the aim of the trajectory clustering was to identify a manageable number of structurally diverse receptor conformation, characterized by a different arrangements of key structural elements.

Ptraj incorporates different statistical parameters to evaluate the quality of the clustering process, as well as the optimal number of clusters recognized in whole ensemble of structures (for a review of the use of these parameters see ref. 407). Two main parameters have been monitored during clustering analysis: the Davies-Bouldin index (DBI) and the pseudo-F statistic (pSF). DBI is mainly used to evaluate the compactness of identified clusters:[408,409] this parameter tends to decrease if the recognized clusters are well-separated from each other. On the other hand, the pSF metric is proportional to the ratio

between SSR and SSE, where SSR and SSE are the explained and residual variations calculated on the distribution of RMSD values:[410] thus, the pSF tends to increases as a consequence of a better clustering procedure.

Another additional parameter useful to evaluate the clustering performance is the so-called critical distance, that is simply the distance between clusters that were just merged or split (depending on the employed algorithm): a steep variation in the critical distance is often seen when the optimal number of clusters is reached.

Taken together, these information indicate that, in an ideal situation, the optimal number of clusters could be recognized by a peak of the pSF metric, a minimum value of DBI and a steep increase (or decrease) of the critical distance. However, the identification of the optimal number of clusters is often not straightforward, due to the lack of an "ideal" trend for these three parameters. In this case one could first consider a manageable number of clusters (e.g. 10-12) and then evaluate the presence of a common trend for pSF, DBI and critical distance within this cluster range.

Among available clustering algorithm, the average linkage was selected for the analysis, since several studies showed its ability in clustering different binding site conformations obtained through MD simulations.[407,411,412,413]

Results of the MD simulation

A visual inspection of trajectories revealed that the overall structure of the A_{2A} receptor was stable during 30 ns of MD simulation. (Figure 74, left).

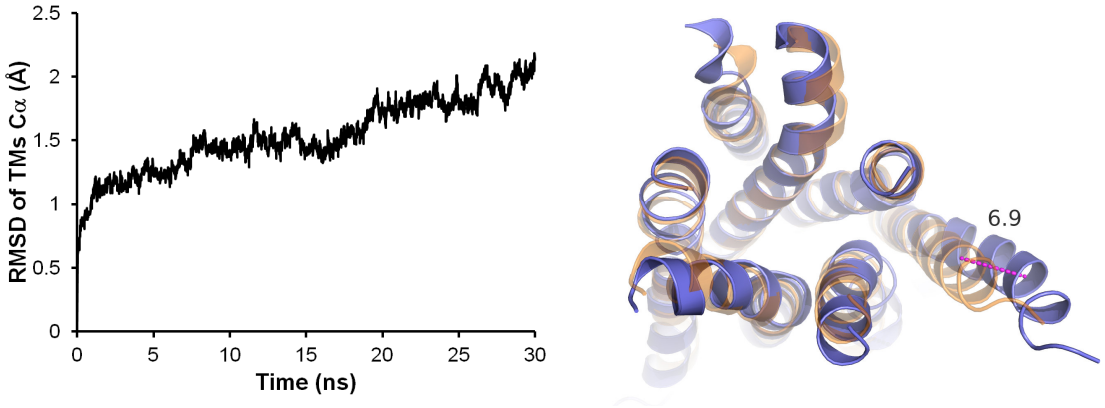

Figure 74: Left: RMSD graph calculated on TMs alpha carbons. Right: extracellular view of the starting (transparent orange) and final (opaque blue) conformations of the A_{2A} adenosine receptor. The displacement of the TM1 tip is represented with a magenta dashed line.

However, the RMSD graph (calculated on TM Cα carbons) did not show a clear plateau, suggesting that the receptor structure was undertaking a conformation transition. Among

all the seven TM segments TM1 underwent the largest displacement, showing an outward movement of about 7 Å of its the extracellular tip (Figure 74, right). Also TM6 showed high values of RMSD during MD simulation. A visual inspection of trajectories revealed that, in contrast to TM1, the major movement of TM6 occurred at its intracellular end. This movement was mainly driven by the re-establishment of the "ionic lock" interaction, located at the extracellular ends of TM3 and TM6. Indeed, the formation of the salt bridge between Arg102$^{3.50}$ and Glu228$^{6.30}$ caused a inward relocation of the C-terminus domain of TM6 of about 5 Å. Interestingly, the "ionic lock" interaction, not present at the beginning of the MD simulation, formed spontaneously in the first stages of the simulation: this observation suggested, once again, the presence of a conformational equilibrium for this specific polar interaction, between an "open" and a "closed" conformation. The dynamic behavior of this peculiar interaction was recently investigated by microsecond-timescale MD simulations:[414] also in this case, the formation of the Arg102$^{3.50}$-Glu228$^{6.30}$ salt bridge was observed during the first stages of the simulation.

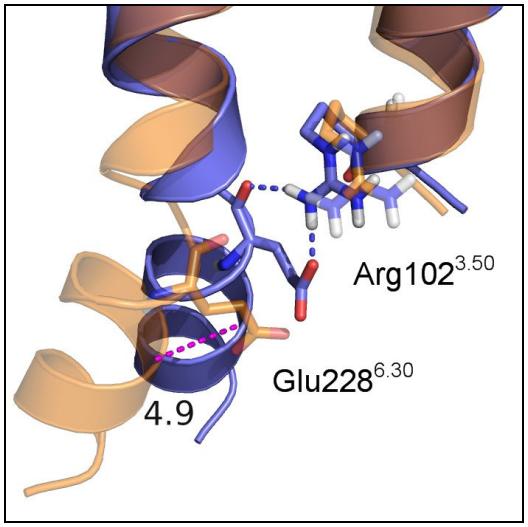

Figure 75: superposition of the starting (orange) and final (blue) conformations of the A_{2A} adenosine receptor taken from the MD simulation. Residues forming the "ionic lock" interaction are represented in sticks.

The other TM domains did not undertake significant rearrangements during MD simulation: accordingly, their RMSD graphs revealed only slight movements, with a maximum RMSD comprised between 1 and 1.5 Å (Figure 76).

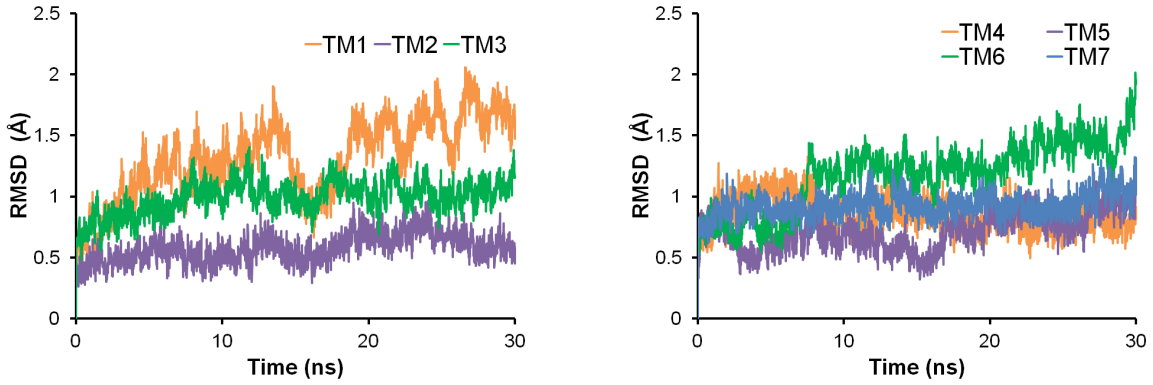

Figure 76: time evolution of the RMSD of each TM domain. RMSD was calculated on alpha carbons.

Although MD simulation did not show remarkable rearrangements of the secondary and tertiary structures of the A_{2A} receptor, an interesting behavior of the co-crystallized antagonist could be observed. To evaluate the dynamic stability of the ligand-receptor interactions detected in the X-ray crystal structure, distances between ligand atoms and amino acids counterparts involved in H-bond contacts were monitored during the MD simulation.

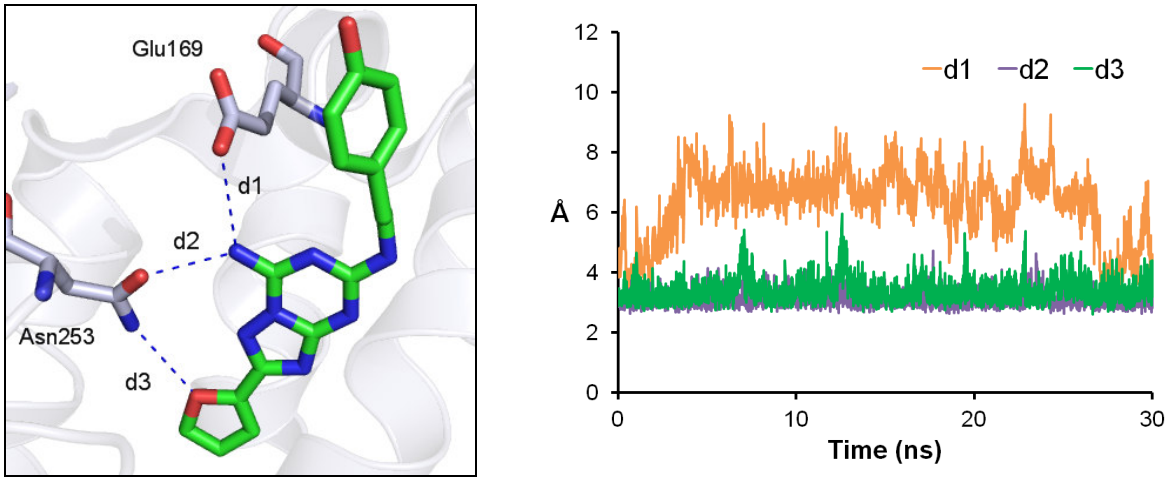

Figure 77: Left: ZM241385 into the A_{2A} ligand binding site. Monitored distances are depicted with dashed blue lines. Right: time evolution of distances d1, d2, and d3.

Interestingly, while H-bond interactions involving Asn253$^{6.55}$ side chain were retained for the whole simulation, the polar interaction occurring between Glu169 side chain and the exocyclic NH_2 group of the co-crystallized antagonist was lost during the first 5 ns of the MD simulation (Figure 77, right). The disruption of this H-bond interaction brought to a remarkable rearrangement of the ligand molecule into the binding site region. In particular, the terminal phenol group of ZM241385 moved from its initial position to a cavity delimited by TM1, TM2 and TM7, causing an outward shift of the C-terminus of TM1 from the TM

bundle. Thus, the relocation of the terminal group of ZM241385 towards the tips of TM1 could explain the increased RMSD values observed for this helical segment compared to other TM domains.

The final structure obtained from MD simulation was compared with the newly released crystal structure of the ZM241385-A_{2A} complex (PDB: 3PWH). Intriguingly, the conformation of the co-crystallized antagonist resembled that obtained with the MD simulation, with the terminal phenol group accommodated into an additional cleft delimited by TM1, TM2 and TM7. Although in the structure extracted from the MD simulation the TM1 segment is more shifted towards the membrane bilayer compared to the crystal structure, these two receptor structures could be easily superposed, showing an overall RMSD value of 3.7 Å (Figure 78, left).

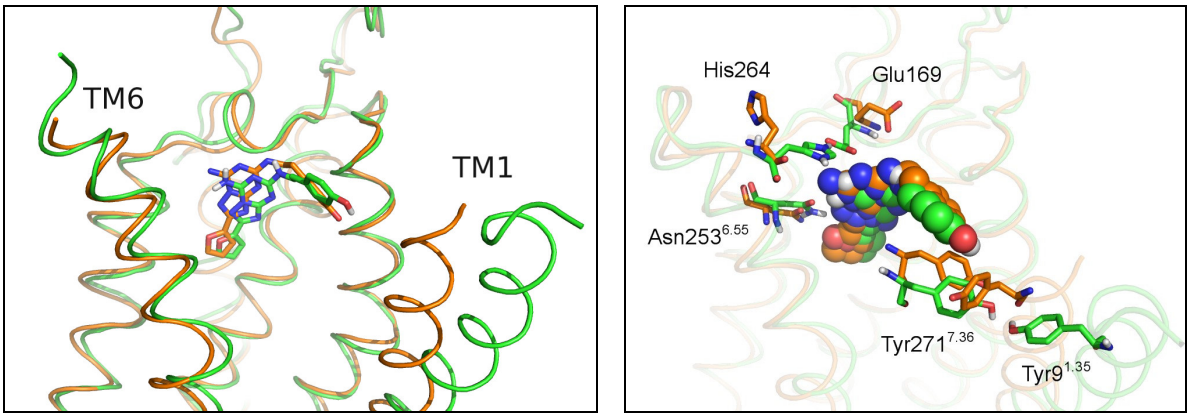

Figure 78: Left: superposition of the final structure obtained from MD simulation (green carbons) and the crystal structure of the ZM241385-A_{2A} complex (PDB: 3PWH, orange carbons). Ligand molecules are represented in sticks. Right: extracellular view of residues delimiting the binding site region. ZM241385 is represented with spheres.

Looking at the main ligand-receptor interactions occurring in the binding site region of the crystallized structure, it could be seen that Glu169 formed a H-bond contact with the NH group present on the ethylamino chain of the ligand molecule. Similarly, also in the structure obtained from MD simulation, Glu169-NH_2 interaction was lost and the NH group belonging to the ethylamino chain of ZM241385 pointed towards the Glu169 side chain. The intrinsic instability seen for the Glu169-NH_2 interaction during MD simulation was consistent with the presence of two conformations of ZM241385 into the A_{2A} binding site (PDB: 3EML and 3PWH). Indeed, Glu169 side chain seems to act like a “gate”, that allows the terminal phenol group of the antagonist to assume different orientations into the binding site region. To guarantee the relocation of the antagonist terminal moiety, this residue has to be characterized by a high intrinsic flexibility.

The trajectory obtained from the MD simulation was analyzed through a clustering procedure.

Results of the cluster analysis

A cluster analysis was conducted on the MD trajectory to identify a manageable number of structurally different receptor conformations: the analysis of these structures could lead to identify other accessible pockets as well as additional residue counterparts that could be targeted by newly designed A_{2A} antagonists.

To investigate the major structural rearrangements of the ligand binding site, residues comprised in a shell of 3 Å centered on the ligand molecule were included in the analysis: Leu167, Phe168, Glu169, Met177$^{5.38}$, Trp246$^{6.48}$, Leu249$^{6.51}$, His250$^{6.52}$, Asn253$^{6.55}$, Met270$^{7.35}$ and Ile274$^{7.39}$ (Figure 79). The cluster analysis was conducted taking into account the carbonyl carbon of the backbone along with the Cα, Cβ and Cγ belonging to the side chain.

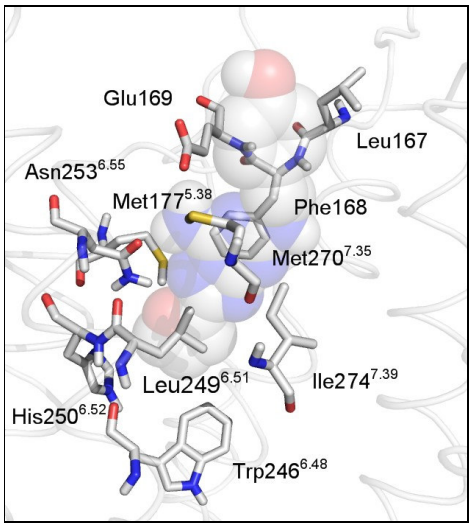

Figure 79: residues included in the clustering analysis. ZM241385 is represented with transparent spheres.

Results clearly showed a peak in the pSF metric for 2 clusters, whereas two minimum values for DBI could be detected for a number of clusters equal to 3 and 6 (Figure 80). Moreover, the critical distance showed steep decreases for 3 and 7 clusters. Taken together these results suggested an optimal number of clusters comprised from 3 to 7. Although the DBI-based selection identified 3 main clusters in the structures ensemble, the aim of this study was to create a heterogeneous set of protein conformations as numerous as possible, to avoid the deletion of important structural information. Thus, it was decided

to include 6 clusters in the present analysis, corresponding to a “local” minimum of the DBI metric.

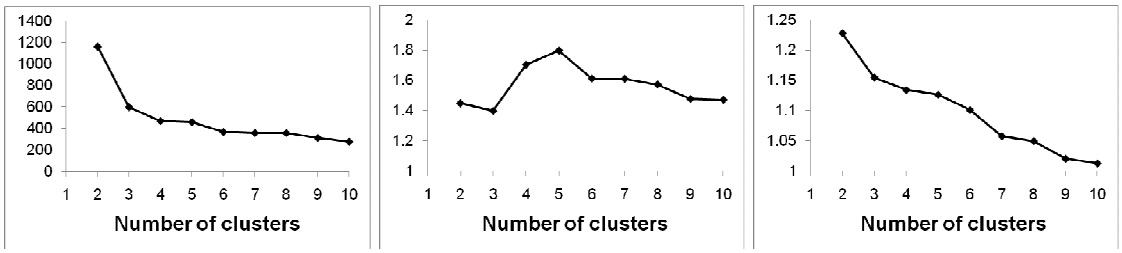

Figure 80: graphs of pSF (left), DBI (center) and critical distance (right) as a function of the number of clusters.

At the end of the clustering process, striking differences in cluster population could be detected among different clusters. For example, while one cluster contained about 41% of the receptor conformations (1020 out of 2502 snapshots), another cluster was found to be a singleton and contained only one receptor structure.

At the end of the clustering procedure Ptraj returns two different receptor structures for each cluster: an average structure and a representative structure. While the former is obtained by averaging the 3D coordinates of all the receptor structures included in a specific cluster, the latter is the structure showing the minimal sum of the squared deviations between other receptor structures comprised the cluster and itself. Since one of the main risks of averaging the 3D coordinates is to normalize the structural variation between different receptor structures, the representative structures were extracted from each cluster and subsequently used for docking studies (Figure 81).

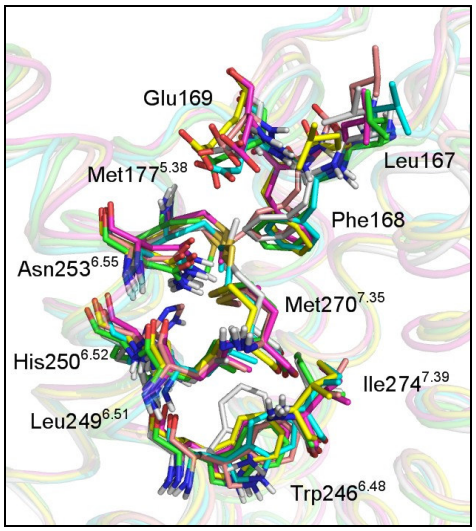

Figure 81: superposition of the 6 representative structures obtained from the clustering procedure.

Docking studies on representative structures

Docking studies were performer with Glide software.[392] Docking grids were centered on the co-crystallized antagonist and both enclosing and bounding boxes were retained at default dimensions: during grid generation, no scaling factors were applied on protein non-polar atoms. Van der Waals radii of ligand non-polar atoms (i.e. atoms having a partial charge lower than ±0.15) were down-scaled to 0.8 during docking runs to achieve a better ligand accommodation and to allow the generation of alternative binding modes. The Coulomb-vdW energy potential threshold was increased to 100 kcal/mol and post-docking minimizations were conducted for all the generated ligand conformations. 20 poses were retained for each docking run and they were ranked according to the Emodel scoring function.

Since xanthine derivatives represent promising therapeutic agents for the treatment of Parkinson's disease[415,416] and have been extensively investigated as important dual active MAOB inhibitors-A_{2A} antagonists,[417] KW-6002 and CSC were used as "probes" to evaluate possible modifications of the main xanthine ring that could improve the binding affinity profile. Although docking results were similar among different representative protein structures, some striking differences could be detected. For example, in the fifth representative structure (here the structure numbering used by Ptraj is maintained) an upward shift of the imidazole ring of His250$^{6.52}$ could be detected. This relocation of His250$^{6.52}$ side chain was favored by the formation of an additional H-bond interaction with the carbonyl group of Asn181$^{5.42}$ side chain (Figure 82, left). As a consequence of the His250$^{6.52}$ shift, an accessible cavity delimited by TM5 and TM6 is formed. Docking of KW-6002 into the fifth representative structure showed the presence of the key interaction between Asn253$^{6.55}$ and the carbonyl oxygen located at position 6 of the xanthine ring. Interestingly, the ethyl substituent bound to position 1 of KW-6002 pointed towards the newly formed cavity, in the proximity of His250$^{6.52}$ (Figure 82, right). On the basis of docking studies it could be hypothesized that bulkier substituents inserted at position 1 of the xanthine core could be accommodated into this additional cleft, leading to an increase in binding affinity. The presence of such a cavity could also explain, at least in part, the increase in binding affinity seen for xanthine derivatives carrying a propargyl group at position 1.[418,419] Taken together, both SAR studies and MD simulations suggested the presence of an accessible cavity located in the proximity of position 1 of the xanthine ring. Also the newly released crystal structure of the XAC-A_{2A} complex (PDB: 3REY) revealed the presence of an accessible cavity located between TM5 and TM6, which is able to

accommodate the 1-propryl group of the co-crystallized antagonist: however, this cavity is slightly shifted towards Met177$^{5.38}$ compared to that found in the MD simulation. Although it cannot be excluded that the cavity present in the fifth representative structure might be an artifact of the MD simulation, it could be also hypothesized that the orientation of the 1-propyl group of XAC is due to the peculiar substituent bound to position 8 of the antagonist: indeed, the 8-phenyl group lays on the extracellular tip of TM7 and could act as a lever, shifting the xanthine ring towards TM3 and ECL2.

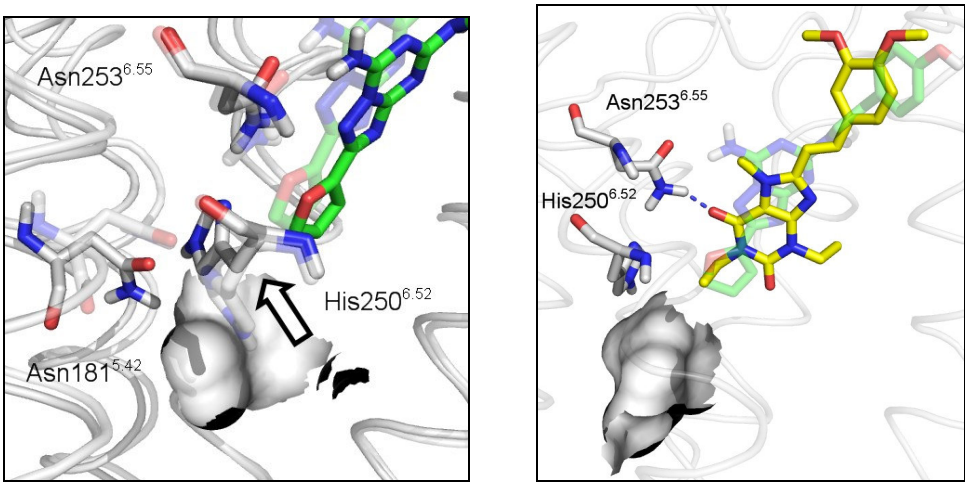

Figure 82: Left: superposition of the starting conformations of the MD simulation (transparent) and the fifth representative structure (opaque). The accessible cavity between TM5 and TM6 is represented with a white surface and ZM241385 is depicted with green carbons. Right: best docking pose obtained for KW-6002 (yellow carbons) in the fifth representative structure. ZM241385 is depicted with green transparent carbons. Also in this case the additional cavity is represented with a white surface.

A significant protein rearrangement could be also observed in the first representative structure. In this receptor conformation, the terminal phenol group of ZM241385 was accommodated in a cleft formed by TM1, TM2 and TM7, forming an OH-π interaction with Tyr271$^{7.36}$ side chain. The terminal phenethyl chain of ZM241385 was further stabilized by additional hydrophobic interactions with Ser67$^{2.65}$ and Met270$^{7.35}$. This specific ligand conformation resembled that observed in the newly released crystal structure of the ZM241385-A_{2A} complex, in which the phenylalkyl chain of the co-crystallized antagonist is inserted in a cleft formed by Ser67$^{2.65}$, Tyr271$^{7.36}$ and Ile274$^{7.39}$. Docking of KW-6002 and CSC within the first representative structure showed the proposed orientation of xanthine derivatives, with the xanthine ring located at the bottom of the binding site region and the lipophilic chain extended towards the extracellular portion of the receptor. Interestingly, while the key interaction with Asn253$^{6.55}$ was preserved, the terminal lipophilic chains of KW-6002 and CSC tended to occupy the additional cavity delimited by TM1, TM2 and TM7, in the proximity of Tyr271$^{7.36}$. In particular, in the best docking poses of both xanthine

derivatives the *meta*-chloro and *meta*-methoxy groups bound to the terminal phenyl ring faced the additional cavity entrance. In this scenario, the insertion of bulkier lipophilic (or polar) functionalities at position *meta* could be used to target a wider pattern of amino acids delimiting the small crevice (e.g. Tyr271$^{7.36}$ and Ser67$^{2.65}$), leading to an increase in ligand binding affinity.

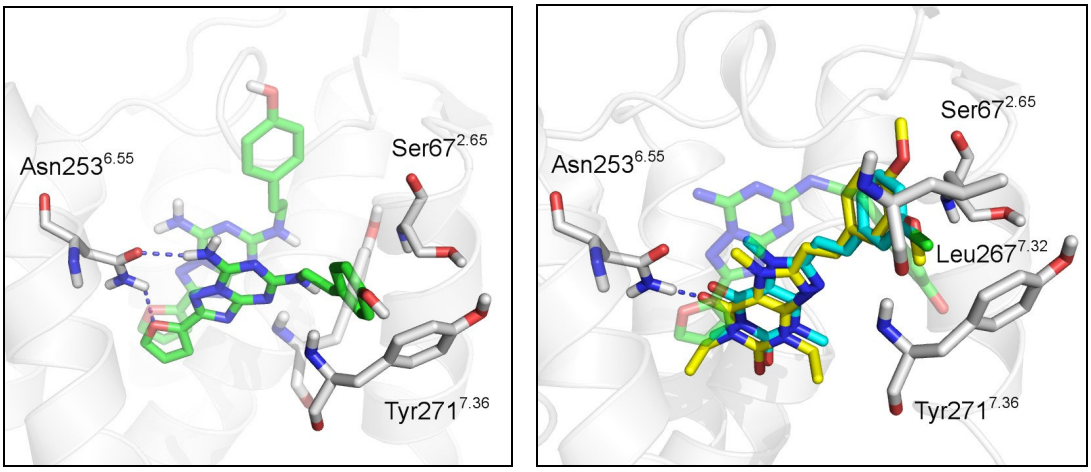

Figure 83: Left: superposition of the starting conformation of the MD simulation (transparent) and the fisrt representative structure (opaque). ZM241385 is represented with green carbons. Right: superposition of the best docking poses obtained for KW-6002 (yellow carbons) and CSC (cyan carbons) into the first representative structure. The co-crystallized pose of ZM241385 (PDB: 3PWH) is depicted with green transparent carbons.

MD simulations of triazolyl-purines

Two triazolyl-purine derivatives, namely compounds 7 and 8, have been already investigated by means of docking studies.

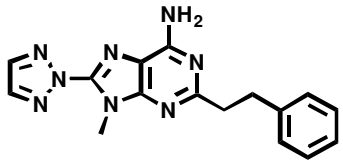

Compound 7
Ki = 4.7 nM

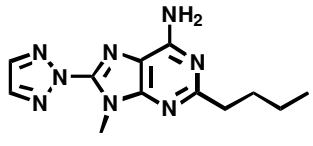

Compound 8
Ki = 6.6 nM

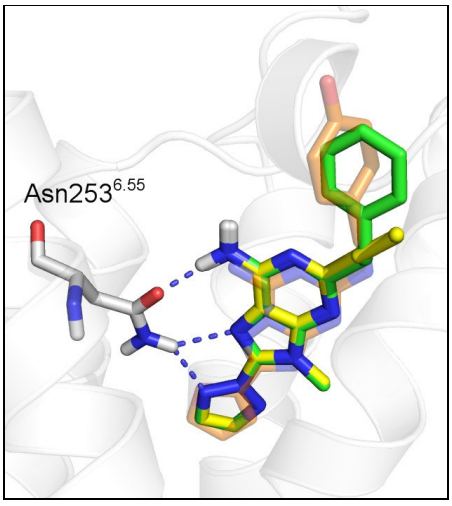

Figure 84: docking poses obtained for compounds 7 (green carbons) and 8 (yellow carbons) into the A_{2A} receptor binding site. Co-crystallized pose of ZM241385 (PDB: 3EML) is represented with transparent orange carbons.

The best docking poses obtained for these compounds into the A_{2A} receptor binding site shared a similar orientation compared to the co-crystallized antagonist, in which Glu169 side chain preferably interacted with the exocyclic NH_2 group of the antagonist and Asn253$^{6.55}$ formed H-bond interactions with both the purine and the triazolyl ring.

In the best docking pose obtained for compound 7, the terminal phenethyl chain was bent toward the TM bundle: since this pose disrupted the highly hydrated cleft found in the A_{2A} receptor structure, it was discarded from the analysis. Conversely, the second best pose showing an orientation of the terminal group similar to that observed in the co-crystallized pose of ZM241385 (PDB: 3EML) was selected for MD simulation. The final docking poses of compounds 7 and 8 used for the MD simulations are depicted in Figure 84.

Resulting complexes were then prepared using the same protocol applied for ZM241385. In brief, water molecules comprised in a shell of 15 Å centered on ZM241385 were reintroduced and their orientation was optimized through a Monte Carlo sampling. Finally, resulting ligand-receptor complexes were energy-minimized applying a restrained geometrical optimization, setting a maximum RMSD of 0.3 Å as convergence criterion. OPLS2005 was used as force field.

The same settings applied for ZM241385 were used for the equilibration and the production phases; production phases were run for 10 ns.

Results of the MD simulations

Results obtained for MD simulations confirmed the stability of the A_{2A} adenosine receptor structure, even in the presence of ligands different from the co-crystallized one. The RMSD graphs (depicted in Figure 85) reached a plateau at 1.4-1.8 Å after about 6 ns of simulation. These small geometrical fluctuations from the initial receptor structure clearly indicated stable secondary and tertiary structures.

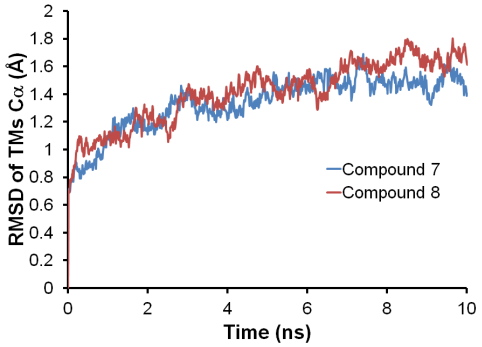

Figure 85: time evolution of the RMSD of TM alpha carbons for A_{2A} receptor complexes with compounds 7 (blue) and 8 (red).

Although both receptor structures showed a similar behavior during MD simulations, remarkable differences could be detected in the pattern of ligand-receptor interactions occurring at the ligand binding region. To evaluate the stability of the main ligand-receptor contacts 3 distances were monitored during MD simulations: d1 (between the NH_2 nitrogen atom and the carboxyl carbon of Glu169 side chain), d2 (between the NH_2 nitrogen atom and the amide oxygen of Asn253$^{6.55}$ side chain) and d3 (between the triazolyl nitrogen and the amide nitrogen of Asn253$^{6.55}$ side chain).

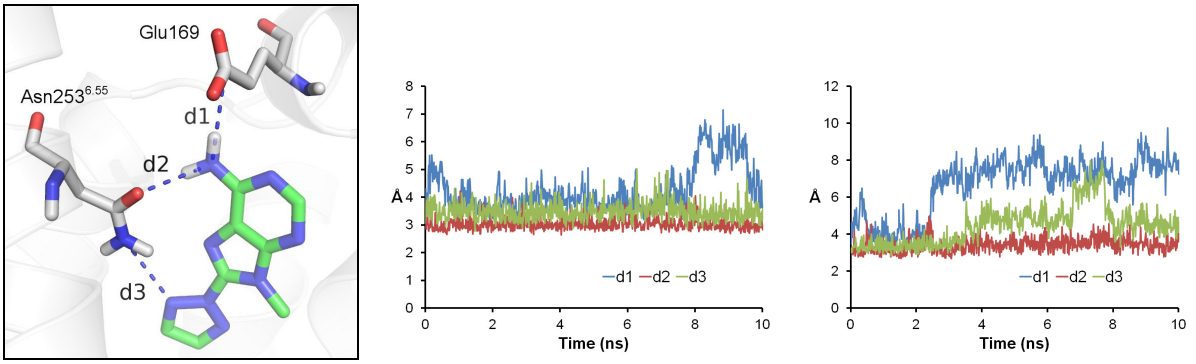

Figure 86: Left: schematic representation of the distances monitored for compounds 7 and 8 during the MD simulations. The common trazolyl-purine core is depicted with transparent green carbons. Center and right: time evolution of distances d1 (blue), d2 (red) and d3 (green) for compounds 7 (center) 8 (right).

Figure 86 showed clear differences in the dynamic behavior of compounds 7 and 8 into the binding site region. Indeed, while compound 7 was able to maintain key H-bond interactions with Glu169 and Asn253$^{6.55}$ during the whole simulation, compound 8 showed a high instability into the A_{2A} binding site. As a consequence, the main polar contact between the exocyclic NH_2 group and Asn253$^{6.55}$ side chain was lost. Also average d3 distances strongly differed between the two triazolyl-purine derivatives: indeed, compounds 7 and 8 showed average d3 values of 3.5 Å and 4.4 Å, respectively.

The different behavior of these two molecules could be rationalized considering their terminal lipophilic groups. During MD simulation, the phenethyl chain of compound 7 shifted towards TM2 and TM7: due to this outward movement, the phenyl group was accommodated in a pocket delimited by Ser67$^{2.65}$, Leu267$^{7.32}$ and Tyr271$^{7.36}$ (Figure 87, left). In this peculiar conformation, the phenyl ring of compound 7 formed extensive hydrophobic interactions with neighboring residues and was sandwiched between the extracellular tips of TM1, TM2 and TM7. In this arrangement, both the steric hindrance of the phenyl ring and the extensive network of hydrophobic contacts concurred to the overall stabilization the terminal phenethyl chain. Interestingly, the final conformation adopted by the phenethyl substituent of compound 7 resembled that observed for the phenethylamino

moiety of ZM241385 in its alternative orientation (PDB: 3PWH). Indeed, the two phenyl rings accommodated in the same cleft, located at the extracellular interface of TM1, TM2 and TM7 (Figure 87, right).

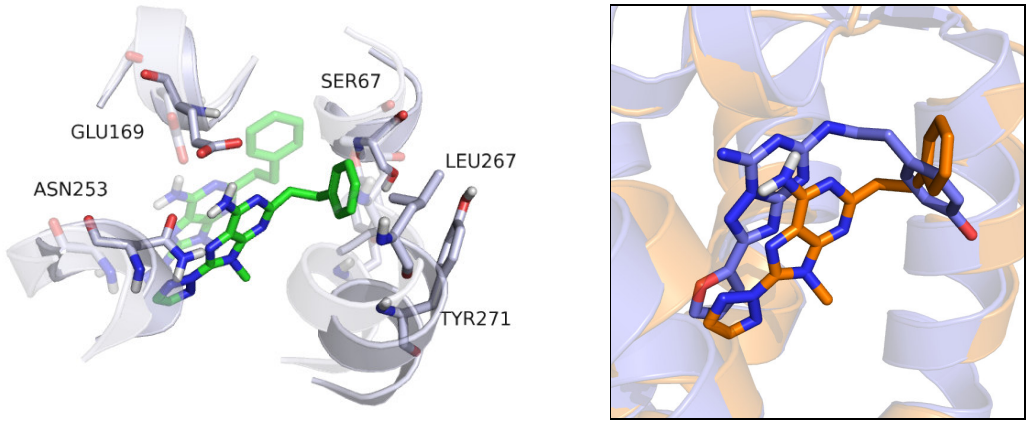

Figure 87: Left: superposition of the starting (transparent) and final (opaque) conformations of the MD simulation of compound 7. The ligand molecule is represented with green carbons. Right: superposition of the final snapshot taken from MD simulation of compound 7 (orange carbons) and the recently published X-ray crystal structure of the ZM241385-A_{2A} complex (blue carbons).

Compound 8 is characterized by a more flexible butyl chain bound to position 9. Due to its high mobility, this alkyl chain could adopt different conformations into the binding site region, accommodating in different accessible clefts. While one of these additional cavities is located near the tips of TM1, TM2 and TM7 (Figure 88, left), trajectories revealed the presence of another accessible volume placed near TM2 and TM3, oriented towards the inner side of the TM bundle (Figure 88, right).

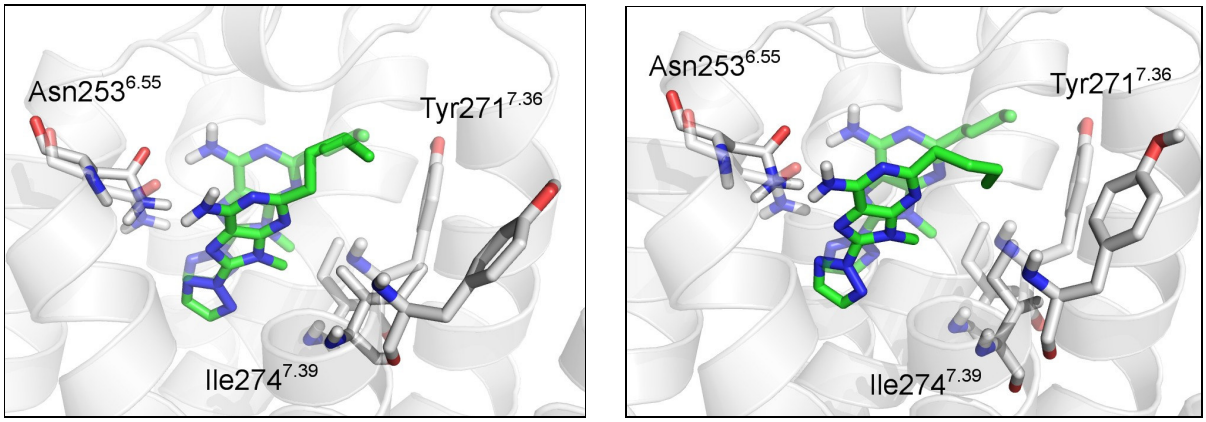

Figure 88: Left: starting (transparent) and final (opaque) conformations taken from the MD simulation of compound 8. Right: starting (transparent) and intermediate snapshots (opaque) extracted from the MD trajectory of compound 8. Ligand molecule is represented with green carbons.

Interestingly, this latter pocket located between TM2 and TM3 (Figure 88, right) corresponded to the highly hydrated volume found in the first A_{2A} crystal structure. Docking

studies also showed that the same pocket could accommodate the *para*-chlorophenyl and the furan substituents of compounds 5 and 6, respectively (Figure 89). Taken together, these evidences suggested the presence of an accessible volume near TM2 and TM3: thus, it could be hypothesized that substituents able to target this additional crevice might lead to an increase in binging affinity.

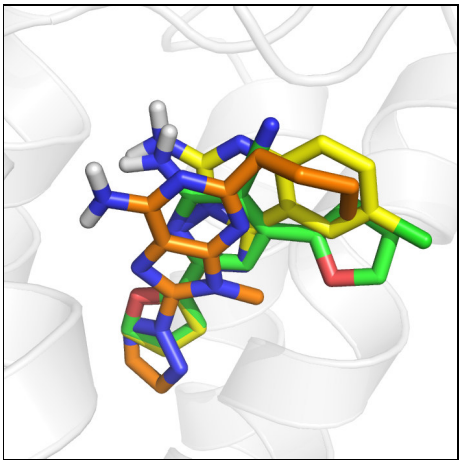

Figure 89: superposition of docking poses of compounds 5 (yellow carbons) and 6 (green carbons) into the A_{2A} receptor structure. The intermediate snapshot taken from the MD simulation of compound 8 is depicted with orange carbons.

Conclusions

Docking studies and MD simulations performed on the A_{2A} adenosine receptor threw light on the ligand recognition process, as well as on the main protein rearrangements occurring upon ligand binding. While docking studies correctly predicted the ligand-receptor interactions for xanthine derivatives, MD simulations were able to reproduce the alternative binding mode observed for the non-xanthine antagonist ZM241385. Moreover, these studies suggested the presence of additional clefts in the proximity of the binding site region: i) between TM5 and TM6 in the proximity of $His250^{6.52}$ (C1 in Figure 90), ii) at the extracellular ends of TM1, TM2 and TM7 (C2 in Figure 90) and iii) between TM3 and TM2, in the proximity of Phe168 (C3 in Figure 90). In conclusion, computational studies provided novel structural information, that could be exploited to either design novel chemical entities or to optimize the scaffold of known structures.

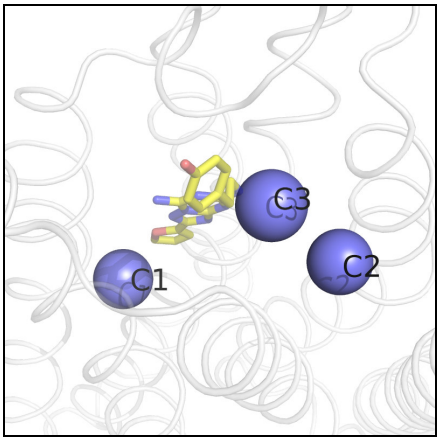

Figure 90: additional cavities found in the A_{2A} adenosine receptor during the present study. Co-crystallized pose of the antagonist ZM241385 is depicted with yellow transparent carbons.

CHAPTER 6

β_2 adrenergic receptor

Therapeutic relevance

The β_2 adrenergic receptor is a member of the GPCR superfamily and is activated by endogenous catecholamines. This specific receptor subtype is mainly located in the airways smooth muscle, epithelial cells, mast cells and type II alveolar cells.[420] The activation of the β_2 adrenergic receptor brings to bronchodilatation, inhibition of the release of pro-inflammatory mediators from activated mast cells,[421] increase of beat frequency of cilia[422] and inhibition of the extravasation of plasma proteins in the airways.[423,424] For these reasons, selective β_2-adrenergic agonists are clinically used for the treatment of respiratory diseases.[425,426] In the last decade, impressive efforts have been focused on the discovery of "once daily" β_2 adrenoceptor agonists, to be used as effective agents in the treatment of asthma and chronic obstructive pulmonary disease (COPD).[427]

Receptor signalling pathways

The main intracellular signalling route that follows the β_2 receptor stimulation involves the activation of the G protein subtype G_s, that brings to a subsequent activation of the adenylyl cyclase and to an increase in intracellular cAMP concentrations. Although this pathway represents the primary transduction mechanism exploited by the β_2 adrenergic receptor, several evidences suggested that this specific receptor subtype can couple with other G protein partners as well as other target effectors. For example, it is known that cAMP is able to activate the cAMP-dependent protein kinase (PKA): several studies confirmed that a PKA-mediated phosphorylation of the ICL3 segment of the β_2 adrenergic receptor led to a reduced interaction with G_s[428] and an enhanced affinity for G_i.[429] Thus, it could be hypothesized that the ICL3 portion of the β_2 adrenergic receptor might act as a "multipotential" G protein selector, whose functionality and specificity are regulated by the PKA-mediated phosphorylation.

Available crystal structures

Nowadays, 11 X-ray crystal structures of the β_2 adrenergic receptor are available in the Protein Data Bank: while 8 of them were co-crystallized with inverse agonists or antagonists, the remainder were crystallized in the presence of agonist molecules. All the

β_2 crystal structures solved so far share a conserved arrangement of the TM bundle, showing no remarkable dissimilarities between different crystallized receptors. As described previously, one of the peculiar structural features of the β_2 receptor is represented by the ECL2 portion. This loop region is characterized by a complex architecture, in which the sequence spanning from the tip of TM4 and the conserved cysteine residue is arranged in a short α-helix segment. The constrained geometry of the ECL2 stabilizes an open conformation of the overall extracellular portion of the receptor, facilitating the penetration of diffusible ligands from the extracellular milieu (Figure 91, left).

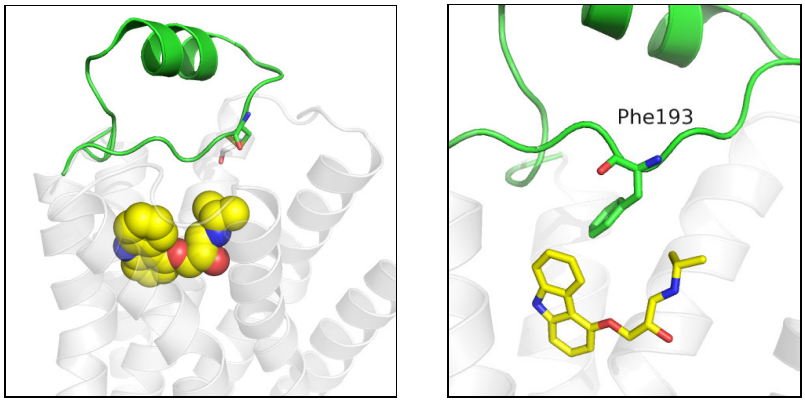

Figure 91: Left: β_2 receptor crystal structure in complex with carazolol (PDB: 2RH1). While the ECL2 is depicted in green, the carazolol molecule is represented with yellow spheres. The conserved disulphide bridge linking ECL2 with TM3 is depicted with sticks. Right: schematic representation of the interaction between Phe193 (green carbons) and carazolol (yellow carbons) into the β_2 receptor binding site (PDB: 2RH1) the ECL2 is represented with green cartoons.

The geometry and the position of the ECL2 segment have strong impact on the ligand binding site shape and characteristics. Indeed, residues belonging to the ECL2 portion form favorable interactions with both antagonist and agonist molecules into the ligand binding site. One clear example is represented by Phe193 that protrudes into the binding site crevice and forms edge-to-face interactions with the aromatic core present in a variety of β_2 receptor ligands (Figure 91, right).

Although the peculiar conformation of the ECL2 portion facilitates the exposure of the ligand binding site to the solvent, no water-mediated contacts were observed within the binding site region among all available β_2 receptor crystal structures.

Recent studies evidenced a crucial role of the ECL2 segment also in the receptor activation mechanism.[91] In particular, a recent NMR study on ligand-specific conformational changes at the extracellular surface of β_2 receptor has shown that agonist binding gives a weakening of the Lys305-Asp192 salt bridge, compared to what observed with inverse agonists.[91] Surprisingly, in available agonist-bound forms of the β_2 receptor

this salt bridge interaction can be either formed (e.g. PDB: 3PDS) or broken (e.g. PDB: 3P0G). This discrepancy could be rationalized taking into account the different "activation level" exhibited by β_2-agonist complexes: indeed, while the Lys305-Asp192 salt bridge is still present in the "partially" activated β_2 receptor structure co-crystallized with a covalent agonist (PDB: 3PDS, Figure 92), this interaction is broken in the "full" active state of the β_2 receptor (PDB: 3P0G, Figure 92). However, due to the low resolution of available β_2-agonist complexes (>3 Å), structural information provided by these crystal structures have to be carefully evaluated.

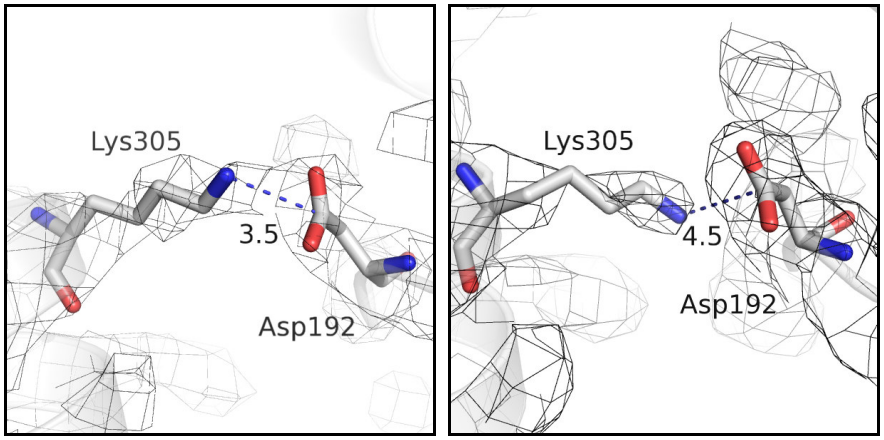

Figure 92: electron density maps depicted for two β_2-agonist complexes, namely 3PDS (left) and 3P0G (right). Lys305 and Asp192 are represented with white sticks. 2Fo– Fc electron density maps contoured at 1.0 σ.

Both the agonist- and antagonist-bound structures of the β_2 receptor share a similar location of the binding site region, shifted towards the extracellular side of the TM bundle. The ligand binding site spans from TM5 and TM6 to TM3 and TM7, extending perpendicularly respect to the helices vertical axis. Interestingly, co-crystallized agonists and antagonists share the same binding cleft, showing a similar accommodation of common ligand features. The ligand aromatic core is sandwiched between Val114$^{3.33}$ and Phe290$^{6.52}$ and faces three serine residues placed on TM5, namely Ser203$^{5.42}$, Ser204$^{5.43}$ and Ser207$^{5.46}$. The ethanolamine fragment of the ligand molecule is involved in a H-bond network with Asp113$^{3.32}$ and Asn312$^{7.39}$, where the first accepts H-bonds from both the protonated amine and the hydroxyl group of the ligand, while Asn312$^{7.39}$ acts both as a H-bond acceptor and donor, with the amine nitrogen and the hydroxyl oxygen of the ligand, respectively.

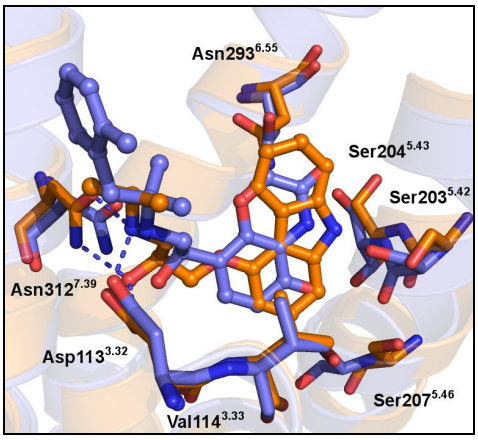

Figure 93: superpostion of the inverse agonist- (PDB: 2RH1, orange carbons) and agonist-bound (PDB: 3P0G, blue carbons) forms of the β_2 receptor. Ligands are represented with ball and sticks.

It is interesting to note that, despite the chemical diversity of co-crystallized ligands, no remarkable structural differences were observed within the binding site region among available β_2 receptor crystal structures.

MD simulations of carmoterol-β_2 complexes

At the time of this study, only the inverse agonist- or antagonist-bound forms of the β_2 adrenergic receptor were available: since β_2 agonists represent the most attractive class of compounds from a therapeutic point of view, this work tried to investigated the molecular basis of agonist recognition by means of docking studies and MD simulations.

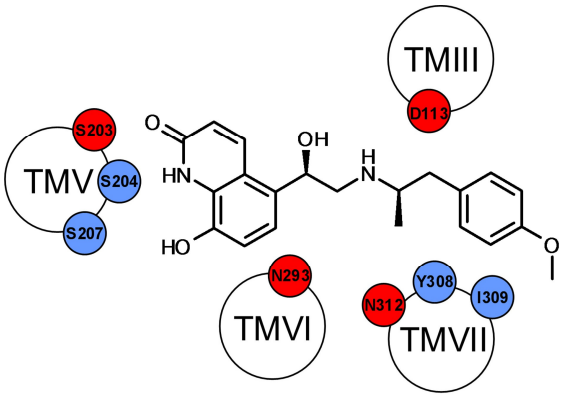

Figure 94: putative interactions between the β_2-adrenergic agonist carmoterol and residues within the receptor binding site, resulting from mutagenesis data. Residues (one-letter code) essential for carmoterol binding are depicted in blue, while residues depicted in red had been pointed out from mutagenesis studies performed with other adrenergic ligands. See text for references.

Recently, carmoterol (Figure 94, also reported as CHF-4226 or TA-2005) has emerged as a promising compound, endowed with a long duration of action.[430,431] Characteristic

features of carmoterol are the 8-hydroxy-carbostyril nucleus and the *para*-methoxyphenyl substituent on the lipophilic chain. While the first mimics the catechol group of the endogenous agonists, the methoxyphenyl group has been found to be critical for the β_2-selectivity of the molecule.[432]

Mutagenesis studies[432] revealed that the 8-hydroxyl group on the carbostyril scaffold interacts with Ser207$^{5.46}$ of transmembrane (TM) 5. Also Ser204$^{5.43}$, located on TM5, has been found to be crucial for carmoterol binding, as the point mutation Ser204$^{5.43}$Ala brings to a 56-fold decrease in carmoterol affinity for the β_2 receptor.[433] Several amino acids belonging to TM7 have been shown to interact with the *para*-methoxyphenyl group of carmoterol.[432] In particular, Tyr308$^{7.35}$Ala and Ile309$^{7.36}$Ala mutants showed 16-fold and 5-fold reduction in ligand affinity, respectively. Conversely, the binding affinity of isoproterenol, having an N-isopropyl group instead of the *para*-methoxyphenyl one, was rather unaffected.[432] These evidences suggest a specific orientation of carmoterol into the binding site, with the carbostyril ring facing TM5 and the *para*-methoxyphenyl group accommodated in the proximity of TM7. Further mutagenesis data, obtained from other compounds, identified other residues that can be involved in agonist recognition. These include: i) Ser203$^{5.42}$ (TM3), an anchor point for the hydroxyl groups of catecholamines;[273] ii) Asn293$^{6.55}$ (TM6), known to participate to the stereospecific recognition of norepinephrine stereoisomers;[356,434] iii) Asp113$^{3.32}$ (TM3), acting as the counterpart of the charged nitrogen carried by endogenous amines;[110,111] iv) Asn312$^{7.39}$ (TM7) also interacting with the catecholamine nitrogen.[435]

Considering that the β-hydroxy-β-phenylethylamine substructure of β_2-adrenergic agonists is also shared by carmoterol, it had been proposed that all the cited residues can also interact with this compound, as represented in Figure 94. Starting from this hypothesis, two different binding modes have been recently proposed. In the first one, resulting from docking studies on a rhodopsin-based receptor model, carmoterol was accommodated in an extended conformation, spanning from TM5 to TM7 and TM2.[436] In the second one, deriving from docking into a crystal structure of β_2 receptor, the lipophilic chain assumes a bent conformation, with the *para*-methoxyphenyl group pointing toward TM6 and TM7 (Figure 95).[437]

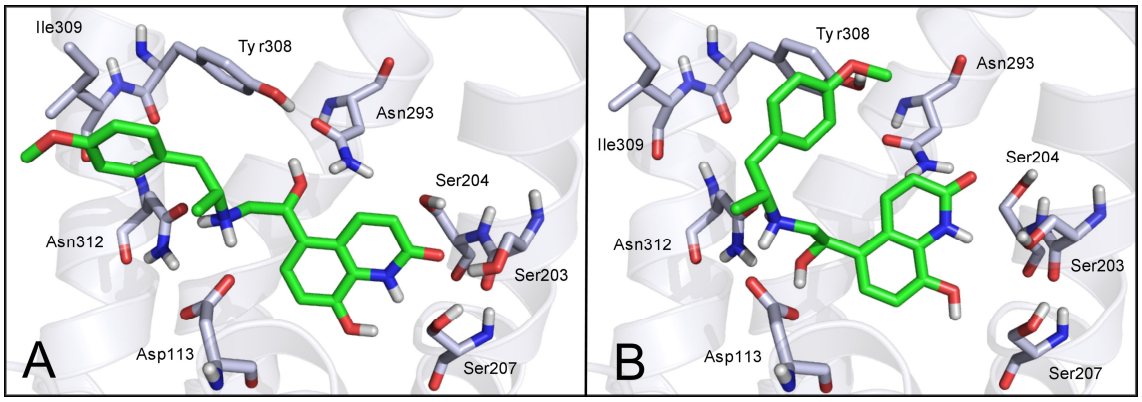

Figure 95: proposed binding modes for carmoterol (green carbons) into the β_2 receptor binding site in its extended (panel A) and bent (panel B) conformations. Residues thought to be involved in carmoterol binding are shown.

Considering that the available structures of β_2 receptor had been crystallized in the presence of antagonists or inverse agonists, it is reasonable to expect a significant induced-fit rearrangement in the protein when an agonist is docked into the binding site with a correct pose. Large-scale movements involved in GPCR activation require a modification of TM assembly, and significant rearrangement at the intracellular loops. However, while a MD simulation in ns-scale is not expected to accurately reproduce TM rearrangements, it may simulate limited modifications of the agonist-receptor complex in the proximity of the binding site, providing an assessment of proposed binding schemes. In this view, MD simulations starting from different agonist poses should converge to a single stable ligand accommodation, or at least allow to discriminate between "good" and "bad" ones. Furthermore, a proper agonist accommodation should favor some modifications of protein conformation, consistent with experimental evidences related to receptor activation. In fact, previous studies had reported that MD simulations are able to discriminate among alternative docking poses, furnishing useful insights for drug design.[438,439,440]

In the present work, two series of independent, 10-ns long, MD simulations of the β_2 receptor in complex with carmoterol, in an extended (hereinafter referred as conformation A) or bent conformation (hereinafter referred as conformation B), were performed in an explicit membrane environment. The two complexes corresponded to the best poses resulting from a docking procedure applied to the β_2-receptor crystal structure, and corresponded to the two binding modes previously proposed. A MD simulation with the co-crystallized ligand carazolol was performed for comparison. Our results suggest that carmoterol binds to β_2 receptor in a bent conformation, corresponding to one of the

previously-proposed poses (conformation B),[437] and that adaptation of the receptor to the agonist is consistent with an event (weakening of the salt bridge between Asp192 and Lys305) supposed to be involved in receptor activation.[91]

Docking and MD protocols

Hydrogen atoms were added to the high-resolution crystal structure of β_2 receptor-T4L (PDB entry 2RH1),[58] using Maestro 9.0.[283] All non-protein molecules were removed, including the acetamide protecting Cys265, the palmitoyl group attached to Cys341 and the crystallographic water molecules, except the carazolol molecule. Chain termini were capped with neutral groups (acetyl and methylamino). All histidines were singly protonated, all arginines and lysines were fully protonated. After deleting the T4L residues, Modeller 9.7[270,271] was used to cap the newly-exposed termini of Leu230 and Lys263 with a bridge of 3 alanines. It was previously shown experimentally that partial removal of ICL3 results in functional protein:[441] therefore, removal of the T4 during system construction for the MD simulation was not expected to significantly alter the protein's potential functional properties and hence expected fluctuations.

(*R*,*R*)-carmoterol was docked with Glide 5.5[392] into the β_2 receptor binding site. The location of carazolol was taken as binding site for docking of carmoterol. The ligand docking calculations were done in the standard precision mode of Glide. During the docking process, the receptor was treated as fixed while ligand was flexible. The scaling factor for the van der Waals radii of nonpolar atoms (those with an absolute partial charge lower than 0.15) was set to 0.8 and the Coulomb-van der Waals energy cutoff was set to 100 kcal/mol. Initial carmoterol conformations into the β_2 receptor binding site were inferred from those previously reported[436,437] and used as reference conformations to restrict the position of ligand heavy atoms during docking procedure. The AMBER* force field[291,292,293] and the GB/SA water model implemented in MacroModel 9.7[442] were used to minimize all complexes. Partial minimization of docked complexes were performed in two steps. First, distance constraints were applied between ligand and protein groups involved in hydrogen bonds. These constraints were characterized by a force constant of 100 kJ/(mol$Å^2$) and a distance of 2 Å. All protein residues within 4 Å of the ligand were allowed for full flexibility, while position restraints of 20 kJ/(mol$Å^2$) were applied to residues between 4 to 10 Å from the ligand. The rest of the atoms were retained fixed. In the

second step of minimization only protein side chains in a 6-Å proximity of the ligand molecule were free to move. The Polak-Ribiere conjugate gradient method was used for minimizations with a convergence threshold of 0.05 kJ/(molÅ).

Carmoterol and carazolol-β_2 receptor complexes were embedded in a POPC lipid bilayer by aligning the receptor to the 2RH1 crystal structure deposited into the Orientations of Protein in Membranes database (OPM),[297] with at least 13 Å between the protein and its closest periodic image. Protein-membrane systems were solvated by approximately 9200 SPC water molecules in a simulation box of approximately 80 Å x 70 Å x 100 Å. The Amber99SB force field[298] was used to model the protein, while ligands and lipids were parameterized using the GAFF.[299] All the systems were relaxed using a modified version of a membrane relaxation protocol implemented in the Schrodinger 2009 Suite.[414] Minimizations and molecular dynamics calculations were performed with Desmond v22623.[296] All simulations were performed in the NPT ensemble under constant pressure of 1 atm and a temperature of 310 K, thermostated and barostated using the Langevin method.[301] All bond lengths to hydrogen atoms were constrained using M-SHAKE.[302] Short-range electrostatic interactions were cut off at 9 Å whereas long-range electrostatic interactions were computed using the Particle Mesh Ewald method.[303] A RESPA integrator[304] was used with a timestep of 2 fs, and long-range electrostatics were computed every 6 fs. Snapshots were saved every 12 fs, resulting in 834 structures for each simulation. Three independent simulations were conducted for all systems using different initial random velocity seeds.

Results

Automated docking with Glide[392] was performed to guide the placement of carmoterol within the β_2 receptor binding site. The first 10 solutions presented alternatively an extended or a bent conformation of the ligand, corresponding to the previously reported A and B binding modes, respectively. The top ranked poses (G-score) presented an extended conformation of carmoterol; one of these poses, consistent with mutagenesis data, was partially minimized and taken as the starting point for MD simulations on the so-called "conformation A". The other family of docking poses was characterized by bent conformations of carmoterol; one of these, allowing interaction of the ligand with the key residues, was the starting point for simulations on the "conformation B", after partial minimization. The two starting geometries of MD simulations are represented in Figure 95.

For each conformation, two series of 10-ns MD simulations were run. Each simulation was replicated three times, starting from different random seeds for the initial velocity distribution. Figure 96 reports the total root mean square deviations (RMSD) from the initial structures, computed for TM α-carbons. After the first 1-2 ns, the RMSD values converged to 1.2-1.4 Å, indicating, for both complexes, overall conservation of the secondary structure for the TM domains.

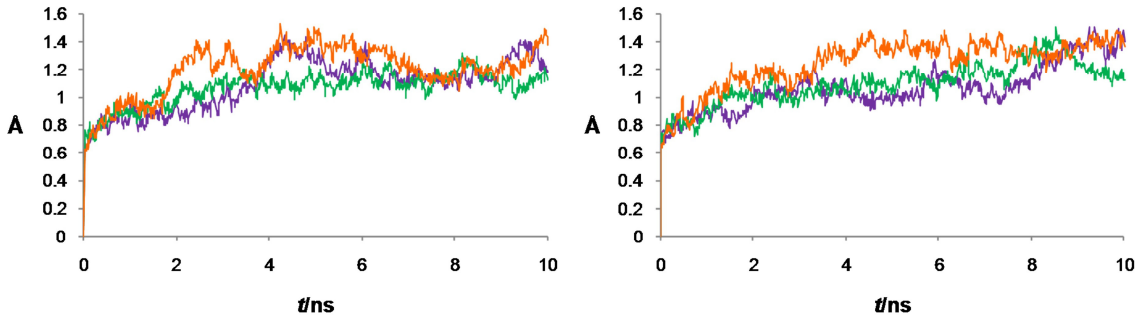

Figure 96: RMSD plots for the MD-simulated structures of receptor-carmoterol complexes calculated for □-carbons of TM regions. Conformation A (left) and B (right). Purple line: simulation 1; green line: simulation 2; orange line: simulation 3.

However, the dynamic behavior of carmoterol was different in the two systems, with conformation A being significantly less stable than conformation B. For conformation A, during MD simulations the carbostyril ring shifted considerably from its initial position (Figure 97, left).

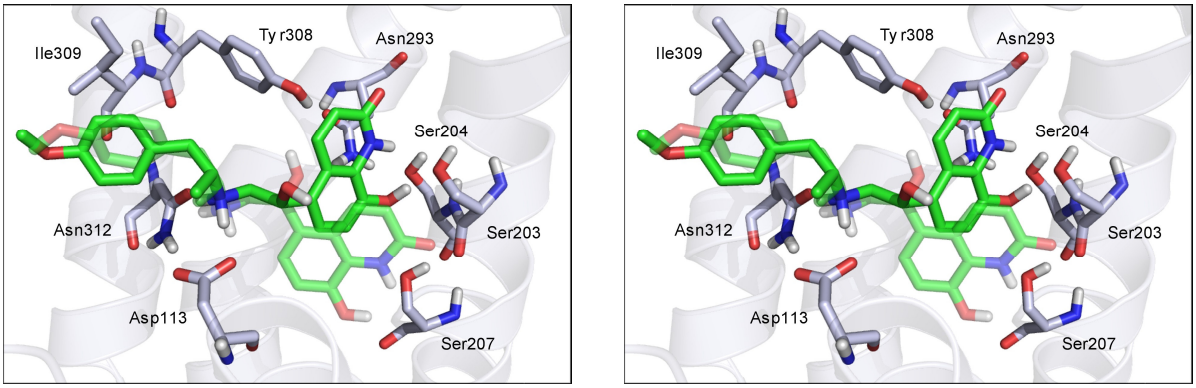

Figure 97: Left: starting (transparent) and final (opaque) conformation of carmoterol (green carbons) obtained with MD simulation of conformation A. Right: starting (transparent) and final (opaque) conformation of carmoterol (green carbons) obtained from MD simulation of conformation B.

In fact, during the early stages of the simulations, hydrogen bond interactions with Ser203$^{5.42}$ and Ser204$^{5.43}$ were lost. Time-averaged distances between Ser203$^{5.42}$ or Ser204$^{5.43}$ hydroxyl oxygens and the carboxylic oxygen of carmoterol were 6.10 ± 0.73 Å and 4.65 ± 0.83 Å, respectively. The H-bond between the 8-hydroxyl group of carmoterol

and Ser207$^{5.46}$ resulted more stable, as indicated by the O-O average distance of 3.25 ± 0.45 Å. In its starting conformation, carmoterol also interacted with the amide group of Asn293$^{6.55}$ through its aliphatic hydroxyl group. A rearrangement from the anticlinal to a gauche orientation of the C-CH-CH_2-N dihedral angle, occurring during the early stages of the simulations, caused a reorientation of the hydroxyl group towards TM3, with loss of the H-bond interaction with Asn293$^{6.55}$. On the other hand, the methoxyphenyl substituent showed little displacement from its starting accommodation, probably due to a H-bond interaction between the methoxy group and the indole ring of Trp313$^{7.40}$, located on TM7 (not shown in Figure 97). This behavior was observed in all the three independent simulations.

Conversely, MD simulations for conformation B showed remarkable conservation of the H-bond network between the carbostyril ring of carmoterol and the serines on TM5 (Figure 97, right). The average distance between Ser203$^{5.42}$ hydroxyl oxygen and the amide nitrogen of carmoterol was 3.18 ± 0.23 Å. The distance between the oxygen atom of Ser207$^{5.46}$ and that of the 8-hydroxyl group of carmoterol was 2.90 ± 0.18 Å, indicative of a stable H-bond interaction. During the simulation, a rotation around χ1 of the Asn293$^{6.55}$ side chain, was observed, leading to a re-orientation of the side chain toward TM5. This led to the formation of an extensive hydrogen bonding network, with Asn293$^{6.55}$ bridging between the side chain of Ser204$^{5.43}$ and the carbonyl oxygen of carmoterol. The ethanolamine fragment of carmoterol was involved in a H-bond network with Asp113$^{3.32}$ and Asn312$^{7.39}$, where the first accepts H-bonds from both the protonated amine and the hydroxyl group of the ligand, while Asn312$^{7.39}$ acts both as a H-bond acceptor and donor, with the amine nitrogen and the hydroxyl oxygen of carmoterol, respectively. During the early stage of the calculation, a slight rotation about carmoterol N-CH bond was observed. Due to this movement, the methoxyphenyl substituent moved toward Tyr308$^{7.35}$ and Ile309$^{7.36}$ on TM7, reaching a stable accommodation. Similar outcomes were observed for the three independent simulations of conformation B.

A closer inspection of carmoterol binding site and its neighboring residues revealed critical structural differences between MD simulations for A and B conformations. The most relevant difference between the two complexes was observed at the receptor extracellular domain, where a salt bridge between Asp192 and Lys305 connects the ECL2 to ECL3. Several breaks of this salt bridge were observed in the simulations with conformation B. The average distances between the ε-N atom of lysine and the carboxyl carbon of aspartic acid (N-C distance) were 3.89 ± 1.03 Å, 3.56 ± 0.54 Å and 3.55 ± 0.43 Å for the three

simulations, respectively. Interestingly, no such movements were observed during the MD simulations of conformation A, where the salt bridge was conserved through the entire trajectory, with average N-C distances of 3.37 ± 0.22 Å, 3.44 ± 0.23 Å and 3.40 ± 0.27 Å (Figure 98).

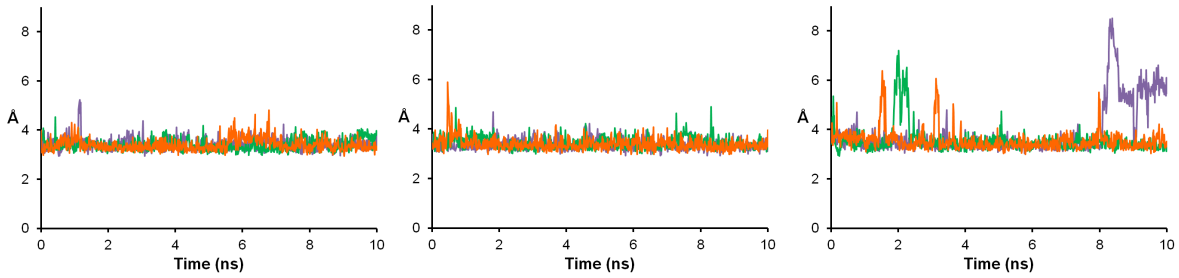

Figure 98: time series of N-C distance for Lys305-Asp192, monitored during MD simulation of β_2 receptor-ligand complexes: left: carazolol; center: carmoterol, conformation A; right: carmoterol, conformation B. Purple line: simulation 1; green line: simulation 2; orange line, simulation 3.

Visual inspection of MD trajectories showed that, in the B orientation, carmoterol tends to weaken the Lys305-Asp192 salt bridge by steric interference with the methoxyphenyl moiety. During the last two ns of one of the three simulation, the N-C distance increased from that of the β_2 receptor crystal structure (4.2 Å) to 8-9 Å, which is consistent with the disruption of the geometrical criteria for a salt bridge, as recently defined by Kumar and Nussinov.[443,444] To better analyze the occurrence of Lys305-Asp192 salt bridge disruptions, we prolonged to 100 ns a simulation of conformation B. As depicted in Figure 99, although the salt bridge is maintained during most of the simulation time, several breaks occurred during the trajectory. This confirms that this agonist-induced weakening of the salt bridge is not an event occurring only during the equilibration of the system, in the first nanoseconds.

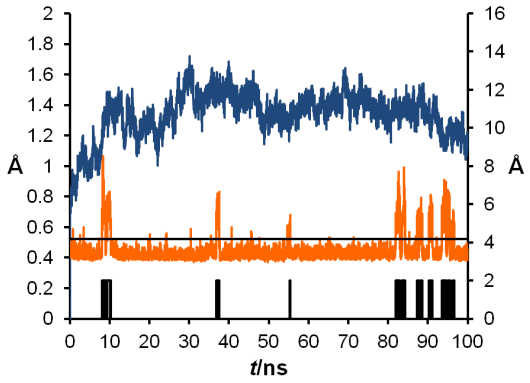

Figure 99: RMSD values (blue) for the 100-ns simulation of β_2 receptor-carmoterol complex in conformation B, calculated over TM α-carbons (left y-axis). N-C distance values for Lys305-Asp192 are reported in orange (right y-axis). The black horizontal line indicates the N-C distance observed in the β_2 receptor-carazolol crystal structure 2RH1. The black bars indicate disruptions of Lys305-Asp192 salt bridge.

Remarkably, a recent NMR study on ligand-specific conformational changes at the extracellular surface of β_2 receptor has shown that agonist binding gives a weakening of the Lys305-Asp192 salt bridge, compared to what observed with inverse agonists.[91]

For comparison, MD simulations were also performed for the β_2 receptor crystal structure in complex with carazolol. Three 10-ns simulations showed a stable complex (RMSD on TM α-carbons of 1.35 ± 0.26 Å, 1.00 ± 0.13 Å and 1.38 ± 0.22 Å), with a stable arrangement of carazolol within its binding site (all the polar interactions between ligand and receptor were conserved). Moreover, the salt bridge between Lys305 and Asp192 was conserved throughout the simulations, with average N-C distances of 3.43 ± 0.25 Å, 3.40 ± 0.24 Å and 3.41 ± 0.25 Å.

The binding mode obtained at the end of the MD simulations of conformation B was compared to the recent crystal structure of the β_1 adrenergic receptor in complex with carmoterol (PDB: 2Y02). Interestingly, the two binding modes were almost identical, showing a similar orientation of the ligand functional groups: indeed, while the carbostyril ring of carmoterol formed extensive polar interactions with conserved serines on TM5, the terminal methoxyphenyl moiety was sandwiched between the side chains of residues located at positions 7.35 and 7.36. A closer inspection revealed that also the orientation of residues delimiting the binding site region was predicted with good accuracy (Figure 100).

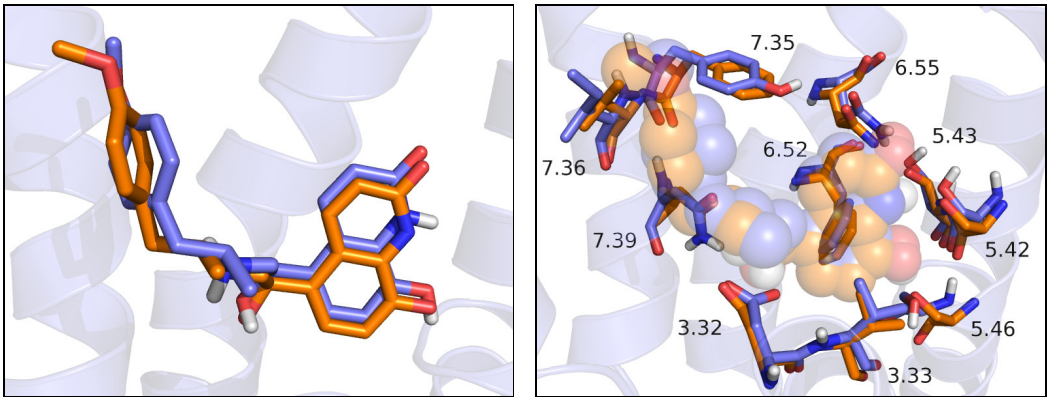

Figure 100: superposition of the last frame of simulation 1 conducted for conformation B of carmoterol (blue carbons) with the co-crystallized pose of carmoterol within the β_1 adrenergic receptor (PDB: 2Y02, orange carbons). Left: carmoterol molecules are represented with sticks. Right: view of residues delimiting the binding site region: while carmoterol molecules are depicted with transparent spheres, residues surrounding the binding site are shown with sticks. Residues are numbered according to the Ballesteros numbering scheme.

Conclusions

Here we report molecular dynamics simulations on membrane-embedded β_2 receptor in complex with the agonist carmoterol. Starting from two docking poses, corresponding to the two previously proposed binding modes of this ligand, we observed different evolutions of the MD trajectories. For the pose with an extended conformation of carmoterol (A), we observed substantial loss of the interactions initially taken by the carbostyril moiety with the serine residues, which had been suggested to be critical for agonist recognition by mutagenesis data. Moreover, in this case no remarkable alteration of the extracellular loops was observed. Conversely, starting from a bent conformation of carmoterol (B), MD shows mutual arrangements of ligand and receptor, resulting in stable interactions with key amino acids and in weakening of a salt bridge between Asp192 and Lys305. The disruption of this salt bridge, connecting ECL2 and ECL3, has been recently recognized by NMR data as involved in receptor binding with agonists. Consistently, MD simulations on the complex crystallized with the inverse agonist carazolol showed stable ligand receptor interactions and no weakening of the Asp192-Lys305 salt bridge.

Although the nanosecond time scale of these MD simulations was certainly not sufficient for capturing the slow transition to the active receptor conformation, our study provides new insights into the molecular basis of carmoterol recognition process, showing conformational coupling between the extracellular motifs and the orthosteric binding site of β_2 receptor. More interestingly, results retrieved from MD simulations were in good agreement with the recently published β_1-carmoterol crystal structure, showing an almost identical orientation of the ligand into the receptor binding site.

The stable orientation found for carmoterol, as well as indications given by MD simulations, can be used in the structure-based design of new β_2-adrenergic agonists.

CHAPTER 7

H_3 histamine receptor

Therapeutic relevance

Identified for the first time in 1983,[445] the histamine H_3 receptors are mainly located in the central nervous system. They are primarily distributed in the presynaptic regions and they modulate the biosynthesis and the release of histamine through a negative feed-back mechanism.[446] Beside their role in the histaminergic transmission, H_3 receptors can act also on non-histaminergic neurons, influencing the release of different neurotransmitters, such as dopamine,[447] norepinephrine,[448,449] serotonin[450] and acetylcholine.[451] Several experimental evidences showed that the administration of H_3 antagonists in the central nervous system causes an increase of neurotransmitters concentrations, leading to an improvement of cognition and attention in animal models.[452,453] Due to this reason, H_3 antagonists have been proposed as attractive therapeutics for the treatment of cognitive disorders, (e.g. Parkinson's and Alzheimer's diseases) as well as for other pathological conditions, including narcolepsy, obesity and epilepsy.[454,455,456,457,458]

Receptor signalling pathways

The H3 histamine receptor is mainly coupled to the G protein subtype G_i.[459,460] The H_3-mediated activation of the G_i protein brings to an inactivation of the adenylyl cyclase and a consequent decrease in cAMP levels. Beside the adenylyl cyclase pathway, the G_i protein can activate other downstream effectors, such as the mitogen-activated protein kinase (MAPK)[461,462] and the phosphatidylinositol 3-kinase (PI3K). The signal transduction pathway of the H_3 receptor might also cause the activation of the phospholipase A2 (that causes an increase of arachidonic acid concentration),[463] the decrease of intracellular calcium concentration[464,465] and the inhibition of the Na^+/H^+ exchanger.[466]

Computational studies on novel dibasic H_3 receptor antagonists

A series of non-imidazole dibasic H_3-antagonists carrying a biphenyl scaffold has been recently characterized.[467,468] The compound showing the highest potency within this series (compound 1, Figure 101) was characterized by subnanomolar affinities for both human and rat H_3 receptors (human H_3 pK_i = 9.47, rat H_3 pK_i = 8.92). A rhodopsin-based homology model of the rat H_3 receptor, showed two possible accommodations for compound 1 in the receptor binding site. In the "horizontal" orientation, compound 1 is

accommodated perpendicular to the helix bundle, occupying the typical orthosteric binding site identified in class A GPCRs. In this orientation, the piperidine nitrogens form ionic interactions with both Asp114$^{3.32}$ and Glu206$^{5.46}$. Mutagenesis studies conducted on these two residues to investigate the binding mode of histamine, indicated that while Asp114$^{3.32}$ preferably interacted with the histamine basic nitrogen, Glu206$^{5.46}$ represented the imidazole ring counterpart. On the contrary, in the "vertical" arrangement, compound 1 lays in a cavity parallel to the transmembrane domains, delimited by TM1, TM2 and TM7. In this alternative orientation, the two basic nitrogens interact with Asp114$^{3.32}$ and Asn404$^{7.45}$: this latter residue is located on the intracellular portion of the TM7, in the proximity of the conserved Trp371$^{6.48}$.

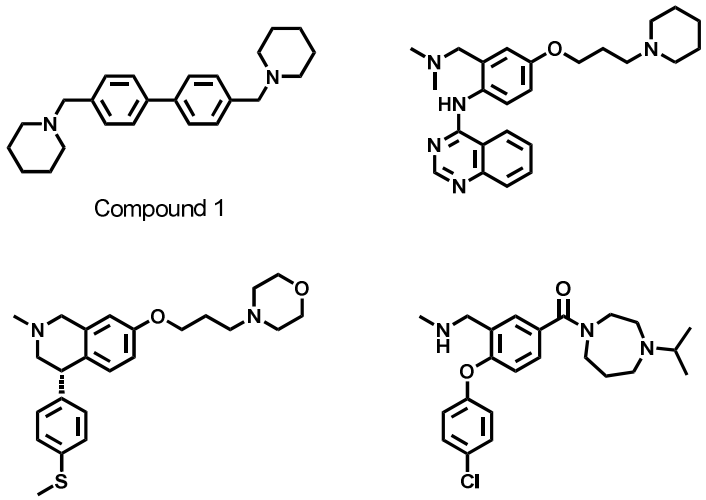

Figure 101: structures of compound 1 and of three dibasic H_3 antagonists carrying a lipophilic side chain.

The presence of these two cavities into the H_3 receptor homology model has been already investigated by other modeling studies, which provided "horizontal" and "vertical" poses for a number of different H_3 antagonists.[469,470,471,472,473] In this scenario it could be speculated that, due to the existence of two perpendicular pockets into the H_3 receptor, dibasic H_3 antagonists carrying a suitable side chain could simultaneously occupy both cavities, forming addtional favorable interactions within the H_3 receptor binding site. This hypothesis is further supported by some recent examples of novel H_3 antagonists, characterized by a lipophilic side chain connected to a dibasic scaffold (Figure 101).[474,475,476]

Therefore, to evaluate the impact of an additional lipophilic chain on the biphenyl scaffold, a new series of derivatives has been characterized.[477]

Conformational analysis

Novel dibasic H_3-antagonists carrying an additional lipophilic chain have been synthesized as mixtures of two diastereoisomers.[477] Since only the configuration of one chiral center was determined (i.e. C2 within the 2-methylpyrrolidin substituent), the complete assignment of their absolute configuration was attained combining NMR experiments and computational studies. With the aim to define an unambiguous rule to assign the correct stereochemical configuration based on their NMR spectra, this study focused on two intermediate structures, namely compounds 2a and 2b (Figure 102), lacking the second cyclic amine which gave NMR signals overlapping the interesting region. Identification of the two diasteroisomers for this model compound allowed the assignment of correct configuration to target compounds in the series.

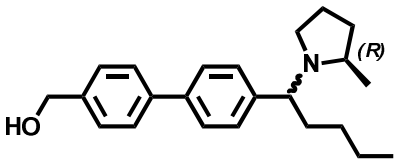

Compounds 2a and 2b

Figure 102: compounds selected for the conformational analysis.

Protocol

Molecular modeling studies were performed with Macromodel 9.8.[478] Starting conformations of (*S*,*R*) and (*R*,*R*) isomers of {4'-[1-(2-methylpyrrolidin-1-yl)pentyl]biphenyl-4-yl}methanol (Figure 103) were energy-minimized applying the MM3 force field,[479] setting a convergence criterion of 0.05 kJ/(molÅ).

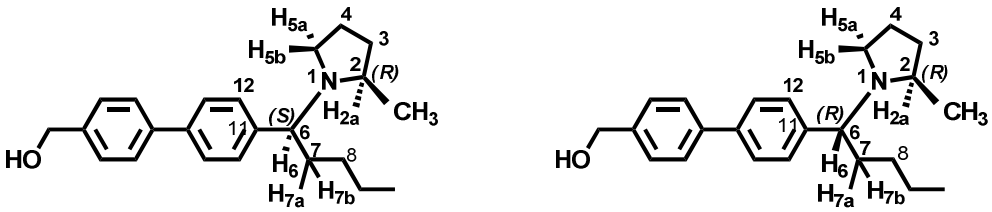

(*S*,*R*)-isomer (*R*,*R*)-isomer

τ_1: C2-N-C6-C11
τ_2: N-C6-C7-C8

Figure 103: compounds selected for the SD simulations. Protons are marked "a" or "b" according to their relative position with respect to the pyrrolidine plane: while protons "a" lay below the ring plane, protons "b" are placed above the plane.

Stochastic dynamics (SD) simulations were run using the GB/SA implicit-solvation model[480] for chloroform, with the MM3 force field. Equilibration and production phases were run for 1000 ps and 1 µs, respectively. SD were conducted to a temperature of 298 K, applying a time step of 1 fs. Snapshots were collected every 100 ps, resulting in 10000 structures for each SD simulation. SD has already proved to reproduce the conformational equilibrium of small molecules in solution, applying an implicit-solvation model for chloroform.[313,314,315,316,317,318,319] Coupling constants were calculated with Maestro 9.1,[481] applying the Karplus equation.[320]

Results

The conformational analysis of (*S*,*R*) and (*R*,*R*) isomers showed remarkable differences in the dynamic behavior of both the butyl chain and the pyrrolidine ring. The time evolution of the τ_1 dihedral angle for the (*S*,*R*)-isomer revealed that the pyrrolidine ring adopted one preferred orientation ($\tau_1 \approx 300°$ in Figure 104), in which the methyl substituent is located in the proximity of the benzylic hydrogen H6.

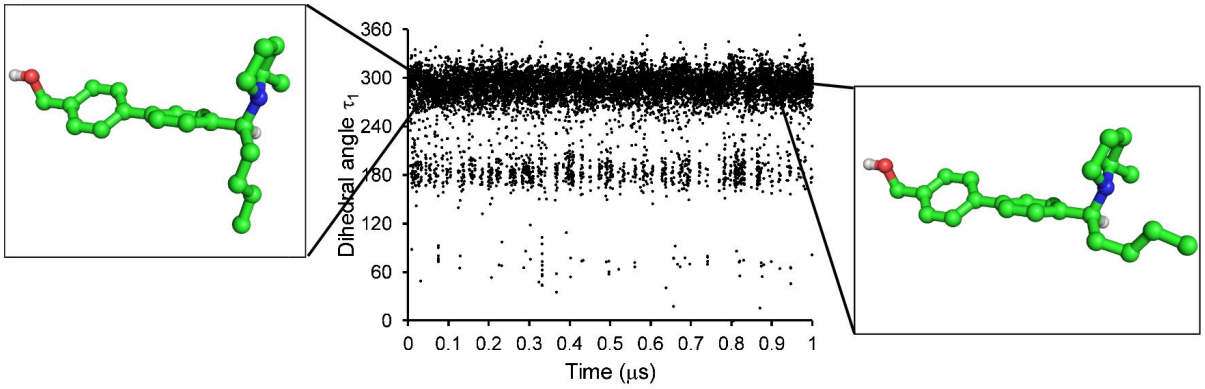

Figure 104: time evolution of dihedral angles τ_1 for the (*S*,*R*)-isomer. Representative conformations with $\tau_1 \approx 300°$ and $\tau_2 \approx 180°$ (left) or $\tau_2 \approx 300°$ (right) are depicted with green carbons. Only the H6 is represented for clarity.

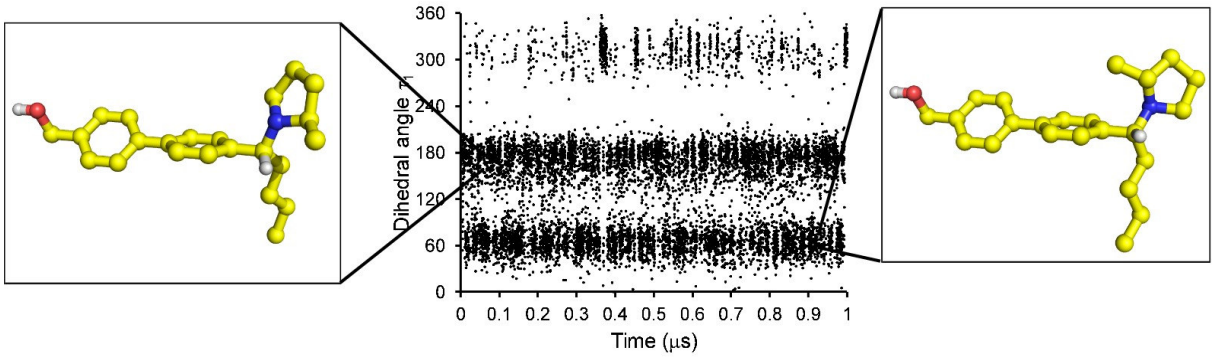

Figure 105: time evolution of dihedral angles τ_1 for the (*R*,*R*)-isomer. Representative conformations with $\tau_1 \approx 60°$ (light) and $\tau_1 \approx 180°$ (left) are depicted with yellow carbons. Only the H6 is represented for clarity.

Conversely, SD simulation of the (*R*,*R*)-isomer showed rapid interconversions of the pyrrolidine ring between two orientations ($\tau_1 \approx 60°$ and 180° in Figure 105): while in the former ($\tau_1 \approx 60°$), the methyl substituent points toward the biphenyl scaffold (Figure 105, right), in the latter ($\tau_1 \approx 180°$) the methyl lays in the proximity of the benzylic hydrogen H6 (Figure 105, left).

Time evolution of the dihedral angle τ_2 showed the presence of two preferred orientations for the butyl chain of the (*S*,*R*)-isomer ($\tau_2 \approx 180°$ and $\tau_2 \approx 300°$, Figure 106), with the first rotatable bond arranged in *anti* or *gauche* conformation. Conversely, during SD simulation of the (*R*,*R*)-isomer the butyl chain retained an almost fixed orientation, with $\tau_2 \approx 180°$ (Figure 106): only a limited number of snapshots (~ 9%) showed a different alkyl chain orientation, characterized by a τ_2 value around 60°.

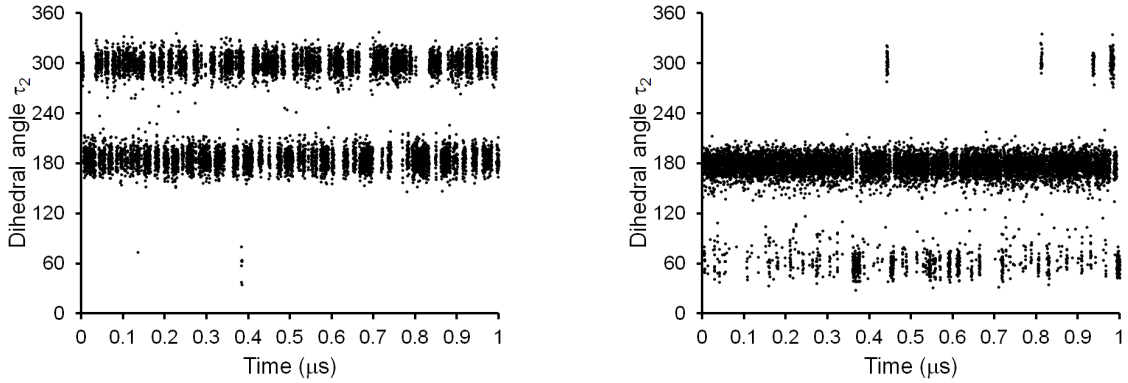

Figure 106: time evolution of dihedral angles τ_2 for the (*S*,*R*)- (left) and the (*R*,*R*)-isomer (right).

NMR data for compounds 2a is in agreement with SD results obtained for the (*S*,*R*)-isomer. The preferred orientation of the pyrrolidine ring seen in the SD simulation is supported by the presence of significant NOE signals between the *ortho*-aromatic protons (H12) and H2a, H5a, H5b and CH_3 protons: on the contrary, no detectable signals were found between H12 and H3a, H3b, H4a and H4b. Accordingly, calculated average distances between H12 and H5a, H5b and CH_3 protons are 2.81 Å, 3.26 Å and 3.07 Å, respectively (for the methyl group the average minimum distance between CH_3 protons and H12 was considered). Proton-proton coupling constants obtained for the butyl chain of compound 2a are consistent with the presence of two favored orientations: indeed, both $J_{H7a\text{-}H6}$ and $J_{H7b\text{-}H6}$ values can be considered as a combination of *anti* and *gauche* arrangements (Table 3).

Also in the case of the (*R*,*R*)-isomer, results obtained from the SD simulation are in good agreement with the NMR data for compound 2b. The preferred conformation found for the

butyl chain in the SD simulation is consistent with i) the *gauche* and *anti* values assumed by $J_{H7a\text{-}H6}$ and $J_{H7b\text{-}H6}$, respectively; ii) the presence of a significant NOE signal between H12 and H7b, but not between H12 and H7a. The rotation of the pyrrolidine ring seen during the SD simulation of the (*R*,*R*)-isomer is also consistent with a number of weak NOE signals detected from H12, H7a and H7b to the pyrrolidine protons of compound 2b.
In Table 3 are listed ^3J values obtained from SD simulations of (*S*,*R*) and (*R*,*R*) isomers and NMR spectra of compounds 2a and 2b: as could be observed, ^3J values calculated for the (*S*,*R*) and (*R*,*R*) isomers showed good agreement with ^3J values measured for compounds 2a and 2b, respectively. In addition, the assignment (*S*,*R*)-compound 2a and (*R*,*R*)-compound 2b was also confirmed by the different δ values obtained for both H2a (more shielded in compound 2a) and CH_3 (more shielded in compound 2b) protons. Indeed, in the majority of conformations observed for the (*S*,*R*)-isomer the H2a proton laid above the plane of the phenyl ring (Figure 104): conversely, in one of the two preferred conformations of the pyrrolidine ring of the (*R*,*R*)-isomer the methyl group pointed above the phenyl ring (Figure 105).

	(*S*,*R*)-isomer (compound 2a)		**(*R*,*R*)-isomer (compound 2b)**	
Coupling constant	**Measured**	**Calculated**	**Measured**	**Calculated**
H_2-H_{3a}	6.6	7.1	-	-
H_2-H_{3b}	6.6	7.5	-	-
H_{5b}-H_{4a}	3.0	3.2	-	-
H_{5b}-H_{4b}	8.4	8.3	-	-
H_{7a}-H_6	6.0	6.8	3.6	4.6
H_{7b}-H_6	9.6	7.3	10.8	10.0

Table 3: coupling constants (Hz) observed for compounds 2a and 2b and calculated for (*S*,*R*) and (*R*,*R*) isomers.

For all the newly synthesized compounds, while one isomer showed NMR features similar to those of compound 2a (e.g. closer $J_{H7a\text{-}H6}$ and $J_{H7b\text{-}H6}$, shielded H2a proton) the second one showed a spectrum resembling that of compound 2b (e.g. distinct $J_{H7a\text{-}H6}$ and $J_{H7b\text{-}H6}$, shielded methyl group). Thus, the combination of SD simulations and experimental NMR data allowed the assignment of the correct configuration to all the compounds in the series, based on peculiar differences observed within each diastereomeric couple.

Homology modeling of the H_3 histamine receptor

To evaluate the accommodation of novel dibasic compounds into the H_3 receptor binding site, a homology model of the human H_3 histamine receptor was built starting from the newly released crystal structure of the H_1 histamine receptor.

Receptor model building and refinement

Considering their whole amino acid sequences, H_1 and H_3 histamine receptors are characterized by 21% identity and 43% homology. Although homology-models should be considered as heuristic, previously published H_3 receptor models showed good performances in virtual screening campaigns[471] as well as in reproducing SARs of antagonist molecules,[482] even if they were constructed from templates having lower sequence similarity. TM domains of H_1 and H_3 receptors are characterized by 36% identity and 68% homology of residues, sharing some crucial amino acids involved in ligand stabilization. For example, the conserved aspartic acid located at position 3.33 in the H_1 crystal structure (Asp107$^{3.32}$) interacts with the basic group of the co-crystallized ligand (doxepin). Asn198$^{5.46}$, located on TM5 of the H_1 receptor, is thought to be the counterpart for the imidazole ring of the histamine molecule:[483] interstingly, this residue does not form interactions with doxepin in the H_1 receptor crystal structure. The corresponding amino acid located at position 5.46 in the H_3 receptor is Glu206$^{5.46}$: mutagenesis studies highlighted the importance of this amino acid for histamine and (*R*)-α-methylhistamine binding.[484] A pattern of amino acids delimiting the ligand binding site in the H_1 receptor were found to be conserved in the H_3 receptor, inclusing Tyr108$^{3.33}$ on TM3, Trp428$^{6.48}$ on TM6 (belonging to the CWXP motif), Thr112$^{3.37}$, Phe199$^{5.47}$, Phe424$^{6.44}$ and Tyr431$^{6.51}$.

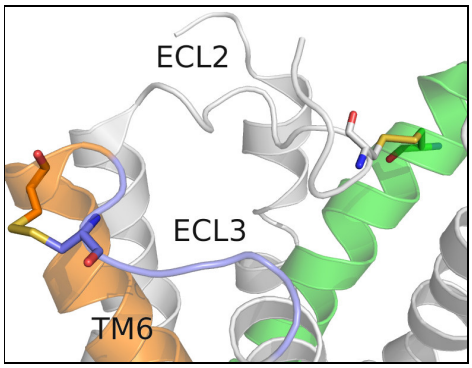

Figure 107: x-ray crystal structure of the H1 histamine receptor. TM3, TM6 and the ECL3 portions are depicted with green, orange and blue cartoon, respectively. Residues forming the two disulphide bridges linking ECL2 with TM3 and ECL3 with TM6 are depicted in sticks.

The H_1 histamine receptor crystal structure (PDB: 3RZE)[65] was retrieved from the Protein Data Bank.[74] The amino acid sequence of the human H_3 receptor (UniProt ID: Q9Y5N1) was retrieved from the Universal Protein Resource.[267,268] ClustalW[269] was employed to build an initial sequence alignment: a following alignment optimization was carried out taking into account conserved common motifs of class A GPCRs.[14,164] Moreover, a characteristic disulfide bridge connecting the ECL3 to the tip of TM6 in the H_1 receptor crystal structure was taken into account during the optimization of the sequence alignment (Figure 107).

```
H1    28 MPLVVVLSTICLVTVGLNLLVLYAVRSERKLHTVGNLYIVSLS 70
H3    35 AVLAALMALLIVATVLGNALVMLAFVADSSLRTQNNFFLLNLA 77

H1    71 VADLIVGAVVMPMNILYLLMSKWSLGRPLCLFWLSMDYVASTA 113
H3    78 ISDFLVGAFCIPLYVPYVLTGRWTFGRGLCKLWLVVDYLLCTS 120

H1   114 SIFSVFILCIDRYRSVQQPLRYLKYR-TKTRASATILGAWFLS 155
H3   121 SAFNIVLISYDRFLSVTRAVSYRAQQGDTRRAVRKMLLVWVLA 163

H1   156 FLWVIP-ILGWNH-------RREDKCETDFYDVTWFKVMTAII 197
H3   164 FLLYGPAILSWEYLSGGSSIP-EGHCYAEFFYNWYFLITASTL 205

H1   198 NFYLPTLLMLWFYAKIYKAVRQHC---LHMNRERKAAKQLGFI 420
H3   206 EFFTPFLSVTFFNLSIYLNIQRRT---FRLSRDRKVAKSLAVI 363

H1   421 MAAFILCWIPYFIFFMVIAFCK-NCCNEHLHMFTIWLGYINST 462
H3   364 VSIFGLCWAPYTLLMIIRAACHGHCVPDYWYETSFWLLWANSA 406

H1   463 LNPLIYPLCNENFKKTFKRILHI 485
H3   407 VNPVLYPLCHHSFRRAFTKLLCP 429
```

Figure 108: sequence alignment between human H_1 and H_3 receptor sequences. While the TM sequences of the H_1 receptor are shaded, highly conserved residues in class A GPCRs are shown in bold.

As seen for other GPCR crystal structures, also in the H_1 histamine receptor the deletion of the ICL3 segment and the subsequent introduction of the T4-lysozyme fragment were employed to increase the receptor stability during the crystallization phase. Since no structural information were available for the ICL3 portion, the corresponding fragment of the H_3 receptor was not modeled: thus, Thr229 at the extracellular end of TM5 was directly linked to Phe348 belonging to the C-terminus of ICL3. This modeling procedure should not impact docking studies, since the binding pocket of the H_3 receptor is located more than 30 Å far from the ICL3 domain. The final alignment is reported in Figure 108.

Modeller 9.7[270,271] was used for the comparative modeling procedure. Thirty H_3 receptor models were initially built using the alignment shown in Figure 108: the stereochemical quality of resulting models was assessed employing Procheck[282] as well as the Protein Report application of Maestro 9.1.[481] The best H_3 receptor model was chosen according to the quality of geometrical parameters and to the objective function implemented in the Modeller software. Available GPCR crystal structures evidenced a key role of the ECL2

portion in shaping the binding site region and in ligand stabilization. Thus, an additional refinement procedure was conducted on the terminal segment of the ECL2 (from Tyr189 to Asn195) employing Modeller 9.7. The final H_3 receptor structure was prepared with the Protein Preparation Wizard workflow. Hydrogen atoms were added to the structure as well as capping terminal groups (acetyl and methylamino). To relax the receptor 3D coordinates without losing the overall secondary and tertiary structure arrangements, a constrained minimization was performed: OPLS2005 was employed as force field[290] while a maximum RMSD of 0.3 Å was set as convergence criterion. The Ramachandran plot for the final H_3 receptor model is reported in Figure 109.

Docking protocol

To better evaluate the accommodation of the addtional lipophilic side chain into the H_3 receptor binding site, compounds 3 and 4 were selected for docking studies: indeed, the presence of a bulky lipophilic moiety could allow for a better evaluation of ligand-receptor interactions occurring within the additional crevice.

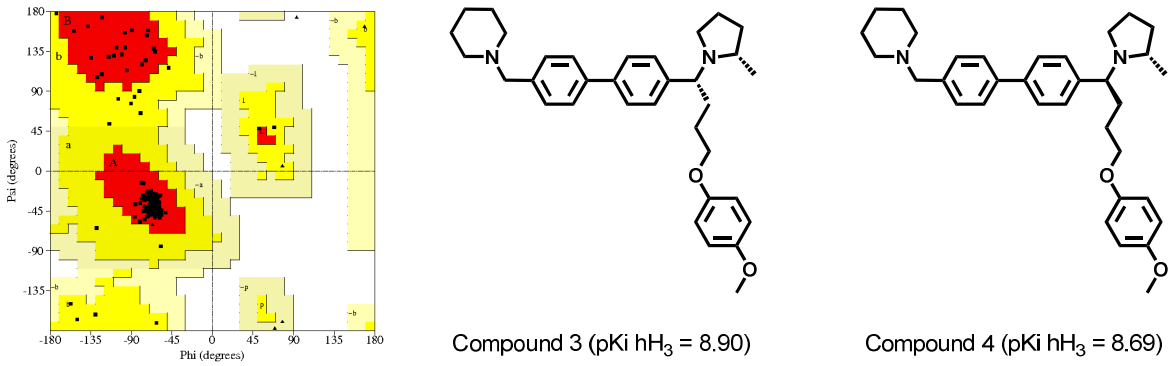

Figure 109: Left: Ramachandran plot of the H_3 receptor model after the refinement procedure. Center and right: compounds used for docking studies.

Initial geometries of compounds 1 (Figure 101), 3 and 4 (Figure 109) were energy-minimized applying the OPLS2005 force field[290] to a convergence gradient of 0.05 kJ/(molÅ). To account for protein flexibility during docking simulations, an induced fit docking (IFD)[485,486] protocol was applied.

During the initial docking phase, van der Waals (vdW) radii of both ligand and protein non-polar atoms were down-scaled to 0.5. Side chains of Leu76$^{2.46}$, Asp80$^{2.50}$, Val83$^{2.53}$, Ser121$^{3.39}$, Met378$^{6.55}$, Trp402$^{7.43}$ and Asn408$^{7.49}$ were temporarily trimmed to favor a better ligand accommodation into the binding site. Docking grids were centered on Asp114$^{3.32}$, retaining their default dimensions. A H-bond constraint was applied during the initial docking run on Asp114$^{3.32}$: in particular, the charged pyrrolidine nitrogen of

compounds 4 and 5 was forced to take interaction with Asp114$^{3.32}$. Docking studies were conducted in standard precision (SP) mode, collecting the twenty best-ranked ligand poses for further structural refinements. Prime was then used to refine the resulting ligand-receptor complexes. Side chains removed in the previous stage were reintroduced and all residues located in a shell of 6.0 Å centered on the ligand molecule were included in the Prime refinement stage. The tryptophan residue belonging to the CWXP motif (Trp371$^{6.48}$) was not refined and its initial position was maintained fixed: indeed, no remarkable conformational changes involving this specific residue are expected upon antagonist binding. In the last docking stage, the ligand was re-docked into the induced-fit receptor conformation using default settings (no vdW radii scaling for protein and a 0.8 scaling factor applied on ligand non-polar atoms). Also in this stage, a H-bond constraint was applied on Asp114$^{3.32}$. Final ligand-receptor complexes were ranked using an composite scoring function, called IFD score: this scoring method incorporates both protein-ligand interaction energy (GScore) and the total energy of the system (Prime Energy). Receptor-ligand complexes of compounds 3 and 4 showing the highest IFD score were subjected to an energy minimization procedure, applying the OPLS2005 force field and setting a convergence gradient of 0.1 kJ/(molÅ).

Results

Preliminary docking studies were conducted on compound 1 to search for alternative binding poses of the ligand into the H_3 receptor binding site. Results highlighted the presence of two different binding modes of compound 1, similar to those already observed in a previous H_3 receptor model.[467] While in one orientation (“horizontal”) compound 1 laid perpendicular to the TM bundle and formed two salt bridge interactions with Asp114$^{3.32}$ and Glu206$^{5.46}$ via its protonated nitrogens, in the second orientation (“vertical”) compound 1 accommodated parallel to the TM bundle, in a crevice delimited by TM1, TM2 and TM7.

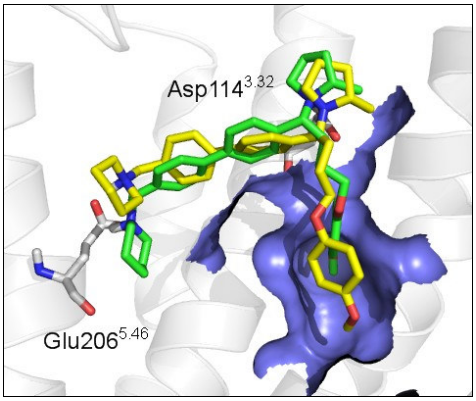

Figure 110: Superposition of the best-ranked H3-compound 3 (green carbons) and H3-compound 4 (yellow carbons) complexes obtained from the IFD. Asp114$^{3.32}$ and Glu206$^{5.46}$ are represented with gray sticks.

The best docking poses of compounds 3 and 4 show an “horizontal” orientation of the biphenyl scaffold, in which the piperidine nitrogen forms a H-bond contact with Glu206$^{5.46}$ and the pyrrolidine nitrogen undertakes a H-bond interaction with the conserved Asp114$^{3.32}$: this orientation resembles the “horizontal” pose previously reported for compound 1 (Figure 110).[467] A π-π stacking interaction was observed between the phenyl ring of the benzylpiperidine moiety and Tyr115$^{3.33}$ side chain (not shown in Figure 110). Interestingly, no interactions were detected between ligand molecules and residues belonging to extracellular loops. The 4-methoxyphenoxypropyl chains of compounds 3 and 4 protrude into the "vertical" additional pocket delimited by TM1, TM2 and TM7. Taken together, these results confirm that the two pockets previously identified in the H_3 receptor binding site can be simultaneously occupied by antagonist molecules. The similar docking poses obtained for compounds 3 and 4 into the H_3 receptor binding site could also explain the lack of stereoselectivity observed throughout the series.[477] Although this binding pose showed the highest docking score, alternative docking solutions were obtained. In one of them, while the pyrrolidine nitrogen interacts with Asp114$^{3.32}$ through a H-bond, the piperidine ring extends into the “vertical” crevice, forming favorable contacts with polar amino acids, including Asp80$^{2.50}$, Ser121$^{3.39}$ and Ser405$^{7.46}$: interestingly, this pose is consistent with the “vertical” arrangement previously described for compound 1. Another pose was found during docking studies, in which the two basic nitrogens exchange their amino acid counterparts: indeed, while the pyrrolidine nitrogen interacts with Glu206$^{5.46}$, the piperidine one forms an ionic interaction with the conserved Asp114$^{3.32}$; in this specific case, the lipophilic side chain points toward the extracellular side of the receptor.

The importance of the two basic centers for ligand affinity was proved by compounds 5 and 6 (see below). These two derivatives lack one of the two basic amine fragments either

in the proximity of the lipophilic chain or at the opposite side. Both compounds showed a notable decrease in ligand binding affinity (pKi < 5), indicating that the presence of the two basic group is crucial to form favorable interactions within the H_3 receptor binding site.

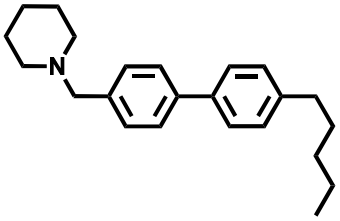

Compound 5 (pKi hH_3 = 4.89)

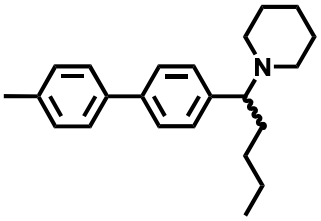

(±)-Compound 6 (pKi hH_3 = 4.87)

CHAPTER 8

Conclusions

Although the recent breakthroughs in the field of GPCR structural biology provided valuable structural information, there is an overwhelming difference between the number of available crystal structures and the number of “druggable” receptors. Despite the extraordinary efforts made by researchers during the last decade, only 7 out of ~800 GPCRs encoded by the human genome have been crystallized so far and they all belong to class A. Moreover, even though the recent advances in crystallization techniques led to characterize some of the intimate functional mechanisms of the GPCR machinery at a molecular level, recent literature showed that the optimization of such experimental protocols requires years of work and that a “tailored” crystallization procedure could be necessary for each receptor structure. In this scenario, an alternative approach that allows to overcome the lack of GPCR crystal structures is needed. The availability of a receptor 3D structure is crucial to investigate the molecular basis of ligand recognition, as well as the main receptor rearrangements that occur upon ligand binding. In drug design, the clarification of the overall binding mechanism at a molecular level could help the design of new ligands and suggest potential structural modifications aimed at improving the desired properties, such as binding affinity, intrinsic activity, receptor subtype selectivity, etc.

Comparative modeling represents one of the most widely-used *in silico* techniques employed to predict the three-dimensional structure of a receptor for which no structural information is available. In this Ph.D. thesis the application of comparative modeling to some therapeutically relevant targets is presented.

One of the main drawbacks of comparative modeling techniques found in this study was the strong dependency of the ligand binding site shape and architecture on the template structure. Indeed, in all the examined GPCR homology models, the starting geometry of the binding site was not suitable to accommodate known ligands, being somehow still tailored on the template structure. Thus, simulated annealing procedures and/or induced fit docking had to be applied to create suitable room and to adapt the binding site shape to ligands of the target GPCR. Unfortunately, the automatic placement of ligands into the ligand binding site failed most of times, producing poses not consistent with available experimental and ligand-based information, such as mutagenesis data, pharmacophore models and structure-activity relationships. Therefore, it became clear that common scoring functions are not suitable to identify the best docking poses and, consequently, the best ligand-receptor complexes. For this reason, high-quality information retrieved from literature was fundamental to guide pose selection during docking studies and to identify the best ligand-receptor complexes.

Inclusion of prior knowledge during homology modeling procedure and receptor structural refinement is a crucial step in the overall workflow, since it allowes to combine structural information derived from the available GPCRs crystal structures with receptor-specific data, including mutagenesis studies and ligand-based information. Not surprisingly, the use of external knowledge during homology modeling had a remarkable impact in the case of GPCRs showing low identity/homology percentages with available crystal structures. A clear example of this aspect is represented by melatonin receptors. In this case, "rough" structural information derived directly from the template was misleading, selecting a ligand accommodation not consistent with mutagenesis data. Indeed, while in the template structure the ligand binding site spanned through TM5 to TM7, mutagenesis data for melatonin receptors suggested a different binding site location, extending from TM4 to TM6. Thus, a ligand-based refinement of the binding site region was performed to obtain a binding site able to accommodate structurally different melatoninergic ligands in an orientation consistent not only with mutagenesis studies but also with pharmacophore models and SARs. Conversely, the 5-HT_{2C} and the H_3 receptors were built starting from template structures that bind the same class of endogenous ligands, i.e. the endogenous amines. Due to the high identity percentages/homologies shared by these receptors and their templates, structural information derived from the template crystal structures appeared suitable to identify a sound ligand binding site location.

Docking studies helped to identify alternative ligand-binding orientations into the binding site region. In all the GPCRs investigated in this project, mutagenesis data and SARs were used as filters during pose selection. Indeed, alternative ligand poses often showed similar scores and the identification of a preferred binding mode was not possible. For example, the use of such knowledge-guided filters helped to identify the correct orientation of xanthine antagonists in the A_{2A} adenosine receptor.

Once a pose consistent with available experimental and ligand-based information was found, molecular dynamics (MD) simulations allowed to correctly describe the dynamic rearrangements occurring upon ligand binding, leading to the prediction of the preferred ligand conformation into the binding site. This was the case of the A_{2A} antagonist ZM241385 and of the β_2-selective agonist carmoterol. In these studies, MD simulations were used to investigate the stability of the main ligand-receptor interactions and the main rearrangements occurring at the protein level: results showed a significant agreement between the co-crystallized binding mode and that predicted by MD simulations.

Although the prediction of some specific GPCR structural elements is still challenging for current homology-modeling protocols, an impressive amount of structural information was recently provided by the newly released GPCR crystal structures. While in some cases the inclusion of novel structural information was crucial for model building (e.g., the availability of the H_1 histamine receptor crystal structure to built the H_3 histamine receptor model), in other cases the structural data available for GPCRs seems to be still inadequate to build a reliable receptor model (e.g., in the case of melatonin receptors). In this latter case, the inclusion of prior knowledge during the homology-modeling procedure was found to be a fundamental step to obtain receptor models able to explain structure-activity relationships.
Even though the receptor models built in this study have been submitted to only a limited evaluation in structure-based drug design campaigns, these receptors gave fundamental clues on the molecular basis of ligand recognition, as well on the main rearrangements occurring upon ligand binding: all these information could be exploited in further studies to design novel compounds with good binding affinity, for virtual screening campaigns, as well as to suggest scaffold modifications aimed at discovering novel classes of GPCR ligands.

Bibliography

[1] Gloriam D.E., Fredriksson R., Schioth H.B.; The G protein-coupled receptor subset of the rat genome; BMC Genomics **2007**, *8*, 338-405.

[2] Kroeze K.W., Sheffler D.J., Roth B.L.; G-protein-coupled receptors at a glance; J. Cell. Sci. **2003**, *116*, 4867-4869.

[3] Takeda S., Kadowaki S., Haga T., Takaesu H., Mitaku S.; Identification of G protein-coupled receptor genes from the human genome sequence; FEBS Lett. **2002**, *520*, 97-101.

[4] Hopkins A.L, Groom C.R.; The druggable genome; Nat. Rev. Drug Discov. **2002**, *1*, 727-730.

[5] Attwood T.K., Findlay J.B.C.; Design of a discriminating fingerprint for G-protein-coupled receptors; Protein Eng. **1993**, *6*, 167-176.

[6] Attwood T.K., Findlay J.B.C.; Fingerprinting G-protein-coupled receptors; Protein Eng. **1994**, *7*, 195-203.

[7] Kolakowski L. F. Jr.; GCRDb: a G-protein-coupled receptor database; Receptors Channels **1994**, *2*, 1-7.

[8] Foord S.M., Bonner T.I., Neubig R.R., Rosser E.M., Pin J.P., Davenport A.P., Spedding M., Harmar A.J.; International Union of Pharmacology. XLVI. G Protein-Coupled receptor list; Pharmacol. Rev. **2005**, *57*, 279-288.

[9] Bockaert J., Pin J.P.; Molecular tinkering of G protein-coupled receptors: an evolutionary success; EMBO J. **1999**, *18*,1723-1729.

[10] Fredriksson R., Lagerstrom M.C., Lundin L.G., Schioth H.B. The G-protein-coupled receptors in the human genome form five main families. Phylogenetic analysis, paralogon groups, and fingerprints; Mol. Pharmacol. **2003**, *63*, 1256-1272.

[11] Overington J.P., Al-Lazikani B., Hopkins A.L.; How many drug targets are there?; Nat. Rev. Drug Disc. **2006**, *5*, 993-996.

[12] Tyndall J.D.A, Sandilya R.; GPCR agonists and antagonists in the clinic; Med. Chem. **2005**, *1*, 405-421.

[13] Schwartz T. W. Locating ligand-binding sites in 7TM receptors by protein engineering; Curr. Opin. Biotechnol. **1994**, *5*, 434-444.

[14] Ballesteros J.A, Weinstein H.; Integrated methods for the construction of three-dimensional models and computational probing of structure-function relations in G protein-coupled receptors, in: S.C. Sealfon, P.M. Conn (Eds.) Methods in Neurosciences, Academic Press, San Diego (CA), 1995, 25, pp. 366-428.

[15] Hofmann B.A., Sydow S., Jahn O., Van Werven L., Liepold T., Eckart K., Spiess J.; Functional and protein chemical characterization of the N-terminal domain of the rat corticotropin-releasing factor receptor; Protein. Sci. **2001**, *10*, 2050-2062.

[16] Grauschopf U., Lilie H., Honold K., Wozny M., Reusch D., Esswein A., Schäfer W., Rücknagel K.P., Rudolph R.; The N-terminal fragment of human parathyroid hormone receptor 1 constitutes a hormone binding domain and reveals a distinct disulfide pattern; Biochemistry, **2000**, *39*, 8878-8887.

[17] Bazarsuren A., Grauschopf U., Wozny M., Reusch D., Hoffmann E., Schaefer W., Panzner S., Rudolph R.; In vitro folding, functional characterization, and disulfide pattern of the extracellular domain of human GLP-1 receptor; Biophys. Chem. **2002**, *96*, 305-318.

[18] Grace C.R.R, Perrin M.H., DiGruccio M.R., Miller C.L., Rivier J.E., Vale W.W., Riek R.; NMR structure and peptide hormone binding site of the first extracellular domain of a type B1 G protein-coupled receptor; Proc. Natl. Acad. Sci. USA **2004**, *101*, 12836-12841.

[19] Unson C.G., Wu C.-R., Jiang Y., Yoo B., Cheung C., Sakmar T.P., Merrifield R.B.; Roles of specific extracellular domains of the glucagon receptor in ligand binding and signaling; Biochemistry **2002**, *41*, 11795-11803.

[20] Dong M., Pinon D.I., Cox R.F., Miller L.J.; Importance of the amino terminus in secretin family G protein-coupled receptors. Intrinsic photoaffinity labeling establishes initial docking constraints for the calcitonin receptor.; J. Biol. Chem. **2004**, 279, 1167-1175.

[21] Dong M., Li Z., Pinon D.I., Lybrand T.P., Miller L.J.; Spatial approximation between the amino terminus of a peptide agonist and the top of the sixth transmembrane segment of the secretin receptor. J. Biol. Chem. **2004**, *279*, 2894-2903.

[22] Bjarnadóttir T.K., Fredriksson R., Höglund P.J., Gloriam D.E., Lagerström M.C., Schiöth H.B.; The human and mouse repertoire of the adhesion family of G-protein-coupled receptors; Genomics **2004**, *84*, 23-33.

[23] Krasnoperov V.G., Bittner M.A., Beavis R., Kuang Y., Salnikow K.V., Chepurny O.G., Little A.R., Plotnikov A.N., Wu D., Holz R.W., Petrenko A.G; alpha-Latrotoxin stimulates exocytosis by the interaction with a neuronal G-protein-coupled receptor; Neuron **1997**, *18*, 925-37.

[24] Lin H.H., Stacey M., Saxby C., Knott V., Chaudhry Y., Evans D., Gordon S., McKnight A.J., Handford P., Lea S.; Molecular analysis of the epidermal growth factor-like short consensus repeat domain-mediated protein-protein interactions: dissection of the CD97-CD55 complex; J. Biol. Chem. **2001**, *276*, 24160-24169.

[25] Kunishima N., Shimada Y., Tsuji Y., Sato T., Yamamoto M., Kumasaka T., Nakanishi S., Jingami H., Morikawa K.; Structural basis of glutamate recognition by a dimeric metabotropic glutamate receptor; Nature 2000, 407, 971-977.

[26] Wang Y., Macke J.P., Abella B.S., Andreasson K., Worley P., Gilbert D.J., Copeland N.G., Jenkins N.A., Nathans J.; A large family of putative transmembrane receptors homologous to the product of the Drosophila tissue polarity gene frizzled; J. Biol. Chem. **1996**, *271*, 4468-4476.

[27] Conte C., Ebeling M., Marcuz A., Nef P., Andres-Barquin P. J.; Identification and characterization of human taste receptor genes belonging to the TAS2R family; Cytogenet. Genome Res. **2002**, *98*, 45-53.

[28] Behrens M., Brockhoff A., Kuhn C., Bufe B., Winnig M., Meyerhof W.; The human taste receptor hTAS2R14 responds to a variety of different bitter compounds; Biochem. Biophys. Res. Commun. **2004**, *319*, 479-85.

[29] Pronin A. N., Tang H., Connor J., Keung, W.; Identification of ligands for two human bitter T2R receptors; Chem. Senses **2004**, *29*, 583-593.

[30] Liebmann C., Bohmer F.D.; Signal Transduction Pathways of G Protein-coupled Receptors and Their Cross-Talk with Receptor Tyrosine Kinases Lessons from Bradykinin Signaling; Curr. Med. Chem. **2000**, *7*, 911-943

[31] Simon M.I., Strathmann M.P., Gautam N.; Diversity of G proteins in signal transduction; Science **1991**, *252*, 802-808.

[32] Neer E.J.; Heterotrimeric C proteins: organizers of transmembrane signals; Cell **1995**, *80*, 249-257.

[33] Fields T.A., Casey P.J.; Signalling functions and biochemical properties of pertussis toxin-resistant G-proteins; Biochem. J. **1997**, *321*, 561-571.

[34] Jiang Y., Ma W., Wan Y., Kozasa T., Hattori S., Huang X.-Y.; The G protein Gα12 stimulates Bruton's tyrosine kinase and a rasGAP through a conserved PH/BM domain; Nature **1998**, *395*, 808-813.

[35] Treisman R.; Regulation of transcription by MAP kinase cascades; Curr. Opin. Cell. Biol. **1996**, *8*, 205-215.

[36] Logothetis D.E., Kurachi Y., Galper J., Neer E.J., Clapham D.E.; The βγ subunits of GTP-binding proteins activate the muscarinic K+ channel in heart; Nature **1987**, *325*, 321-326.

[37] Clapham D.E., Neer E.J.; New roles for G-protein βγ-dimers in transmembrane signalling; Nature **1993**, *365*, 403-406.

[38] Tang W.J., Gilman A.G.; Type-specific regulation of adenylyl cyclase by G protein beta gamma subunits; Science **1991**, *254*, 1500-1503.

[39] Casey P.J., Lipid modifications of G proteins; Curr. Opin. Cell. Biol. **1994**, *6*, 219-225.

[40] Mumby S.M.; Reversible palmitoylation of signaling proteins; Curr. Opin. Cell. BIol. **1997**, *9*, 148-154.

[41] Duzic E., Coupry I., Downing S., Lanier S.M.; Factors determining the specificity of signal transduction by guanine nucleotide-binding protein-coupled receptors. I. Coupling of alpha 2-adrenergic receptor subtypes to distinct G-proteins; J. Biol. Chem. **1992**, *267*, 9844-9851.

[42] Duzic E., Lanier S.M.; Factors determining the specificity of signal transduction by guanine nucleotide-binding protein-coupled receptors. III. Coupling of alpha 2-adrenergic receptor subtypes in a cell type-specific manner; J. Biol. Chem. **1992**, *267*, 24045-24052.

[43] Laugwitz K.-L., Offermanns S., Spicher K., Schultz G.; μ and δ opioid receptors differentially couple to G protein subtypes in membranes of human neuroblastoma SH-SY5Y cells; Neuron **1993**, *10*, 233-242.

[44] Law S.F, Reisine T.; Agonist binding to rat brain somatostatin receptors alters the interaction of the receptors with guanine nucleotide-binding regulatory proteins; Mol. Pharmacol. **1992**, *42*, 398-402.

[45] Law S.F., Yasuda K., Bell G.I., Reisine T.; Gi alpha 3 and G(o) alpha selectively associate with the cloned somatostatin receptor subtype SSTR2; J. Biol. Chem. **1993**, *268*, 10721-10727.

[46] Munshi R., Pang I.H., Sternweis P.C., Linden J.; A1 adenosine receptors of bovine brain couple to guanine nucleotide-binding proteins Gi1, Gi2, and Go; J. Biol. Chem. **1991**, *266*, 22285-22289.

[47] Parker E.M., Kameyama K., Higashijima T., Ross E.M.; Reconstitutively active G protein-coupled receptors purified from baculovirus-infected insect cells; J. Biol. Chem. **1991**, *266*, 519-527.

[48] Schmidt A., Hescheler J., Offermanns S., Spicher K., Hinsch K.D., Klinz F.J., Codina J., Birnbaumer L., Gausepohl H., Frank R.; Involvement of pertussis toxin-sensitive G-proteins in the hormonal inhibition of dihydropyridine-sensitive Ca2+ currents in an insulin-secreting cell line (RINm5F); J. Biol. Chem. **1991**, *266*, 18025-18033.

[49] Birnbaumer L., Abramowitz J., Brown A.M.; Receptor-effector coupling by G proteins; Biochim. Biophys. Acta **1990**, *1031*, 163-224.

[50] Gierschik P., Sidiropoulos D., Jakobs K.H.; Two distinct Gi-proteins mediate formyl peptide receptor signal transduction in human leukemia (HL-60) cells; J. Biol. Chem. **1989**, *264*, 21470-21473.

[51] Offermans S., Schäfer R., Hoffmann B., Bombien E., Spicher K., Hinsch K.-D., Schultz G., Rosenthal W.; Agonist-sensitive binding of a photoreactive GTP analog to a G-protein α-subunit in membranes of HL-60 cells; FEBS Lett. **1990**, *260*, 14-18.

[52] Offermanns S., Laugwitz K.L., Spicher K., Schultz G.; G proteins of the G12 family are activated via thromboxane A2 and thrombin receptors in human platelets; Proc. Natl. Acad. Sci. USA **1994**, *91*, 504-508.

[53] Shenker A., Goldsmith P., Unson C.G., Spiegel A.M.; The G protein coupled to the thromboxane A2 receptor in human platelets is a member of the novel Gq family; J. Biol. Chem. **1991**, *266*, 9309-9313.

[54] Birnbaumer L.; Receptor-to-effector signaling through G proteins: Roles for βγ dimers as well as α subunits; Cell **1992**, *71*, 1069-1072.

[55] Lustig K.D., Conklin B.R., Herzmark P., Taussig R., Bourne H.R.; Type II adenylyl cyclase integrates coincident signals from Gs, Gi, and Gq; J. Biol. Chem. **1993**, *268*, 13900-13905.

[56] Taussig R., Iniguez-Lluhi J.A., Gilman A.G.; Inhibition of adenylyl cyclase by Gi alpha; Science **1993**, *261*, 218-221.

[57] Palczewski K., Kumasaka T., Hori T., Behnke C.A., Motoshima H., Fox B.A., Le Trong I., Teller D.C., Okada T., Stenkamp R.E., Yamamoto M., Miyano M.; Crystal structure of rhodopsin: a G protein-coupled receptor; Science **2000**, *289*, 739-745.

[58] Cherezov V., Rosenbaum D.M., Hanson M.A., Rasmussen S.G.F., Thian F.S., Kobilka T.S., Choi H.-J., Kuhn P., Weis W.I., Kobilka B.K., Stevens R.C.; High-resolution crystal structure of an engineered human β_2-adrenergic G protein–coupled receptor; Science **2007**, *318*, 1258-1265.

[59] Rosenbaum D.M., Cherezov V., Hanson M.A., Rasmussen S.G.F., Thian F.S., Kobilka T.S., Choi H.-J., Yao X.-J., Weis W.I., Stevens R.C., Kobilka B.K.; GPCR engineering yields high-resolution structural insights into β_2-adrenergic receptor function; Science **2007**, *318*, 1266-1273.

[60] Rasmussen S.G.F, Choi H.-J., Rosenbaum D.M., Kobilka T.S., Thian F.S., Edwards P.C., Burghammer M., Ratnala V.R.P., Sanishvili R., Fischetti R.F., Schertler G.F.X., Weis W.I., Kobilka B.K.; Crystal structure of the human β_2 adrenergic G-protein-coupled receptor; Nature **2007**, *450*, 383-387.

[61] Warne T., Serrano-Vega M.J., Baker J.G., Moukhametzianov R., Edwards P.C., Henderson R., Leslie A.G.W., Tate C.G., Schertler G.F.X.; Structure of a β_1-adrenergic G-protein-coupled receptor; Nature **2008**, *454*, 486-491.

[62] Jaakola V.-P., Griffith M.T., Hanson M.A., Cherezov V., Chien E.Y.T, Lane J.R., IJzerman A.P., Stevens R.C.; The 2.6 Angstrom crystal structure of a human A_{2A} adenosine receptor bound to an antagonist; Science **2008**, *322*, 1211-1217.

[63] Wu B., Chien E.Y.T, Mol C.D., Fenalti G., Liu W., Katritch V., Abagyan R., Brooun A., Wells P., Bi F.C., Hamel D.J., Kuhn P., Handel T.M., Cherezov V., Stevens R.C.; Structures of the CXCR4 chemokine GPCR with small-molecule and cyclic peptide antagonists; Science **2010**, *330*, 1066-1071.

[64] Chien E.Y.T., Liu W., Zhao Q., Katritch V., Han G.W., Hanson M.A., Shi L., Newman A.H., Javitch J.A., Cherezov V., Stevens R.C.; Structure of the human dopamine D3 receptor in complex with a D2/D3 selective antagonist; Science **2010**, *330*, 1091-1095.

[65] Shimamura T., Shiroishi M., Weyand S., Tsujimoto H., Winter G., Katritch V., Abagyan R., Cherezov V., Liu W., Han G.W., Kobayashi T., Stevens R.C., Iwata S.; Structure of the human histamine H_1 receptor complex with doxepin; Nature **2011**, *475*, 65-70.

[66] Park J.H., Scheerer P., Hofmann K.P., Choe H.-W., Ernst O.P.; Crystal structure of the ligand-free G-protein-coupled receptor opsin; Nature **2008**, *454*, 183-187.

[67] Scheerer P., Park J.H., Hildebrand P.W., Kim Y.J., Krauß N., Choe H.-W., Hofmann K.P., Ernst O.P.; Crystal structure of opsin in its G-protein-interacting conformation; Nature **2008**, *455*, 497-502.

[68] Rasmussen S.G.F., Choi H.-J., Fung J.J., Pardon E., Casarosa P., Chae P.S., DeVree B.T., Rosenbaum D.M., Thian F.S., Kobilka T.S., Schnapp A., Konetzki I., Sunahara R.K., Gellman S.H., Pautsch A., Steyaert

J., Weis W.I., Kobilka B.K.; Structure of a nanobody-stabilized active state of the β_2 adrenoceptor; Nature **2011**, *469*, 175-180.

[69] Rosenbaum D.M., Zhang C., Lyons J.A., Holl R., Aragao D., Arlow D.H., Rasmussen S.G.F, Choi H.-J., DeVree B.T., Sunahara R.K., Chae P.S., Gellman S.H., Dror R.O., Shaw D.E., Weis W.I., Caffrey M., Gmeiner P., Kobilka B.K.; Structure and function of an irreversible agonist-β2 adrenoceptor complex; Nature **2011**, *469*, 236-240.

[70] Rasmussen S.G.F., DeVree B.T., Zou Y., Kruse A.C., Chung K.Y., Kobilka T.S., Thian F.S., Chae P.S., Pardon E., Calinski D., Mathiesen J.M., Shah S.T.A, Lyons J.A., Caffrey M., Gellman S.H., Steyaert J., Skiniotis G., Weis W.I., Sunahara R.K., Kobilka B.K.; Crystal structure of the β_2 adrenergic receptor–Gs protein complex; Nature **2011**, *477*, 549-555.

[71] Warne T., Moukhametzianov R., Baker J.G., Nehmé R., Edwards P.C., Leslie A.G.W., Schertler G.F.X., Tate C.G.; The structural basis for agonist and partial agonist action on a β_1-adrenergic receptor; Nature **2011**, *469*, 241-244.

[72] Lebon G., Warne T., Edwards P.C., Bennett K., Langmead C.J., Leslie A.G.W., Tate C.G.; Agonist-bound adenosine A_{2A} receptor structures reveal common features of GPCR activation; Nature **2011**, *474*, 521-525.

[73] Xu F., Wu H., Katritch V., Han G.W., Jacobson K.A., Gao Z.-G., Cherezov V., Stevens R.C.; Structure of an agonist-Bound human A_{2A} adenosine receptor; Science **2011**, *332*, 322-327.

[74] Berman H.M., Westbrook J., Feng Z., Gilliland G., Bhat T.N., Weissig H., Shindyalov I.N., Bourne P.E.; The Protein Data Bank; Nucl. Acids Res. **2000**, *28*, 235-242.

[75] Li J., Edwards P.C., Burghammer M., Villa C., Schertler G.F.X.; Structure of bovine rhodopsin in a trigonal crystal form; J. Mol. Biol. **2004**, *343*, 1409-1438.

[76] Okada T., Fujiyoshi Y., Silow M., Navarro J., Landau E.M., Shichida Y.; Functional role of internal water molecules in rhodopsin revealed by x-ray crystallography; Proc. Natl. Acad. Sci. USA **2002**, *99*, 5982-5987.

[77] Teller D.C., Okada T., Behnke C.A., Palczewski K., Stenkamp R.E.; Advances in determination of a high-resolution three-dimensional structure of rhodopsin, a model of G-protein-coupled receptors (GPCRs); Biochemistry **2001**, *40*, 7761-7772.

[78] Salom D., Lodowski D.T., Stenkamp R.E., Le Trong I., Golczak M., Jastrzebska B., Harris T., Ballesteros J.A., Palczewski K.; Crystal structure of a photoactivated deprotonated intermediate of rhodopsin; Proc. Natl. Acad. Sci. USA **2006**, *103*, 16123-16128.

[79] Makino C.L., Riley C.K., Looney J., Crouch R.K., Okada T.; Binding of more than one retinoid to visual opsins; Biophys. J. **2010**, *99*, 2366-2373.

[80] Stenkamp R.E.; Alternative models for two crystal structures of bovine rhodopsin; Acta Cryst. **2008**, *D64*, 902-904.

[81] Standfuss J., Xie G., Edwards P.C., Burghammer M., Oprian D.D., Schertler G.F.X.; Crystal structure of a thermally stable rhodopsin mutant; J. Mol. Biol. **2007**, *372*, 1179-1188.

[82] Nakamichi H., Buss V., Okada T.; Photoisomerization mechanism of rhodopsin and 9-cis-rhodopsin revealed by X-ray crystallography; Biophys. J. **2007**, *92*, L106-L108.

[83] Nakamichi H., Okada T.; Crystallographic analysis of primary visual photochemistry; Angew. Chem. Int. Ed. Engl. **2006**, *45*, 4270-4273.

[84] Nakamichi H., Okada T.; Local peptide movement in the photoreaction intermediate of rhodopsin; Proc. Natl. Acad. Sci. USA **2006**, *103*, 12729-12734.

[85] Standfuss J., Edwards P.C., D'Antona A., Fransen M., Xie G., Oprian D.D., Schertler G.F.X.; The structural basis of agonist-induced activation in constitutively active rhodopsin; Nature **2011**, *471*, 656-660.

[86] Choe H.-W., Kim Y.J., Park J.H., Morizumi T., Pai E.F., Krauß N., Hofmann K.P., Scheerer P., Ernst O.P.; Crystal structure of metarhodopsin II; Nature **2011**, *471*, 651-655.

[87] Shimamura T., Hiraki K., Takahashi N., Hori T., Ago H., Masuda K., Takio K., Ishiguro M., Miyano M.; Crystal structure of squid rhodopsin with intracellularly extended cytoplasmic region; J. Biol. Chem. **2008**, *283*, 17753-17756.

[88] Murakami M., Kouyama T.; Crystal structure of squid rhodopsin; Nature **2008**, *453*, 363-367.

[89] Hanson M.A., Cherezov V., Griffith M.T., Roth C.B., Jaakola V.P., Chien E.Y., Velasquez J., Kuhn P., Stevens R.C.; A specific cholesterol binding site is established by the 2.8 Å structure of the human β_2-adrenergic receptor; Structure, **2008**, *16*, 897-905.

[90] Wacker D., Fenalti G., Brown M.A., Katritch V., Abagyan R., Cherezov V., Stevens R.C.; Conserved binding mode of human β_2 adrenergic receptor inverse agonists and antagonist revealed by X-ray crystallography; J. Am. Chem. Soc. **2010**, *132*, 11443-11445.

[91] Bokoch M.P., Zou Y., Rasmussen S.G.F., Liu C.W., Nygaard R., Rosenbaum D.M., Fung J.J., Choi H.-J., Thian F.S., Kobilka T.S., Puglisi J.D., Weis W.I., Pardo L., Prosser R.S., Mueller L., Kobilka B.K.; Ligand-specific regulation of the extracellular surface of a G-protein-coupled receptor; Nature **2010**, *463*, 108-112.

[92] Moukhametzianov R., Warne T., Edwards P.C., Serrano-Vega M.J., Leslie A.G.W., Tate C.G., Schertler G.F.X.; Two distinct conformations of helix 6 observed in antagonist-bound structures of a β_1-adrenergic receptor; Proc. Natl. Acad. Sci. USA **2011**, *108*, 8228-8232.

[93] Doré A.S., Robertson N., Errey J.C., Ng I., Hollenstein K., Tehan B., Hurrell E., Bennett K., Congreve M., Magnani F., Tate C.G., Weir M., Marshall F.H.; Structure of the adenosine A_{2A} receptor in complex with ZM241385 and the xanthines XAC and caffeine; Structure **2011**, *19*, 1283-1293.

[94] Peeters M.C., van Westen G.J.P., Li Q., IJzerman A.P.; Importance of the extracellular loops in G protein-coupled receptors for ligand recognition and receptor activation; Trends Pharmacol. Sci. **2011**, *32*, 35-42.

[95] Klco J. M., Nikiforovich G.V., Baranski T.J.; Genetic analysis of the first and third extracellular loops of the C5a receptor reveals an essential WXFG motif in the first loop; J. Biol. Chem. **2006**, *281*, 12010-12019.

[96] Hawtin S.R., Simms J., Conner M., Lawson Z., Parslow R.A., Trim J., Sheppard A., Wheatley M.; Charged extracellular residues, conserved throughout a G-protein-coupled receptor family, are required for ligand binding, receptor activation, and cell-surface expression; J. Biol. Chem. **2006**, *281*, 38478-38488.

[97] Clark S.D., Tran H.T., Zeng J., Reinscheid R.K.; Importance of extracellular loop one of the neuropeptide S receptor for biogenesis and function; Peptides **2010**, *31*, 130-138.

[98] Fillion D., Lemieux G., Basambombo L.L., Lavigne P., Guillemette G., Leduc R., Escher E.; The amino-terminus of angiotensin II contacts several ectodomains of the angiotensin II receptor AT1; J. Med. Chem. **2010**, *53*, 2063-2075.

[99] Wheatley M., Simms J., Hawtin S.R., Wesley V.J., Wootten D., Conner M., Lawson Z., Conner A.C., Baker A., Cashmore Y., Kendrick R., Parslow R.A.; Extracellular loops and ligand binding to a subfamily of Family A G-protein-coupled receptors; Biochem. Soc. Trans. **2007**, *35*, 717-720.

[100] Härterich S., Koschatzky S., Einsiedel J., Gmeiner P.; Novel insights into GPCR-peptide interactions: mutations in extracellular loop 1, ligand backbone methylations and molecular modeling of neurotensin receptor 1; Bioorg. Med. Chem. **2008**, *16*, 9359-9368.

[101] Nygaard R., Frimurer T.M., Holst B., Rosenkilde M.M., Schwartz T.W.; Ligand binding and micro-switches in 7TM receptor structures; Trends Pharmacol. Sci. **2009**, *30*, 249-259.

[102] Avlani V.A., Gregory K.J., Morton C.J., Parker M.W., Sexton P.M., Christopoulos A.; Critical role for the second extracellular loop in the binding of both orthosteric and allosteric G protein-coupled receptor ligands; J. Biol. Chem. **2007**, *282*, 25677-25686.

[103] Scarselli M., Li B., Kim S.-K., Wess J.; Multiple residues in the second extracellular loop are critical for M_3 muscarinic acetylcholine receptor activation; J. Biol. Chem. **2007**, *282*, 7385-7396.

[104] Massotte D., Kieffer B.L.; The second extracellular loop: a damper for G protein–coupled receptors?; Nat. Struct. Mol. Biol. **2005**, *12*, 287-288.

[105] Sum C.S., Tikhonova I.G., Costanzi S., Gershengorn M.C.; Two arginine-glutamate ionic locks near the extracellular surface of FFAR1 gate receptor activation; J. Biol. Chem. **2009**, *284*, 3529-3536.

[106] Zhang X., Chien E.Y.T., Chalmers M.J., Pascal B.D., Gatchalian J., Stevens R.C., Griffin P.R.; Dynamics of the β_2-adrenergic G-protein coupled receptor revealed by hydrogen–deuterium exchange; Anal. Chem. **2010**, *82*, 1100-1108.

[107] West G.M., Chien E.Y.T., Katritch V., Gatchalian J., Chalmers M.J., Stevens R.C., Griffin P.R.; Ligand-dependent perturbation of the conformational ensemble for the GPCR β_2 adrenergic receptor revealed by HDX; Structure **2011**, *19*, 1424-1432.

[108] Katritch V., Cherezov V., Stevens R.C.; Diversity and modularity of G protein-coupled receptor structures; Trends Pharmacol. Sci. **2011**, *33*, 17-27.

[109] Kleinau G., Jaeschke H., Mueller S., Raaka B.M., Neumann S., Paschke R., Krause G.; Evidence for cooperative signal triggering at the extracellular loops of the TSH receptor; FASEB J. **2008**, *22*, 2798-2808.

[110] Strader C.D., Sigal I.S., Register R.B., Candelore M.R., Rands E., Dixon R.A.; Identification of residues required for ligand binding to the beta-adrenergic receptor; Proc. Natl. Acad. Sci. USA **1987**, *84*, 4384-4388.

[111] Strader C.D., Sigal I.S., Candelore M.R., Rands E., Hill W.S., Dixon R.A.; Conserved aspartic acid residues 79 and 113 of the beta-adrenergic receptor have different roles in receptor function; J. Biol. Chem. **1988**, *263*, 10267-10271.

[112] Muntasir H.A., Takahashi J., Rashid M., Ahmed M., Komiyama T, Hossain M., Kawakami J., Nashimoto M., Nagatomo T.; Site-directed mutagenesis of the serotonin 5-hydroxytryptamine2C receptor: identification of amino acids responsible for sarpogrelate binding; Biol. Pharm. Bull. **2006**, *29*, 1645-1650.

[113] Wang C.D., Gallaher T.K., Shih J.C.; Site-directed mutagenesis of the serotonin 5-hydroxytrypamine2 receptor: identification of amino acids necessary for ligand binding and receptor activation; Mol. Pharmacol. **1993**, *43*, 931-940.

[114] Duvernay M.T., Dong C., Zhang X., Robitaille M., Hébert T.E., Wu G.; A single conserved leucine residue on the first intracellular loop regulates ER export of G protein-coupled receptors; Traffic **2009**, *10*, 552-566.

[115] Kleinau G., Jaeschke H., Worth C.L., Mueller S., Gonzalez J., Paschke R., Krause G.; Principles and determinants of G-protein coupling by the rhodopsin-like thyrotropin receptor; PLoS ONE **2010**, 5, e9745.

[116] Zhang L., Huang G., Wu J., Ruan K.-H.; A profile of the residues in the first intracellular loop critical for Gs-mediated signaling of human prostacyclin receptor characterized by an integrative approach of NMR-experiment and mutagenesis; Biochemistry **2005**, *44*, 11389–11401.

[117] Zhang L., Wu J., Ruan H.-K.; Solution structure of the first intracellular loop of prostacyclin receptor and implication of its interaction with the C-terminal segment of Gαs protein; Biochemistry **2006**, *45* 1734–1744.

[118] Dai W., You Z., Zhou H., Zhang J., Hu Y.; Structure-function relationships of the human bitter taste receptor hTAS2R1: insights from molecular modeling studies; J. Recept. Signal. Transduct. **2011**, *31*, 229-240.

[119] Shacham S., Cheifetz M.N., Fridkin M., Pawson A.J., Millar R.P., Naor Z.; Identification of Ser^{153} in ICL2 of the Gonadotropin-releasing hormone (GnRH) receptor as a phosphorylation-independent site for inhibition of Gq coupling; J. Biol. Chem. **2005**, *280*, 28981-28988.

[120] Chee M.J.S, Mörl K., Lindner D., Merten N., Zamponi G.W., Light P.E., Beck-Sickinger A.G., Colmers W.F.; The third intracellular loop stabilizes the inactive state of the neuropeptide Y1 receptor; J. Biol. Chem. **2008**, *283* 33337-33346.

[121] Wess J.; Molecular basis of receptor/G-protein-coupling selectivity; Pharmacol. Ther. **1998**, *80*, 231-264.

[122] Gether U; Uncovering molecular mechanisms involved in activation of G protein-coupled receptors; Endocr Rev. **2000**, *21*, 90-113.

[123] Wess J.; G-protein-coupled receptors: molecular mechanisms involved in receptor activation and selectivity of G-protein recognition; FASEB J. **1997**, *11*, 346-354.

[124] Ballesteros J.A., Jensen A.D., Liapakis G., Rasmussen S.G.F., Shi L., Gether U., Javitch J.A.; Activation of the β_2-adrenergic receptor involves disruption of an ionic lock between the cytoplasmic ends of transmembrane segments 3 and 6; J. Biol. Chem. **2001**, *276*, 29171-29177.

[125] Rasmussen S.G.F., Jensen A.D., Liapakis G., Ghanouni P., Javitch J.A., Gether U.; Mutation of a highly conserved aspartic acid in the β_2 adrenergic receptor: constitutive activation, structural instability, and conformational rearrangement of transmembrane segment 6; Mol. Pharmacol. **1999**, *56*, 175-184.

[126] Cohen G.B., Yang T., Robinson P.R., Oprian D.D.; Constitutive activation of opsin: influence of charge at position 134 and size at position 296; Biochemistry **1993**, *32*, 6111-6115.

[127] Alewijnse A.E., Timmerman H., Jacobs E.H., Smit M.J., Roovers E., Cotecchia S., Leurs R.; The effect of mutations in the DRY motif on the constitutive activity and structural instability of the histamine H_2receptor; Mol. Pharmacol. **2000**, *57*, 890-898.

[128] Shi L., Liapakis G., Xu R., Guarnieri F., Ballesteros J.A., Javitch J.A.; β_2 adrenergic receptor activation: MODULATION OF THE PROLINE KINK IN TRANSMEMBRANE 6 BY A ROTAMER TOGGLE SWITCH; J. Biol. Chem. **2002**, *277*, 40989-40996.

[129] Crocker E., Eilers M., Ahuja S., Hornak V., Hirshfeld A., Sheves M., Smith S.O.; Location of Trp265 in metarhodopsin II: implications for the activation mechanism of the visual receptor rhodopsin; J. Mol. Biol. **2006**, *357*, 163-172.

[130] Lin S.W.; Sakmar T.P.; Specific tryptophan UV-absorbance changes are probes of the transition of rhodopsin to its active state; Biochemistry **1996**, *35*, 11149-11159.

[131] Borhan B., Souto M.L., Imai H., Shichida Y., Nakanishi K.; Movement of retinal along the visual transduction path; Science **2000**, *288*, 2209-2212.

[132] Farrens D.L., Altenbach C., Yang K., Hubbell W.L., Khorana H.G.; Requirement of rigid-body motion of transmembrane helices for light activation of rhodopsin; Science **1996**, *274*, 768-770.

[133] Sheikh S.P., Zvyaga T.A., Lichtarge O., Sakmar T.P., Bourne H.R.; Rhodopsin activation blocked by metal-ion-binding sites linking transmembrane helices C and F; Nature **1996**, *383*, 347-350.

[134] Gether U., Lin S., Ghanouni P., Ballesteros J.A., Weinstein H., Kobilka B.K.; Agonists induce conformational changes in transmembrane domains III and VI of the β_2 adrenoceptor; EMBO J. **1997**, *16*, 6737-6747.

[135] Javitch J.A., Fu D., Liapakis G., Chen J.; Constitutive activation of the β_2 adrenergic receptor alters the orientation of its sixth membrane-spanning segment; J. Biol. Chem. **1997**, *272*,18546-18549.

[136] Jensen A.D., Guarnieri F., Rasmussen S.G.F., Asmar F., Ballesteros J.A., Gether U.; Agonist-induced conformational changes at the cytoplasmic side of transmembrane segment 6 in the β_2 adrenergic receptor mapped by site-selective fluorescent labeling; J. Biol. Chem. **2001**, *276*, 9279-9290.

[137] Huber T., Sakmar T.P.; Rhodopsin's active state is frozen like a DEER in the headlights; Proc. Natl. Acad. Sci. USA **2008**, *105*, 7439-7444.

[138] Ruprecht J.J., Mielke T., Vogel R., Villa C., Schertler G.F.X.; Electron crystallography reveals the structure of metarhodopsin I; EMBO J. **2004**, *23*, 3609-3620.

[139] Pellissier L.P., Sallander J., Campillo M., Gaven F., Queffeulou E., Pillot M., Dumuis A., Claeysen S., Bockaert J., Pardo L.; Conformational toggle switches implicated in basal constitutive and agonist-induced activated states of 5-hydroxytryptamine-4 receptors; Mol. Pharmacol. **2009**, *75*, 982-990.

[140] Mobarec J.C., Sanchez R., Filizola M.; Modern homology modeling of G-protein coupled receptors: which structural template to use?; J. Med. Chem. **2009**, *52*, 5207-5216.

[141] de Graaf C., Rognan D.; Customizing G Protein-Coupled receptor models for structure-based virtual screening; Curr. Pharm. Des. **2009**, *15*, 4026-4048.

[142] Worth C.L., Kleinau G., Krause G.; Comparative sequence and structural analyses of G-protein-coupled receptor crystal structures and implications for molecular models; PLoS One **2009**, *4*, e7011.

[143] Kneissl B., Leonhardt B., Hildebrandt A., Tautermann C.A.; Revisiting automated G-protein coupled receptor modeling: the benefit of additional template structures for a neurokinin-1 receptor model; J. Med. Chem. **2009**, *52*, 3166-3173.

[144] Larsson P., Wallner B., Lindahl E., Elofsson A.; Using multiple templates to improve quality of homology models in automated homology modeling; Protein Sci. **2008**, *17*, 990-1002.

[145] Michino M., Abola E., GPCR Dock 2008 participants, Brooks C.L., Dixon J.S., Moult J., Stevens R.C.; Community-wide assessment of GPCR structure modelling and ligand docking: GPCR Dock 2008; Nat. Rev. Drug Discov. **2009**, *8*, 455-463.

[146] Trabanino R.J., Hall S.E., Vaidehi N., Floriano W.B., Kam V.W.T., Goddard W.A.; First principles predictions of the structure and function of G-protein-coupled receptors: validation for bovine rhodopsin; Biophys. J. **2004**, *86*, 1904-1921.

[147] Vaidehi N., Floriano W.B., Trabanino R., Hall S.E., Freddolino P., Choi E.J., Zamanakos G., Goddard W.A. III; Prediction of structure and function of G protein-coupled receptors; Proc. Natl. Acad. Sci. USA **2002**, *99*, 12622-12627.

[148] Shacham S., Marantz Y., Bar-Haim S., Kalid O., Warshaviak D., Avisar N., Inbal B., Heifetz A., Fichman M., Topf M., Naor Z., Noiman S., Becker O.M.; PREDICT modeling and in-silico screening for G-protein coupled receptors; Proteins **2004**, *57*, 51-86.

[149] Floriano W.B., Vaidehi N., Goddard W.A. III, Singer M.S., Shepherd G.M.; Molecular mechanisms underlying differential odor responses of a mouse olfactory receptor; Proc. Natl. Acad. Sci. USA **2000**, *97*, 10712-10716.

[150] Bray J.K., Goddard W.A. III; The structure of human serotonin 2c G-protein-coupled receptor bound to agonists and antagonists; J. Mol. Graph. Model. **2008**, *27*, 66-81.

[151] Kim S.-K., Fristrup P., Abrol R., Goddard W.A. III; Structure-based prediction of subtype selectivity of histamine H_3 receptor selective antagonists in clinical trials; J. Chem. Inf. Model **2011**, *51*, 3262–3274.

[152] Becker O.M., Marantz Y., Shacham S., Inbal B., Heifetz A., Kalid O., Bar-Haim S., Warshaviak D., Fichman M., Noiman S.; G protein-coupled receptors: in silico drug discovery in 3D; Proc. Natl. Acad. Sci. USA **2004**, *101*, 11304-11309.

[153] Costanzi S; On the applicability of GPCR homology models to computer-aided drug discovery: a comparison between in silico and crystal structures of the β_2-adrenergic receptor; J. Med. Chem. **2008**, 51, 2907-2914.

[154] Ivanov A.A., Barak D., Jacobson K.A.; Evaluation of homology modeling of G-protein-coupled receptors in light of the A_{2A} adenosine receptor crystallographic structure; J. Med. Chem. **2009**, *52*, 3284-3292.

[155] Nikiforovich G.V., Taylor C.M., Marshall G.R., Baranski T.J.; Modeling the possible conformations of the extracellular loops in G-protein-coupled receptors; Proteins **2010**, *78*, 271-285.

[156] Mehler E.L., Hassan S.A., Kortagere S., Weinstein H.; Ab initio computational modeling of loops in G-protein-coupled receptors: Lessons from the crystal structure of rhodopsin; Proteins **2006**, *64*, 673-690.

[157] Mehler E.L., Periole X., Hassan S.A.; Weinstein H.; Key issues in the computational simulation of GPCR function: representation of loop domains; J. Comp. Aided Mol. Design **2002**, *16*, 841-853.

[158] Watanabe Y.S., Fukunishi Y., Nakamura H.; Modelling of third cytoplasmic loop of bovine rhodopsin by multicanonical molecular dynamics; J. Mol. Graph. Model. **2004**, *23*, 59-68.

[159] Goldfeld D.A., Zhu K., Beuming T., Friesner R.A.; Successful prediction of the intra- and extracellular loops of four G-protein-coupled receptors; Proc. Natl. Acad. Sci. USA **2011**, *108*, 8275-8280.

[160] Zhao S., Zhu K., Li J., Friesner R.A.; Progress in super long loop prediction; Proteins **2011**, *79*, 2920-2935.

[161] de Graaf C., Foata N., Engkvist O., Rognan D.; Molecular modeling of the second extracellular loop of G-protein coupled receptors and its implication on structure-based virtual screening; Proteins **2008**, *71*, 599-620.

[162] Reynolds K.A., Katritch V., Abagyan R.; Identifying conformational changes of the β_2 adrenoceptor that enable accurate prediction of ligand/receptor interactions and screening for GPCR modulators; J. Mol. Graph. Model. **2009**, *23*, 273-288.

[163] Probst W.C., Snyder L.A., Schuster D.I., Brosius J., Sealfon S.C.; Sequence alignment of the G-protein coupled receptor superfamily; DNA Cell Biol. **1992**, *11*, 1-20.

[164] Mirzadegan T., Benkö G., Filipek S., Palczewski K.; Sequence analyses of G-protein-coupled receptors: similarities to rhodopsin; Biochemistry **2003**, *42*, 2759-2767.

[165] Rayan A.; New vistas in GPCR 3D structure prediction; J. Mol. Model **2010**, *16*, 183-191.

[166] Katritch V., Rueda M., Lam P. C.-H., Yeager M., Abagyan R.; GPCR 3D homology models for ligand screening: Lessons learned from blind predictions of adenosine A2a receptor complex; Proteins **2010**, *78*, 197-211.

[167] Cavasotto C.N., Orry A.J.W., Murgolo N.J., Czarniecki M.F., Kocsi S.A., Hawes B.E., O'Neill K.A., Hine H., Burton M.S., Voigt J.H., Abagyan R.A., Bayne M.L., Monsma F.J. Jr.; Discovery of novel chemotypes to a G-protein-coupled receptor through ligand-steered homology modeling and structure-based virtual screening; J. Med. Chem. **2008**, *51*, 581-588.

[168] Kufareva I., Rueda M., Katritch V., GPCR Dock 2010 participants, Stevens R.C., Abagyan R.; Status of GPCR modeling and docking as reflected by community wide GPCR Dock 2010 assessment; Structure **2011**, *19*, 1108-1126.

[169] Obiol-Pardo C., López L., Pastor M., Selent J.; Progress in the structural prediction of G protein-coupled receptors: D3 receptor in complex with eticlopride; Proteins **2011**, *79*, 1695-1703.

[170] Jaakola V.P., Lane J.R., Lin J.Y., Katritch V., Ijzerman A.P., Stevens R.C.; Ligand binding and subtype selectivity of the human A_{2A} adenosine receptor: identification and characterization of essential amino acid residues; J. Biol. Chem. **2010**, *285*, 13032–13044.

[171] Katritch V., Rueda M., Lam P.C., Yeager M., Abagyan R.; GPCR 3D homology models for ligand screening: lessons learned from blind predictions of adenosine A2a receptor complex; Proteins **2010**, *78*, 197-211.

[172] Klepeis J.L., Lindorff-Larsen K., Dror R.O., Shaw D.E.; Long-timescale molecular dynamics simulations of protein structure and function; Curr. Opin. Struct. Biol. **2009**, *19*, 120-127.

[173] Dror R.O., Arlow D.H., Borhani D.W., Jensen M.Ø., Piana S., Shaw D.E.; Identification of two distinct inactive conformations of the β_2-adrenergic receptor reconciles structural and biochemical observations; Proc. Natl. Acad. Sci. USA **2009**, *106*, 4689-4694.

[174] Romo T.D., Grossfield A., Pitman M.C.; Concerted interconversion between Ionic lock substates of the β_2 adrenergic receptor revealed by microsecond timescale molecular dynamics; Biophys. J. **2010**, *98*, 76-84.

[175] Jójárt B., Kiss R., Viskolcz B., Keserű G.M.; Activation mechanism of the human histamine H_4 receptor - an explicit membrane molecular dynamics simulation study; J. Chem. Inf. Model. **2008**, *48*, 1199-1210.

[176] Khelashvili G., Grossfield A., Feller S.E., Pitman M.C., Weinstein H.; Structural and dynamic effects of cholesterol at preferred sites of interaction with rhodopsin identified from microsecond length molecular dynamics simulations; Proteins **2009**, *76*, 403-417.

[177] Provasi D., Bortolato A., Filizola M.; Exploring molecular mechanisms of ligand recognition by opioid receptors with metadynamics; Biochemistry **2009**, *48*, 10020-10029.

[178] Kolb P., Rosenbaum D.M., Irwin J.J., Fung J.J., Kobilka B.K., Shoichet B.K.; Structure-based discovery of β_2-adrenergic receptor ligands; Proc. Natl. Acad. Sci. USA **2009**, *106*, 6843-6848.

[179] Sabio M., Jones K., Topiol S.; Use of the X-ray structure of the β_2-adrenergic receptor for drug discovery. Part 2: Identification of active compounds; Bioorg. Med. Chem. Lett. **2008**, *18*, 5391-5395.

[180] Topiol S., Sabio M.; Use of the X-ray structure of the Beta2-adrenergic receptor for drug discovery; Bioorg. Med. Chem. Lett. **2008**, *18*, 1598-1602.

[181] Carlsson J., Yoo L., Gao Z.-G., Irwin J.J., Shoichet B.K., Jacobson K.A.; Structure-based discovery of A_{2A} adenosine receptor ligands; J. Med. Chem. **2010**, *53*, 3748-3755.

[182] de Graaf C., Kooistra A.J., Vischer H.F., Katritch V., Kuijer M., Shiroishi M., Iwata S., Shimamura T., Stevens R.C., de Esch I.J.P., Leurs R.; Crystal structure-based virtual screening for fragment-like ligands of the human histamine H_1 receptor; J. Med. Chem. **2011**, *54*, 8195-8206.

[183] Carlsson J., Coleman R.G., Setola V., Irwin J.J., Fan H., Schlessinger A., Sali A., Roth B.L., Shoichet B.K.; Ligand discovery from a dopamine D_3 receptor homology model and crystal structure; Nat. Chem. Biol. **2011**, *7*, 769-778.

[184] Bissantz C., Bernard P., Hibert M., Rognan D.; Protein-based virtual screening of chemical databases. II. Are homology models of g-protein coupled receptors suitable targets?; Proteins **2003**, *50*, 5-25.

[185] Radestock S., Weil T., Renner S.; Homology model-based virtual screening for GPCR ligands using docking and target-biased scoring; J. Chem. Inf. Model. **2008**, *48*, 1104-1117.

[186] Singh N., Chevé G., Ferguson D.M., McCurdy C.R.; A combined ligand-based and target-based drug design approach for G-protein coupled receptors: application to salvinorin A, a selective kappa opioid receptor agonist; J. Comp. Aided Mol. Design **2006**, *20*, 471-493.

[187] Evers A., Hessler G., Matter H., Klabunde T.; Virtual screening of biogenic amine-binding G-protein coupled receptors: comparative evaluation of protein- and ligand-based virtual screening protocols, J. Med. Chem. **2005**, *48*, 5448-5465.

[188] Renault N., Gohier A., Chavatte P., Farce A.; Novel structural insights for drug design of selective 5-HT_{2C} inverse agonists from a ligand-biased receptor model; Eur. J. Med. Chem. **2010**, *45*, 5086-5099.

[189] McRobb F.M., Capuano B., Crosby I.T., Chalmers D.K., Yuriev E.; Homology modeling and docking evaluation of aminergic G protein-coupled receptors; J. Chem. Inf. Model. **2010**, *50*, 626-637.

[190] Kiss R., Kiss B., Könczöl A., Szalai F., Jelinek I., László V., Noszál B., Falus A., Keserű G.M.; Discovery of novel human histamine H_4 receptor ligands by large-scale structure-based virtual screening; J. Med. Chem. **2008**, *51*, 3145-3153.

[191] Engel S., Skoumbourdis A.P., Childress J., Neumann S., Deschamps J.R., Thomas C.J., Colson A.-O., Costanzi S., Gershengorn M.C.; A virtual screen for diverse ligands: discovery of selective G protein-coupled receptor antagonists; J. Am. Chem. Soc. **2008**, *130*, 5115-5123.

[192] Tikhonova I.G., Sum C.S., Neumann S., Engel S., Raaka B.M., Costanzi S., Gershengorn M.C.; Discovery of novel agonists and antagonists of the Free Fatty Acid Receptor 1 (FFAR1) using virtual screening; J. Med. Chem. **2008**, *51*, 625-633.

[193] Evers A., Klebe G.; Successful virtual screening for a submicromolar antagonist of the Neurokinin-1 receptor based on a ligand-supported homology model; J. Med. Chem. **2004**, *47*, 5381-5392.

[194] Evers A., Klabunde T.; Structure-based drug discovery using GPCR homology modeling: successful virtual screening for antagonists of the Alpha1A adrenergic receptor; J. Med. Chem. **2005**, *48*, 1088-1097.

[195] Varady J., Wu X., Fang X., Min J., Hu Z., Levant B., Wang S.; Molecular modeling of the three-dimensional structure of Dopamine 3 (D_3) subtype receptor: discovery of novel and potent D_3 ligands through a hybrid pharmacophore- and structure-based database searching approach; J. Med. Chem. **2003**, *46*, 4377-4392.

[196] Tautermann C.S.; The use of G-protein coupled receptor models in lead optimization; Future Med. Chem. **2011**, *3*, 709-721.

[197] Tautermann C.S., Pautsch A.; The implication of the first agonist bound activated GPCR X-ray structure on GPCR in silico modeling; ACS Med. Chem. Lett. **2011**, *2*, 414–418.

[198] Kolb P., Klebe G.; The golden age of GPCR structural biology: any impact on drug design? Angew. Chem. Int. Ed. Engl. **2011**, 50, 11573-11575.

[199] Inouye S.T., Kawamura H.; Persistence of circadian rhythmicity in a mammalian hypothalamic “island” containing the suprachiasmatic nucleus; Proc. Natl. Acad. Sci. USA **1979** ,*76*, 5962-5966.

[200] Cardinali D.P., Rosner J.M.; Metabolism of serotonin by the rat retina “in vitro”; J. Neurochem. **1971**, *18*, 1769-70.

[201] Tosini G., Menaker M.; The clock in the mouse retina: melatonin synthesis and photoreceptor degeneration; Brain Res. **1998**, *789*, 221-228.

[202] Carrillo-Vico A., Calvo J.R., Abreu P., Lardone P.J., García-Mauriño S., Reiter R.J., Guerrero J.M.; Evidence of melatonin synthesis by human lymphocytes and its physiological significance: possible role as intracrine, autocrine and/or paracrine substance; FASEB J. **2004**, *18*, 537-539.

[203] Cajochen C., Kräuchi K., Wirz-Justice A.; Role of melatonin in the regulation of human circadian rhythms and sleep; J. Neuroendocrinol. **2003**, *15*, 432-437.

[204] Maestroni G.J.; The immunotherapeutic potential of melatonin; Expert Opin. Investig. Drugs **2001**, *10*, 467-476.

[205] Arangino S., Cagnacci A., Angiolucci M., Vacca A.M., Longu G., Volpe A., Melis G.B.; Effects of melatonin on vascular reactivity, catecholamine levels and blood pressure in healthy men; Am. J. Cardiol. **1999**, *83*, 1417-1419.

[206] Ambriz-Tututi M., Rocha-Gonzalez H.I., Cruz S.L., Granados-Soto V.; Melatonin: a hormone that modulates pain; Life Sci. **2009**, *84*, 489-498.

[207] Satomura K., Tobiume S., Tukoyama R., Yamasaki Y., Kudoh K., Maeda E., Nagayama M.; Melatonin at pharmacological doses enhances human osteoblastic differentiation in vitro and promotes mouse cortical bone formation in vivo; J. Pineal Res. **2007**, *42*, 231-239.

[208] Korkmaz A., Reiter R.J., Topal T., Manchester L.C., Oter S., Tan D.X.; Melatonin: an established antioxidant worthy of use in clinical trials; Mol. Med. **2009**, *15*, 43-50.

[209] Turek, F. W.; Gillette, M. U.; Melatonin, sleep, and circadian rhythms: rationale for development of specific melatonin agonists; Sleep Med. **2004**, *5*, 523-532.

[210] Lewy A.J.; Circadian misalignment in mood disturbances; Curr. Psychiatry Rep. **2009**, *11*, 459-465.

[211] Hirsch-Rodriguez E., Imbesi M., Manev R., Uz T., Manev H.; The pattern of melatonin receptor expression in the brain may influence antidepressant treatment; Med. Hypotheses **2006**, *69*, 120-124.

[212] Medeiros C.A.M., Carvalhedo de Bruin P.F., Lopes L.A., Magalhães M.C., Seabra M.deL., Sales de Bruin V.M.; Effect of exogenous melatonin on sleep and motor dysfunction in Parkinson's disease. A randomized, double blind, placebo-controlled study; J. Neurol. **2007**, *254*, 459-464.

[213] Mills E., Wu P., Seely D., Guyatt G.; Melatonin in the treatment of cancer: a systematic review of randomized controlled trials and meta-analysis; J. Pineal Res. **2005**, *39*, 360-366.

[214] Solmaz I., Gurkanlar D., Gokcil Z., Göksoy C., Ozkan M., Erdoğan E.; Antiepileptic activity of melatonin in guinea pigs with pentylenetetrazol-induced seizures; Neurol. Res. **2009**, *31*, 989-995.

[215] Macleod M. R., O'Collins T., Horky L.L., Howells D.W., Donnan G.A.; Systematic review and meta-analysis of the efficacy of melatonin in experimental stroke; J. Pineal Res. **2005**, *38*, 35-41.

[216] Spadoni G., Bedini A., Mor M., Rivara S.; in *Sleep Disorders: Diagnosis and Therapeutics*, (Eds.: Pandi-Pemural S.R., Verster J.C., Monti J.M., Lader M.H., Langer S.Z.), Informa Healthcare, London, **2008**, pp. 402-416.

[217] Mor M., Rivara S., Pala D., Bedini A., Spadoni G., Tarzia G.; Recent advances in the development of melatonin MT(1) and MT(2) receptor agonists; Expert Opin. Ther. Pat. **2010**, *20*, 1059-1077.

[218] Wade A.G., Ford I., Crawford G., McMahon A.D., Nir T., Laudon M., Zisapel N.; Efficacy of prolonged release melatonin in insomnia patients aged 55–80 years: quality of sleep and next-day alertness outcomes; Curr. Med. Res. Opin. **2007**, *23*, 2597-2605.

[219] Simpson D., Curran M.P.; Ramelteon: a review of its use in insomnia; Drugs **2008**, *68*, 1901-1919.

[220] Yous S., Andrieux J., Howell H.E., Morgan P.J., Renard P., Pfeiffer B., Lesieur D., Guardiola-Lemaître B.; Novel naphthalenic ligands with high affinity for the melatonin receptor; J. Med. Chem. **1992**, *35*, 1484-1486.

[221] Kennedy S., Emsley R.; Placebo-controlled trial of agomelatine in the treatment of major depressive disorder; Eur. Neuropsychopharmacol. **2006**, *16*, 93-100.

[222] Vachharajani N.N., Yeleswaram K., Boulton D.W.; Preclinical pharmacokinetics and metabolism of BMS-214778, a novel melatonin receptor agonist; J. Pharm. Sci. **2003**, *92*, 760-772.

[223] Mulchahey J.J., Goldwater D.R., Zemlan F.P.; A single blind, placebo controlled, across groups dose escalation study of the safety, tolerability, pharmacokinetics and pharmacodynamics of the melatonin analog β-methyl-6-chloromelatonin; Life Sci. **2004**, *75*, 1843-1856.

[224] Reppert S.M., Weaver D.R., Godson C.; Melatonin receptors step into the light: cloning and classification of subtypes; Trends Pharmacol. Sci. **1996**, *17*, 100-102.

[225] Dubocovich M.L., Delagrange P., Krause D.N., Sugden D., Cardinali D.P., Olcese J.; International Union of Basic and Clinical Pharmacology. LXXV. Nomenclature, classification, and pharmacology of G protein-coupled melatonin receptors; Pharmacol. Rev. **2010**, *62*, 343-380.

[226] Duncan M.J., Takahashi J.S., Dubocovich M.L.; 2-[125I] iodomelatonin binding sites in hamster brain membranes: pharmacological characteristics and regional distribution; Endocrinology **1988**, *122*, 1825-1833.

[227] Dubocovich M.L.; Melatonin receptors: are there multiple subtypes?; Trends Pharmacol. Sci. **1995**, *16*, 50-56.

[228] Nosjean O., Ferro M., Cogé F., Beauverger P., Henlin J.-M., Lefoulon F., Fauchère J.-L., Delagrange P., Canet E., Boutin J.A.; Enzyme catalysis and regulation; J. Biol. Chem. **2000**, *275*, 31311-31317.

[229] Tan D.X., Manchester L.C., Terron M.P., Flores L.J., Tamura H., Reiter R.J.; Melatonin as a naturally occurring co-substrate of quinone reductase-2, the putative MT3 melatonin membrane receptor: hypothesis and significance; J. Pineal Res. **2007**, *43*, 317-320.

[230] Petit L., Lacroix I., de Coppet P., Strosberg A.D., Jockers R.; Differential signaling of human Mel1a and Mel1b melatonin receptors through the cyclic guanosine 3-5-monophosphate pathway; Biochem. Pharmacol. **1999**, *58*, 633-639.

[231] Hardeland R.; Melatonin: signaling mechanisms of a pleiotropic agent; Biofactors **2009**, *35*, 183-192.

[232] Witt-Enderby P.A., Bennett J., Jarzynka M.J., Firestine S., Melan M.A.; Melatonin receptors and their regulation: biochemical and structural mechanisms; Life Sci. **2003**, *72*, 2183-2198.

[233] Weaver D.R., Reppert S.M.; The Mel1a melatonin receptor gene is expressed in human suprachiasmatic nuclei; Neuroreport **1996**, *8*, 109-112.

[234] Savaskan E., Ayoub M.A., Ravid R., Angeloni D., Fraschini F., Meier F., Eckert A., Müller-Spahn F., Jockers R.; Reduced hippocampal MT2 melatonin receptor expression in Azheimer's disease; J. Pineal Res. **2005**, *38*, 10-16.

[235] Uz T., Arslan A.D., Kurtuncu M., Imbesi M., Akhisaroglu M., Dwivedi Y., Pandey G.N., Manev H.; The regional and cellular expression profile of the melatonin receptor MT1 in the central dopaminergic system; Brain Res. Mol. Brain Res. **2005**, *136*, 45-53.

[236] Ekmekcioglu C., Thalhammer T., Humpeler S., Mehrabi M.R., Glogar H.D., Hölzenbein T., Markovic O., Leibetseder V.J., Strauss-Blasche G., Marktl W.; The melatonin receptor subtype MT2 is present in the human cardiovascular system; J. Pineal Res. **2003**, *35*, 40-44.

[237] Savaskan E., Wirz-Justice A., Olivieri G., Pache M., Kräuchi K., Brydon L., Jockers R., Müller-Spahn F., Meyer P.; Distribution of melatonin MT1 receptor immunoreactivity in human retina; J. Histochem. Cytochem. **2002**, *50*, 519-526.

[238] Maestroni G.J., Sulli A., Pizzorni C., Villaggio B., Cutolo M.; Melatonin in rheumatoid arthritis: synovial macrophages show melatonin receptors.; Ann. N.Y. Acad. Sci. **2002**, *966*, 271-275.

[239] Jin X., von Gall C., Pieschl R.L., Gribkoff V.K., Stehle J.H., Reppert S.M., Weaver D.R.; Targeted disruption of the mouse Mel1b melatonin receptor. Mol. Cell. Biol. **2003**, *23*, 1054-1060.

[240] von Gall C., Garabette M.L., Kell C.A., Frenzel S., Dehghani F., Schumm-Draeger P.M., Weaver D.R., Korf H.W., Hastings M.H., Stehle J.H.; Rhythmic gene expression in pituitary depends on heterologous sensitization by the neurohormone melatonin; Nat. Neurosci. **2002**, *5*, 234-238.

[241] Drazen D.L., Bilu D., Bilbo S.D., Nelson R.J.; In vitro melatonin enhancement of splenocyte proliferation is attenuated in mice by luzindole, a melatonin receptor antagonist; Am. J. Physiol. **2001**, *280*, R1476-1482.

[242] Dubocovich M.L., Masana M.I., Iacob S., Sauri D.M.; Melatonin receptor antagonists that differentiate between the human Mel1a and Mel1b recombinant subtypes are used to assess the pharmacological profile of the rabbit retina ML1 presynaptic heteroreceptor; Naunyn-Schmied. Arch. Pharmacol. **1997**, *355*, 365-375.

[243] Ersahin C., Masana M.I., Dubocovich M.L.; Constitutively active melatonin MT1 receptors in male rat caudal artieries; Eur. J. Pharmacol. **2002**, *439*, 171-172.

[244] Masana M.I., Doolen S., Ersahin C., Al-Ghoul W.M., Duckles S.P., Dubocovich M.L., Krause D.N.; MT2 melatonin receptors are present and functional in rat caudal artery; J. Pharmacol. Exp. Ther. **2002**, *302*, 1295-1302.

[245] Farce A., Chugunov A.O., Logé C., Sabaouni A., Yous S., Dilly S., Renault N., Vergoten G., Efremov R.G., Lesieur D., Chavatte P.; Homology modeling of MT_1 and MT_2 receptors; Eur. J. Med. Chem. **2008**, *43*, 1926-1944.

[246] Voronkov A.E., Ivanov A.A., Baskin I.I., Palyulin V.A., Zefirov N.S.; Molecular modeling study of the mechanism of ligand binding to human melatonin receptors; Dokl. Biochem. Biophys. **2005**, *403*, 284-288.

[247] Grol C.J., Jansen J.M.; The high affinity melatonin binding site probed with conformationally restricted ligands—II. Homology modeling of the receptor; Bioorg. Med. Chem. **1996**, *4*, 1333-1339.

[248] Chugunov A.O., Farce A., Chavatte P., Efremov R.G.; Differences in binding sites of two melatonin receptors help to explain their selectivity to some melatonin analogs: a molecular modeling study; J. Biomol. Struct. Dyn. **2006**, *24*, 91-107.

[249] Kokkola T., Salo O.M.H., Poso A., Laitinen J.T.; The functional role of cysteines adjacent to the NRY motif of the human MT1 melatonin receptor; J. Pineal Res. **2005**, *39*, 1-11.

[250] Mazna P., Obsilova V., Jelinkova I., Balik A., Berka K., Sovova Z., Ettrich R., Svoboda P., Obsil T., Teisinger J.; Molecular modeling of human MT2 melatonin receptor: the role of Val204, Leu272 and Tyr298 in ligand binding; J. Neurochem. **2004**, *91*, 836-842.

[251] Sovova Z., Mazna P., Teisinger J., Stys D., Obsil T., Ettrich R.; A structural model of human MT2 melatonin receptor and its melatonin recognition site; Materials Structure 2004, 11, 12-14.

[252] Mseeh F., Gerdin M.J., Dubocovich M.L.; Identification of cysteines involved in ligand binding to the human melatonin MT_2 receptor; Eur. J. Pharmacol. **2002**, *449*, 29-38.

[253] Navajas C., Kokkola T., Poso A., Honka N., Gynther J., Laitinen J.T., A rhodopsin-based model for melatonin recognition at its G protein-coupled receptor; Eur. J. Pharmacol. **1996**, *304*, 173-183.

[254] Sugden D., Chong N.W., Lewis D.F.; Structural requirements at the melatonin receptor; Br. J. Pharmacol. **1995**, *114*, 618-623.

[255] Ivanov A.A., Voronkov A.E., Baskin I.I., Palyulin V.A., Zefirov N.S.; The study of the mechanism of binding of human ML1A melatonin receptor ligands using molecular modeling; Dokl. Biochem. Biophys. **2004**, *394*, 49-52.

[256] Rivara S., Lorenzi S., Mor M., Plazzi P.V., Spadoni G., Bedini A., Tarzia G.; Analysis of structure-activity relationships for MT_2 selective antagonists by melatonin MT_1 and MT_2 receptor models; J. Med. Chem. **2005**, *48*, 4049-4060.

[257] Castevens C.M., Shillady D.D.; Computational models of the sevene-helix trans-membrane human melatonin receptor MT1, one of the nature's common nano-assemblies; Clusters and nano-assemblies, **2003**, 415-422.

[258] Mazna P., Berka K., Jelinkova I., Balik A., Svoboda P., Obsilova V., Obsil T., Teisinger J.; Ligand binding to the human MT2 melatonin receptor: the role of residues in transmembrane domains 3, 6, and 7; Biochem. Biophys. Res. Commun. **2005**, *332*, 726-734.

[259] Rivara S., Mor M., Silva C., Zuliani V., Vacondio F., Spadoni G., Bedini A., Tarzia G., Lucini V., Pannacci M., Fraschini F., Plazzi P.V.; Three-dimensional quantitative structure-activity relationship studies on selected MT1 and MT2 melatonin receptor ligands: requirements for subtype selectivity and intrinsic activity modulation; J. Med. Chem. **2003**, *46*, 1429-1439.

[260] Rivara S., Diamantini G., Di Giacomo B., Lamba D., Gatti G., Lucini V., Pannacci M., Mor M., Spadoni G., Tarzia G.; Reassessing the melatonin pharmacophore--enantiomeric resolution, pharmacological activity, structure analysis, and molecular modeling of a constrained chiral melatonin analogue; Bioorg. Med. Chem. **2006**, *14*, 3383-3391.

[261] Rivara S., Lodola A., Mor M., Bedini A., Spadoni G., Lucini V., Pannacci M., Fraschini F., Scaglione F., Sanchez R.O., Gobbi G., Tarzia G.; N-(substituted-anilinoethyl)amides: design, synthesis, and

pharmacological characterization of a new class of melatonin receptor ligands; J. Med. Chem., **2007**, *50*, 6618–6626.

[262] Hu Y., Ho M.K., Chan K.H., New D.C., Wong Y.H.; Synthesis of substituted N-[3-(3-methoxyphenyl)propyl] amides as highly potent MT(2)-selective melatonin ligands; Bioorg. Med. Chem. Lett. **2010**, *20*, 2582-2585.

[263] Li G., Zhou H., Jiang Y., Keim H., Topiol S.W., Poda S.B., Ren Y., Chandrasena G., Doller D.; Design and synthesis of 4-arylpiperidinyl amide and N-arylpiperdin-3-yl-cyclopropane carboxamide derivatives as novel melatonin receptor ligands; Bioorg. Med. Chem. Lett. **2011**, *21*, 1236-1242.

[264] Carocci A., Catalano A., Lovece A., Lentini G., Duranti A., Lucini V., Pannacci M., Scaglione F., Franchini C.; Design, synthesis, and pharmacological effects of structurally simple ligands for MT_1 and MT_2 melatonin receptors. Bioorg. Med. Chem. **2010**, *18*, 6496-6511.

[265] Forrest L.R., Tang C.L., Honig B.; On the accuracy of homology modeling and sequence alignment methods applied to membrane proteins; Biophys. J. **2006**, *91*, 508-517.

[266] Vroling B., Sanders M., Baakman C., Borrmann A., Verhoeven S., Klomp J., Oliveira L., de Vlieg J., Vriend G.; GPCRDB: information system for G protein-coupled receptors; Nucleic Acids Res. **2011**, *39*, D309-D319.

[267] The UniProt Consortium; Ongoing and future developments at the Universal Protein Resource; Nucleic Acids Res. **2011**, *39*, D214-D219.

[268] Jain E., Bairoch A., Duvaud S., Phan I., Redaschi N., Suzek B.E., Martin M.J., McGarvey P., Gasteiger E.; Infrastructure for the life sciences: design and implementation of the UniProt website; BMC Bioinformatics **2009**, *10*, 136.

[269] Thompson J.D., Higgins D.G., Gibson T.J.; CLUSTAL W: improving the sensitivity of progressive multiple sequence alignment through sequence weighting, position-specific gap penalties and weight matrix choice; Nucleic Acids Res. **1994**, *22*, 4673-4680.

[270] Eswar N., Marti-Renom M.A., Webb B., Madhusudhan M.S., Eramian D., Shen M., Pieper U., Sali A.; Comparative protein structure modeling with MODELLER; Current Protocols in Bioinformatics, John Wiley & Sons, Inc., Supplement 15, 5.6.1-5.6.30, **2006**.

[271] Sali A., Blundell T.L.; Comparative protein modelling by satisfaction of spatial restraints; J. Mol. Biol. **1993**, *234*, 779-815.

[272] Gerdin M.J., Mseeh F., Dubocovich M.L.; Mutagenesis studies of the human MT_2 melatonin receptor; Biochem. Pharmacol. **2003**, 66, 315-320.

[273] Sato T., Kobayashi H., Nagao T., Kurose H.; Ser203 as well as Ser204 and Ser207 in fifth transmembrane domain of the human beta2-adrenoceptor contributes to agonist binding and receptor activation; Br. J. Pharmacol. **1999**, *128*, 272-274.

[274] Audinot V., Mailliet F., Lahaye-Brasseur C., Bonnaud A., Le Gall A., Amossé C., Dromaint S., Rodriguez M., Nagel N., Galizzi J.P., Malpaux B., Guillaumet G., Lesieur D., Lefoulon F., Renard P., Delagrange P., Boutin J.A.; New selective ligands of human cloned melatonin MT_1 and MT_2 receptors; Naunyn-Schmiedeberg's Arch. Pharmacol. **2003**, *367*, 553–561.

[275] Liapakis G., Ballesteros J.A., Papachristou S., Chan W.C., Chen X., Javitch J.A.; The Forgotten Serine: A crticial role for Ser-203$^{5.42}$ in ligand binding to and activation of the β_2-adrenergic receptor; J. Biol. Chem. **2000**, *275*, 37779-37788.

[276] Mattson R.J., Catt J.D., Keavy D., Sloan C.P., Epperson J., Gao Q., Hodges D.B., Iben L., Mahle C.D., Ryan E., Yocca F.D.; Indanyl piperazines as melatonergic MT_2 selective agents; Bioorg. Med. Chem. Lett. **2003**, *13*, 1199-1202.

[277] Spadoni G., Balsamini C., Diamantini G., Tontini A., Tarzia G., Mor M., Rivara S., Plazzi P.V., Nonno R., Lucini V., Pannacci M., Fraschini F., Stankov B.M.; 2-N-acylaminoalkylindoles: design and quantitative structure-activity relationship studies leading to MT2-selective melatonin antagonists; J. Med. Chem. **2001**, *44*, 2900-2912.

[278] Glide, version 4.5, Schrödinger, LLC, New York, NY, 2008

[279] Maestro, version 8.5, Schrödinger, LLC, New York, NY, 2008

[280] Lucini V., Pannacci M., Scaglione F., Fraschini F., Rivara S., Mor M., Bordi F., Plazzi P.V., Spadoni G., Bedini A., Piersanti G., Diamantini G., Tarzia G.; Tricyclic alkylamides as melatonin receptor ligands with antagonist or inverse agonist activity; J. Med. Chem.; **2004**, *47*, 4202-4212.

[281] Armstrong S.M., McNulty O.M., Guardiola-Lemaitre B., Redman J.R.; Successful use of S20098 and melatonin in an animal model of delayed sleep-phase syndrome (DSPS); Pharmacol. Biochem. Behav.; **1993**, *46*, 45-49.

[282] Laskowski R.A., MacArthur M.W., Moss D.S., Thornton J.M.; PROCHECK: a program to check the stereochemical quality of protein structures; J. Appl. Cryst. **1993**, *26*, 283-291.

[283] Maestro, version 9.0, Schrödinger, LLC, New York, NY, 2009.

[284] Liu W., Eilers M., Patel A.B., Smith S.O.; Helix packing moments reveal diversity and conservation in membrane protein structure; J. Mol. Biol. **2004**, *337*, 713-729.

[285] Li H., Robertson A.D., Jensen J.H.; Very fast empirical prediction and interpretation of protein pKa values; Proteins **2005**, *61*, 704-721.

[286] Bas D.C., Rogers D.M., Jensen J.H.; Very fast prediction and rationalization of pKa values for protein-ligand complexes; Proteins **2008**, *73*, 765-783.

[287] Olsson M.H.M., Søndergard C.R., Rostkowski M., Jensen J.H.; PROPKA3: consistent treatment of internal and surface residues in empirical pKa predictions; J. Chem. Theory Comput. **2011**, *7*, 525-537.

[288] Georgescu R.E., Alexov E.G., Gunner M.R.; Combining conformational flexibility and continuum electrostatics for calculating pKa's in proteins; Biophys J. **2002**, *83*, 1731-1748.

[289] Alexov E., Gunner M.R.; Incorporating protein conformational flexibility into pH- titration calculations: results on T4 lysozyme; Biophys. J. **1997**, *74*, 2075-2093.

[290] Kaminski G.A., Friesner R.A., Tirado-Rives J., Jorgensen W.J.; Evaluation and reparametrization of the OPLS-AA force field for proteins via comparison with accurate quantum chemical calculations on peptides; J. Phys. Chem. B **2001**, *105*, 6474-6487.

[291] Weiner S.J., Kollman P.A., Case D.A., Singh U.C., Ghio C., Alagona G., Profeta S., Weiner P.; A new force field for molecular mechanical simulation of nucleic acids and proteins; J. Am. Chem. Soc. **1984**, *106*, 765-784.

[292] Ferguson D. M., Kollman P.A.; Can the Lennard-Jones 6-12 function replace the 10-12 form in molecular mechanics calculations?; J. Comput. Chem. **1991**, *12*, 620-626.

[293] McDonald D.Q., Still W.C.; AMBER torsional parameters for the peptide backbone; Tetrahedron Lett. **1992**, *33*, 7743-7746.

[294] Cavalli A., Fanelli F., Taddei C., De Benedetti P.G., Cotecchia S.; Amino acids of the alpha1B-adrenergic receptor involved in agonist binding: differences in docking catecholamines to receptor subtypes; FEBS Lett. **1996**, *399*, 9-13.

[295] Parnot C., Bardin S., Miserey-Lenkei S., Guedin D., Corvol P., Clauser E.; Systematic identification of mutations that constitutively activate the angiotensin II type 1A receptor by screening a randomly mutated cDNA library with an original pharmacological bioassay; Proc. Natl. Acad. Sci. USA **2000**, *97*, 7615-7620.

[296] Bowers K.J., Chou E., Xu H., Dror R.O., Eastwood M.P., Gregersen B.A., Klepeis J.L., Kolossvary I., Moraes M.A., Sacerdoti F.D., Salmon J.K., Shan Y., Shaw D.E. Proceedings of the ACM/IEEE Conference on Supercomputing (SC06) Tampa, Florida, November 11-17, **2006**.

[297] Lomize M.A., Lomize A.L., Pogozheva I.D., Mosberg H.I.; OPM: Orientations of Proteins in Membranes database; Bioinformatics **2006**, *22*, 623-625.

[298] Hornak V., Abel R., Okur A., Strockbine B., Roitberg A., Simmerling C.; Comparison of multiple Amber force fields and development of improved protein backbone parameters; Proteins **2006**, *65*, 712-725.

[299] Wang J., Wolf R.M., Caldwell J.W., Kollman P.A., Case D.A.; Development and testing of a general amber force field; J. Comput. Chem. **2004**, *25*, 1157-1174.

[300] Jojart B., Martinek T. A.; Performance of the general amber force field in modeling aqueous POPC membrane bilayers; J. Comput. Chem. **2007**, *28*, 2051-2058.

[301] Feller S.E., Zhang Y., Pastor R.W., Brooks B.R.; Constant pressure molecular dynamics simulation: The Langevin piston method; J. Chem. Phys. **1995**, *103*, 4613-4621.

[302] Krautler V., van Gunsteren W.F., Hunenberger P.H.; A fast SHAKE algorithm to solve distance constraint equations for small molecules in molecular dynamics simulations; J. Comput. Chem. **2001**, *22*, 501-508.

[303] Darden T., York D., Pedersen L.; Particle mesh Ewald: An N·log(N) method for Ewald sums in large systems; J. Chem. Phys. **1993**, *98*, 10089-10092.

[304] Tuckerman M., Berne B.J., Martyna G.J.; Reversible multiple time scale molecular dynamics; J. Chem. Phys. **1992**, *97*, 1990-2001.

[305] Dubocovich M.L., Masana M.I., Iacob S., Sauri D.M.; Melatonin receptor antagonists that differentiate between the human Mel1a and Mel1b recombinant subtypes are used to assess the pharmacological profile of the rabbit retina ML1 presynaptic heteroreceptor; Naunyn Schmiedebergs Arch. Pharmacol. 1997, 355, 365-375.

[306] Spadoni G., Balsamini C., Diamantini G., Tontini A., Tarzia G., Mor M., Rivara S., Plazzi P.V., Nonno R., Lucini V., Pannacci M., Fraschini F., Stankov B.M.; 2-N-Acylaminoalkylindoles: design and quantitative structure–activity relationship studies leading to MT_2-selective melatonin antagonists; J. Med. Chem. **2001**, *44*, 2900-2912.

[307] Gatti G., Piersanti G., Spadoni G.; Conformation by NMR of two tetralin-based receptor ligands; Farmaco **2003**, *58*, 469-476.

[308] Mor M., Spadoni G., Di Giacomo B., Diamantini G., Bedini A., Tarzia G., Plazzi P.V., Rivara S., Nonno R., Lucini V., Pannacci M., Fraschini F., Stankov B.M.; Synthesis, pharmacological characterization and QSAR studies on 2-substituted indole melatonin receptor ligands; Bioorg. Med. Chem. **2001**, *9*, 1045-1057.

[309] Bedini A., Lucarini S., Spadoni G., Tarzia G., Scaglione F., Dugnani S., Pannacci M., Lucini V., Carmi C., Pala D., Rivara S., Mor M.; Toward the definition of stereochemical requirements for MT_2-selective antagonists and partial agonists by studying 4-phenyl-2-propionamidotetralin derivatives; J. Med. Chem. **2011**, *54*, 8362–8372.

[310] Orlando P.; PhD Thesis, University of Urbino (I), 2011.

[311] MacroModel, version 9.7, Schrödinger, LLC, New York, NY, 2009.

[312] Allinger N.L.; Conformational Analysis 130. MM2. A hydrocarbon force field utilizing V1 and V2 torsional terms; J. Am. Chem. Soc. **1977**, *99*, 8127-8134.

[313] Brunne R.M., van Gusteren W.F., Bruschweiler R., Ernst R.R.; Molecular dynamics simulation of the proline conformational equilibrium and dynamics in antamanide using the GROMOS force field; J. Am. Chem. Soc. **1993**, *115*, 4764-4768.

[314] Christianson L.A., Lucero M.J., Appella D.H., Klein D.A., Gellman S.H.; Improved treatment of cyclic β-amino acids and successful prediction of β-peptide secondary structure using a modified force field: AMBER*C; J. Comput. Chem. **2000**, *21*, 763-773.

[315] Dolain C., Léger J.-M., Delsuc N., Gornitzka H., Huc I.; Probing helix propensity of monomers within a helical oligomer; Proc. Natl. Acad. Sci. USA **2005**, *102*, 16146-16151.

[316] McDonald D.Q., Still W.C.; An AMBER* study of Gellman's amides; Tetrahedron Lett. **1992**, *33*, 7747-7750.

[317] Palocci C., Falconi M., Alcaro S., Tafi A., Puglisi R., Ortuso F., Botta M., Alberghina L., Cernia E.; An approach to address Candida rugosa lipase regioselectivity in the acylation reactions of trytilated glucosides; J. Biotech. **2007**, *128*, 908-918.

[318] Berl V., Huc I., Khoury R.G., Lehn J.-M.; Helical molecular programming: folding of oligopyridine-dicarboxamides into molecular single helices; Chem. Eur. J. **2001**, *7*, 2798-2809.

[319] Berl V., Huc I., Khoury R.G., Lehn J.-M.; Helical molecular programming: supramolecular double helices by dimerization of helical oligopyridine-dicarboxamide strands; Chem. Eur. J. **2001**, *7*, 2810-2820.

[320] Haasnoot C.A.G., de Leeuw F.A.A.M., Altona C.; The relationship between proton-proton NMR coupling constants and substituent electronegativities-I : An empirical generalization of the karplus equation; Tetrahedron **1979**, *36*, 2783-2792.

[321] Jansen J.M., Copinga S., Gruppen G., Molinari E.J., Dubocovich M.L., Grol C.J.; The high affinity melatonin binding site probed with conformationally restricted ligands-I. Pharmacophore and minireceptor models; Bioorg. Med. Chem. **1996**, *4*, 1321-1332.

[322] Barnes N.M., Sharp T.; A review of central 5-HT receptors and their function; Neuropharmacology **1999**, *38*, 1083-1152.

[323] Gillman P.K.; A review of serotonin toxicity data: implications for the mechanisms of antidepressant drug action; Biol. Psychiatry **2006**, *59*, 1046-1051.

[324] Garfield A.S., Heisler L.K.; Pharmacological targeting of the serotonergic system for the treatment of obesity; J. Physiol. **2009**, *587*, 49-60.

[325] Wood M.D., Reavill C., Trail B., Wilson A., Stean T., Kennett G.A., Lightowler S., Blackburn T.P., Thomas D., Gager T.L., Riley G., Holland V., Bromidge S.M., Forbes I.T., Middlemiss D.N.; SB-243213; a selective 5-HT_{2C} receptor inverse agonist with improved anxiolytic profile: lack of tolerance and withdrawal anxiety; Neuropharmacology **2001**, *41*, 186-199.

[326] Kennett G.A., Bailey F., Piper D.C., Blackburn T.P.; Effect of SB 200646A, a 5-HT_{2C}/5-HT_{2B} receptor antagonist in two conflict models of anxiety; Psychopharmacology **1995**, *118*, 178-182.

[327] Iwamoto K., Nakatani N., Bundo M., Yoshikawa T., Kato T.; Altered RNA editing of serotonin 2C receptor in a rat model of depression; Neurosci. Res. **2005**, *53*, 69-76.

[328] Sodhi M.S., Burnet P.W., Makoff A.J., Kerwin R.W., Harrison P.J.; RNA editing of the 5-HT_{2C} receptor is reduced in schizophrenia; Mol. Psychiatry. **2001**, *6*, 373-379.

[329] Isaac M.; Serotonergic 5-HT_{2C} receptors as a potential therapeutic target for the design antiepileptic drugs; Curr. Top. Med. Chem. **2005**, *5*, 59-67.

[330] Leysen J.E.; 5-HT2 receptors; Curr. Drug Targets CNS Neurol. Disord. **2004**, *3*, 11-26.

[331] Bubar M.J., Cunningham K.A.; Distribution of serotonin 5-HT_{2C} receptors in the ventral tegmental area; Neuroscience **2007**, *146*, 286-297.

[332] Nilsson C., Lindvall-Axelsson M., Owman C.; Neuroendocrine regulatory mechanisms in the choroid plexus-cerebrospinal fluid system; Brain Res. Brain Res. Rev. **1992**, *17*, 109-138.

[333] Pranzatelli M.R., Murthy J.N., Pluchino R.S.; Identification of spinal 5-HT_{1C} binding sites in the rat: characterization of [^{3}H]mesulergine binding; J. Pharmacol. Exp. Ther. **1992**, *261*, 161-165.

[334] Abramowski D., Rigo M., Due D., Hoyer D., Staufenbiel M.; Localization of the 5-hydroxytryptamine2C receptor protein in human and rat brain using specific antisera; Neuropharmacology **1995**, *34*, 1635-1645.

[335] Becamel C., Alonso G., Galeotti N., Demey E., Jouin P., Ullmer C., Dumuis A., Bockaert J., Marin P.; Synaptic multiprotein complexes associated with 5-HT(2C) receptors: a proteomic approach; Embo J. **2002**, *21*, 2332-2342.

[336] Forbes I.T., Dabbs S., Duckworth D.M., Ham P., Jones G.E., King F.D., Saunders D. V., Blaney F.E., Naylor C.B., Baxter G.S., Blackburn T.P., Kennett G.A., Wood M.D.; Synthesis, biological activity and molecular modeling studies of selective 5-HT2C/2B receptor antagonists; J. Med. Chem. **1996**, *39*, 4966-4977.

[337] Bromidge S.M., Dabbs S., Davies D.T., Duckworth D.M., Forbes I.T., Ham P., Jones G.E., King F.D., Saunders D.V., Starr S., Thewlis K.M., Wyman P.A., Blaney F.E., Naylor C.B., Bailey F., Blackburn T.P., Holland V., Kennett G.A., Riley G.J., Wood M.D.; Novel and selective 5-HT2C/2B receptor antagonists as potential anxiolytic agents: synthesis, quantitative structure-activity relationships, and molecular modeling of substituted 1-(3-pyridylcarbamoyl)indulines; J. Med. Chem. **1998**, *41*, 1598-1612.

[338] Marshall G.R., Barry C.D., Bosshard H.E., Dammkoehler R.A., Dunn D.A.; The conformational parameter in drug design: the active analog approach; Computer-assisted drug design; Olson E.C., Christoffersen R.E., Eds.; American Chemical Society: Washington, DC, **1979**; pp 205-226.

[339] Brea J., Rodrigo J., Carrieri A., Sanz F., Cadavid M.I., Enguix M.J., Villazón M., Mengod G., Caro Y., Masaguer C.F., Raviña E., Centeno N.B., Carotti A., Loza M.I.; New serotonin 5-HT(2A), 5-HT(2B), and 5-HT(2C) receptor antagonists: synthesis, pharmacology, 3D-QSAR, and molecular modeling of (aminoalkyl)benzo and heterocycloalkanones; J. Med. Chem. **2002**, *45*, 54-71.

[340] Rashid M., Manivet P., Nishio H., Pratuangdejkul J., Rajab M., Ishiguro M., Launay J.M., Nagatomo T.; Identification of the binding sites and selectivity of sarpogrelate, a novel 5-HT2 antagonist, to human 5-HT_{2A}, 5-HT_{2B} and 5-HT_{2C} receptor subtypes by molecular modeling; Life Sci. **2003**, *73*, 193-207.

[341] Brea J., Castro M., Loza M.I., Masaguer C.F., Raviña E., Dezi C., Pastor M., Sanz F., Cabrero-Castel A., Galán-Rodríguez B., Fernández-Espejo E., Maldonado R., Robledo P.; QF2004B, a potential antipsychotic butyrophenone derivative with similar pharmacological properties to clozapine; Neuropharmacology **2006**, *51*, 251-262.

[342] Farce A., Dilly S., Yous S., Berthelot P., Chavatte P.; Homology modelling of the serotoninergic 5-HT_{2C} receptor; J. Enzyme Inhib. Med. Chem.; **2006**, *21,* 285-92.

[343] Zuo Z., Chen G., Luo X., Puah C., Zhu W., Chen K., Jiang H.; Pharmacophore-directed homology modeling and molecular dynamics simulation of G protein-coupled receptor: study of possible binding modes of 5-HT2C receptor agonists; Acta Biochim. Biophys. Sin. (Shanghai) **2007**, *39*, 413-422.

[344] Dao-Pin S., Baase W.A., Matthews B.W.; A mutant T4 lysozyme (Val 131 → Ala) designed to increase thermostability by the reduction of strain within an α-helix; Proteins **1990**, *7*, 198-204.

[345] Lyu P.C., Liff M.I., Marky L.A., Kallenbach N.R.; Side chain contributions to the stability of alpha-helical structure in peptides; Science **1990**, *250*, 669-673.

[346] Marqusee S., Robbins V.H., Baldwin R.L.; Unusually stable helix formation in short alanine-based peptides; Proc. Natl. Acad. Sci. USA **1989**, *86*, 5286-5290.

[347] Merutka G., Lipton W., Shalongo W., Park S.H., Stellwagen E.; Effect of central-residue replacements on the helical stability of a monomeric peptide; Biochemistry **1990**, *29*, 7511-7515.

[348] O'Neil K.T., DeGrado W.F.; A thermodynamic scale for the helix-forming tendencies of the commonly occurring amino acids; Science **1990**, *250*, 646-651.

[349] Herrick-Davis K., Grinde E., Harrigan T.J., Mazurkiewicz J.E.; Inhibition of serotonin 5-hydroxytryptamine2c receptor function through heterodimerization: receptor dimers bind two molecules of ligand and one G-protein; J. Biol. Chem. **2005**, *280*, 40144-40151.

[350] Cho S.J., Jensen N.H., Kurome T., Kadari S., Manzano M.L., Malberg J.E., Caldarone B., Roth B.L., Kozikowski A.P.; Selective 5-hydroxytryptamine 2C receptor agonists derived from the lead compound tranylcypromine: identification of drugs with antidepressant-like action; J. Med. Chem. **2009**, *52*, 1885-1902.

[351] Wacker D.A., Varnes J.G., Malmstrom S.E., Cao X., Hung C.P., Ung T., Wu G., Zhang G., Zuvich E., Thomas M.A., Keim W.J., Cullen M.J., Rohrbach K.W., Qu Q., Narayanan R., Rossi K., Janovitz E., Lehman-McKeeman L., Malley M.F., Devenny J., Pelleymounter M.A., Miller K.J., Robl J.A.; Discovery of (*R*)-9-ethyl-1,3,4,10b-tetrahydro-7-trifluoromethylpyrazino[2,1-a]isoindol- 6(2H)-one, a selective, orally active agonist of the 5-HT(2C) receptor; J. Med. Chem. **2007**, *50*, 1365-1379.

[352] Rosenzweig-Lipson S., Zhang J., Mazandarani H., Harrison B.L., Sabb A., Sabalski J., Stack G., Welmaker G., Barrett J.E., Dunlop J.; Antiobesity-like effects of the 5-HT_{2C} receptor agonist WAY-161503. Brain Res. **2006**, *1073-1074*, 240-251.

[353] Schrödinger Suite 2009 Induced Fit Docking protocol; Glide version 5.5, Schrödinger, LLC, New York, NY, 2009; Prime version 2.1, Schrödinger, LLC, New York, NY, 2009.

[354] Shapiro D.A., Kristiansen K., Kroeze W.K., Roth B.L.; Differential modes of agonist binding to 5-hydroxytryptamine(2A) serotonin receptors revealed by mutation and molecular modeling of conserved residues in transmembrane region 5; Mol. Pharmacol. **2000**, *58*, 877-886.

[355] Choudhary M.S., Craigo S., Roth B.L.; A single point mutation (Phe340→Leu340) of a conserved phenylalanine abolishes 4-[125I]iodo-(2,5-dimethoxy)phenylisopropylamine and [^{3}H]mesulergine but not [^{3}H]ketanserin binding to 5-hydroxytryptamine2 receptors; Mol. Pharmacol. **1993**, *43*, 755-761.

[356] Wieland K., Zuurmond H.M., Krasel C., Ijzerman A.P., Lohse M.J.; Involvement of Asn-293 in stereospecific agonist recognition and in activation of the beta 2-adrenergic receptor; Proc. Natl. Acad. Sci. USA **1996**, *93*, 9276-9281.

[357] Schubert P., Komp W., Kreutzberg G.W.; Correlation of 5'-nucleotidase activity and selective transneuronal transfer of adenosine in the hippocampus; Brain Res. **1979**, *168*, 419-424.

[358] Zimmermann H., Braun N., Kegel B., Heine P.; New insights into molecular structure and function of ectonucleotidases in the nervous system; Neurochem. Int. **1998**, *32*, 421-425.

[359] Broch O.J., Ueland P.M.; Regional and subcellular distribution of Sadenosylhomocysteine hydrolase in the adult rat brain; J. Neurochem. **1980**, *35*, 484-488.

[360] Carswell H.V., Graham D.I., Stone T.W.; Kainate-evoked release of adenosine from the hippocampus of the anaesthetised rat: possible involvement of free radicals; J. Neurochem. **1997**, *68*, 240-247.

[361] Delaney S.M., Geiger J.D.; Levels of endogenous adenosine in rat striatum. II. Regulation of basal and N-methyl-D-aspartate-induced levels by inhibitors of adenosine transport and metabolism; J. Pharmacol. Exp. Ther. **1998**, *285*, 568-572.

[362] Fredholm B.B., IJzerman A.P., Jacobson K.A., Klotz K.N., Linden J.; International Union of Pharmacology. XXV. Nomenclature and classification of adenosine receptors; Pharmacol. Rev. **2001**, *53*, 527-552.

[363] Linden J.; Adenosine in tissue protection and tissue regeneration; Mol. Pharmacol. **2005**, *67*, 1385-1387.

[364] Satoh S., Matsumura H., Hayaishi O.; Involvement of adenosine A_{2A} receptor in sleep promotion; Eur. J. Pharmacol. **1998**, *351*, 155-162.

[365] Zablocki J.A., Wu L., Shryock J., Belardinelli L.; Partial A1 adenosine receptor agonists from a molecular perspective and their potential use as chronic ventricular rate control agents during atrial fibrillation (AF); Curr. Top. Med. Chem. **2004**, *4*, 839-854.

[366] Fraser H., Gao Z., Ozeck M.J., Belardinelli L.; N-[3-(R)-tetrahydrofuranyl]-6-aminopurine riboside, an A1 adenosine receptor agonist, antagonizes catecholamine-induced lipolysis without cardiovascular effects in awake rats; J. Pharmacol. Exp. Ther. **2003**, *305*, 225-231.

[367] Ledent C., Vaugeois J.M., Schiffmann S.N., Pedrazzini T., El Yacoubi M., Vanderhaeghen J.J., Costentin J., Heath J.K., Vassart G., Parmentier M.; Aggressiveness, hypoalgesia and high blood pressure in mice lacking the adenosine A_{2A} receptor; Nature **1997**, *388*, 674-678.

[368] Huang Z.L., Qu W.M., Eguchi N., Chen J.F., Schwarzschild M.A., Fredholm B.B., Urade Y., Hayaishi O.; Adenosine A_{2A}, but not A1, receptors mediate the arousal effect of caffeine. Nature Neurosci. **2005**, *8*, 858-859.

[369] Sawynok J.; Adenosine receptor activation and nociception; Eur. J. Pharmacol. **1998**, *347*, 1-11.

[370] Chen J.F., Huang Z., Ma J., Zhu J., Moratalla R., Standaert D., Moskowitz M.A., Fink J.S., Schwarzschild M.A.; A_{2A} adenosine receptor deficiency attenuates brain injury induced by transient focal ischemia in mice; J. Neurosci. **1999**, *19*, 9192-9200.

[371] Dubey R.K., Gillespie D.G., Mi Z., Jackson E. K.; Adenosine inhibits PDGF-induced growth of human glomerular mesangial cells via A_{2B} receptors; Hypertension **2005**, *46*, 628-634.

[372] Bayes M., Rabasseda X., Prous J.R.; Gateways to clinical trials; Methods Find. Exp. Clin. Pharmacol. **2003**, *25*, 831-855.

[373] Ellenbogen K.A., O'Neill G., Prystowsky E.N., Camm J.A., Meng L., Lieu H.D., Jerling M., Shreeniwas R., Belardinelli L., Wolff A.A., TEMPEST Study Group; Trial to evaluate the management of paroxysmal supraventricular tachycardia during an electrophysiology study with tecadenoson; Circulation **2005**, *111*, 3202-3208.

[374] Matherne G.P., Linden J., Byford A.M., Gauthier N.S., Headrick J.P.; Transgenic A1 adenosine receptor overexpression increases myocardial resistance to ischemia; Proc. Natl. Acad. Sci. USA **1997**, *94*, 6541-6546.

[375] Barrett R.J., Lamson M.J., Johnson J., Smith W.B.; Pharmacokinetics and safety of binodenoson after intravenous dose escalation in healthy volunteers; J. Nucl. Cardiol. **2005**, *12*, 166-171.

[376] Hauser R.A., Hubble J.P., Truong D.D.; Randomized trial of the adenosine A_{2A} receptor antagonist istradefylline in advanced PD; Neurology **2003**, *61*, 297-303.

[377] Weiss S.M., Benwell K., Cliffe I.A., Gillespie R.J., Knight A.R., Lerpiniere J., Misra A., Pratt R.M., Revell D., Upton R., Dourish C.T.; Discovery of nonxanthine adenosine A_{2A} receptor antagonists for the treatment of Parkinson's disease; Neurology 2003, 61, S101-S106.

[378] Parkinson F.E., Xiong W., Zamzow C.R.; Astrocytes and neurons: different roles in regulating adenosine levels; Neurol. Res. **2005**, *27*, 153-160.

[379] Varani K., Caramori G., Vincenzi F., Adcock I., Casolari P., Leung E., Maclennan S., Gessi S., Morello S., Barnes P.J., Ito K., Chung K.F., Cavallesco G., Azzena G., Papi A., Borea P.A.; Alteration of adenosine receptors in patients with chronic obstructive pulmonary disease; Am. J. Respir. Crit. Care Med. **2006**, *173*, 398-406.

[380] Russo C., Arcidiacono G., Polosa R.; Adenosine receptors: promising targets for the development of novel therapeutics and diagnostics for asthma; Fund. Clin. Pharm. **2006**, *20*, 9-19.

[381] Merighi S., Mirandola P., Varani K., Gessi S., Leung E., Baraldi P.G., Tabrizi M.A., Borea P.A.; A glance at adenosine receptors: novel target for antitumor therapy; Pharmacol. Ther. **2003**, *100*, 31-48.

[382] Awad A.S., Huang L., Ye H., Duong E.T., Bolton W.K., Linden J., Okusa M.D.; Adenosine A_{2A} receptor activation attenuates inflammation and injury in diabetic nephropathy; Am. J. Physiol. Renal Physiol. **2006**, *290*, F828 -F837.

[383] Fredholm B.B., IJzerman A.P., Jacobson K.A., Klotz K.N., Linden J.; International Union of Pharmacology. XXV. Nomenclature and classification of adenosine receptors; Pharmacol. Rev. **2001**, *53*, 527-552.

[384] Kull B., Svenningsson P., Fredholm B.B.; Adenosine A_{2A} receptors are colocalized with and activate Golf in rat striatum; Mol. Pharmacol. **2000**, *58*, 771-777.

[385] Tucker A.L., Jia L., Holeton D., Taylor A.J., Linden J.; Dominance of Gs in doubly Gs/Gi-coupled chimeric A_1/A_{2A} adenosine receptors in HEK-293 cells; Biochem. J. **2000**, *352*, 203-210.

[386] Kim J., Jiang Q., Glashofer M., Yehle S., Wess J., Jacobson K.A.; Glutamate residues in the second extracellular loop of the human A2a adenosine receptor are required for ligand recognition; Mol. Pharm. **1996**, *49*, 683-691.

[387] Kim J., Wess J., van Rhee A.M., Schöneberg T., Jacobson K.A.; Site-directed Mutagenesis Identifies Residues Involved in Ligand Recognition in the Human A_{2A} Adenosine Receptor; J. Biol. Chem. **1995**, *270*, 13987-13997.

[388] Klotz K.-N., Hessling J., Hegler J., Owman C., Kull B., Fredholm B.B., Lohse, M.J.; Comparative pharmacology of human adenosine receptor subtypes characterization of stably transfected receptors in CHO cells; Naunyn Schmiedebergs Arch. Pharmacol. **1998**, *357*, 1-9.

[389] Dionisotti S., Ongini E., Zocchi C., Kull B., Arslan G., Fredholm B.B.; Characterization of human A2Aadenosine receptors with the antagonist radioligand [^{3}H]-SCH 58261; Br. J. Pharmacol. **1997**, *121*, 353-360.

[390] Ongini E., Dionisotti S., Gessi S., Irenius E., Fredholm B.B.; Comparison of CGS 15943, ZM 241385 and SCH 58261 as antagonists at human adenosine receptors; Naunyn Schmiedebergs Arch. Pharmacol. **1999**, *359*, 7-10.

[391] Kull B., Arslan G., Nilsson C., Owman C., Lorenzen A., Schwabe U., Fredholm B.B.; Differences in the order of potency for agonists, but not antagonists, at human and rat adenosine A_{2A} receptors; Biochem. Pharmacol. **1999**, *57*, 65-75.

[392] Glide, version 5.5, Schrödinger, LLC, New York, NY, 2009.

[393] Jarvis M.F., Williams M., Do U.H., Sills M.A.; Characterization of the binding of a novel nonxanthine adenosine antagonist radioligand, [^{3}H]CGS 15943, to multiple affinity states of the adenosine A_1 receptor in the rat cortex; Mol. Pharmacol. **1991**, *39*, 49-54.

[394] Dionisotti S., Ongini E., Zocchi C., Kull B., Arslan G., Fredholm B.B.; Characterization of human A_{2A} adenosine receptors with the antagonist radioligand [^{3}H]-SCH 58261; Br. J. Pharmacol. **1997**, *121*, 353-360.

[395] Mantri M., de Graaf O., van Veldhoven J., Göblyös A., von Frijtag Drabbe Künzel J.K., Mulder-Krieger T., Link R., de Vries H., Beukers M.W., Brussee J., Ijzerman A.P.; 2-amino-6-furan-2-yl-4-substituted nicotinonitriles as A_{2A} adenosine receptor antagonists; J. Med. Chem. **2008**, *52*, 4449-4455.

[396] Minetti P., Tinti M.O., Carminati P., Castorina M., Di Cesare M.A., Di Serio S., Gallo G., Ghirardi O., Giorgi F., Giorgi L., Piersanti G., Bartoccini F., Tarzia G.; 2-n-Butyl-9-methyl-8-[1,2,3]triazol-2-yl-9H-purin-6-ylamine and analogues as A2A adenosine receptor antagonists. Design, synthesis, and pharmacological characterization; J. Med. Chem. **2005**, *48*, 6887-6896.

[397] Higgs C., Beuming T., Sherman W.; Hydration site thermodynamics explain SARs for triazolylpurines analogues binding to the A_{2A} receptor; ACS Med. Chem. Lett., **2010**, *1*, 160-164.

[398] Jacobson K.A., Kiriasis L., Barone S., Bradbury B.J., Kammula U., Campagne J.M., Daly J.W., Neumeyer J.L, Pfleiderer W., Secunda S.; Sulfur-containing 1,3-dialkylxanthine derivatives as selective antagonists at A_1-adenosine receptors; J. Med. Chem., **1989**, *32*, 1873-1879.

[399] Jacobson K. A., Gallo-Rodriguez C. Melman N., Fischer B., Maillard M., Van Bergen A., Van Galen P.J.M., Karton Y.J.; Structure-activity relationships of 8-styrylxanthines as A2-selective adenosine antagonists; J. Med. Chem. **1993**, *36*, 1333-1342.

[400] Muller C.E., Geis U., Hipp J., Schobert U., Frobenius W., Pawlowski M., Suzuki F., Sandoval-Ramirez J.; Synthesis and structure–activity relationships of 3,7-dimethyl-1-propargylxanthine derivatives, A_{2A}-selective adenosine receptor antagonists; J. Med. Chem. **1997**, *40*, 4396-4405.

[401] Shimada J., Koike N., Nonaka H., Shiozaki S., Yanagawa K., Kanada T., Kobayashi H., Fumio S.; Adenosine A_{2A} antagonists with potent anti-cataleptic activity; Bioorg. Med. Chem. Lett. **1997**, *7*, 2349-2352.

[402] Suzuki F., Shimada J., Koike N., Nakamura J., Shioazaki S., Ichikawa S., Ishii A., Nonaka H.; United States Patent, Jan 16 1996. PN/5,484,920.

[403] Pretorius J., Malan S.F., Castagnoli Jr. N., Bergh J.J., Petzer J.P.; Dual inhibition of monoamine oxidase B and antagonism of the adenosine A_{2A} receptor by (E,E)-8-(4-phenylbutadien-1-yl)caffeine analogues; Bioorg. Med. Chem., **2008**, *16*, 8676-8684.

[404] Grahner B., Winiwarter S., Lanzner W., Mueller C.E.; Synthesis and structure-activity relationships of deazaxanthines: analogs of potent A_1- and A_2-adenosine receptor antagonists; J. Med. Chem. **1994**, *37*, 1526-1534.

[405] Siu S.W.I., Vacha R., Jungwirth P., Bockmann R.A.; Biomolecular simulations of membranes: Physical properties from different force fields; J. Chem. Phys. **2008**, *128*, 125103-125112.

[406] Case D.A, Darden T.A., Cheatham T.E., Simmerling C.L., Wang J., Duke R.E., Luo R., Crowley M., Walker R.C., Zhang W., Merz K.M., Wang B., Hayik S., Roitberg A., Seabra G., Kolossváry I., Wong K.F., Paesani F., Vanicek J., Wu X., Brozell S.R., Steinbrecher T., Gohlke H., Yang L., Tan C., Mongan J., Hornak V., Cui G., Mathews D.H., Seetin M.G., Sagui C., Babin V., Kollman P.A.; (2008), AMBER 10, University of California, San Francisco.

[407] Shao J., Tanner S. W., Thompson N., Cheatham T. E.; Clustering molecular dynamics trajectories: 1. characterizing the performance of different clustering algorithms; J. Chem. Theory Comput. **2007**, *3*, 2312-2334.

[408] Davies, D. L., Bouldin, D. W.; A cluster separation measure; IEEE Trans. Pattern Anal. Mach. Intelligence **1979**, *1*, 224- 227.

[409] Vesanto J., Alhoniemi E.; Clustering of the self-organizing map; IEEE Trans. Neural Networks **2000**, *11*, 586-600.

[410] Calinski T., Harabasz J.; A dendrite method for cluster analysis; Comm. Stat. **1974**, *3*, 1-27.

[411] Han M., Zhang J.Z.H.; Class I phospho-inositide-3-kinases (PI3Ks) isoform-specific inhibition study by the combination of docking and molecular dynamics simulation; J. Chem. Inf. Model. **2010**, *50*, 136-145.

[412] Xu D., Newhouse E.I., Amaro E.R., Pao H.C., Cheng L.S., Markwick P.R.L., McCammon J.A., Li W.W., Arzberger P.W.; Distinct glycan topology for avian and human sialopentasaccharide receptor analogues upon binding different hemagglutinins: a molecular dynamics perspective; J. Mol. Biol. **2009**, *387*, 465-491.

[413] Grant B.J., Gorfe A.A., McCammon A.J.; Ras conformational switching: simulating nucleotide-dependent conformational transitions with accelerated molecular dynamics; PLoS Comp. Biol., 2009, 5, e1000325.

[414] Lyman E., Higgs C., Kim B., Lupyan D., Shelley J.C., Farid R., Voth G.A.; A role for a specific cholesterol interaction in stabilizing the Apo configuration of the human A_{2A} adenosine receptor; Structure **2009**, *17*, 1660-1668.

[415] Hauser R.A., Shulman L.M., Trugman J.M., Roberts J.W., Mori A., Ballerini R., Sussman N.M., Istradefylline 6002-US-013 Study Group; Study of istradefylline in patients with Parkinson's disease on levodopa with motor fluctuations; Mov. Disord. **2008**, *23*, 2177-2185.

[416] LeWitt P.A., Guttman M., Tetrud J.W., Tuite P.J., Mori A., Chaikin P., Sussman N.M., 6002-US-005 Study Group; Adenosine A_{2A} receptor antagonist istradefylline (KW-6002) reduces "off" time in Parkinson's disease: a double-blind, randomized, multicenter clinical trial (6002-US-005); Ann. Neurol. **2008**, *63*, 295-302.

[417] Petzer J.P., Castagnoli N. Jr., Schwarzschild M.A., Chen J.F., Van der Schyf C.J.; Dual-target-directed drugs that block monoamine oxidase B and adenosine A_{2A} receptors for Parkinson's disease; Neurotherapeutics 2009, 6, 141-151.

[418] Muller C.E., Schobert U., Hipp J., Geis U., Frobenius W., Pawlowski M.; Configurationally stable analogs of styrylxanthines as A_{2A} adenosine receptor antagonist; Eur. J. Med. Chem. **1997**, *32*, 709-719.

[419] Müller C.E., Geis U., Hipp J., Schobert U., Frobenius W., Pawlowski M., Suzuki F., Sandoval-Ramírez J.; Synthesis and structure-activity relationships of 3,7-dimethyl-1-propargylxanthine derivatives, A_{2A}-selective adenosine receptor antagonists; J Med Chem. **1997**, *40*, 4396-4405.

[420] Johnson M.; The β-adrenoceptor; Am. J. Respir. Crit. Care Med. **1998**, *158*, S146–S153.

[421] Church M.K., Hiroi J.; Inhibition of IgE-dependent histamine release from human dispersed lung mast cells by anti-allergic drugs and salbutamol; Br. J. Pharmacol. **1987**, *90*, 421-429.

[422] O'Donnell S.R.; Pharmacology of β-adrenoceptors in lung disease. In: Szabadi, E., Bradshaw, C.M. (Eds.), Adrenoceptors: Structure, Mechanisms, Function, Advances in Pharmacological Sciences. Birkhauser-Verlag, Basel, **1991**, pp. 265–274.

[423] Bolton P.B., Lefevre P., McDonald D.M., Salmeterol reduces early- and late-phase plasma leakage and leukocyte adhesion in rat airways; Am. J. Respir. Crit. Care Med. **1997**, *155*, 1428-1435.

[424] Wither G.D., Kubes P., Ibbotson G., Scott R.B., Anaphylaxis-induced mesenteric vascular permeability, granulocyte adhesion, and platelet aggregates in rat; Am. J. Physiol. **1998**, *275*, H274-H284.

[425] Kim D., Glaum M., Lockey R.; Evaluation of combination long-acting β-2 agonists and inhaled glucocorticosteroids for treatment of asthma; Expert Opin. Drug. Metab. Toxicol. **2009**, *5*, 933-940.

[426] Cazzola M., Molimard M.; The scientific rationale for combining long-acting β_2-agonists and muscarinic antagonists in COPD; Pulm. Pharmacol. Ther. **2010**, *23*, 257-267.

[427] Cazzola M., Matera M.G.; Novel long-acting bronchodilators for COPD and asthma. Br. J. Pharmacol. **2008**, *155*, 291-299.

[428] Benovic J.L., Pike L.J., Cerione R.A., Staniszewski C., Yoshimasa T., Codina J., Caron M.G., Lefkowitz R.J.; Phosphorylation of the mammalian β-adrenergic receptor by cyclic AMP-dependent protein kinase: regulation of the rate of receptor phosphorylation and dephosphorylation by agonist occupancy and effects on coupling of the receptor to the stimulatory guanine nucleotide regulatory protein; J. Biol. Chem. **1985**, *260*, 7094-7101.

[429] Okamoto T., Murayama Y., Hayashi Y., Inagaki M., Ogata E., Nishimoto I.; Identification of a Gs activator region of the β_2-adrenergic receptor that is autoregulated via protein kinase A-dependent phosphorylation. Cell **1991**, *67*, 723-730.

[430] Voss H.P., Shukrula S., Wu T.S., Donnell D., Bast A.; A functional beta-2 adrenoceptor-mediated chronotropic response in isolated guinea pig heart tissue: selectivity of the potent beta-2 adrenoceptor agonist TA 2005; J. Pharmacol. Exp. Ther. **1994**, *271*, 386-389.

[431] Kikkawa H., Kanno K., Ikezawa K.; TA-2005, a novel, long-acting and selective β_2-adrenocepter agonist: characterization of its in vivo bronchodilating action in guinea pigs and cats in comparison with other β_2-agonists; Biol. Pharm. Bull. **1994**, *17*, 1047-1052.

[432] Kikkawa H., Isogaya M., Nagao T., Kurose H.; The role of the seventh transmembrane region in high affinity binding of a β_2-selective agonist TA-2005; Mol. Pharmacol. **1998**, *53*, 128-134.

[433] Kikkawa H., Kurose H., Isogaya M., Sato Y., Nagao T.; Differential contribution of two serine residues of wild type and constitutively active beta2-adrenoceptors to the interaction with beta2-selective agonists; Br. J. Pharmacol. **1997**, *121*, 1059-1064.

[434] Izeboud C.A., Vermeulen R.M., Zwart A., Voss H.P., van Miert A.S., Witcamp R.F.; Stereoselectivity at the β_2-adrenoceptor on macrophages is a major determinant of the anti-inflammatory effects of β_2-agonists; Naunyn-Schmiedeberg's Arch. Pharmacol. **2000**, *362*, 184-189.

[435] Suryanarayana S., Kobilka B.K.; Amino acid substitutions at position 312 in the seventh hydrophobic segment of the beta 2-adrenergic receptor modify ligand-binding specificity; Mol. Pharmacol. **1993**, *44*, 111-114.

[436] Furse K.E., Lybrand T.P.; Three-dimensional models for β-adrenergic receptor complexes with agonists and antagonists; J. Med. Chem. **2003**, *46*, 4450-4462.

[437] Katritch V., Reynolds K.A., Cherezov V., Hanson M.A., Roth C.B., Yeager M., Abagyan R.; Analysis of full and partial agonists binding to β_2-adrenergic receptor suggests a role of transmembrane helix V in agonist-specific conformational changes; J. Mol. Recognit. **2009**, *22*, 307-318.

[438] Grazioso G., Cavalli A., De Amici M., Recanatini M., De Micheli C.; Alpha7 nicotinic acetylcholine receptor agonists: Prediction of their binding affinity through a molecular mechanics Poisson–Boltzmann surface area approach; J. Comput. Chem. **2008**, *29*, 2593-2602.

[439] Neugebauer R.C., Uchiechowska U., Meier R., Hruby H., Valkov V., Verdin E., Sippl W., Jung M.; Structure–activity studies on splitomicin derivatives as sirtuin inhibitors and computational prediction of binding mode; J. Med. Chem. **2008**, *51*, 1203-1213.

[440] Cavalli A., Bottegoni G., Raco C., De Vivo M., Recanatini M.; A computational study of the binding of propidium to the peripheral anionic site of human acetylcholinesterase; J. Med. Chem. **2004**, *47*, 3991-3999.

[441] Rubenstein R.C., Wong S.K.F., Ross E.M.; The hydrophobic tryptic core of the beta-adrenergic receptor retains Gs regulatory activity in response to agonists and thiols; J. Biol. Chem. **1987**, *262*, 16655-16662.

[442] MacroModel, version 9.7, Schrodinger, LLC, New York, NY, 2009.

[443] Kumar S., Nussinov R.; Fluctuations in ion pairs and their stabilities in proteins; Proteins **2001**, *43*, 433-454.

[444] Kumar S., Nussinov R.; Relationship between ion pair geometries and electrostatic strengths in proteins; Biophys. J. **2002**, *83*, 1595-1612.

[445] Arrang J.-M., Garnabg M., Schwartz J.-C.; Auto-inhibition of brain histamine release mediated by a novel class (H_3) of histamine receptor; Nature, **1983**, *302*, 832-837.

[446] Gomez-Ramirez J., Ortiz J., Blanco I.; Presynaptic H_3 autoreceptors modulate histamine synthesis through cAMP pathway; Mol. Pharmacol. **2002**, *61*, 239-245.

[447] Schlicker E., Fink K., Detzner M., Gothert M.; Histamine inhibits dopamine release in the mouse striatum via presynaptic H_3 receptors; J. Neural. Transm. Gen. Sect. **1993**, *93*, 1-10.

[448] Schlicker E., Fink K., Hinterthaner M., Gothert M.; Inhibition of noradrenaline release in the rat brain cortex via presynaptic H_3 receptors; Naunyn-Schmiedeberg's Arch. Pharmacol. **1989**, *340*, 633-638.

[449] Blandizzi C., Toghetti M., Colucci R., Del Tacca M.; Histamine H_3 receptors mediate inhibition of noradrenaline release from intestinal sympathetic nerves; Br. J. Pharmacol. **2000**, *129*, 1387-1396.

[450] Schlicker E., Berz R., Gothert M.; Histamine H_3 receptor-mediated inhibition of serotonin release in the rat brain cortex; Naunyn-Schmiedeberg's Arch. Pharmacol. **1988**, *337*, 588-590.

[451] Blandina P., Giorgetti M., Bartolini L., Cecchi M., Timmerman H., Leurs R., Pepeu G., Giovannini M.G.; Inhibition of cortical acetylcholine release and cognitive performance by histamine H_3 receptor activation in rats; Br. J. Pharmacol. **1996**, *119*, 1656-1664.

[452] Hancock A.A., Fox G.B.; Drugs that target histaminergic receptors, In: J.J. Buccafusco, (Eds.), Cognition Enhancing Drugs, Birkhäuser Verlag, Basel Switzerland, **2004**, pp. 97-114.

[453] De Almeida M.A.M.R, Izquierdo I.; Intracerebroventricular histamine, but not 48/80, causes posttraining memory facilitation in the rat; Arch. Int. Pharmacodyn. Ther. **1988**, *291*, 202-207.

[454] Leurs R., Bakker R.A., Timmerman H., de Esch I.J.P; The histamine H_3 receptor: from gene cloning to H_3 receptor drugs; Nature Rev. Drug Discov. **2005**, *4*, 107-120.

[455] Sander K., Kottke T., Stark H.; Histamine H_3 receptor antagonists go to clinics; Biol. Pharm. Bull. **2008**, *31*, 2163-2181.

[456] Gemkow M.J., Davenport A.J., Harich S., Ellenbroek B.A.; The histamine H_3 receptor as a therapeutic drug target for CNS disorders; Drug Discov. Today **2009**, *14*, 509-515.

[457] Lazewska D., Kiec-Kononowicz K.; Recent advances in histamine H_3 receptor antagonists/inverse agonists; Expert Opin. Ther. Patents, **2010**, *20*, 1147-1169.

[458] Berlin M., Boyce C.W., de Lera Ruiz M.; Histamine H_3 receptor as a drug discovery target; J. Med. Chem. **2011**, *54*, 26-53.

[459] Clark E. A., Hill S.J.; Sensitivity of histamine H_3 receptor agonist-stimulated [^{35}S]GTPγS binding to pertussis toxin; Eur. J. Pharmacol. **1996**, *296*, 223-225.

[460] Lovenberg T.W., Roland B.L., Wilson S.J., Jiang X., Pyati J., Huvar A., Jackson M.R., Erlander M.G.; Cloning and functional expression of the human histamine H3 receptor; Mol. Pharmacol. **1999**, *55*, 1101-1107.

[461] Drutel G., Peitsaro N., Karlstedt K., Wieland K., Smit M.J., Timmerman H., Panula P., Leurs R.; Identification of rat H_3 receptor isoforms with different brain expression and signaling properties; Mol. Pharmacol. **2001**, *59*, 1-8.

[462] Giovannini M.G., Efoudebe M., Passani M.B., Baldi E., Bucherelli C., Giachi F., Corradetti R., Blandina P.; Improvement in fear memory by histamine-elicited ERK2 activation in hippocampal CA3 cells; J. Neurosci. **2003**, *23*, 9016-9023.

[463] Rouleau A., Ligneau X., Tardivel-Lacombe J., Morisset S., Gbahou F., Schwartz J.C., Arrang J.M.; Histamine H_3-receptor-mediated [35S]GTPγS binding: evidence for constitutive activity of the recombinant and native rat and human H_3 receptors; Br. J. Pharmacol. *2002*, *135*, 383-392.

[464] Silver R.B., Poonwasi K.S., Seyedi N., Wilson S.J., Lovenberg T.W., Levi R.; Decreased intracellular calcium mediates the histamine H_3-receptor-induced attenuation of noradrenaline exocytosis from cardiac sympathetic nerve endings; Proc. Natl. Acad. Sci. USA **2002**, *99*, 501-506.

[465] Molina-Hernández A., Nuñez A., Sierra J.J., Arias-Montaño J.A.; Histamine H_3 receptor activation inhibits glutamate release from rat striatal synaptosomes; Neuropharmacology **2001**, *41*, 928-934.

[466] Silver R.B., Mackins C.J., Smith N.C., Koritchneva I.L., Lefkowitz K., Lovenberg T.W., Levi R.; Coupling of histamine H_3 receptors to neuronal Na+/H+ exchange: a novel protective mechanism in myocardial ischemia; Proc. Natl. Acad. Sci. USA **2001**, *98*, 2855-2859.

[467] Morini G., Comini M., Rivara M., Rivara S., Lorenzi S., Bordi F., Mor M., Flammini L., Bertoni S., Ballabeni V., Barocelli E., Plazzi P.V.; Dibasic non-imidazole histamine H_3 receptor antagonists with a rigid biphenyl scaffold; Bioorg. Med. Chem. Lett. **2006**, *16*, 4063-4067.

[468] Morini G., Comini M., Rivara M., Rivara S., Bordi F., Plazzi P.V., Flammini L., Saccani F., Bertoni S., Ballabeni V., Barocelli E., Mor M.; Synthesis and structure-activity relationships for biphenyl H_3 receptor antagonists with moderate anti-cholinesterase activity; Bioorg. Med. Chem. **2008**, *16*, 9911-9924.

[469] Yao B.B., Hutchins C.W., Carr T.L., Cassar S., Masters J.N., Bennani Y.L., Esbenshade T.A., Hancock A.A.; Molecular modeling and pharmacological analysis of species-related histamine H(3) receptor heterogeneity; Neuropharmacology **2003**, *44*, 773-786.

[470] Axe F.U., Bembenek S.D., Szalma S.; Three-dimensional models of histamine H_3 receptor antagonist complexes and their pharmacophore; J. Mol. Graph. Model. **2006**, *24*, 456-464.

[471] Schlegel B., Laggner C., Meier R., Langer T., Schnell D., Seifert R., Stark H., Holtje H.-D., Sippl W.; Generation of a homology model of the human histamine H(3) receptor for ligand docking and pharmacophore-based screening; J. Comput. Aided Mol. Des. **2007**, *21*, 437-453.

[472] Levoin N., Calmels T., Poupardin-Oliveier O., Labeeuw O., Danvy D., Robert P., Berrebi-Bertrand I., Ganellin C.R., Schunack W., Stark H., Capet M.; Refined docking as a valuable tool for lead optimization: application to histamine H_3 receptor antagonists; Arch. Pharm. Chem. Life Sci. **2008**, *341*, 610-623.

[473] Rai B.K., Tawa G.J., Katz A.H., Humblet C.; Modeling G protein-coupled receptors for structure-based drug discovery using low-frequency normal modes for refinement of homology models: application to H_3 antagonists; Proteins **2010**, *78*, 457-473.

[474] Roche O., Rodriguez Sarmiento R.M.; A new class of histamine H_3 receptor antagonists derived from ligand based design; Bioorg. Med. Chem. Lett. **2007**, *17*, 3670-3675.

[475] Ly K.S., Letavic M.A., Keith J.M., Miller J.M., Stocking E.M., Barbier A.J., Bonaventure P., Lord B., Jiang X., Boggs J.D., Dvorak L., Miller K.L., Nepomuceno D., Wilson S.J., Carruthers N.I.; Synthesis and biological activity of piperazine and diazepane amides that are histamine H_3 antagonists and serotonin reuptake inhibitors; Bioorg. Med. Chem. Lett. **2008**, *18*, 39-43.

[476] Letavic M.A., Keith J.M., Jablonowski J.A., Stocking E.M., Gomez L.A., Ly K.S., Miller J.M., Barbier A.J., Bonaventure P., Boggs J.D., Wilson S.J., Miller K.L., Lord B., McAllister H.M., Tognarelli D.J., Wu J., Abad

M.C., Schubert C., Lovenberg T.W., Carruthers N.I.; Novel tetrahydroisoquinolines are histamine H3 antagonists and serotonin reuptake inhibitors; Bioorg. Med. Chem. Lett. **2007**, *17*, 1047-1051.

[477] Bordi F., Rivara S., Dallaturca E., Carmi C., Pala D., Lodola A., Vacondio F., Flammini L., Bertoni S., Ballabeni V., Barocelli E., Mor M.; Dibasic biphenyl H3 receptor antagonists: steric tolerance for a lipophilic side chain; Eur. J. Med. Chem. **2012**, http://dx.doi.org/10.1016/j.ejmech.2011.12.019.

[478] MacroModel, version 9.8, Schrödinger, LLC, New York, NY, 2010.

[479] Allinger N.L., Yuh Y.H., Lii J.-H.; Molecular mechanics. The MM3 force field for hydrocarbons. 1; J. Am. Chem. Soc. **1989**, *99*, 8127-8134.

[480] Still W.C., Tempczyk A., Hawley R.C., Hendrickson T.; Semianalytical treatment of solvation for molecular mechanics and dynamics; J. Am. Chem. Soc. **1990**, *112*, 6127-6129.

[481] Maestro, version 9.1, Schrödinger, LLC, New York, NY, 2010.

[482] Lorenzi S., Mor M., Bordi F., Rivara S., Rivara M., Morini G., Bertoni S., Ballabeni V., Barocelli E., Plazzi P.V.; Validation of a histamine H_3 receptor model through structure-activity relationships for classical H_3 antagonists; Bioorg. Med. Chem. **2005**, *19*, 5647-5657.

[483] Leurs R., Smit M.J., Tensen C.P., Terlaak A.M., Timmerman H.; Site-directed mutagenesis of the histamine H_1-receptor reveals a selective interaction of asparagine207 with subclasses of H_1-receptor agonists; Biochem. Biophys. Res. Commun. **1994**, *201*, 295-301.

[484] Uveges A.J., Kowal D., Zhang Y., Spangler T.B., Dunlop J., Semus S., Jones P.G.; The role of transmembrane Helix5 in agonist binding to the human H3 receptor; J. Pharmacol. Exp. Ther. **2002**, *301*, 451-458.

[485] Sherman W., Day T., Jacobson M.P., Friesner R.A., Farid R.; Novel procedure for modeling ligand/receptor induced fit effects; J. Med. Chem. **2006**, *49*, 534-553.

[486] Schrödinger Suite 2010 Induced Fit Docking protocol; Glide version 5.6, Schrödinger, LLC, New York, NY, 2010; Prime version 2.2, Schrödinger, LLC, New York, NY, 2010.